SYNTHESIS AND BIOLOGICAL CHARACTERISATION OF POTENTIAL INHIBITORS OF MICROBIAL β-LACTAMASES

AISOSA IMAS IYOHA

Doctor of Philosophy

ASTON UNIVERSITY

February 2023

Aston University

Synthesis and Biological Characterisation of Potential Inhibitors of Microbial β-Lactamases

Thesis Submitted by Aisosa Imas Iyoha

For the Degree of Doctor of Philosophy

February 2023.

Abstract

Antibiotic resistance remains a global health challenge and arguably, could be described as a silent pandemic. Bacterial β-lactamases are among the major promoters of antibiotic resistance owing to their virulence against the most commonly used class of antibiotics. β-Lactamases such as NDM-1 and Bla$_{Mab}$ are broad-spectrum, antibiotic-degrading enzymes that are associated with life-threatening infections. The therapeutic relevance of β-lactam antibiotics remains obscure considering the absence of clinically significant NDM-1 inhibitor(s) while the cure rate of *Mycobacterium abscessus* (*Mab*) infection in patients with cystic fibrosis remains low due to the lack of Bla$_{Mab}$ inhibitor as part of the treatment regimen for *Mab* infection. These have prompted the development of potential NDM-1 and Bla$_{Mab}$ inhibitors respectively.

Potential bis cyclo-oxamide prodrugs/α,β-unsaturated carbonyl compounds and bicyclic/tricyclic *N,S*-acetals were successfully synthesised and characterised as potential inhibitors of NDM-1 and Bla$_{Mab}$ enzymes respectively. Potential NDM-1 polar and hydrophobic interactions with the respective bis cyclo-oxamide and the unsaturated carbonyl compounds were identified by crystallographic studies while TLC-based inhibitory screening of the bis cyclo-oxamide prodrugs showed some of the compounds functioned as NDM-1 inhibitors, rather than a prodrug that was expected to release oxalate anion in the presence of NDM-1, at a concentration of ≥1.78 mM. However, a rapid nitrocefin test identified oxalate anion as a potential inhibitor of NDM-1. The synthesised bicyclic and tricyclic *N,S*-acetals are analogues of a potent Bla$_{Mab}$ inhibitor (lead compound). The bioisosteric modification of the lead compound resulted in the loss of inhibitory activity but two of these analogues displayed limited antimicrobial activity against some Gram-negative bacteria.

The study demonstrates that the bis cyclo-oxamides are potential inhibitors of NDM-1 and the enzyme is also sensitive to oxalate anion, hence, the anion can be employed as an active drug agent in the development of NDM-1 prodrugs.

Acknowledgements

"No one who achieves success does so without acknowledging the help of others. The wise and confident acknowledge this help with gratitude (Alfred North Whitehead)"

First, I offer thanks to God for granting me the courage and ability to complete the PhD programme despite challenging times.

I sincerely appreciate Aston University for awarding me the Vice-Chancellor's International Scholarship. This generous support (scholarship) enabled me to undertake this life-changing journey.

It is important to offer my sincere gratitude to my supervisor, Dr. Dan Rathbone, for his supervision. His support and guidance were instrumental throughout this challenging Journey (PhD programme). It is equally worthwhile to express my gratitude to the microbiology team, Dr. Jonathan Cox and Dr. James Harrison, for their assistance and guidance with the biological screening of the synthesised compounds.

Also, thanks to Dr. Eshtiwi Amani for undertaking the protein-docking studies and to the postdoctoral researchers, Dr. Brahman Medapi, Dr. Florian Dato and Dr. Subramanian Govindan for teaching me some technical skills (chemistry).

My appreciation to colleagues in the chemistry laboratory, Bassant Rateb and the postdocs earlier mentioned as well as the technical staff, Hayley Shearer and Daniel Burrell, for their support and kindness.

Equally, many thanks to Dr. William Fraser and Dr. Dan Rathbone for allowing me to gain teaching experience which was a prerequisite for obtaining my AFHEA qualification.

My heartfelt gratitude, to my ever-loving and caring wife, Mrs. P.A. IYOHA, for her amazing support and encouragement and, to my precious daughter, Etiosasere, for her love and warmth.

Lastly, my sincere thanks to my parents, Mr. and Mrs. IYOHA, for their prayers, financial and moral support, and thanks to my siblings for their kindness and prayers.

List of Contents

List of Abbreviations

ABR   Antibacterial resistance

AMR   Antimicrobial resistance

BcII   *Bacillus cereus* Metallo-β-lactamase

Bla$_{Mab}$ *Mycobacterium abscessus* β-lactamase

Bla$_{Mmas}$ *Mycobacterium massiliense* β-lactamase

$CBrCl_3$ Bromotrichloromethane

$CDCl_3$ Deuterated chloroform

CDC   Centers for Disease Control and Prevention

CDI   1,1'-carbonyldiimidazole

CphA   Carbapenemase hydrolysing *Aeromonas*

d_6-DMSO   Deuterated dimethylsulfoxide

DBU   1,8-Diazabicyclo[5.4.0]undec-7-ene

DCM   Dichloromethane

DHSC   Department for Health and Social Care

DMF   *N,N*-dimethylformamide

D_2O Deuterium oxide

EDC.HCl   N-(3-Dimethylaminopropyl)-N'-ethylcarbodiimide hydrochloride

ESMS   Electrospray mass spectrometry

ESI-MS   Electrospray ionisation mass spectrometry

HOBt   1-Hydroxybenzotriazole

IMP-1   Imipenemase 1

IR   Infrared

$KMnO_4$ Potassium permanganate

Mab   *Mycobacterium abscessus*

MBLs   Metallo-β-lactamases

MS   Mass spectrometry

NDM-1   New Delhi Metallo-β-lactamase-1

PBPs   Penicillin-binding proteins

PBS   Phosphate-Buffered Saline

SBLs   Serine-β-lactamases

SPR   Surface plasmon resonance

TFA   Trifluoroacetic acid

TLC   Thin-layer chromatography

TMS   Tetramethylsilane

VIM-2   Verona-integron encoded metallo-β-lactamase 2

WHO   World Health Organisation

^{1}H NMR   Proton nuclear magnetic resonance

^{13}C NMR   Carbon-13 nuclear magnetic resonance

List of Tables

List of Figures

List of Schemes

Chapter 1

1. Introduction to antibiotics resistance

1.1 Introduction

The most notable medical accomplishment of the twentieth century was the discovery of antibiotics (Alexander Fleming in 1928), antibacterial compounds that have saved countless lives and enabled several medical procedures (surgery, chemotherapy) (Singh and Barrett, 2006; Drawz and Bonomo, 2010). This life-saving therapy is in peril due to the development and proliferation of antibacterial resistance (ABR) resulting from the overuse and misuse of antibiotics (WHO, 2017). More worrisome is the emergence and proliferation of multidrug-resistant bacteria, causing infections with few to no therapeutic options (Unemo and Nicholas, 2012). The consistent development of bacteria resistance to current antibiotics, including the most important and commonly-used class, known as the β-lactams (Bush and Bradford, 2016), has made the supremacy of antibiotics over bacterial infections temporary for decades.

Several recognised organisations, such as the World Health Organisation (WHO), Centers for Disease Control and Prevention (CDC), the Department for Health and Social Care (DHSC), and notable individuals continue to highlight the increased threat of antibiotic resistance. The CDC report (2019) shows that each year, in the US, a minimum of 2.8 million people are infected with antibiotic-resistant bacteria which results in not less than 35,000 deaths while a recent article, on the global burden of bacterial AMR in 2019, estimated 1.27 million deaths specifically attributed to bacterial AMR and 3.68 million bacterial AMR-related deaths (Murray *et al*., 2022). Similarly, according to the DHSC, AMR causes more than 700,000 deaths annually across the globe. In August 2019, the then England's chief medical officer, Dame Sally Davies, warned on Sky News that the threat of antimicrobial resistance was more imminent than climate change and a 2014 Review on Antimicrobial Resistance, chaired by Jim O'Neill, also warned that if there is no intervention, antimicrobial resistance could lead to 10 million deaths annually by 2050. However, this estimate might increase as a result of the overuse of antibiotics during the Covid-19 pandemic (Arshad *et al*., 2020).

In light of the therapeutic failure of current antibiotics against infections from resistant bacteria, the WHO (2012) has warned that the positive outcome of major surgeries and cancer treatments would be severely compromised, resulting in an increased ABR-associated mortality rate.

1.2 Antibiotic resistance

Antibiotic resistance occurs when bacteria develop the capability, through different mechanisms, to defeat antibiotics such that the antibiotics become less effective or ineffective against bacterial infections. Bacteria develop resistance to antibiotics via different mechanisms

➤ Alteration/modification of outer membrane proteins,

➤ Modification of antibiotics targets (penicillin-binding proteins),

➤ Expression of a hydrolytic enzyme(s) and

➤ Efflux pump

1.2.1 Alteration/modification of outer membrane proteins

The unique outer membrane of Gram-negative bacteria harbours lipoproteins and integral membrane proteins generally called outer membrane proteins (Figure 1.1) which are classified as general/nonspecific porins, substrate-specific porins, gated porins, and efflux porins (Hancock and Brinkman, 2002; Martinez-Martinez, 2008).

These porins are β-barrel structured transmembrane pore-forming proteins which facilitate the passive diffusion of antibiotics across the outer membrane to access the target, PBPs, on the inner plasma membrane (Nikaido, 2003; Pages *et al*., 2008; Choi and Lee, 2019).

Decreased expression of porin proteins lowers the permeability of the outer membrane (Bush, 2010) and mutant porin proteins, produced due to gene mutation, are unable to facilitate the passage of antibiotics across the outer membrane, resulting in antibiotic resistance. For example, the modification of the non-specific porin protein OmpF, a protein that transports β-lactams across the outer membrane into the periplasmic space in Gram-negative bacteria, results in β-lactam antibiotics resistance (Delcour, 2009; Choi and Lee, 2019).

[Figure redacted]

Figure 1.1: Gram-negative cell wall (Dahl, 2008).

1.2.2 Modification of antibiotics target

β-Lactam antibiotics function via covalent modification of transpeptidase/penicillin-binding proteins (PBPs), an enzyme that catalyses the final step of peptidoglycan synthesis via 4→3 amino acid cross-linkage (D, D-transpeptidases) of one stem peptide to the adjacent stem peptide (Figure 1.2), leading to the loss of enzymatic activity and consequently cell lysis.

[Figure redacted]

Figure 1.2: Peptidoglycan Synthesis. N-acetylglucosamine (1st hexagonal structure) and N-acetylmuramic acid (2nd hexagonal structure) (Lavollay *et al*., 2011).

The modification of the PBPs binding site or the production of different PBP (target) subtypes may result in reduced affinity or loss of affinity for β-lactam antibiotics and consequently the development of bacteria resistance to this class of antibiotics (Fisher and Mobashery, 2016). A classic example is the presence of PBP2a, which has a low affinity for β-lactam antibiotics, in Methicillin-resistant *Staphylococcus aureus* (MRSA) (Finch *et al*., 2012).

1.2.3 Expression of hydrolytic enzymes

Concerning the expression of a hydrolytic enzyme(s), bacteria may become resistant to antibiotics through the acquisition of virulent gene(s) or the development of mutant gene(s) that code for the production of an enzyme(s), capable of hydrolysing antibiotics (Figure 1.3) and these genes (plasmids) are mobile as they can be transferred from one group of bacteria to another (Bush, 2013).

Figure 1.3: Generic representation of hydrolysis of β-lactam by β-lactamase.

1.2.4 Efflux pump

Bacterial efflux pumps, located in the plasma membrane, are proteins that transport toxic compounds, such as antibiotics, from the periplasmic space to the external environment (Pagès, and Amaral, 2009; Pagès *et al*., 2011) and these pumps may be substrate-specific or non-specific. The non-substrate specific pumps transport a wide range of substrates and are associated with multiple drug resistance (Webber and Piddock, 2003; Amaral *et al*., 2014).

A high concentration of toxins (like antibiotics) in the periplasmic space, which threatens the survival of the bacterium, triggers the overexpression of efflux pumps which extrude the toxins out of the periplasm, resulting in antibiotic resistance (Piddock, 2006; Gootz, 2006; Amaral *et al*., 2014).

Similarly, a mutation in bacteria can prompt overexpression of efflux pumps which in turn facilitates the extrusion of antibiotics and consequently lead to the development of resistance (Webber and Piddock, 2003).

1.3 Bacterial resistance: Gram-positive versus Gram-negative

As earlier stated, bacteria develop antibiotic resistance by altering their normal physiology to minimise or abrogate the therapeutic effect of most antibiotics, including the most commonly used class, β-lactam antibiotics (Bush and Bradford, 2016), which exerts its therapeutic effect by inhibiting the enzymes associated with cell wall biosynthesis (Bonomo, 2017). The mechanism of bacterial resistance to β-lactam antibiotics depends on the class of the bacterial pathogen. The main mechanism of β-lactam antibiotics resistance for Gram-positive bacterial pathogens is target modification while the main mechanism for Gram-negative bacteria is the expression of the hydrolytic enzyme, called β-lactamases, that catalyses the hydrolysis of the β-lactam ring of the antibiotics, rendering them inactive (Fisher and Mobashery, 2016; Ogawara, 2015; Finch *et al*., 2012; Livermore 2012; Babic *et al*., 2006).

1.4 β-Lactamases

The discovery of β-lactamase, in *Bacillus* (*Escherichia*) *coli*, dates back to the late 80s (Abraham and Chain 1988) but its clinical challenge became apparent, several years later, when *Staphylococcus aureus* developed resistance to penicillin due to the production of staphylococcal penicillinase. Over the years, the introduction of several novel β-lactams into clinical settings further exacerbated the pressure on bacteria, promoting the survival of multitudes of bacteria with effective β-lactamase (Massova and Mobashery 1998; Bonomo, 2017). Currently, there are over 2,000 naturally occurring β-lactamases and each possesses a distinct amino acid sequence and enzymatic profile (Bonomo, 2017). According to Ambler's classification, β-lactamases are classified into four classes, A, B, C and D, based on the active site amino acid and catalytic residues. Classes A, C and D are serine-based hydrolases (Serine-β-lactamases, SBLs), which utilise a serine to catalyse the cleavage of the β-lactam ring of the antibiotics, while Class B enzymes are Zn-Metallo hydrolases (Metallo-β-lactamases, MBLs) and they utilise one or two Zn (II) ions to catalyse the hydrolysis of the β-lactam ring (Bush and Jacoby, 2010). Class B enzymes are further divided into three subclasses: B1, B2 and B3. The B1 subclass contains the most pathogenic MBL enzyme, called New Delhi Metallo-β-lactamase-1 (NDM-1), which can degrade nearly all clinically available β-lactam antibiotics, including last-resort antibiotics (carbapenems), except monobactams (aztreonam) which are subject to hydrolysis by SBLs that are usually coproduced with NDM-1 (Bush and Jacoby, 2010; Shaikh *et al*., 2015; Drawz and Bonomo, 2010; Groundwater *et al*., 2016; Khan, Maryam and Zarrilli, 2017; Yong *et al*., 2009).

1.5 New Delhi Metallo-β-lactamase-1 (NDM-1)

New Delhi Metallo-β-lactamase-1 (NDM-1), first discovered in a *Klebsiella pneumoniae* strain isolated from a Swedish patient in New Delhi, India (Yong *et al*., 2009), has been identified as a recent and emerging concern among versatile β-lactamases (carbapenemases) and consequently presents a serious threat to public health due to its rapid spread across the globe through occurrence in diverse

species of *Enterobacteriaceae*, *Acinetobacter* and *Pseudomonas* (Khan, Maryam and Zarrilli, 2017; Moellering, 2010; Dortet, Poirel, Nordmann, 2014; Wu *et al*., 2019). In a few years, NDM-1 has evolved over 20 variants, and at present, there is no clinically significant inhibitor to co-administer with NDM-1 susceptible β-lactam antibiotics, hence NDM-1-induced infections have become a major public health challenge as these infections are associated with high morbidity and mortality rate (Wu *et al*., 2019; Linciano *et al*., 2019).

1.5.1   Architecture and structural catalytic insight of NDM-1

To understand the enzymatic characteristics of NDM-1, several studies on the architecture and structural catalytic residues have been conducted with emphasis on the structure/nature/composition of the active site, mechanism of action (formation of one or two transition states), the nature of the nucleophile, source of the proton donor and substrate binding mode.

1.5.2   Architecture of NDM-1

NDM-1 is structurally characterised by unique αβ/βα domains with an embedded active site, flanked by several loops, consisting of two zinc (II) ions (Zn1 and Zn2) linked by a water/hydroxide molecule (w1) (Figure 1.4) (Linciano *et al*., 2019). Among these loops, flexible (subject to conformational change) loop3 and loop10 play essential roles, with loop3 involved in substrate binding recognition due to the presence of hydrophobic amino residues (Leu65, Met67, Phe70, and Val73) which interact with the substrate hydrophobic substituents while loop10 consist of amino residues that interact with the carboxyl group of the substrate (Lys211 and Asn220) as well as residues that coordinate Zn2 (Cys 208) (King and Strynadka, 2011; Zhang and Hao, 2011). Zn1, which functions to align the carbonyl group of the substrate for nucleophilic attack by the hydroxide, is tetrahedrally coordinated to His120, His122, His189 and the bridging hydroxide (w1) while Zn2, which interacts with the carboxyl group and amide nitrogen of the substrate, is trigonal-bipyramidally coordinated to Asp124, Cys208, His250, the bridging hydroxide (w1) (Figure 1.5 and Figure 1.6) and an apical water molecule (w2) (Linciano *et al*., 2019; Mojica, Bonomo and Fast, 2016; Zhang and Hao, 2011; King and Strynadka, 2011; Kim *et al*., 2011; Lassaux *et al*., 2011).

[Figure redacted]

Figure 1.4: The architecture of NDM-1 (3spu) (A) Protein folding with the two zinc ions, Loops 3 and 10. (B) The core of the active site with essential amino residues and water molecules (King and Strynadka, 2011; Kim *et al*., 2011; Linciano *et al*., 2019).

1.5.3 Structural catalytic insight of NDM-1

NDM-1 hydrolytic mechanism of β-lactams generally involves two key steps, the scission of the C-N bond and the protonation of the newly formed anionic intermediate respectively (King and Strynadka, 2013; Meini *et al*., 2015; Feng *et al*., 2017). However, during hydrolysis, the occurrence of these steps differs based on the class of the substrate. While NDM-1 hydrolysis of penicillin involves a straightforward process of nucleophilic attack on the carbonyl carbon of the β-lactam ring (Figure 1.5 B) which prompts the scission of the C-N bond and consequently results in the formation of anionic intermediate with negatively charged nitrogen (Figure 1.5 C) that is protonated and released from the enzymes' active site (Figure 1.5 D) (King and Strynadka, 2013; Meini *et al*., 2015), cephalosporin and carbapenem involve tautomerisation of the double bond upon cleavage of C-N bond and concomitant formation of respective carbanionic species (Feng *et al*., 2014; Feng *et al*., 2017).
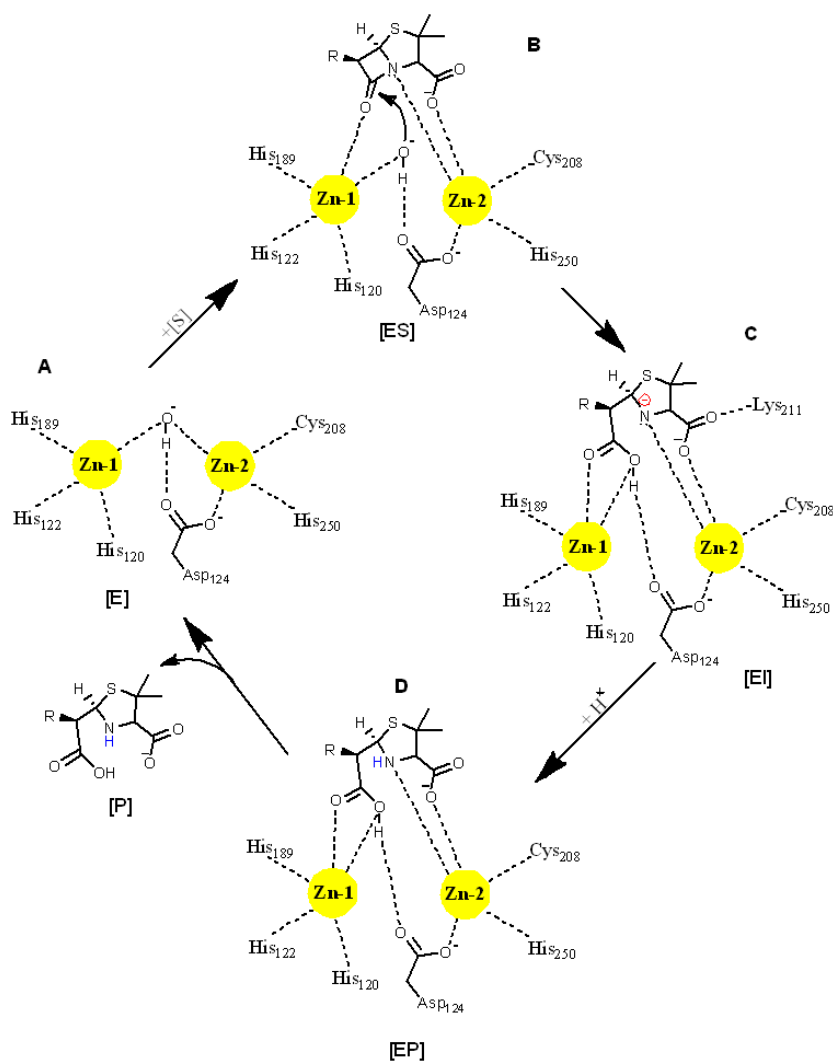
Figure 1.5: Generic representation of hydrolysis of penicillin by NDM-1, B1 enzyme (Llarrull *et al*., 2008). (A) NDM-1 active state; (B) binding of penicillin and nucleophilic attack; (C) scission of the amide bond and binding of the intermediate (hydrolysed substrate) to the active site; (D) neutralization of the intermediate, followed by the release of the hydrolysed substrate and reactivation of NDM-1 active state (Meini *et al*., 2015; Feng *et al*., 2017; Linciano *et al*., 2019).

[Figure redacted]

Figure 1.6: Generic representation of hydrolysis of cephalosporin NDM-1 (Feng *et al*., 2014): (A) NDM-1 active state; (B) binding of substrate and nucleophilic attack (C) scission of the amide bond and binding of the intermediate (hydrolysed substrate) to the active site; (D) tautomerisation of the double bond and formation of carbanion; (E) neutralization of the intermediate product, the release of the hydrolysed substrate and reactivation of NDM-1 active state (Feng *et al*., 2014; Feng *et al*., 2017; Linciano *et al*., 2019).

In NDM-1 hydrolysis of cephalosporin, the formation of the negatively charged nitrogen, which stems from the C-N bond scission, facilitates the tautomerisation of the double bond in the dihydrothiazine ring, from position C-3/C-4 to C-4/N-5, resulting in the formation of carbanion at position 3 (Feng *et al*., 2014). The carbanionic intermediate is neutralised by protonation of C-3 (Figure 1.6 E) and the hydrolysed substrate is released from the active site, triggering the regeneration of the bridging hydroxide which consequently reactivates the enzyme (Figure 1.6 A) for a new hydrolytic cycle (Feng *et al*., 2014; Feng *et al*., 2017). However, following the double bond rearrangement, the characteristics of R2 determine the type of intermediate, and the subsequent product, that is formed. Cephalosporins

with good R2 leaving group, such as cephalothin (Mobashery and Johnston, 1986) and cefoxitin (Chen *et al.,* 2005) respectively, form an intermediate with the exo-methylene group due to the elimination of the leaving while cephalosporins with poor R2 leaving group, such as cephalexin, retain their R2 group (Figure 1.6 D and E) (Feng *et al.*, 2014).

[Figure redacted]

Figure 1.7: Generic representation of hydrolysis of carbapenem NDM-1 (Feng *et al.*, 2017): (A) NDM-1 active state; (B) binding of substrate and nucleophilic attack; (C, D) scission of amide bond, binding of the intermediate, tautomerisation of the double bond and formation of carbanion; (E) protonation and EI$_3$ intermediate; (F) unprotonated EP complex; (G) protonated EP complex, the release of the hydrolysed substrate and reactivation of NDM-1 (Feng *et al.*, 2017; Linciano *et al.*, 2019).

Contrary to the NDM-1 hydrolytic mechanism of penicillin and cephalosporin respectively (Figures 5 and 6), carbapenems display a distinct NDM-1 hydrolytic mechanism (Feng *et al.*, 2017), thus indicating substrate-induced NDM-1 catalytic variation. Crystal structures of NDM-1 complexed with the

hydrolysed intermediates and products of carbapenems (imipenem and meropenem) revealed the following key variations

➤ The opening of the lactam ring prompts double bond rearrangement (tautomerisation) of the dihydropyrrole ring, from position C-2/C-3 to C-3/N-4, resulting in the formation of two enzyme-intermediate species (EI1 and EI2) in equilibrium (Figure 1.7 C and D).

➤ Contrary to the presence of a water molecule intercalating both zinc (II) ions in the NDM-1-penicillin/cephalosporin complex respectively (Meini *et al*., 2015; Zhu, 2013; Tripathi and Nair, 2015), there is no such bridging-hydroxide/water molecule in NDM-1-meropenem complex. The absence of the bridging water, a potential protonating agent, makes the protonation of the negatively charged dihydropyrrole nitrogen highly unlikely (Figure 1.7 C, EI1) and as such favours the accumulation of EI2 (Figure 1.7 D).

➤ The favoured EI2 can undergo two respective pathways before releasing the hydrolysed substrate. It can generate an EI3 intermediate (Figure 1.7 E) following protonation at C-2 or it can generate a transient unprotonated-EP^I complex (Figure 1.7 F) which in turn generates an EP complex (Figure 1.7 G). This is contrary to the NDM-1-penicillin/cephalosporin complex where one enzyme-intermediate complex is formed.

➤ The oxygen atom of the newly formed carboxylate coordinates both zinc (II) ions in the EP state (Figure 1.7 G), unlike the NDM-1-cephalosporin complex, where this group coordinates with only Zn1

Another substrate-induced NDM-1 catalytic variation is the differential penicillin/cephalosporin- and carbapenem-NDM-1 binding modes. This variation is due to the plasticity of the binding site which anchors on the flexibility of loop3 as its conformation is fine-tuned by the binding of substrate(s). This is evident in the NDM-1 binding of penicillin/cephalosporin and carbapenems respectively as the binding of carbapenems prompts the catalytic pocket to moderately cave-in with loop3 closing the groove of the active site while in the case of cephalosporin, loop3 moves rearward, creating space for larger moieties (Feng *et al*., 2017; Huntley *et al*., 2000).

As earlier stated, one of the key steps of NDM-1 catalysis is the protonation of the newly formed anionic/carbanionic intermediate and several studies have validated the proton-neutralisation of the anionic/carbanionic intermediate, as the rate-limiting step in NDM-1 hydrolysis of β-lactam antibiotics (Feng *et al*., 2017; King and Strynadka, 2013). However, the identity of the proton donor remains vague (Meini *et al*., 2015) as different concepts have been proposed, concerning the proton donor, and they are enumerated below

➤ A Zn2 ligand, D120, was once suggested as the proton donor (Carfi *et al.,* 1998) or a general base (Carfi *et al.,* 1995) that protonates the anionic nitrogen atom but the discovery of the actual function of D120 – orientation of the hydroxide and stabilisation of Zn2 (Yamaguchi *et al*., 2005) – has long invalidated this concept.

➤ A Zn2 coordinated water molecule, in apo NDM-1, was also proposed as the proton donor (Concha *et al*., 1996; Dal Peraro *et al*., 2007) but, according to Zhang and Hao, 2011, it is highly unlikely

because the bound water is replaced by the amide nitrogen and carboxyl oxygen coordination to Zn2 respectively in the NDM-1-ampicillin (EP) crystal structure. However, Meini *et al*., 2015 reaffirm this concept of the Zn2-bound water being the potential protonating agent. The bound water repositions closer to Zn1 and swiftly takes up the vacant position initially occupied by the nucleophile (OH⁻) after the C-N bond scission. This possibly accounts for the absence of the Zn2-bound water in the NDM-1-ampicillin (EP) crystal structure.

➤ A water molecule from a bulk solvent was similarly proposed as the source of the proton during its coordination with the zinc ions which results in the formation of a new hydroxide (Hu *et al*., 2008). However, this is less likely, especially in B1 subclass MBLs, because the water molecule is located below the active site and cannot readily access the active site because the substrate/intermediate is still bound to the active site, hence the water molecule cannot occupy the position left by the nucleophile (Meini *et al*., 2015; Zhang and Hao, 2011).

➤ Zhang and Hao, 2011 proposed that the proton might be from the newly formed carboxylic acid, of the β-lactam ring, whose formation is facilitated by the nucleophilic proton (O$\underline{H}$⁻). Their concept anchors on the proximity of the carboxylate to the anion as well as the acidity of the carboxylate proton.

Although the concepts of water-bound Zn2 and carboxylic acid of the β-lactam ring respectively, as a protonating agent, sound reasonable and it is applicable in all subclasses of MBLs, to date, the identity of the proton donor remains controversial.

1.6 Trends in NDM-1 inhibitor(s) synthesis

In a world where current antibiotic therapy is in peril as a result of the emergence and spread of resistant bacteria with infections of few to no therapeutic options, there is a need for the development of clinically useful inhibitors that can resensitise bacterial infections to current antibiotics. Concerning the NDM-1 susceptibility of almost all β-lactam antibiotics and the absence of clinically significant NDM-1 inhibitors, several efforts are being made to develop ideal NDM-1 inhibitors of clinical importance with high specificity, low to non-toxicity and remarkable potency.

Currently, two main strategies exist in the development of NDM-1 inhibitors and they are further subclassed based on mechanism (Ju *et al*., 2018; Rotondo and Wright, 2017).

1) Zn-independent
a) Covalent bond formation
2) Zn-dependent
a) Zinc binding inhibitors (ternary complex formation)
i)   Thiol compounds
ii)   Transition state analogues
iii)   Dicarboxylic acid derivatives
b) Zinc chelating/stripping Inhibitors

The exploitation of the two main strategies is not a trivial task as the presence of a shallow active site pocket is a drawback of the Zn-independent strategy while the Zn-dependent approach, sometimes,

results in the development of inhibitors with significant toxicity due to the presence of human metal-dependent enzymes competing for the Zn-dependent inhibitor (Ju *et al*., 2018; Rotondo and Wright, 2017). However, both strategies are vital in the development of NDM-1 inhibitors despite these hurdles.

1.6.1 Zn-independent NDM-1 inhibitors

These inhibitors function by modification of essential catalytic amino residue(s) present in the NDM-1 active site. As far as can be determined to date, only two catalytic amino residues – Cys208 and recently discovered Lys211 – have been successfully targeted for covalent modification in the development of NDM-1 inhibitors (Zervosen *et al*., 2001; Thomas *et al*., 2014).

1.6.1.1 NDM-1-covalent inhibitors - irreversible/reversible

Covalent inhibition is an essential biochemical and therapeutic strategy for overcoming enzyme-induced (over-expression) diseases. Inhibitors of this class deactivate enzyme(s) via covalent bond formation between the inhibitor (reactive group) and the targeted residue(s) in the enzymes' active site (Tuley and Fast, 2018). Concerning serine-β-lactamase-mediated antibiotic resistance, this approach is useful in deactivating serine-β-lactamases via covalent modification of the active site nucleophilic serine. Examples include clavulanic acid, sulbactam, tazobactam and avibactam.

Unfortunately, this approach is unproductive with NDM-1 as this type of enzyme hydrolyses substrate with a non-covalently zinc-bound hydroxide nucleophile (that is, the nucleophilic hydroxide is not covalently attached) (Yang *et al*., 2012; Wang *et al*.,1998) and as such NDM-1 lacks suitable core catalytic nucleophile for covalent modification. Despite this drawback, reports on covalent inhibition of CphA (B2) and mutant FEZ-1 (B3) by cephalosporins (moxalactam/cefoxitin and cefuroxime respectively) (Figures 1.10 and 1.11), mediated through Cys-substrate disulphide bond formation, are well documented (Mercuri *et al*., 2004; Zervosen *et al*., 2001).

Following the discovery of the significance of Cys and Lys residues, in the covalent inhibition process of Metallo-β-lactamases, several research groups are now exploiting the active site Cys and Lys residues, respectively, in the development of potential NDM-1 covalent inhibitors that can target the Cys208 (e.g ebselen), a ligand of Zn2, and Lys211 respectively (e.g cefaclor, 3-cyanochromone, 3-formylchromone) (González and Vila, 2016; Christopeit *et al*., 2016; Chiou *et al*, 2015; Thomas *et al*., 2014).
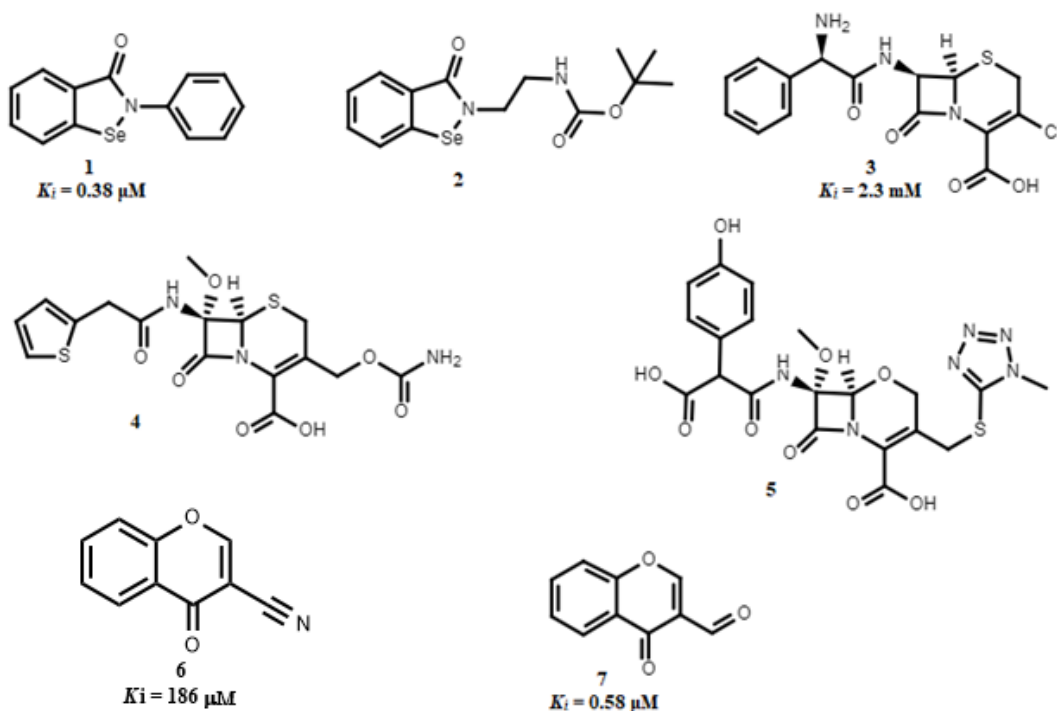
Figure 1.8: NDM-1 Inhibitors resulting in covalent modification of enzyme's active site (González and Vila, 2016; Christopeit *et al*., 2016; Chiou *et al*, 2015; Thomas *et al*., 2014).

1.6.1.1.1 Ebselen and its derivatives

Ebselen (compound **1)** is a selenium-containing drug with several therapeutic potentials such as a neuroprotective effect in cerebral ischemia (Dawson *et al*., 1995; Johshita *et al*., 1990), anti-inflammatory effect (Cheng *et al.,* 2019; Sies and Parnham, 2020), antioxidant property (Sies, 1993; Parnham and Sies, 2013), applicable in the treatment of acute stroke (Saito *et al*., 1998; Yamaguchi *et al*.,1998) as well as in the treatment of hearing loss and Meniere's disease (Kil *et al*., 2017; Kil *et al*., 2022, Lynch and Kil, 2009), a potent inhibitor of the main protease (involved in gene expression and replication the virus) of severe acute respiratory syndrome coronavirus 2 (SARS-CoV-2) and currently in phase II clinical trial for the treatment of Covid-19 patients (Ramli *et al*., 2022). Besides the aforementioned potentials, ebselen also displays antibacterial properties against Gram-positive and Gram-negative bacteria (Thakare *et al*., 2020). Similarly, ebselen functions as a time- and concentration-dependent reversible inhibitor of NDM-1 via covalent modification of the Cys208 thiol group (Chiou *et al*, 2015). ESI-MS analysis revealed that ebselen binds to NDM-1 through the formation of an S-Se bond, resulting in the displacement of Zn2 from the active site and consequently disrupting the Zn coordination with the catalytic amino residues (Figure 1.9) (Chiou *et al*, 2015). A combination of ebselen with ampicillin and meropenem revealed 16 and 128-fold MICs reduction respectively when tested against *E. coli* expressing NDM-1. Ebselen can be a broad-spectrum B1 and B2 inhibitor as Cys residue is well conserved in both subclasses.
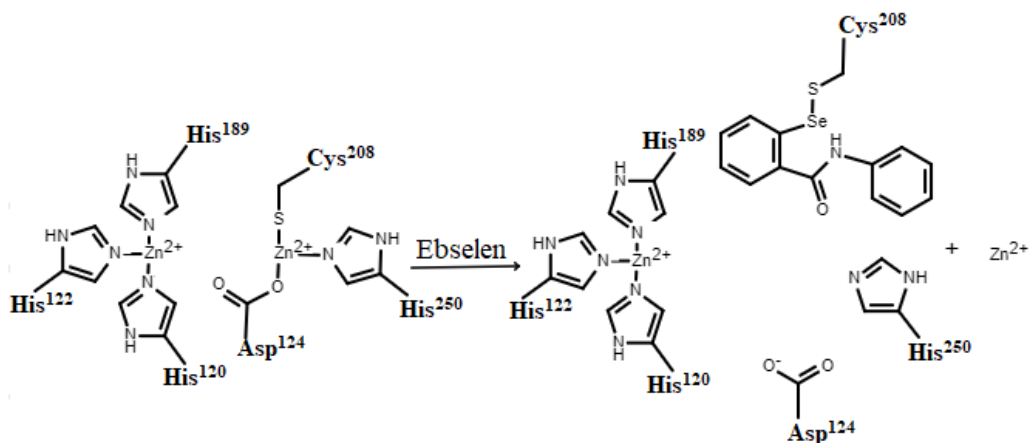
Figure 1.9: Ebselen-NDM-1 Inhibition (Chiou *et al*, 2015).

Despite ebselen's therapeutic potential, there are major drawbacks hindering the development of ebselen as an NDM-1 inhibitor. Besides its antioxidant property which possibly negates its activity with respect to other enzymes *in vivo*, the selenium moiety is a major concern of toxicity.

In light of its remarkable inhibitory and synergistic properties, Jin *et al*., (2018) exploited possible SAR modification of ebselen to enhance its therapeutic potential. This group was able to obtain an analogue, 1, 2-benzisoselenazol-3(2H)-one, (compound **2**) of ebselen with strong synergistic antimicrobial activity with meropenem and low cytotoxicity when tested against *E. coli* expressing NDM-1 and HeLa cell line respectively.

1.6.1.1.2   Cephalosporin scaffold derivatives

The evaluation of cephalosporin scaffold derivatives revealed cefaclor (compound **3**), a derivative of cephalothin obtained via substitution of the methyl thiophene and methyl acetate fragments with benzylamine and chlorine respectively, cefoxitin (compound **4**) and moxalactam (compound **5**) as irreversible inhibitors of MBLs (Thomas *et al*., 2014).

Although moxalactam and cefoxitin are poor substrates of the B2 MBL, CphA, their respective hydrolysed intermediates are reactive species that deactivate the enzyme CphA through the formation of respective covalent adducts as judged by ESMS analysis (Zervosen *et al*., 2001). CphA-induced formation of carbanionic intermediate of moxalactam, emanating from tautomerisation of the dihydrothiazine double bond, facilitates the elimination of the 3' leaving group,1-methyl-5-mercaptotetrazole, which forms a disulphide bond with CphA active site cysteine residue, thus abrogating enzyme activity (Figure 1.10) while cefoxitin inhibits CphA via two potential mechanisms:

➢ The CphA active site cysteine residue can form a disulphide bond with the dihydrothiazine sulphur and abrogate CphA activity (Figure 1.11) and/or

➢ The exo-methylene group of the hydrolysed cefoxitin, which appears after the elimination of the 3' leaving group, can react with a free thiol group. This was established when D-cysteine was incubated with the hydrolysed cefoxitin and HPLC/MS results, following the incubation period, showed that the free thiol group of the D-cysteine reacted with the 3-exomethylene group of the hydrolysed cefoxitin (Figure 1.11).

The findings of Zervosen *et al.*, 2001 entrenched the importance of cephalosporins with a good 3' leaving group in the development of MBLs inhibitors.
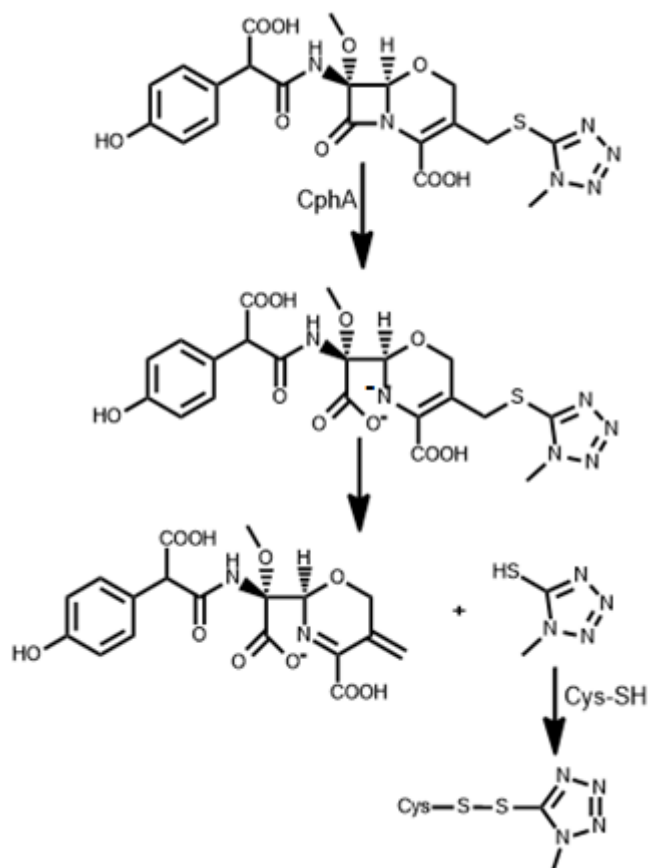
Figure 1.10: Proposed moxalactam-CphA irreversible inhibition pathway (Zervosen *et al.*, 2001).
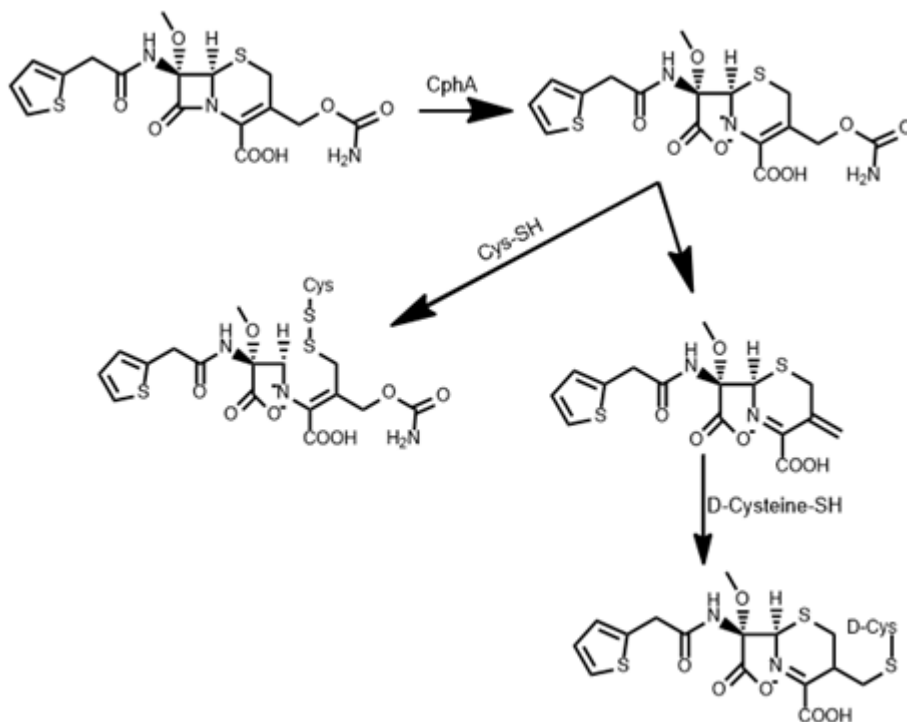
Figure 1.11: Proposed cefoxitin-CphA irreversible inhibition pathway (Zervosen *et al.*, 2001)

Furthermore, while the CphA (B2) inactivation by cefoxitin (compound **4**) and moxalctam (compound **5**) respectively is mediated through the active site Cys residue (Zervosen *et al.*, 2001),

NDM-1 (B1) deactivation by cefaclor (compound **3**) is mediated through multiple pathways, possibly through the Lys211 and Cys208 residues as judged by site-directed mutagenesis (Thomas *et al*., 2014). According to Thomas *et al*. (2014), NDM-1 inactivation by cefaclor is a time- and concentration-dependent inhibition and the potential inhibition mechanism involves the transannular-induced generation of a reactive electrophilic species (episulphonium ion), upon cleavage of the β-lactam ring and loss of the dihydrothiazine chloride ion followed by the incorporation of nucleophilic Lys211 amine group via covalent bond formation (Figure 1.12). This process also yields negatively charged dihydrothiazine sulphur that can form a disulphide bond with the thiol group of the active site Cys residue (Thomas *et al*., 2014; Mercuri *et al*., 2004; Zervosen *et al*., 2001).

Thomas *et al*. (2014) also pointed out that cephalothin and moxalactam respectively, are inactivators of NDM-1 and the inhibition is mediated through the active site Cys residue. Their result further validates the findings of Zervosen *et al*. (2001).

[Figure redacted]

Figure 1.12: Proposed Cefaclor-NDM-1 irreversible deactivation pathway (Thomas *et al*., 2014).

Despite cefaclor's irreversible deactivation potential of NDM-1, it is clinically irrelevant as a high therapeutic dose (≥ 60 higher than therapeutic plasma concentration) is required in the treatment of NDM-1 mediated infections while at a lower concentration, the kinetic analysis showed that cefaclor behaved like a typical substrate. Despite this drawback, the cefaclor-NDM-1 deactivation mechanism has given insight into the development of NDM-1 covalent inhibitors that can target the active site Lys residue.

1.6.1.1.3   3-Cyanochromone and 3-Formylchromone

Consequent to the discovery of the role of Lys residue in the inhibition of NDM-1, Christopeit and Leiros, (2016) discovered 3-cyanochromone (compound **6**) and its aldehyde derivative, 3-formylchromone (compound **7**) with enhanced affinity (Christopeit *et al*., 2016), as potential NDM-1 covalent/competitive reversible inhibitors with the ability to modify the active site Lys residue as revealed by ESI-MS analysis, SPR (surface plasmon resonance) based biosensor assay, kinetic study and site-directed mutagenesis. Molecular docking revealed compound **6** probably coordinates with Zn2, via its carbonyl group, and interacts with the amine group (side chain) of active site Lys residue via its nitrile group while compound

7 is assumed to display similar interaction with its aldehyde interacting with the side chain amine group of Lys residue (Figure 1.13).

[Figure redacted]

Figure 1.13: Proposed 3-Formylchromone-NDM-1 reversible inhibition pathway (Christopeit and Leiros, 2016).

1.6.2   Zinc-dependent inhibitors

A unique characteristic of the MBL family (B1-3) is the conservation of zinc (II) ion(s), which plays an essential role in the catalytic activity of MBLs. The exploitation of this advantage by developing inhibitors with remarkable affinity for the active site zinc (II) ions may lead to the discovery of broad-spectrum MBLs inhibitor(s). This class of compounds may initiate their activity by either

➢ binding to the active site zinc ions, via displacement of the nucleophile, thus forming a complex in the active site or

➢ binding and removing essential zinc ion(s) from the active site

1.6.2.1 Zinc coordinating inhibitors (ternary complex formation)

Zinc binding inhibitors function by interacting with both active site zinc (II) ions, displacing the nucleophilic bridging hydroxide, as well as interacting with essential active site amino residues. This class of inhibitors contains functional group(s) with atoms (sulphur, nitrogen and oxygen) that have a high affinity for metal ions. They have three key advantages essential for the deactivation of NDM-1

1) They are zinc-binding
2) They can interact with active site amino residues
3) They can displace the nucleophilic bridging hydroxide

1.6.2.1.1   Thiol compounds

Most thiol compounds function as zinc coordinating inhibitors as their thiol group can oust the nucleophilic hydroxide with concurrent intercalation of the deprotonated thiol (sulphur) group between Zn1 and Zn2 while the other fragment(s) of the molecule interacts with essential active site residues, thus stabilizing the inhibitor-enzyme complex. With several reports validating the catalytic importance of the nucleophilic hydroxide, displacing the hydroxide may induce inhibition while the residue-binding property of the inhibitor would likely enhance selectivity and potency.
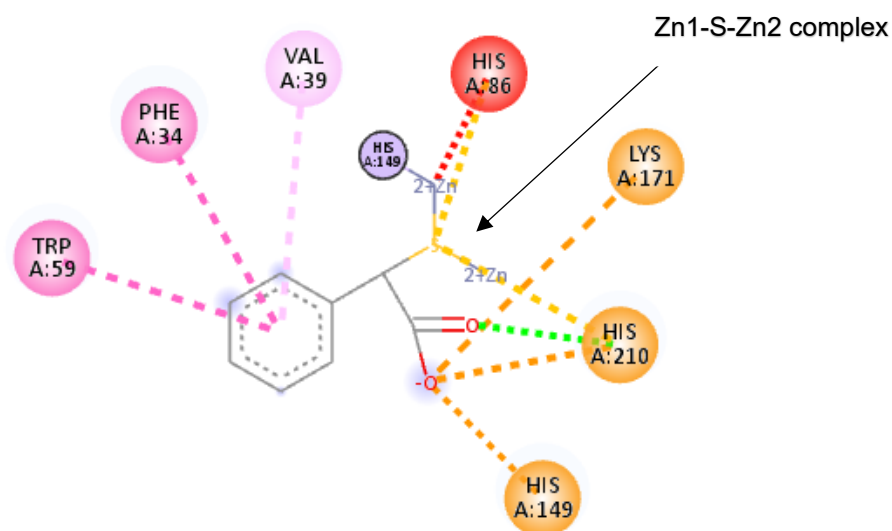
Figure 1.14: R-Thiomandelic acid – BcII complex (Karsisiotis *et al*., 2013).

The discovery of thiomandelic acid (compound **8**) as the first broad-spectrum inhibitor (B1 and B3), before the emergence of NDM-1, revealed that its inhibitory activity is a function of the deprotonated thiol group intercalating both zinc (II) ions, irrespective of the stereochemistry of the inhibitor, while the carboxylate enhances potency through interaction with the histidine residues (Figure 1.14) (Mollard *et al*., 2001). In light of the role of the thiol group in MBLs inhibition, a survey on the importance of approved thiol-based drugs as suitable MBLs inhibitors revealed only D/L-captopril (D = **9**; L = **10**), D/L-thiophan (compound **11**), 2,3-dimercaprol (compound **12**) and tiopronin (compound **13**) (Figure 1.15) exhibited, low to high micromolar, inhibitory activity towards NDM-1, via direct binding of the deprotonated thiol group to Zn1 and Zn2, despite the eleven tested compounds possessing a thiol group (Klingler *et al*., 2015). The lack of inhibitory activity of the other compounds may be due to no/poor binding to the NDM-1 active site. The synergetic activity of these compounds revealed a reduction in MIC (minimum inhibitory concentration) of imipenem when tested against respective *E. coli* and *K. pneumoniae* expressing NDM-1.
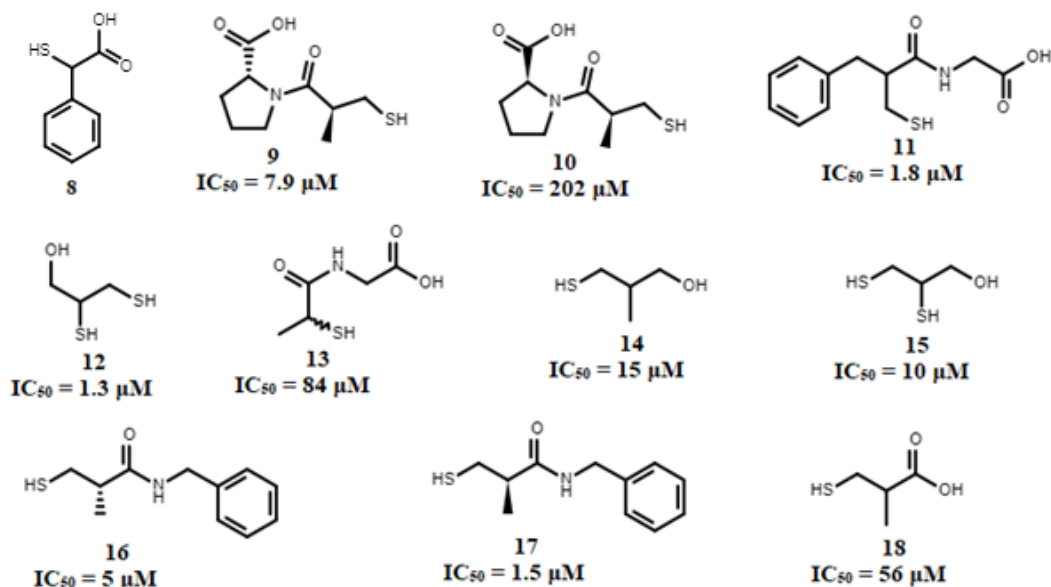
Figure 1.15: Thiol compounds – NDM-1 Inhibitors resulting in ternary formation complex in the enzyme's active site (Mollard *et al.*, 2001; Klingler *et al.*, 2015; Guo *et al.*, 2011; Li *et al.*, 2014).

In light of the inhibitory property of captopril, an X-ray study was conducted to determine the binding mode of L-captopril and the result revealed that L-captopril (compound **10**) displays a similar sulphur-mediated nucleophile displacement mechanism (Figure 1.16 B), as observed in thiomandelic acid-B1 enzyme inhibition, with the hydrophobic and hydrophilic (carboxyl group) moieties, of L-captopril, interacting with NDM-1 loop3 (substrate-binding recognition) hydrophobic residues (Val73 and Met67) and loop10 hydrophilic residues (Asn220, hydrogen bonding N220) respectively (King *et al.*, 2012).

The discovery that captopril diastereomers display inhibitory activity towards NDM-1 at different rates, with D-captopril (compound **9**) (7.9 µM) more active than L-captopril (202 µM) (Guo *et al.*, 2011), gave an insight on the relationship between stereoisomerism and NDM-1 inhibition and as such the importance of stereochemistry in the development of NDM-1 inhibitors.

The revelation of the binding mode of L-captopril enabled the evaluation of how stereoisomerism affects the binding mode of D- and L-captopril respectively. The crystal structure of NDM-1 bound L-captopril (King *et al.*, 2012) was overlaid with the crystal structure of BlaB (have similar active site arrangement and Zn coordination geometries but low amino acid residue sequence identity with NDM-1) bound D-captopril (García-Sáez *et al.*, 2003). The superimposition of these crystal structures showed that the two diastereomers bind oppositely but insert their deprotonated thiol moiety (S) between Zn1 and Zn2 in the same manner (Figure 1.16 C and D). Based on the similarity of the active sites of NDM-1 and BlaB, D-captopril may likely adopt the same BlaB-type orientation in the NDM-1 active site. Such orientation might facilitate more productive interactions between the proline moiety as well as the amide and methyl group of the aliphatic fragment of D-captopril with the amino residues of the NDM-1 active site, thus enhancing the potency of D-captopril over L-captopril.
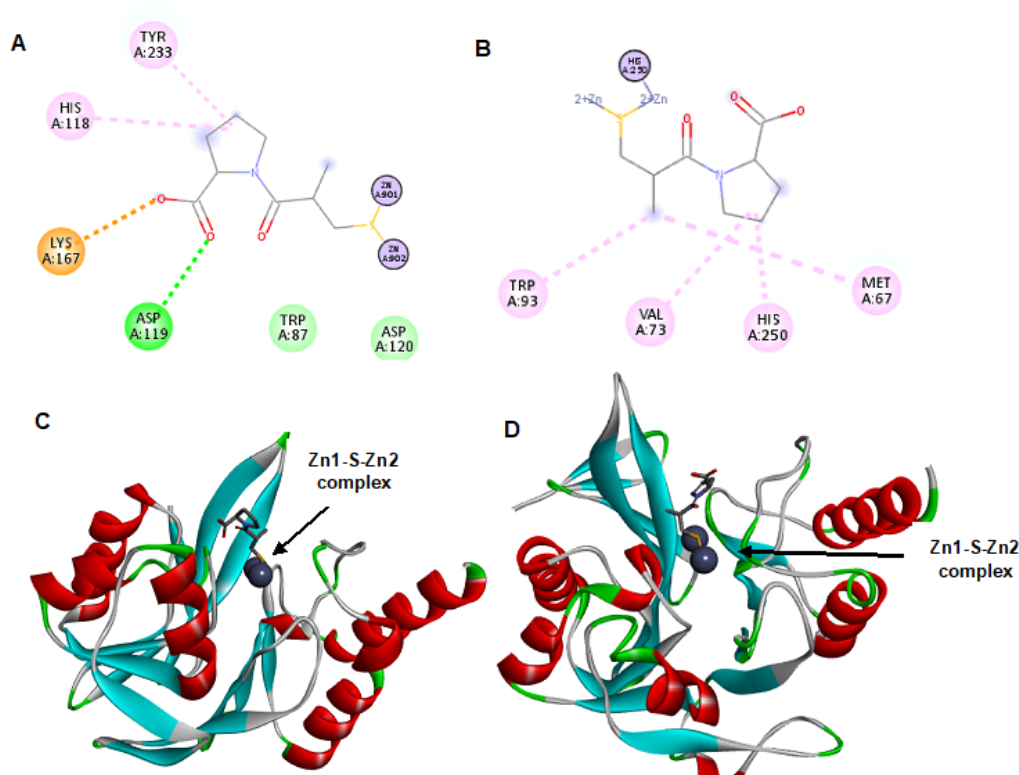
Figure 1.16: A and C = BlaB-D-Captopril complex; B and D = NDM-1-L-captopril complex (King *et al*., 2012).

Consequent to the inhibitory potential of captopril, several SAR studies of captopril were undertaken by Li *et al*. (2014), Skagseth *et al*. (2017) and Buttner *et al.* (2018) and their respective results revealed the following:

➢ The 3-mercapto-2-methylpropanoyl moiety is the pharmacophore of captopril and free thiol and carboxyl/hydroxyl groups were essential for biological activity (compounds **14** and **15**) (Li *et al*., 2014). Esterification of the carboxyl group of 3-mercapto-2-methylpropanoic acid resulted in the loss of biological activity despite the presence of the free thiol group (Li *et al*., 2014), thus supporting the findings of King *et al*. (2012) – the free carboxyl group is essential for substrate binding. It is important to highlight that compounds **12** and **15** are the same, possibly a racemic mixture, but when assayed against NDM-1 in two different studies by Klingler *et al*., 2015 and Li *et al*., 2014 respectively, the IC_{50} values were different (Figure 1.15).

➢ The substitution of the proline ring with benzylamine enhanced potency (compounds **16** and **17**) (Li *et al*., 2014), possibly due to the aromatic interaction of the substrate with the enzyme's many aromatic residues.

➢ The mercaptophosphonic and mercaptotetrazole scaffolds (compounds **20 - 22**) are better substitutes for the 3-mercapto-2-methylpropanoic scaffold (compounds **18** and **19**) while aryl groups are better substitutes (compounds **19 - 23**) for the methyl group in 3-mercapto-2-methylpropanoyl (Figure 1.17) (Skagseth *et al*., 2017; Buttner *et al*., 2018).
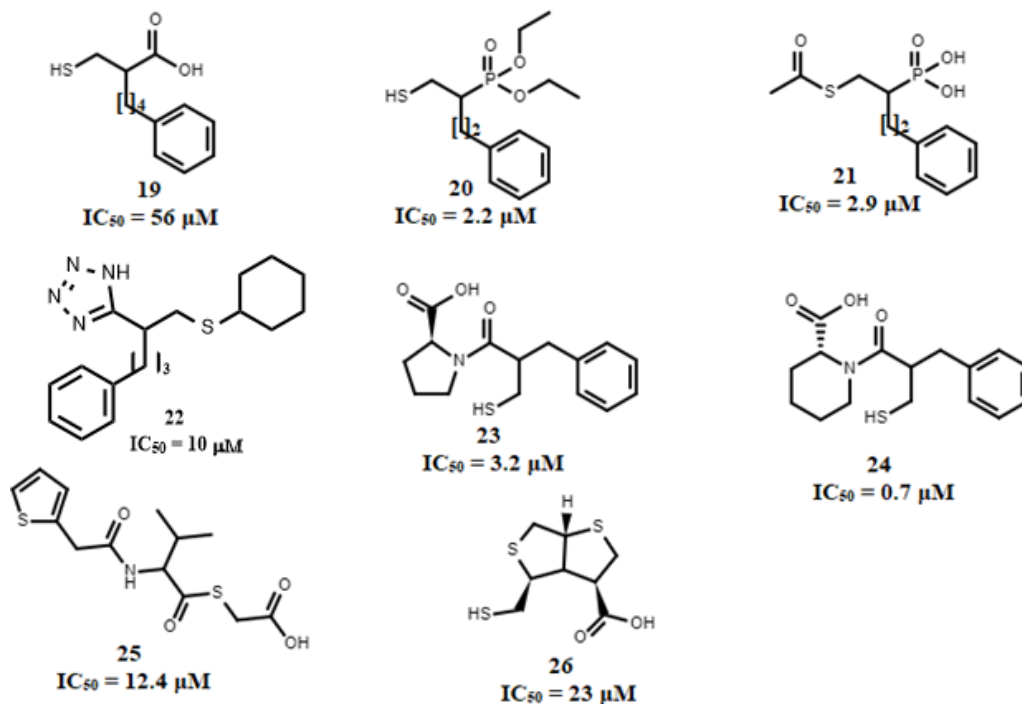
Figure 1.17: Thiol compounds – NDM-1 Inhibitors resulting in ternary formation complex in the enzyme's active site (Skagseth *et al*., 2017; Buttner *et al*., 2018).

➤ The esterification of the phosphonic acid (compound **20**) improved the potency, in the presence of a free thiol group, contrary to the findings of Li *et al*. (2014) (when a carboxyl group was used) (Skagseth *et al*., 2017).

➤ The acetylation of the thiol group in the presence of free phosphonic acid (compound **21**) gave an IC_{50} value similar to compound **20** (Skagseth *et al*., 2017). This may be due to the presence of two free hydroxyl groups. Despite the inhibitory potential of compounds **20** and **21**, no synergetic effect was observed when combined with meropenem against *K. pneumoniae* expressing NDM-1

➤ The simultaneous esterification and acetylation of the phosphonic acid and thiol groups respectively resulted in the loss of biological activity (Skagseth *et al*., 2017).

➤ The substitution of the captopril proline ring of compound **23** with an S-pipecolic acid slightly decreased the potency (Buttner *et al*., 2018). However, the potency significantly improved when the proline ring was substituted with R-pipecolic acid (compound **24**) (Buttner *et al*., 2018). This further validates the importance of stereoisomerism in the development of NDM-1 inhibitors. Compounds **23** and **24** showed good synergetic effects with imipenem against *E. coli* and *K. pneumoniae* isolates producing NDM-1.

Similarly, the mercaptoacetic acid thiol ester (compound **25**) has been reported as a low double-digit micromolar NDM-1 inhibitor, in synergy with cefazolin, when tested against *E. coli*-producing NDM-1 (Liu *et al*., 2015).

Due to the significance of the thiol and carboxylate groups in the inhibition of NDM-1 as evidenced by several studies, Gonzalez and co-workers (2015) exploited these features in synthesising two novel bisthiazolidines with their respective enantiomers as potential NDM-1 inhibitors. Their study revealed that the most potent, double-digit micromolar, inhibitor (compound **26**) does not possess antibacterial properties but it inhibits imipenem hydrolysis in the presence of *E. coli* cells expressing NDM-1 as well

as restores the activity of imipenem against clinical isolates of *Klebsiella pneumoniae*, *Acinetobacter baumannii*, and *Providencia rettgeri* expressing NDM-1. Meanwhile, the IC$_{50}$ of the enantiomer of compound **26** is about 5-fold higher than compound **26**. This observed difference once more consolidates the relationship between stereoisomerism and NDM-1 inhibition.

Compound **26** acts as thiol mediated-competitive inhibitor like L-captopril, with its free carboxylate interacting with the active site Lys residue via water molecules and it lacks cytotoxicity against the human metalloenzyme, glyoxalase II, as well as the cultured human mammalian cells (HeLa and Hek 293) at the inhibitory concentration (23 μM).

1.6.2.1.2 Cyclic and acyclic boronates (transition state analogues)

The formation of the tetrahedral intermediate during SBL and MBL hydrolysis of β-lactam antibiotics is well documented in several scientific articles. Scientists are currently exploiting this characteristic in the development of dual-action SBL/MBL inhibitors through the design and synthesis of analogues that mimic these transition tetrahedral intermediates (Figure 1.18). The discovery and approval of the first-generation monocyclic boronate, vaborbactam (compound **27**), established the basis for transition state analogue research. Vaborbactam (**27**) was discovered as a potent SBL inhibitor (Hecker *et al*., 2015) but a poor inactivator of NDM-1 (Langley *et al*., 2019). However, progress has been made since the discovery of vaborbactam as evidenced by recent articles that have revealed the bicyclic boronates, compounds **28, 29, 30** and **31**, (Figure 1.19) as dual-action (SBL/MBL) transition state analogues with remarkable potency against NDM-1 (Liu *et al*., 2019; Krajnc *et al*., 2019; Brem *et al*., 2016).

[Figure redacted]

Figure 1.18: Cyclic/bicyclic boronate-MBL/SBL inhibition mechanism (Langley *et al*., 2019; Liu *et al*., 2019).

27
IC$_{50}$ = 631 μM

28
IC$_{50}$ = 0.029 μM

29
IC$_{50}$ = 0.04 μM

30
IC$_{50}$ = 0.004 μM

31
IC$_{50}$ = 0.01 μM

32
K_i = 0.032

33
IC$_{50}$ = 32.47 μM

34
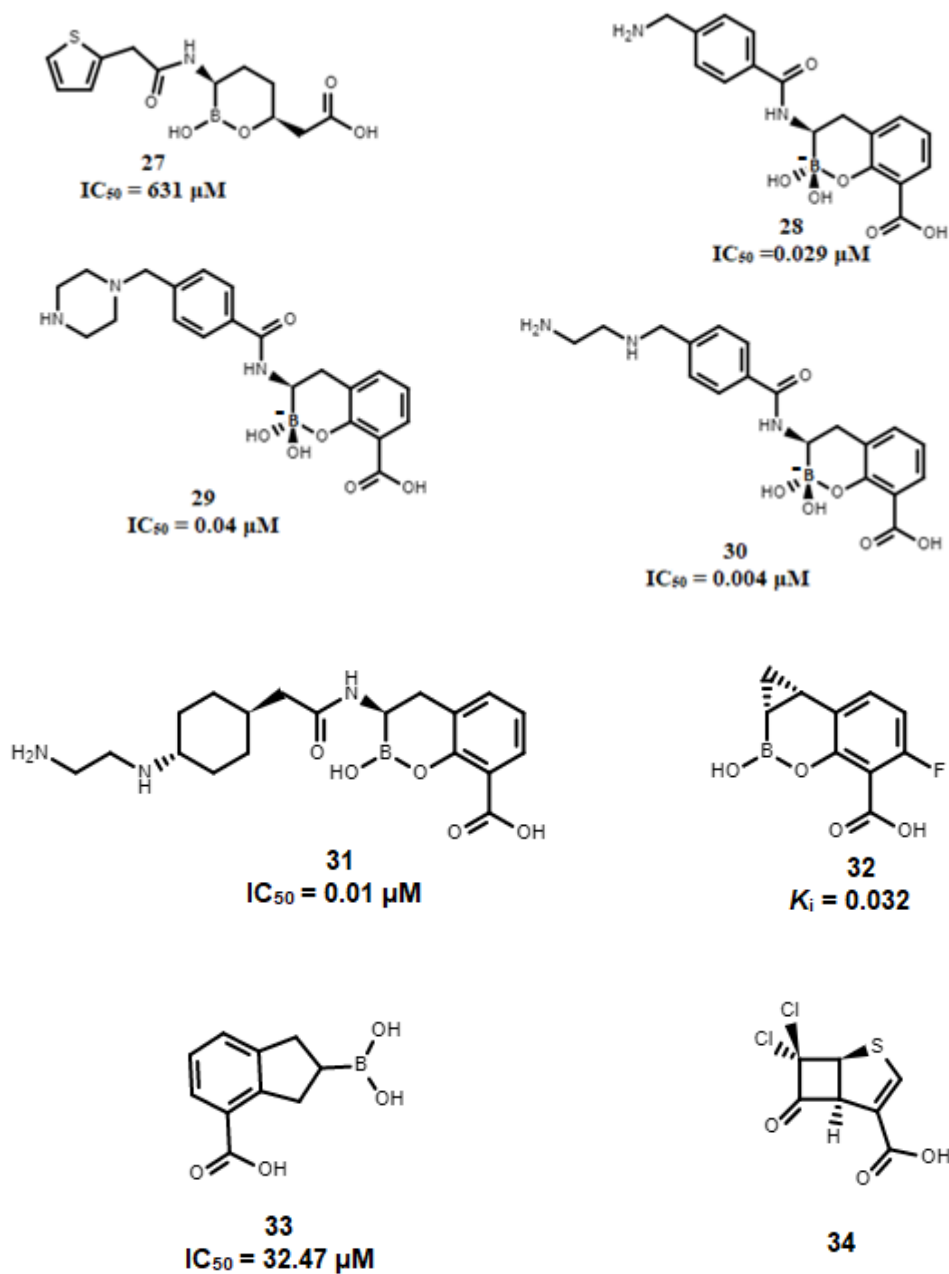
Figure 1.19: Transition State Analogues (Cyclic and Acyclic Boronates) (Liu *et al.*, 2019; Krajnc *et al.*, 2019; Brem *et al.*, 2016; Santucci *et al.*, 2017; Hecker *et al.*, 2020).
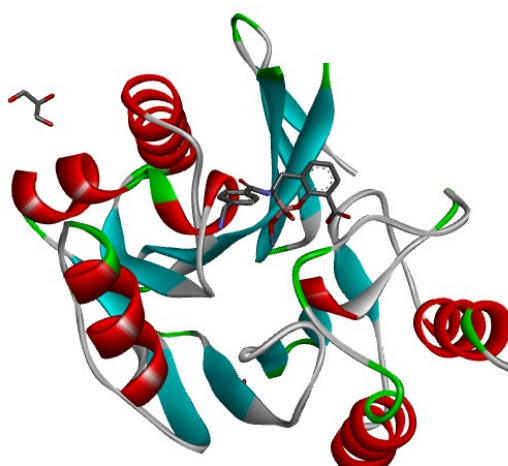
Figure 1.20: 28-BcII Complex, a mimic of the tetrahedral intermediate structure of NDM-1 hydrolysed β-lactam (Brem *et al.*, 2016).

The crystal structures of the **28**-BcII complex and **31**-NDM-1 complex respectively showed that the boron is sp^3 (tetrahedral) and the respective crystal structure resembles the tetrahedral intermediate of NDM-1 hydrolysed β-lactam (Figure 1.18) as evidence by some similar key features:

➤ The hydroxyl oxygen of the C-3 carboxylate (**28**-BcII complex) coordinates with the Zn2 while the carbonyl oxygen atom of the same C-3 carboxylate interacts with the active site Lys residue via electrostatic interaction (Brem *et al*., 2016). These interactions are analogous to those observed in hydrolysed penicillin/cephalosporin where the C-3 carboxylate of penicillin or C-4 carboxylate of cephalosporin binds Zn2 and active site Lys residue respectively (Figure 1.5 C and 6 C) (Meini *et al*., 2015; Feng *et al*., 2014).

➤ **28** is a bicyclic compound that is similar to the bicyclic β-lactams, especially cephalosporin which possesses the dihydrothiazine ring (Feng *et al*., 2014) that is similarly positioned to the phenyl-boronate ring of **28** in the active site and as such they are prone to hydrophobic interactions with the aromatic amino residues, Trp and Phe, in the active site (Brem *et al*., 2016). Also, the coordination of the endocyclic boronate oxygen with Zn2 resembles the coordination of the Zn2 with dihydrothiazine ring nitrogen of the carbanion intermediate (Figure 1.6 D) (Brem *et al*., 2016).

➤ Compound **28** and cephalosporin possess acetamido groups that are similarly positioned in the enzyme active site and as such, they are prone to hydrogen bonding with Ala residue (BcII) or Glu residue (NDM-1) in the enzyme active site (Brem *et al*., 2016).

➤ The coordination and hydrogen bonding of the carboxylate of **28** to Zn1 and Ans236 residue respectively in the 28-BcII complex mimics the interactions of the newly formed carboxylate, of cephalosporin intermediate, with Zn1 and Asn220 (Brem *et al*., 2016).

➤ In addition to the above features, the compound **31**-NDM-1 crystal structure showed that both active site zinc (II) ions are linked together by the boron-bound oxygen. Also, a tricyclic derivative of **31** is unexpectedly generated, at the active site, possibly through cyclization of the acylamino side-chain carbonyl group with the boron atom with resultant loss of water/hydroxide (Figure 1.21) (Krajnc *et al*., 2019).

[Figure redacted]

Figure 1.21: Generation of a tricyclic derivative of **31** in NDM-1 active site (Krajnc *et al*., 2019).

Compound **28** lacks antibacterial activity, and cytotoxicity against human HEK 293 cells at the inhibitory concentration, but synergistically (at 10 μg/mL and 25 μg/mL), it significantly reduces the MIC of meropenem (≤ 32 μg/mL) when tested against recombinant and clinical isolates of *K. pneumoniae* expressing NDM-1 and SBL of different classes (Brem *et al*., 2016) while **31,** at 10 μg/mL, synergistically reduces the MICs of fourth-generation cephalosporin (cefepime; ≤ 16 μg/mL) and carbapenem (meropenem; ≤ 1 μg/mL) respectively when tested against clinical isolates of *E. coli and K. pneumoniae* producing NDM-1 (Krajnc *et al*., 2019).

In addition, the exploitation of the bicyclic boronate scaffold in the ongoing innovation of this class of inhibitor recently lead to the discovery of QPX7728 (compound **32**), a compound that is currently in the preclinical stage of drug development. Compound **32** was discovered, by Hecker and co-workers (2020), as a potent broad-spectrum dual-action (SBL/MBL) inhibitor that is insignificantly affected by fluctuations in porin proteins and efflux pumps (Hecker *et al*., 2020). The binding mode of compound **32** to NDM-1 is similar to the **28**-BcII complex with the carboxylate coordinating and interacting with Zn2 and Lys211 as well Asn220 respectively while the endocyclic boronate oxygen coordinates Zn2 in the same fashion (Hecker *et al*., 2020). Compound **32** is a weak antibacterial agent but in synergy (8 μg/mL) with cefepime and meropenem respectively, it significantly reduces the respective MICs by over 60-fold in *Enterobacterales* expressing NDM-1. Also, computational and biological profiling of the acyclic boronic acid, **33**, revealed compound **33** as a weak NDM-1 inhibitor with a potential binding mode involving the boronic group coordinating with Zn1 and Zn2 while the carboxyl group interacts with Lys211 (Santucci *et al*., 2017).

[Figure redacted]

Figure 1.22: Behaviour of compound **34** in D$_2$O solution (Abboud *et al*., 2018).

[Figure redacted]

Figure 1.23: Binding mode of hydrolytically stable **34** to IMP-1 (Abboud *et al*., 2018).

Furthermore, other derivatives besides boronates are being exploited as potential transition state analogues. In 2018, Abboud *et al*., in search for broad-spectrum SBL/MBL inhibitors, discovered the cyclobutanone derivative, compound **34**, as a potential transition state analogue that mimics the tetrahedral intermediate formed during SBL/MBL hydrolysis of β-lactams. Compound **34** is an analogue of both penems and penams that is hydrolytically stable to IMP-1 possibly due to the substitution of the amide nitrogen with a carbon molecule (Figure 1.23). Under the conditions of the crystal/binding studies, compound **34** favourably exists in the hydrated form (Figure 1.22) as evidenced by ^{13}C NMR analysis, where the peak corresponding to the carbonyl carbon (around 190 ppm) of the ketone form was absent whereas a peak corresponding to the carbon bearing the di-D$_2$O was observed at lower ppm (102 ppm). Considering the characteristics of compound **34** in solution, it is likely that **34** binds to the enzyme, IMP-1, in its hydrated form and this was confirmed by the ^{13}C NMR analysis of the **34**-IMP-1 mixture, where the chemical shift of the carbon-bearing the di-D$_2$O remained unchanged while there was no peak corresponding to the carbonyl carbon of compound **34** (ketone form). The crystal study showed that the formed tetrahedral specie in the **34**-IMP-1 complex is similar to the NDM-1/penam or NDM-1/penem tetrahedral intermediates with respect to the carboxylate and dichlorocyclobutanone ring interactions with the IMP-1 active site residues/moiety (Abboud *et al*., 2018). Although their finding is preliminary, the concept is reasonable and merits further investigation in the development of dual-action (SBL/MBL) transition state analogues.

1.6.2.1.3   Dicarboxylic acid derivatives

In light of the importance of dicarboxylic acid derivatives as good zinc coordinating inhibitors against IMP-1, with the two carboxyl groups interacting with both zinc ions via displacement of the bridging hydroxide and the apical water molecule (Olsen *et al.*, 2006; Moloughney *et al.*, 2005; Toney *et al.*, 2001), Chen *et al.* (2017) exploited the metal-binding pharmacophore that targets both zinc ions in a search for compound(s) that preferentially interact with the essential residues surrounding the zinc (II) ions. This group discovered the novel compound (**35**) (Figure 1.24), among other derivatives, with remarkable selective inhibitory properties against B1 enzymes (NDM-1, VIM-2 and IMP-1), via SAR modification of the metal-chelating 2,6-dipicolinic acid (**36**).

35
IC_{50} = 80 nM

36
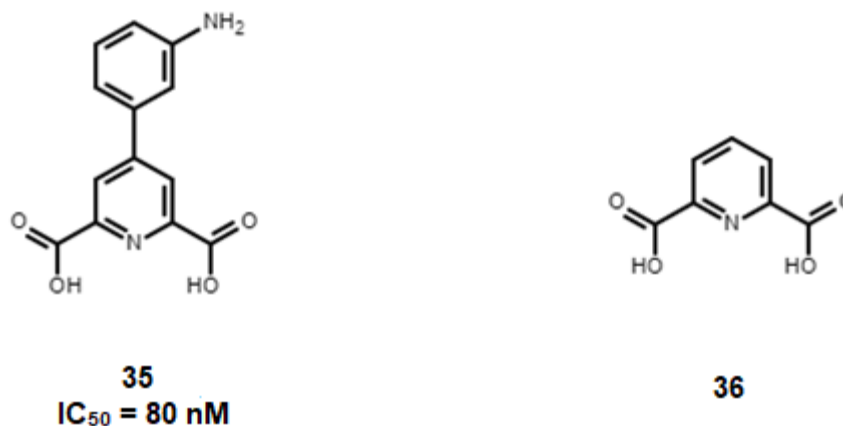
Figure 1.24: Dicarboxylic acid derivative (Chen *et al.*, 2017).

Molecular modelling analysis showed that **35** may form a stable complex with NDM-1 via interactions with His189, Cys208, Lys211, Met 248, Ser249, His250 and Ser251 residues with its aniline group as the most potent inhibitory fragment due to its strong interaction with Lys211, which initiates the formation of four strong stable bonds between **35** and His189, Ser249, His250 and Ser251 (Niu *et al.*, 2019). Initial proton NMR spectroscopy, electron paramagnetic resonance (EPR) spectroscopy and intrinsic tryptophan fluorescence quenching studies revealed **35**, at low inhibitory concentration, as Zn1/Zn2 coordinating inhibitor forming ternary complex (NDM-1/Zn(II)/**35**) similar to NDM-1/Zn(II)/L-captopril complex while at higher concentration, it behaves as a typical metal ion stripping inhibitor, just like compound **36** (Chen *et al.*, 2017). **35** showed no toxicity (at ≤10 μM) against mammalian cells and it lacks antibacterial activity but in synergy with imipenem reduces its MIC values in clinical isolates of *E. coli* and *K. pneumoniae* producing NDM-1.

1.6.2.1.4   Other Compounds with zinc coordinating characteristics

Scientific research on antibiotics as well as MBL inhibitors has been wide-ranging but the discovery of a new class of compounds/inhibitors has been limited. However, the research community is exploiting other scaffold derivatives with zinc-coordinating properties as potential NDM-1 inhibitors.

Drug repurposing studies by Song *et al.* (2018) identified methisazone, a drug molecule used for the treatment of smallpox infection, as a weak NDM-1 inhibitor. Considering the NDM-1 inhibitory property of methisazon, Song *et al.* (2018) synthesised several methisazone derivatives and *in vitro* tests showed all the derivatives displayed a low micromolar range inhibitory activity against NDM-1 with

compound **37** being the most potent. Molecular docking prediction showed that **37** likely elicits its inhibitory effect through hydrogen bond formation, with Gly69 and His189, and hydrophobic interactions with many residues (Thr34, Val73, Trp93, Gly219, Asn220 and Gly222) with the sulphur atom coordinating both zinc ions (Bauer, 1965; Song *et al.*, 2018).

37
IC_{50} = 2.72 µM

38
K_i = 0.43

39
IC_{50} = 0.16 µM

40
IC_{50} = 0.17 µM
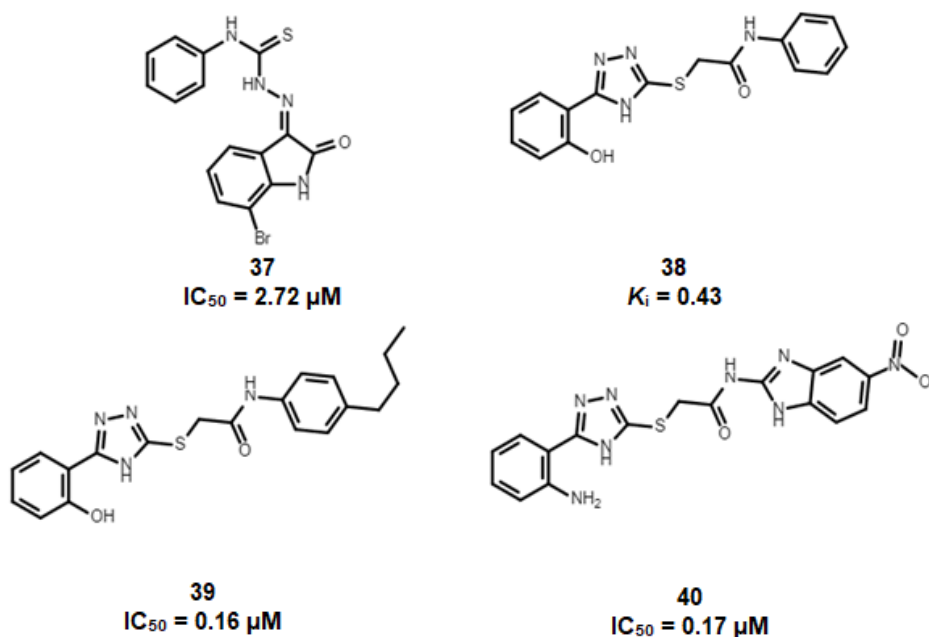
Figure 1.25: Methisazone and Mercapto-azole derivatives (Song *et al.*, 2018; Zhang *et al.*, 2014; Zhai *et al.*, 2016; Xiang *et al.*, 2017).

Similarly, azolylthioacetamide was discovered as a promising scaffold in the development of MBL inhibitors. In 2014, Zhang *et al.*, synthesised eighteen diaryl-substituted-azolylthioacetamide derivatives, compound **38** inclusive, and an enzyme assay revealed most of these derivatives are potent NDM-1 inhibitors, with K_i value range of 0.35 – 6.8 µM, while few of the derivatives displayed broad-spectrum activity against the three subclasses of MBLs (ImiS and L1) (Zhang *et al.*, 2014). Molecular docking prediction suggested that compound **38** interacts with NDM-1 active site through the deprotonated triazole bridging the two zinc (II) ions with the 2-phenol and the amide carbonyl groups interacting with Lys211 and Gln123 respectively (Zhang *et al.*, 2014). In furtherance of the diaryl-substituted-azolylthioacetamide studies, Zhai *et al.* (2016) synthesised and evaluated twenty-four triazolylthioacetamide derivatives, compound **39** inclusive, and their findings showed that these derivatives as potent narrow-spectrum NDM-1 inhibitors with an IC_{50} value range of 0.15 −1.90 µM (Zhai *et al.*, 2016). Compound **39** displayed low micromolar inhibitory activity against NDM-1 and the substitution of the 2-phenol group with an amine group did not alter the IC_{50} value. Expectedly, the molecular docking prediction of **39** with NDM-1 indicates that the binding interaction is similar to the observed interactions in the **38**-NDM-1 complex (Zhai *et al.*, 2016). Considering the positive outcome from earlier studies, Xiang *et al.* (2017) conducted SAR studies on the azolylthioacetamide derivatives and synthesised twenty-eight analogues, compound **40** inclusive (Xiang *et al.*, 2017). These analogues were assayed against MBLs and the result showed that about 68 per cent of the compounds were active specifically against ImiS while the remaining 32 per cent specifically inactivate NDM-1 (Xiang *et al.*, 2017).

Contrary to the observed molecular interactions enumerated in previous studies, the triazole ring does not interact with the zinc (II) ions, rather the nitro group of compound **40** intercalates Zn1 and Zn2 (Zhang *et al*., 2014; Zhai *et al*., 2016; Xiang *et al*., 2017). Also, the substitution of the amine group of **40** with a hydroxyl group increased the IC$_{50}$ value contrary to the behaviour of compound **39** (Zhai *et al*., 2016; Xiang *et al*., 2017).

1.6.2.2 Zinc chelating/stripping inhibitors

Several studies have identified NDM-1 as a zinc-dependent enzyme, therefore sequestering or removal of the zinc ion(s) will alter the structural composition of the active site which will in turn deactivate the enzyme. This metal ion stripping mechanism is the oldest model for zinc-dependent enzyme inhibition as Sabath and Abraham (1966) first identified the relationship between zinc (II) ion removal, using ethylenediamine tetraacetic acid (EDTA) (compound **41**) and 1, 10-phenanthroline (**42**) respectively, and abrogation of MBL's enzymatic activity.

Recently, the S, S, S stereoisomer of the natural compound, aspergillomarasmine A (AMA, irreversible inhibitor) (compound **43**), was discovered to be active against *E. coli* producing NDM-1 via masking of the active site zinc ions, without removing them from the catalytic pocket and SAR studies validate the carboxyl groups are essential for biological activity (Bergstrom *et al*., 2017; Liao *et al*., 2016; Zhang *et al*., 2017; King *et al*., 2014). AMA showed synergistic activity with meropenem in *Enterobacteriaceae* producing NDM-1 (Paul-soto *et al*., 1999).

Also, the inhibitory activity of other chelating compounds, such as EDTA-Ca(II), 1,4,7-triazacyclononane-1,4,7-triacetic acid (NOTA) (compound **44**), 1,4,7,10-tetraazacyclododecane-1,4,7,10-tetraacetic acid (DOTA) (compound **45**), N, N, N′, N′-tetrakis(2-pyridylmethyl)ethylenediamine (TPEN) (compound **46)** and tris(2-pyridylmethyl)amine (TPA) (compound **47**) (Figure 1.26) revealed intriguing characteristics and they are synergistically active, with carbapenems, against several resistant bacterial strains (Yoshizumi *et al*., 2013; Somboro *et al*., 2015; Azumah *et al*., 2016; Schnaars *et al*., 2018).
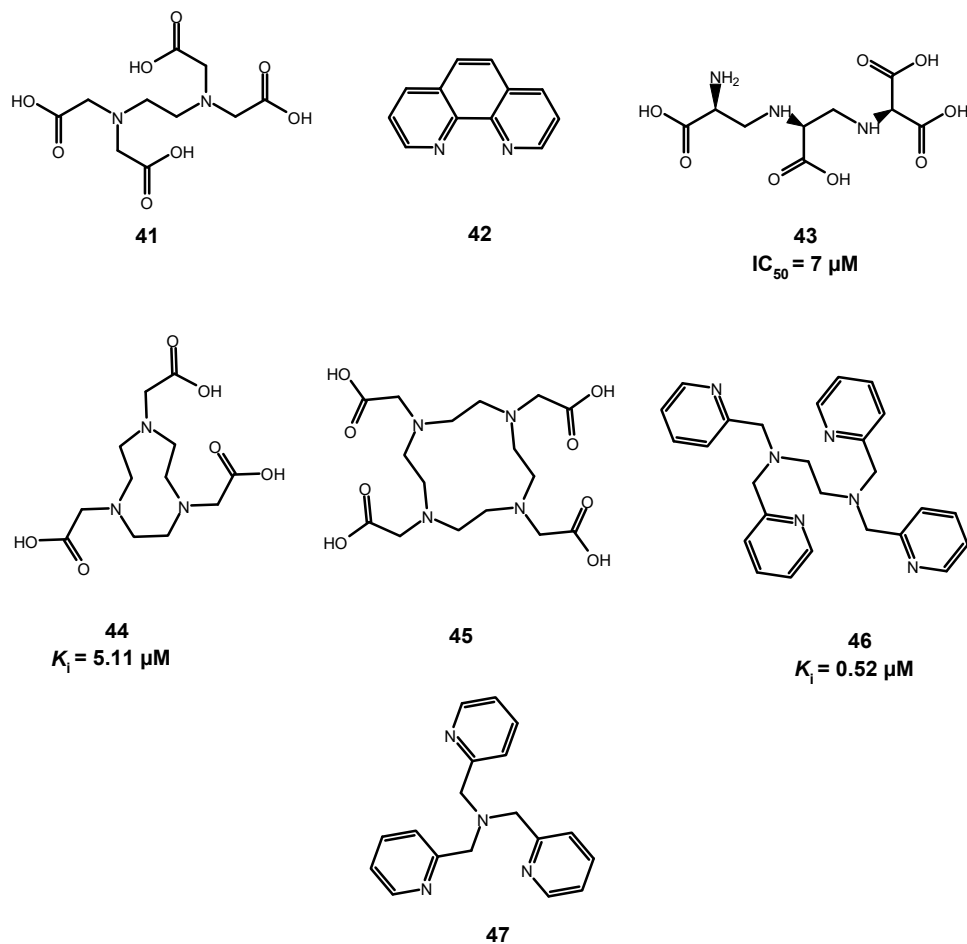
Figure 1.26: Metal chelators - NDM-1 inhibitors resulting in active site's Zn(II) ion expulsion/sequestration (Sabath and Abraham, 1966; Paul-soto *et al*., 1999; Yoshizumi *et al*., 2013; Somboro *et al*., 2015; Azumah *et al*., 2016; Schnaars *et al*., 2018).

These chelators function by removing/sequestering Zn(II) ions and forming stable chelates. Compound **43** (EDTA) and compound **46** (TPEN) inactivate NDM-1 by forming stable octahedral chelates with zinc ions via coordination of carboxyl groups and amide nitrogen and pyridyl groups and amine nitrogen respectively while compound **47** (TPA) functions by forming a stable chelate with lower Zn (II) ion coordination number (Zhu *et al*., 2014).

Despite the extensive research for clinically important NDM-1 inhibitors, none of the aforementioned compounds has been approved, by the FDA, as an NDM-1 inhibitor. However, one of the transition state analogues, tarniborbactam (compound **31**), may be approved by the FDA, as cefepime-tarniborbactam, in the coming months/years should its clinical studies continue to generate positive results.

1.7 Designed compound and proposed inhibitory mechanism

In light of obvious public health challenges, the absence of clinically significant NDM-1 inhibitors and the need to prevent a possible NDM-1 infection pandemic, it is essential to develop novel NDM-1 inhibitor(s) of clinical importance. Recently, a series of mechanism-based NDM-1 inhibitors was developed (*in silico*) by Eshtiwi, A. (2020). The potential inhibition mechanism involves NDM-1-induced activation of compound **48**, resulting in the generation of two reactive species, ketene and thiolate, in

the active site (Figure 1.27). The reactive ketene would react, via its carbonyl group, with the side chain amine group of Lys211 (3-formylchromone-NDM-1 deactivation mechanism) while the reactive thiolate would form a disulphide bond with the thiol group of Cys208 (cefaclor-NDM-1 deactivation mechanism) and/or displace the hydroxide nucleophile and intercalate Zn1 and Zn2 (captopril-NDM-1 deactivation mechanism).
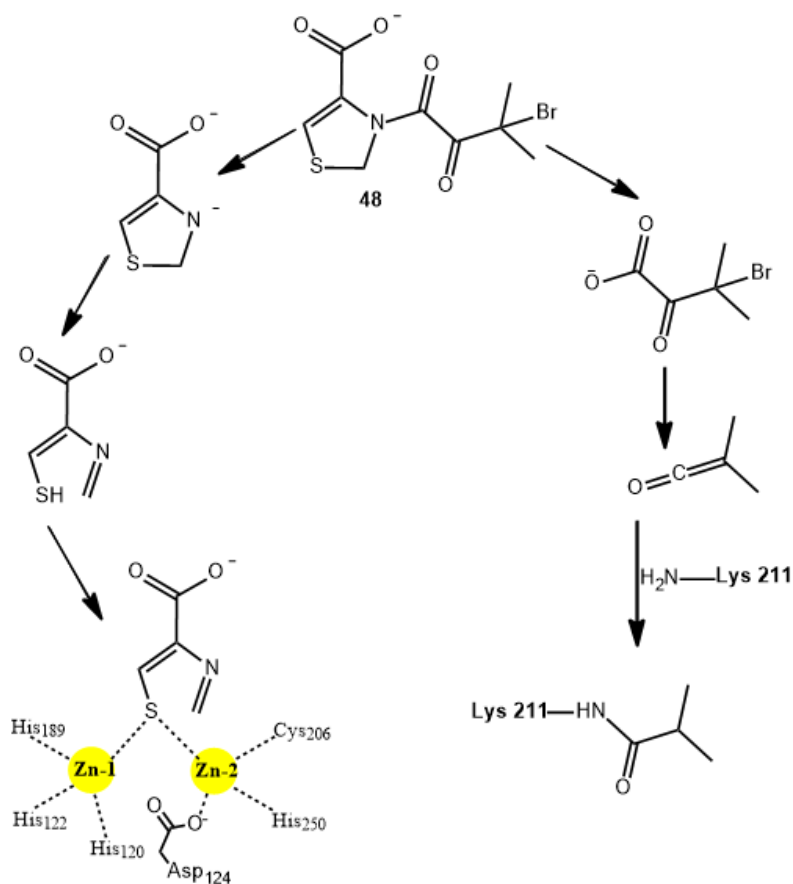
Figure 1.27: Proposed activation/inhibitory mechanism of the designed NDM-1 inhibitor.

1.8 Aim and Objectives

This project aims to develop small molecules as potential inhibitors of microbial β-lactamases (NDM-1 and Bla$_{Mab}$) through chemical synthesis and inhibitory assays. This will be accomplished by the following specific objectives:

- Chemical synthesis of monocyclic and dimeric compounds as potential NDM-1 inhibitors
- Chemical synthesis of bicyclic and tricyclic compounds as potential Bla$_{Mab}$ inhibitors
- Identity characterisation of the synthesised compounds by spectroscopic methods (^{1}H-NMR, ^{13}C-NMR, IR and Mass spectroscopy)
- Purity characterisation of the synthesised compounds by thin-layer chromatography and melting range.
- Evaluation of the inhibitory activity of the synthesised final compounds by:
- TLC-based assay using penicillin V as substrate
- UV-based assay (rapid nitrocefin test).

Chapter 2

2.1 Attempted synthesis of compound 48

Irrespective of the introduction of antibiotics in clinical settings, bacteria continue to strive to cause infections. Despite the usefulness of antibiotics, their application has enabled the survival of a multitude of bacteria with a sophisticated defence mechanism, such as the secretion of β-lactamase (hydrolase) which make antibiotics ineffective or less effective (Bonomo, 2017). More concerning is the emergence and global proliferation of bacteria harbouring the hydrolase called New Delhi Metallo-β-lactamase-1 (NDM-1), an enzyme that can destroy almost all known β-lactam antibiotics (Unemo and Nicholas, 2012; Bush and Bradford, 2016). The ineffectiveness or the low efficacy of β-lactam antibiotics against bacterial infection has turned easily treatable diseases into life-threatening illnesses.

Considering the obvious public health challenge of New Delhi Metallo-β-lactamase-1 (NDM-1), there is a need for the development of an ideal NDM-1 inhibitor. Despite extensive research by the scientific community, no compound has been approved as an NDM-1 inhibitor to date, hence the attempt to prepare and evaluate compound **48** as a potential NDM-1 inhibitor.

2.2 General analytical methods

Chemicals were purchased from Merck, Sigma-Aldrich, Flurochem Ltd., Scientific Laboratory Supplies, Fisher Scientific Ltd. and Apollo Scientific Ltd. and used without further purification. Water-sensitive reactions were carried out in oven-dried glassware under an argon atmosphere. Were possible, reactions were monitored by thin-layer chromatography using precoated silica gel plates (60 F_{254}, Merck) as a stationary phase while visualisation was performed with ultraviolet light (λ = 254/365 nm) and, when necessary, with an aqueous solution of potassium permanganate. Also, reaction products were obtained by flash/column/gradient chromatography (Merck Silicagel 60) when necessary.

The structure of the synthesised compounds was characterised by spectroscopic methods (^{1}H NMR, IR and MS) while the purity of the respective compounds was judged by thin-layer chromatography and melting point analysis respectively.

^{1}H NMR spectra were recorded with a Bruker Avance DPX400 NMR (at 400 MHz) in deuterated chloroform ($CDCl_3$), deuterated dimethylsulfoxide (d_6-DMSO) or deuterium oxide (D_2O) while tetramethylsilane (TMS) was used as internal standard, except for measurements with D_2O. Chemical shifts and coupling constants are reported in parts per million (ppm) and hertz [Hz] respectively while multiplicities are abbreviated as s = singlet, d = doublet, t = triplet, q = quartet and m = multiplet.

IR spectra were recorded on a Thermo Scientific Nicolet iS5 FT-IR spectrometer equipped with an ID5 Diamond ATR accessory at room temperature and intensities of the signals are given as weak (w), medium (m) and strong (s).

Mass spectra were recorded on LTQ Orbitrap XL 1 Instrument (nanoESI).

Analytical TLC was carried out using precoated silica gel plates (60 F_{254}, Merck) while the melting points (uncorrected) were determined on a Reichert-Jung Thermo Galen - hot stage microscope equipped with a Pt 100/RTD temperature sensor.

2.3 Experimental methods

2.3.1 3-Bromo-3-methyl-2-oxobutanoic acid (49)

To a stirred suspension of (S)-2-hydroxy-3-methylbutanoic acid (18.00 g, 152.37 mmol) in tetrachloroethylene (300 mL) was added N-bromosuccinimide (56.95 g, 319.98 mmol, 2.1 eq.). The resulting mixture was heated at reflux under argon for 3 hours and allowed to cool to ambient temperature. The flask was placed in an ice-bath for 30 minutes to facilitate crystallisation and the crystals formed (succinimide) were separated by vacuum filtration while the filtrate was collected. The tetrachloroethylene was removed at low pressure and the residue was dried under vacuum to afford the titled compound as a yellow oil, 30.09 g, 154.30 mmol, 101 %, contaminated with succinimide (33 mol %) as judged by proton NMR integration. The crude compound **49** was used in the next step without further purification.
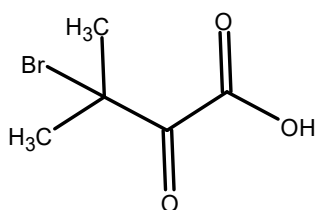
Figure 2.1: Compound **49**.

Molecular Formula: $C_5H_7BrO_3$; R_f (ethyl acetate/hexane, 1:3): 0.4 (major spot).

^{1}H NMR (400 MHz, CDCl$_3$) δ 2.08 (s, 6H, [2 x C$\underline{H_3}$]-C-Br), 2.80 (succinimide, 33 %) ppm.

IR (ATR): ν = 1709 (s, C=O), 1966 (s), 2219 (s), 2576 (m), 2846 (m, C-H), 3139 (m, O-H carboxylic acid) cm^{-1}

MS (-ESI) m/z = Found 192.9507 (M-H)$^-$; calculated for $C_5H_6BrO_3$ 192.9506; 0.6 ppm; ^{79}Br.

2.3.2 3-Bromo-3-methyl-2-oxobutanoyl chloride (50)

To a flask containing the crude compound **49** (30.09 g, 154.30 mmol), at 5 - 10 ºC, was added thionyl chloride (120 mL), while stirring, for over 30 minutes. The resulting mixture was allowed to gradually warm up to ambient temperature and stirred overnight. The mixture was heated at reflux for 2.5 hours and allowed to cool to ambient temperature. The excess thionyl chloride was removed at low pressure and the residue was dried under vacuum to afford the titled compound as a yellow oil, with a nominal yield of 22.44 g, 105.13 mmol, 68 %, contaminated with succinimide (30 mol %) as judged by proton NMR integration. The crude compound **50** was used in the next step without further purification.
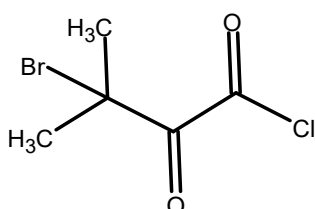
Figure 2.2 Compound **50**.

Molecular Formula: $C_5H_6BrClO_2$.

^{1}H NMR (400 MHz, CDCl$_3$) δ 2.04 (s, 6H, [2 x C$\underline{H_3}$]-C-Br), 2.80 (succinimide, 30 mol %) ppm.

2.3.3 (R)-Ethyl thiazolidine-4-carboxylate (51)

To a stirred suspension of L-4-thiazolidine carboxylic acid (10.00 g, 75.09 mmol) in ethanol (60 mL), at 0 ºC, was added thionyl chloride (6.57 mL, 90.11 mmol, 1.2 eq.) at a rate to maintain the temperature of the reaction ≤ 5 ºC. The resulting mixture was stirred at 0 ºC for 2 hours and was allowed to gradually warm up to ambient temperature and stirred overnight. The mixture was heated at reflux for 1.5 hours, allowed to cool to ambient temperature and the ethanol was removed at low pressure to obtain white crystals. The white crystals were dissolved in distilled water (30 mL) and the solution was neutralised, pH 7, with a saturated aqueous solution of $NaHCO_3$ and the desired compound, was extracted into dichloromethane (3x, 40 mL). The organic portions were combined, dried with anhydrous magnesium sulphate, filtered, and the filtrate was collected. The dichloromethane was removed at low pressure and the residue was dried under vacuum to afford compound **51** as a pale yellow oil, 10.30 g, 63.89 mmol, 85 %, which was used in the next step without further purification.
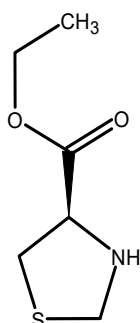
Figure 2.3: Compound **51**.

Molecular Formula: $C_6H_{11}NO_2S$; R_f (ethyl acetate/hexane, 1:3): 0.2 (single spot).

^{1}H NMR (400 MHz, $CDCl_3$) δ 1.31 (t, J = 7.1 Hz, 3H, C$\underline{H}_3$-CH$_2$-O), 2.05 (s, 1H, N$\underline{H}$-CH-CH$_2$), 2.87 (dd, J = 10.4, 8.0 Hz, 1H, NH-CH-C$\underline{H}_2$), 3.27 (dd, J = 10.4, 7.2 Hz, 1H, NH-CH-C$\underline{H}_2$), 3.83 (m, 1H, NH-C$\underline{H}$-CH$_2$), 4.12 (d, J = 9.6 Hz, 1H, S-C$\underline{H}_2$-NH), 4.25 (dq, J = 7.1, 2.6 Hz, 2H, CH$_3$-C$\underline{H}_2$-O), 4.39 (dd, *J* = 9.6, 0.4 Hz, 1H, S-C$\underline{H}_2$-NH) ppm.

IR (ATR): ν = 1027 (m, C-N), 1180 (s, C-O ester), 1341 (m), 1371 (m, C-H), 1445 (w, C-H), 1731 (s, C=O) cm^{-1}.

2.3.4 (R)-Ethyl-3-(3-bromo-3-methyl-2-oxobutanoyl)thiazolidine-4-carboxylate (52)

To a stirred solution of **51** (1.00 g, 6.20 mmol, 1.3 eq.) and triethylamine (0.86 mL, 6.20 mmol, 1.3 eq.) in anhydrous dichloromethane (15 mL), at 0 ºC, was added the crude compound **50** (corrected mass/molarity: 1.02 g, 4.78 mmol, dissolved in 5 mL dichloromethane) at a rate to maintain the reaction temperature ≤ 5 ºC. The resulting mixture was stirred at 0 ºC for 2 hours and allowed to gradually warm up to ambient temperature and stirred overnight. The reaction mixture was diluted with dichloromethane (10 mL), washed with 1N HCl (2x, 20 mL), a saturated aqueous solution of $NaHCO_3$ (2x, 20 mL) and a saturated aqueous solution of NaCl (20 mL), and dried with anhydrous magnesium sulphate, filtered, and the filtrate was collected. The filtrate was concentrated at low pressure and the crude concentrate was subjected to flash chromatography (ethyl acetate/hexane, 1:6) to afford compound **52** as a pale yellow oil, 0.60 g, 1.77 mmol, 37 %.

Figure 2.4: Compound **52** (*cis* and *trans* rotamers).

Molecular Formula: $C_{11}H_{16}BrNO_4S$; R_f (ethyl acetate/hexane, 1:6): 0.2 (single spot).

^{1}H NMR (400 MHz, CDCl$_3$) δ (two rotamers, *cis* and *trans*, at 298 K; ratio of isomers, 1:3): 1.30 (*cis* and *trans*, t, J = 7.1, 2.1 Hz, 6H, CH$_3$-CH$_2$-O), 2.09 (*cis* and *trans*, m, 12H, [2 x CH$_3$]-C-Br), 3.28 (*cis/trans*, dd, *J* = 11.8, 4.4 Hz, 1H, N-CH-CH$_2$), 3.36 (*cis* and *trans*, m, 3H, N-CH-CH$_2$), 4.25 (*cis* and *trans*, qd, *J* = 7.1, 3.9 Hz, 4H, CH$_3$-CH$_2$-O), 4.59 (*cis/trans*, d, *J* = 9.9 Hz, 1H, S-CH$_2$-N), 4.69 (*cis/trans*, s, 2H, S-CH$_2$-N), 4.92 (*cis/trans*, d, *J* = 10.0 Hz, 1H, S-CH$_2$-N), 4.94 (*cis/trans*, m, 0.5H, N-CH-CH$_2$), 5.10 (*cis/trans*, dd, J = 7.0, 4.4 Hz, 1.5H, N-CH-CH$_2$) ppm.

IR (ATR): v = 1187 (m, C-O ester), 1651 (s, C=O amide), 1737 (m, C=O ester), 1956 (m) cm^{-1}.

MS (+ESI) m/z = Found 338.0061 (M+H)$^+$; calculated for $C_{11}H_{17}O_4NBrS$ 338.0056; 1.4 ppm; ^{79}Br.

MS (+ESI) m/z = Found 355.0323 (M+NH$_4$)$^+$; calculated for $C_{11}H_{20}O_4N_2BrS$ 355.0322; 0.4 ppm; ^{79}Br.

MS (+ESI) m/z = Found 359.9876 (M+Na)$^+$; calculated for $C_{11}H_{16}O_4NBrSNa$ 359.9876; 0.1 ppm; ^{79}Br.

2.3.5 (R)-Ethyl-3-(2-ethoxy-2-oxoacetyl)thiazolidine-4-carboxylate (54)

To a stirred solution of **51** (5.00 g, 31.01 mmol) and triethylamine (4.32 mL, 31.01 mmol) in anhydrous dichloromethane (30 mL), at 0 °C, was added ethyl chlorooxoacetate (3.47 mL, 31.01 mmol, dissolved in 15 mL dichloromethane), at a rate to maintain the temperature of the mixture ≤ 5 °C. The resulting mixture was stirred at 0 °C for 2 hours and allowed to gradually warm up to ambient temperature and stirred overnight. The reaction mixture was diluted with ethyl acetate (50 mL) and the flask was placed in an ice-bath for 20 minutes. The precipitate formed was separated by vacuum filtration and the filtrate was collected. The dichloromethane was removed at low pressure and the ethyl acetate portion was washed with 1N HCl (60 mL), a saturated aqueous solution of NaHCO$_3$ (60 mL) and a saturated aqueous solution of NaCl (60 mL) respectively, and dried with anhydrous magnesium sulphate, filtered, and the filtrate was collected. The ethyl acetate was removed at low pressure and the residue was dried under vacuum to afford **54** as a dark yellow oil, 6.80 g, 26.02 mmol, 84 %, which was used in the next step without further purification.

Figure 2.5: Compound **54** (*cis* and *trans* rotamers).

Molecular Formula: $C_{10}H_{15}NO_5S$; R_f (ethyl acetate/hexane, 3:10): 0.3 (single spot).

^{1}H NMR (400 MHz, CDCl$_3$) δ (two rotamers, *cis* and *trans*, at 298 K; ratio of isomers, 1:1): 1.29 (*cis* and *trans*, dt, J = 7.1, 4.2 Hz, 6H, C$\underline{H}_3$-CH$_2$-O), 1.38 (*cis* and *trans*, dt, J = 10.9, 7.1 Hz, 6H, C$\underline{H}_3$-CH$_2$-O, oxo moiety), 3.24 (*cis/trans*, dd, *J* = 11.9, 4.3 Hz, 1H, N-CH-C$\underline{H}_2$), 3.32 (*cis/trans*, dd, *J* = 11.9, 7.0 Hz, 1H, N-CH-C$\underline{H}_2$), 3.41 (*cis/trans*, m, 2H, N-CH-C$\underline{H}_2$), 4.28 (*cis* and *trans*, overlapping m, 8H, CH$_3$-[2 x CH$_2$]-O), 4.74 (*cis/trans*, dd, *J* = 3.7, 0.5 Hz, 2H, S-C$\underline{H}_2$-N), 4.78 (*cis/trans*, dd, *J* = 9.4, 0.5 Hz, 1H, S-C$\underline{H}_2$-N), 4.90 (*cis/trans*, d, J = 9.5 Hz, 1H, S-C$\underline{H}_2$-N), 5.08 (*cis/trans*, dd, J = 7.0, 4.2 Hz, 1H, N-C$\underline{H}$-CH$_2$), 5.39 (*cis/trans*, dd, J = 6.0, 3.2 Hz, 1H, N-C$\underline{H}$-CH$_2$) ppm.

IR (ATR): υ = 1019 (m, C-N), 1186 (s, C-O ester), 1239 (s, C-O ester), 1428 (m), 1660 (s, C=O amide), 1732 (s, C=O ester) cm^{-1}.

MS (+ESI) m/z = Found 262.0747 (M+H)$^+$; calculated for $C_{10}H_{16}O_5NS$ 262.0744; 1.3 ppm.

MS (+ESI) m/z = Found 279.1010 (M+NH$_4$)$^+$; calculated for $C_{10}H_{19}O_5N_2S$ 279.1009; 0.3 ppm.

MS (+ESI) m/z = Found 284.0564 (M+Na)$^+$; calculated for $C_{10}H_{15}O_5NSNa$ 284.0563; 0.3 ppm.

2.3.6 (R)-Ethyl-3-(3-methyl-2-oxobutanoyl)thiazolidine-4-carboxylate (55)

To a stirred solution of **54** (2.50 g, 9.57 mmol) in anhydrous tetrahydrofuran (60 mL), at - 78 °C, was added 0.75 M solution of isopropylmagnesium bromide in tetrahydrofuran (17.86 mL, 13.39 mmol, 1.4 eq.) at a rate to maintain the temperature of the reaction mixture ≤ -70 °C. The resulting mixture was stirred at about -78 to -70 °C for 5 hours and poured into a saturated aqueous solution of ammonium chloride (100 mL). The aqueous solution was extracted with ethyl acetate (3x, 40 mL) and the organic layers were combined, washed with water (40 mL), dried with anhydrous magnesium sulphate, filtered, and the filtrate was collected. The filtrate was concentrated at low pressure and the crude concentrate was subjected to flash chromatography, ethyl acetate/petroleum ether 60-80 °C (3: 10), to afford compound **55** as a colourless oil, 0.97 g, 3.74 mmol, 39 %.
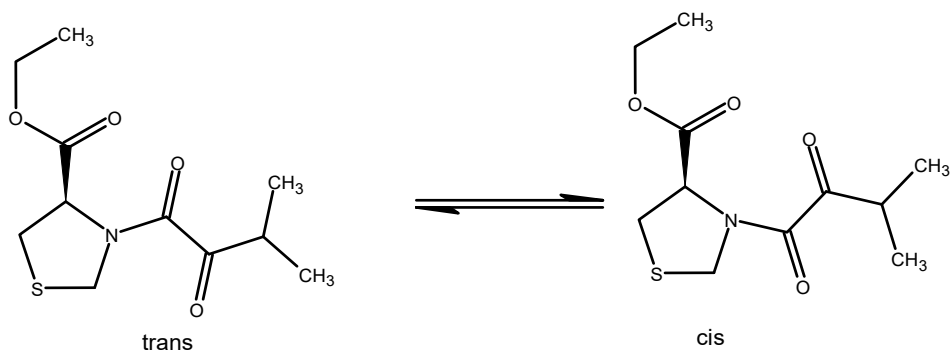
Figure 2.6: Compound **55** (*cis* and *trans* rotamers).

Molecular Formula: $C_{11}H_{17}NO_4S$; R_f (ethyl acetate/petroleum ether 60 - 80 °C, 3:10): 0.4 (single spot).

^1H NMR (400 MHz, $CDCl_3$) δ (two rotamers, *cis* and *trans*, at 298 K; ratio of isomer, 1:1): 1.14 (*cis* and *trans*, m, 9H, [2 x C$\underline{H}_3$]-CH-CO), 1.20 (*cis/trans*, d, J = 7.1 Hz, 3H, [2 x C$\underline{H}_3$]-CH-CO), 1.29 (*cis* and *trans*, t, J = 7.2 Hz, 6H, C$\underline{H}_3$-CH$_2$-O), 2.34 (*cis*/trans, m, 0.5H, [2 x CH$_3$]-C$\underline{H}$-CO), 2.49 (*cis/trans*, m, 0.5H, [2 x CH$_3$]-C$\underline{H}$-CO), 3.23 (*cis/trans*, dd, J = 11.9, 4.0 Hz, 1H, N-CH-C$\underline{H}_2$), 3.31 (*cis/trans*, dd, J = 11.9, 7.0 Hz, 1H, N-CH-C$\underline{H}_2$), 3.40 (*cis/trans*, m, 2H, N-CH-C$\underline{H}_2$, [2 x CH$_3$]-C$\underline{H}$-CO), 3,49 (*cis/trans*, m, 1H, N-CH-C$\underline{H}_2$), 4.23 (*cis* and *trans*, overlapping m, 4H, CH$_3$-C$\underline{H}_2$-O), 4.61 (*cis/trans*, d, J = 9.4 Hz, 1H, S-C$\underline{H}_2$-N), 4.73 (*cis/trans*, dd, J = 2.1, 0.5 Hz, 2H, S-C$\underline{H}_2$-N), 4.82 (*cis/trans*, d, J = 9.5 Hz, 1H, S-C$\underline{H}_2$-N), 5.07 (*cis/trans*, dd, J = 7.0, 4.0 Hz, 1H, N-C$\underline{H}$-CH$_2$), 5.34 (*cis/trans*, dd, J = 6.1, 3.2 Hz, 1H, N-C$\underline{H}$-CH$_2$) ppm.

IR (ATR): v = 1024 (m, C-N), 1186 (s, C-O ester), 1413 (w), 1643 (s, C=O amide), 1738 (s, C=O ester), 2972 (w, C-H) cm^{-1}

MS (+ESI) m/z = Found 260.0954 (M+H)$^+$; calculated for $C_{11}H_{18}O_4NS$ 260.0951; 1.1 ppm.

MS (+ESI) m/z = Found 282.0771 (M+Na)$^+$; calculated for $C_{11}H_{17}O_4NSNa$ 282.0770; 0.2 ppm.

2.3.7 (R)-Ethyl-2,2-dimethylthiazolidine-4-carboxylate (56)

To a stirred suspension of L-cysteine ethyl ester hydrochloride (11.00 g, 59.24 mmol) in acetone (200 mL) was added 2,2-dimethoxypropane (37.88 mL, 308.07 mmol, 5.2 eq.). The resulting mixture was heated at reflux for 3 hours and allowed to cool to ambient temperature. The flask was placed in an ice-bath for 30 minutes and the crystals formed were collected by vacuum filtration. The filtrate was concentrated at low pressure and reconstituted in an acetone-ethyl acetate mixture (80 mL, 4:1) and placed in an ice-bath for another 30 minutes. The second batch of crystals formed was also collected by vacuum filtration. The first and second batches of the crystals were combined, dissolved in water (30 mL) and the solution was neutralised, pH 7, with a saturated aqueous solution of $NaHCO_3$ and the desired compound, was extracted into dichloromethane (3x, 30 mL). The organic portions were combined, dried with anhydrous magnesium sulphate, filtered and the filtrate was collected. The dichloromethane was removed at low pressure and the residue was dried under vacuum to afford **56** as a colourless oil, 8.20 g, 43.32 mmol, 73 %, which was used in the next step without further purification.
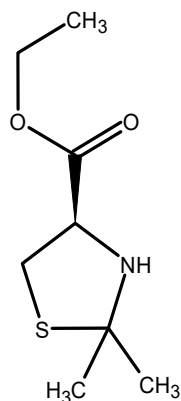
Figure 2.7: Compound **56**.

Molecular Formula: $C_8H_{15}NO_2S$; R_f (ethyl acetate/hexane, 1:3): 0.3 (single spot).

^{1}H NMR (400 MHz, CDCl$_3$) δ 1.32 (t, J = 7.1 Hz, 3H, C$\underline{H}_3$-CH$_2$-O), 1.54 (s, 3H, S-C-C$\underline{H}_3$), 1.72 (s, 3H, S-C-C$\underline{H}_3$), 3.03 (dd, J = 10.4, 9.2 Hz, 1H, NH-CH-C$\underline{H}_2$), 3.45 (dd, J = 10.5, 7.0 Hz, 1H, NH-CH-C$\underline{H}_2$), 4.08 (dd, J = 9.2, 7.0 Hz, 1H, NH-C$\underline{H}$-CH$_2$), 4.25 (dq, *J* = 7.1, 5.0 Hz, 2H, CH$_3$-C$\underline{H}_2$-O) ppm.

IR (ATR): υ = 796 (m), 1025 (m, C-N), 1184 (s, C-O ester), 1225 (m-s), 1332 (m), 1371 (m-s, C-H), 1445 (w, C-H), 1731 (s, C=O ester) cm^{-1}.

2.3.8 (R)-Ethyl-3-(2-ethoxy-2-oxoacetyl)-2,2-dimethylthiazolidine-4-carboxylate (57)

To a stirred solution of **56** (5.00 g, 26.42 mmol) and triethylamine (3.68 mL, 26.42 mmol) in anhydrous dichloromethane (30 mL) at 0 °C, was added ethyl chlorooxoacetate (2.96 mL, 26.42 mmol, dissolved in 15 mL dichloromethane), at a rate to maintain the temperature of the mixture ≤ 5 °C. The resulting mixture was stirred at 0 °C for 2 hours and allowed to gradually warm up to ambient temperature and stirred overnight. The reaction mixture was diluted with ethyl acetate (50 mL) and the flask was placed in an ice-bath for 20 minutes. The precipitate formed was separated by vacuum filtration and the filtrate was collected. The dichloromethane was removed at low pressure and the ethyl acetate portion was washed with 1N HCl (60 mL), a saturated aqueous solution of NaHCO$_3$ (60 mL) and a saturated aqueous solution of NaCl (60 mL) respectively, and dried with anhydrous magnesium sulphate, filtered, and the filtrate was collected. The ethyl acetate was removed at low pressure and the residue was dried under vacuum to afford **57** as a pale yellow oil, 5.01 g, 17.31 mmol, 66 %, which was used in the next step without further purification.
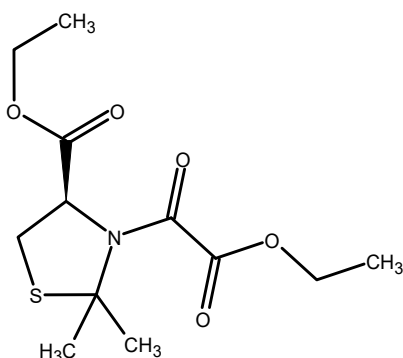
Figure 2.8: Compound **57** (*trans* rotamer).

Molecular Formula: $C_{12}H_{19}NO_5S$; R_f (ethyl acetate/hexane, 3:10): 0.5 (single spot).

^{1}H NMR (400 MHz, CDCl$_3$) δ (only one rotamer at 298 K, possibly *trans*): 1.32 (dt, J = 21.5, 7.2 Hz, 6H, [2 x CH$_3$]-CH$_2$-O), 1.88 (s, 3H, S-C-CH$_3$), 1.94 (s, 3H, S-C-CH$_3$), 3.34 (d, J = 3.9 Hz, 2H, N-CH-CH$_2$), 4.18 – 4.43 (overlapping m, 4H, [2 x CH$_3$]-[2 x CH$_2$]-O), 5.38 (1H, d, J = 3.9 Hz, N-CH-CH$_2$) ppm.

IR (ATR): υ = 1017 (m, C-N), 1193 (s, C-O ester), 1233 (s, C-O ester), 1364 (m), 1666 (s, C=O amide), 1734 (s, C=O ester), 2981 (w, C-H) cm^{-1}.

MS (+ESI) m/z = Found 290.1060 (M+H)$^+$; calculated for C$_{12}$H$_{20}$O$_5$NS 290.1057; 1.1 ppm.

MS (+ESI) m/z = Found 307.1323 (M+NH$_4$)$^+$; calculated for C$_{12}$H$_{23}$O$_5$N$_2$S 307.1322; 0.3 ppm.

MS (+ESI) m/z = Found 312.0876 (M+Na)$^+$; calculated for C$_{12}$H$_{19}$O$_5$NSNa 312.0876; 0.0 ppm.

2.3.9 (R)-Ethyl-2,2-dimethyl-3-(3-methyl-2-oxobutanoyl)thiazolidine-4-carboxylate (58)

To a stirred solution of **57** (2.33 g, 8.05 mmol) in anhydrous tetrahydrofuran (60 mL), at - 78 °C, was added 0.75 M solution of isopropylmagnesium bromide in tetrahydrofuran (13.96 mL, 10.47 mmol, 1.3 eq.) at a rate to maintain the temperature of the reaction mixture ≤ -70 °C. The resulting mixture was stirred at about -78 to -70 °C for 5 hours and poured into a saturated aqueous solution of ammonium chloride (100 mL). The aqueous solution was extracted with ethyl acetate (3x, 40 mL) and the organic layers were combined, washed with water (40 mL), dried with anhydrous magnesium sulphate, filtered, and the filtrate was collected. The filtrate was concentrated at low pressure and the crude concentrate was subjected to flash chromatography, ethyl acetate/petroleum ether 60 - 80 °C (1: 10), to afford compound **58** as a colourless oil, 0.91 g, 3.17 mmol, 39 %.
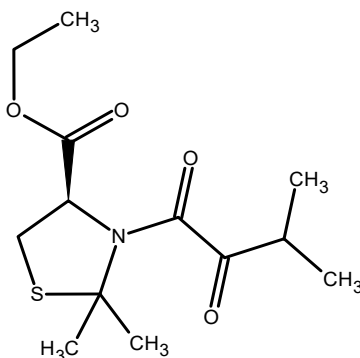
Figure 2.9: Compound **58** (*trans* rotamer).

Molecular Formula: C$_{13}$H$_{21}$NO$_4$S; R$_f$ (ethyl acetate/petroleum ether 60 - 80 °C, 1: 10): 0.2 (single spot).

^{1}H NMR (400 MHz, CDCl$_3$) δ (only one rotamer at 298 K, possibly *trans*): 1.11 (d, J = 7.0 Hz, 3H, CH$_3$-CH-CO), 1.16 (d, *J* = 6.9 Hz, 3H, CH$_3$-CH-CO), 1.28 (t, *J* = 7.1 Hz, 3H, CH$_3$-CH$_2$-O), 1.88 (s, 3H, S-C-CH$_3$), 1.95 (s, 3H, S-C-CH$_3$), 3.32 (d, J = 3.8 Hz, 2H, N-CH-CH$_2$), 3.41 (p, J = 7.0 Hz, 1H, CH$_3$-CH-CO), 4.20 (m, 2H, CH$_3$-CH$_2$-O), 5.37 (dd, J = 4.7, 3.2 Hz, 1H, N-CH-CH$_2$) ppm.

IR (ATR): υ = 1024 (m, C-N), 1187 (s, C-O ester), 1413 (w), 1644 (s, C=O amide), 1741 (s, C=O ester), 2974 (w, C-H) cm^{-1}.

MS (+ESI) m/z = Found 288.1264 (M+H)$^+$; calculated for C$_{13}$H$_{22}$O$_4$NS 288.1264; 0.0 ppm.

MS (+ESI) m/z = Found 305.1530 (M+NH$_4$)$^+$; calculated for C$_{13}$H$_{25}$O$_4$N$_2$S 305.1530; 0.1 ppm.

MS (+ESI) m/z = Found 310.1082 (M+Na)$^+$; calculated for C$_{13}$H$_{21}$O$_4$NSNa 310.1084; 0.5 ppm.

2.3.10 (R)-Ethyl-3-(3-bromo-3-methyl-2-oxobutanoyl)-2,2-dimethylthiazolidine-4-carboxylate (59)

To a stirred solution of compound **56** (1.00 g, 5.28 mmol, 1.3 eq.) and triethylamine (0.74 mL, 5.28 mmol, 1.3 eq.) in anhydrous dichloromethane (15 mL), at 0 ºC, was added compound **50** (corrected mass/molarity: 0.87 g, 4.08 mmol, dissolved in 5 mL dichloromethane) at a rate to maintain the reaction temperature ≤ 5 ºC. The resulting mixture was stirred at 0 ºC for 2 hours and allowed to gradually warm up to ambient temperature and stirred overnight. The mixture was diluted with dichloromethane (10 mL), washed with 1N HCl (2x, 20 mL) and a saturated aqueous solution of NaCl (2x, 20 mL) respectively, and dried with anhydrous magnesium sulphate, filtered, and the filtrate was collected. The filtrate was concentrated at low pressure and the crude concentrate was subjected to column chromatography (ethyl acetate/hexane, 1:5) to afford **59** as a yellow oil, 0.23 g, 0.63 mmol, 15 %.
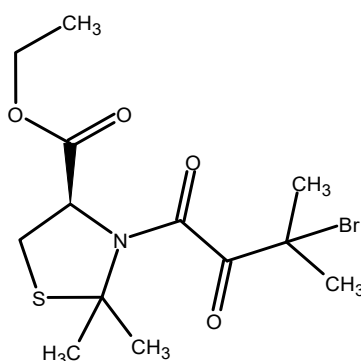
Figure 2.10: Compound **59** (*trans* rotamer).

Molecular Formula: $C_{13}H_{20}BrNO_4S$; R_f (ethyl acetate/hexane, 1:5): 0.4 (single spot).

^{1}H NMR (400 MHz, CDCl$_3$) δ (only one rotamer at 298 K, possibly *trans*): 1.32 (J = 7.1 Hz, 3H, C$\underline{H}_3$-CH$_2$-O), 1.92 (s, 3H, C$\underline{H}_3$-C-Br), 1.93 (s, 3H, C$\underline{H}_3$-C-Br), 1.99 (s, 3H, S-C-C$\underline{H}_3$), 2.15 (s, 3H, S-C-C$\underline{H}_3$), 3.28 (dd, *J* = 12.2, 1.4 Hz, 1H, N-CH-C$\underline{H}_2$), 3.35 (dd, *J* = 12.2, 5.8 Hz, 1H, N-CH-C$\underline{H}_2$), 4.26 (m, 2H, CH$_3$-C$\underline{H}_2$-O), 4.90 (dd, J = 5.9, 1.4 Hz, 1H, N-C$\underline{H}$-CH$_2$) ppm.

IR (ATR): υ = 1205 (s, C-O ester),1384 (s, C-H), 1656 (s, C=O amide), 1712 (s, C=O ester), 2935 (w, C-H), 2981 (w, C-H) cm^{-1}.

MS (+ESI) m/z = Found 366.0374 (M+H)$^+$; calculated for $C_{13}H_{21}O_4NBrS$ 366.0369; 1.3 ppm; ^{79}Br.

MS (+ESI) m/z = Found 383.0634 (M+NH$_4$)$^+$; calculated for $C_{13}H_{24}O_4N_2BrS$ 383.0635; 0.2 ppm; ^{79}Br

MS (+ESI) m/z = Found 388.0187 (M+Na)$^+$; calculated for $C_{13}H_{20}O_4NBrSNa$ 388.0189; 0.4 ppm; ^{79}Br.

2.3.11 (R)-3-*tert*-butyl-4-methyl thiazolidine-3,4-dicarboxylate(62)

To a stirred solution of (R)-3-(*tert*-butoxycarbonyl)thiazolidine-4-carboxylic acid (3.10 g, 13.29 mmol) in anhydrous dimethylformamide (20 mL) was added K$_2$CO$_3$ (7.35 g, 53.15 mmol 4 eq.) and iodomethane (0.99 mL, 15.95 mmol, 1.2 eq.). The resulting mixture was stirred at ambient temperature (21 ºC) under argon overnight. Ethyl acetate (30 mL) was added to the reaction mixture and the white precipitate formed was separated by vacuum filtration and the precipitate was rinsed with ethyl acetate (5 mL). The filtrate was collected and washed with a saturated aqueous solution of NaCl (3x, 30 mL), dried with

magnesium sulphate, filtered and the filtrate was collected. The ethyl acetate was removed at low pressure and the residue was dried under vacuum to afford **62** as a yellow oil, 2.66 g, 10.76 mmol, 81 %, which was used in the next step without further purification.
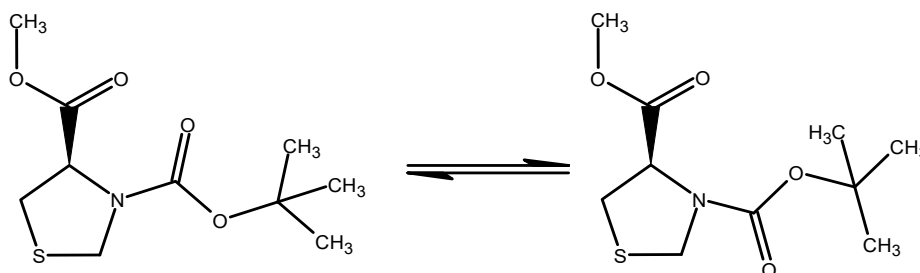
Figure 2.11: Compound **62** (*cis* and *trans* rotamers).

Molecular Formula: $C_{10}H_{17}NO_4S$; R_f (ethyl acetate/pet. ether, 40-60 °C, 3:10): 0.4 (single spot).

^{1}H NMR (400 MHz, DMSO-d_6) δ (two rotamers, *cis* and *trans*, at 298 K, ratio of isomers, 1:1): 1.39 (*cis* and *trans*, s, 18H, [3 x C<u>H</u>$_3$]-O-CO), 3.15 (*cis/trans*, m, 2H, N-CH-C<u>H</u>$_2$), 3.40 (*cis/trans*, m, 2H, N-CH-C<u>H</u>$_2$), 3.68 (*cis* and *trans*, s, 6H, C<u>H</u>$_3$-O-CO), 4.36 (*cis/trans*, t, J = 10.7 Hz, 2H, S-C<u>H</u>$_2$-N), 4.52 (*cis/trans*, d, J = 8.9 Hz, 2H, S-C<u>H</u>$_2$-N), 4.63 (*cis/trans*, s, 1H, N-C<u>H</u>-CH$_2$), 4.75 (*cis/trans*, s, 1H, N-C<u>H</u>-CH$_2$) ppm.

IR (ATR): v = 1155 (s, C-O ester), 1380 (s, C-H), 1698 (s, C=O carbamate), 1749 (m, C=O ester), 2976 (w, C-H) cm^{-1}.

2.3.12 (R)-2,2-Dimethylthiazolidine-4-carboxylic acid hydrochloride (68)

A suspension of anhydrous L-cysteine hydrochloride (9.00 g, 57.10 mmol) in acetone (150 mL) was heated at reflux overnight and allowed to cool to ambient temperature. The precipitate formed was collected by vacuum filtration, washed with cold acetone and dried under vacuum to afford **68** as a white crystalline solid, 9.50 g, 48.06 mmol, 84 %, which was used in the next step without further purification.
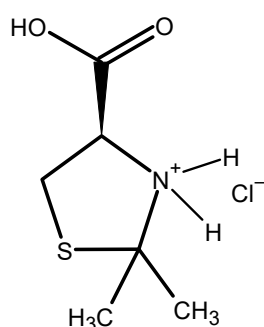
Figure 2.12: Compound **68**.

Molecular Formula: $C_6H_{12}ClNO_2S$; (MeOH/DCM, 1:4): 0.30 (single spot).

^{1}H NMR (400 MHz, D$_2$O) δ 1.63 (d, J = 5.3 Hz, 6H, S-C-[2 x C<u>H</u>$_3$]), 3.34 (ddd, J = 12.2, 7.8, 1.0 Hz, 1H, HN-CH-C<u>H</u>$_2$), 3.48 (dd, J = 12.2, 8.1 Hz, 1H, HN-CH-C<u>H</u>$_2$), 4.63 (m, 1H, HN-C<u>H</u>-CH$_2$) ppm.

IR (ATR): v = 1221 (w), 1376 (w, C-H), 1520 (w), 1740 (s, C=O), 2872 (w, C-H), 3060 (w, O-H) cm^{-1}.

2.3.13 (4R)-3-(*tert*-Butoxycarbonyl)-2,2-dimethylthiazolidine-4-carboxylic acid (69)

A stirred solution of compound **68** (4.0 g, 20.23 mmol) in pyridine (150 mL) was cooled to - 23 ℃ and di-*tert*-butyl dicarbonate (4.42 g, 22.18 mmol, 1.1 eq.) was added in small portions. The ice-bath was removed and the resulting mixture was allowed to gradually warm to ambient temperature and stirred under argon for 3 days. Toluene (200 mL) was added to the mixture and the solution was extracted with ice-cold 2N NaOH (2x, 150 mL). The alkaline extract was washed with toluene (2x, 200 mL) and hexane (200 mL) respectively and acidified, at 8 - 15 ℃, with citric acid to pH 3 – 4. The acidified solution was extracted with dichloromethane (2x, 200 mL) and the organic portions were combined and washed with 10 % NaCl (2x, 200 mL), dried with magnesium sulphate, filtered and the filtrate was collected. The dichloromethane was removed at low pressure and the residue was dried under vacuum to afford compound **69** as a white solid 3.43 g, 13.12 mmol, 65 %, which was used in the next step without further purification.
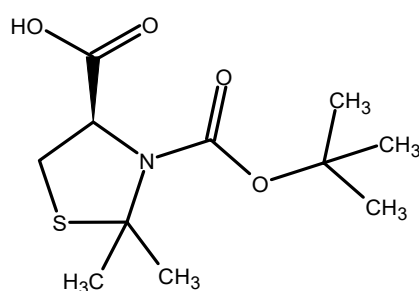
Figure 2.13: Compound **69** (*trans* rotamer).

Molecular Formula: $C_{11}H_{19}NO_4S$; R_f (MeOH/DCM, 1:4): 0.50 (single spot); melting point: 89.3 – 93.5 ℃.

^{1}H NMR (400 MHz, $CDCl_3$) δ (only one rotamer at 298 K, possibly trans): 1.48 (m, 9H, [3 x C$\underline{H_3}$]-O-CO), 1.79 (m, 6H, S-C-[2 x C$\underline{H_3}$]), 3.22 (d, *J* = 38.9 Hz, 2H, N-CH-C$\underline{H_2}$), 4.90 (d, *J* = 36.1 Hz, 1H, N-C$\underline{H}$-CH$_2$) ppm.

IR (ATR): υ = 1079 (m, C-N), 1188 (s, C-O carbamate), 1365 (s, C-H), 1675 (s, C=O, carbamate), 1753 (m-s, C = O, carboxylic acid), 2975 (w, C-H) 3191 (w, O-H) cm^{-1}.

2.3.14 (R)-3-*tert*-Butyl-4-methyl 2,2-dimethylthiazolidine-3,4-dicarboxylate (70)

To a stirred solution of compound **69** (1.13 g, 4.32 mmol) in anhydrous dimethylformamide (30 mL) were added K_2CO_3 (2.39 g, 17.30 mmol 4 eq.) and iodomethane (0.32 mL, 5.19 mmol, 1.2 eq). The resulting mixture was stirred at ambient temperature (21 ℃) under argon overnight. Ethyl acetate (30 mL) was added to the reaction mixture and the white precipitate formed was separated by vacuum filtration and the precipitate was rinsed with ethyl acetate (5 mL). The filtrate was collected and washed with a saturated aqueous solution of NaCl (3x, 40 mL), dried with magnesium sulphate, filtered and the filtrate was collected. The ethyl acetate was removed at low pressure and the residue was dried under vacuum to afford **70** as a yellow oil, 1.09 g, 3.96 mmol, 92 %, which was used in the next step without further purification.
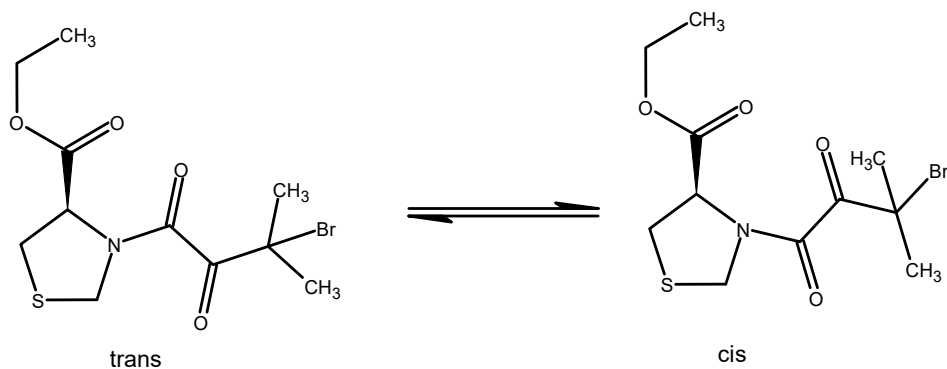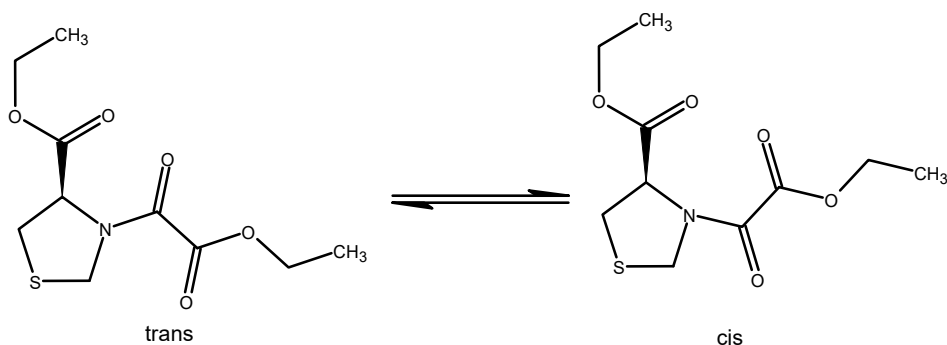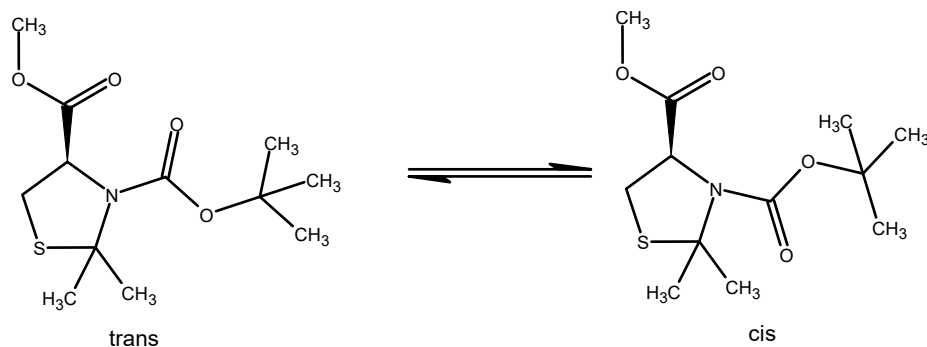
Figure 2.14: Compound **70** (*cis* and *trans* rotamers).

Molecular Formula: $C_{12}H_{21}NO_4S$; R_f (ethyl acetate/hexane, 1:6): 0.3 (single spot).

^{1}H NMR (400 MHz, CDCl₃) δ (two rotamers, *cis* and *trans*, at 298 K; ratio of isomers, 1:1): 1.41 (*cis/trans*, s, 9H, [3 x C$\underline{H}_3$]-O-CO), 1.51 (*cis/trans*, s, 9H, [3 x C$\underline{H}_3$]-O-CO), 1.79 (*cis* and *trans*, m, 9H, S-C-[2 x C$\underline{H}_3$]), 1.87 (*cis/trans*, s, 3H, S-C-[2 x C$\underline{H}_3$]), 3.11 (*cis/trans*, m, 2H, N-CH-C$\underline{H}_2$), 3.28 (*cis/trans*, dd, *J* = 12.0, 6.7 Hz, 2H, N-CH-C$\underline{H}_2$), 3.77 (*cis* and *trans*, s, 6H, C$\underline{H}_3$-O-CO), 4.80 (*cis/trans*, dd, *J* = 6.9, 2.9 Hz, 1H, N-C$\underline{H}$-CH₂), 4.97 (*cis/trans*, d, *J* = 6.2 Hz, 1H, N-C$\underline{H}$-CH₂) ppm.

2.3.15 **(4R)-3-*tert*-Butyl-4-methyl-5ξ-(benzoyloxy)-2,2-dimethylthiazolidine-3,4-dicarboxylate (71)**

To a stirred solution of compound **70** (1.09 g, 3.96 mmol) in tetrachloroethylene (40 mL) was added benzoyl peroxide (2.40 g, 9.90 mmol, 2.5 eq.) and the resulting mixture was heated at reflux for 3 hours. The mixture was allowed to cool to ambient temperature and the reaction solvent was removed at low pressure while the residue was dissolved in ethyl acetate (40 mL) and washed with a saturated aqueous solution of NaHCO₃ (2x, 50 mL) and a saturated aqueous solution of NaCl (2x, 50 mL) respectively. The organic phase was dried with magnesium sulphate, filtered and the filtrate was collected. Hexane (50 mL) was added to the filtrate and the flask was kept at 0°C overnight. The precipitate formed was separated by vacuum filtration and the filtrate was collected. The filtrate was concentrated under reduced pressure and subjected to column chromatography (ethyl acetate/hexane, 1:10) to afford the compound **71** brown oil, 0.23 g, 0.58 mmol, 15 %.
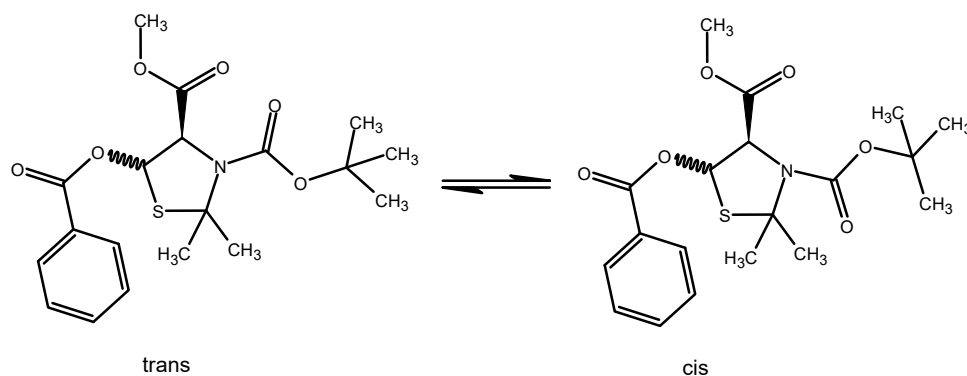
Figure 2.15: Compound **71** (*cis* and *trans* rotamers as well as diastereoisomers).

Molecular Formula: $C_{19}H_{25}NO_6S$; R_f (ethyl acetate/hexane, 1:10): 0.2 (single spot).

^{1}H NMR (400 MHz, CDCl$_3$) δ (two rotamers, *cis* and *trans*, at 298 K; ratio of isomers, 1:1): 1.45 (*cis/trans*, s, 9H, [3 x C<u>H</u>$_3$]-O-CO), 1.56 (*cis/trans*, s, 9H, [3 x C<u>H</u>$_3$]-O-CO), 1.92 (*cis* and *trans* dd, *J* = 24.7, 11.6 Hz, 12H, S-C-[2 x C<u>H</u>$_3$]), 3.82 (*cis* and *trans*, s, 6H, C<u>H</u>$_3$-CO-C), 5.12 (*cis/trans*, s, 1H, N-C<u>H</u>-CH$_2$), 5.33 (*cis/trans*, s, 1H, N-C<u>H</u>-CH$_2$), 6.53 (*cis* and *trans*, d, *J* = 8.9 Hz, 2H, CO-O-C<u>H</u>), 7.48 (*cis* and *trans*, m, 4H, benzoyl group, ortho/meta protons), 7.60 (*cis* and *trans*, dd, *J* = 7.2, 3.1 Hz, 2H, benzoyl group, meta proton), 7.99 (*cis* and *trans*, d, *J* = 7.7 Hz, 1H, benzoyl group, ortho/meta proton), 8.06 (*cis* and *trans*, dd, *J* = 5.6, 3.8 Hz, 3H, benzoyl group, ortho/para proton) ppm.

IR (ATR): ν = 718 (m), 1131 (s, C-O), 1177 (s, C-O), 1243 (w), 1435 (m), 1660 (s, C=O), 2934 (w, C-H) cm^{-1}.

2.3.16 3-*tert*-Butyl-4-methyl-2,2-dimethylthiazole-3,4(2H)-dicarboxylate (72)

To a stirred solution of compound **71** (0.23 g, 0.58 mmol) in dichloromethane (15 mL) was added 1,8-diazabicyclo[5.4.0]undec-7-ene (0.13 mL, 0.87 mmol, 1.5 eq.). The reaction mixture was stirred overnight at ambient temperature and heated at reflux for 1 hour. The reaction mixture was diluted with dichloromethane (10 mL) and washed with a saturated aqueous solution of NaHCO$_3$ (2x, 20 mL) and a saturated aqueous solution of NaCl (20 mL) respectively. The organic phase was dried with magnesium sulphate, filtered and the filtrate was collected. The dichloromethane was removed at low pressure and the residue was dried under vacuum to afford **72** as a brown oil, 0.10 g, 0.37 mmol, 63 %.
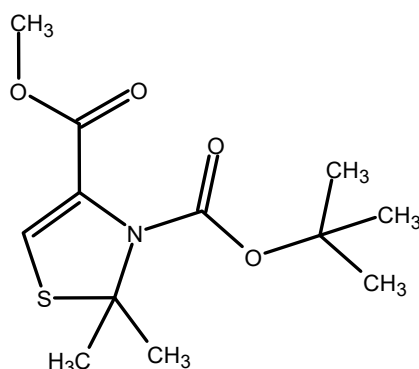
Figure 2.16: Compound **72** (*trans* rotamer).

Molecular Formula: C$_{12}$H$_{19}$NO$_4$S; R$_f$ (ethyl acetate/hexane, 1:6): 0.3 (single spot).

^{1}H NMR (400 MHz, CDCl$_3$) δ (only one rotamer at 298 K, possibly *trans*): 1.45 (s, 9H, [3 x C<u>H</u>$_3$]-O-CO), 1.86 (s, 6H, S-C-[2 x C<u>H</u>$_3$]), 3.77 (s, 3H, C<u>H</u>$_3$-CO-C), 6.58 (s, 1H, N-C-C<u>H</u>) ppm.

IR (ATR): ν = 1245 (w, C-H), 1384 (w, C-H), 1655 (s, C=O carbamate), 1738 (s, C=O ester), 2932 (w, C-H) cm^{-1}.

2.3.17 2-Methoxythiazole-4-carboxylic acid (74)

To a stirred solution of ethyl 2-chlorothiazole-4-carboxylate (0.50 g, 2.61 mmol) in acetonitrile-methanol mixture (10 mL, 1:1) was added 25 % sodium methoxide in methanol (2.68 mL, 11.74 mmol, 4.5 eq.) followed by 2M sodium hydroxide solution (5.09 mL, 10.18 mmol, 3.9 eq.). The resulting mixture was heated at reflux overnight and allowed to cool to ambient temperature. The reaction solvent was removed at low pressure and the residue was acidified with 6M hydrochloric acid. The crude product was extracted with ethyl acetate (3x, 30 mL), dried with magnesium sulphate, filtered, and the filtrate

collected. The filtrate was concentrated, hexane (50 mL) was added to the flask, and the flask was kept at 0°C for 30 minutes. The crystal formed was separated by vacuum filtration while the filtrate was subjected to further crystallisation and the subsequent crystals formed were collected as well. The first and second batches of crystals were combined and dried under vacuum to afford compound **74** as an off-white solid, 0.11 g, 0.69 mmol, 26 %.
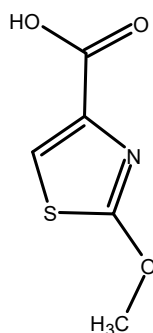
Figure 2.17: Compound **74**.

Molecular Formula: $C_5H_5NO_3S$; R_f (MeOH/DCM/acetic acid, 1:4:0.3 %): 0.33 (single spot), melting point:147.7 – 149.8 °C

^{1}H NMR (400 MHz, DMSO-d_6) δ 4.04 (s, 3H, C-O-C$\underline{H}_3$), 7.85 (s, 1H, C=C$\underline{H}$-S), 12.90 (s, 1H, COO$\underline{H}$) ppm.

IR (ATR): ν = 736 (s, C=C), 1093 (m), 1227 (s, C-O), 1423 (m, C-H), 1531(s), 1602 (w, C=C), 1699 (s, C=O), 3120 (w, O-H) cm^{-1}.

2.3.18 2-Oxo-2,3-dihydrothiazole-4-carboxylic acid (75)

To a stirred solution of **74** (0.06 g, 0.38 mmol) in tetrahydrofuran (10 mL) was added phosphorus tribromide (0.08 mL, 0.80 mmol, 2.1 eq.) and the resulting mixture was heated at reflux overnight. Distilled water (5 mL) was added to the reaction mixture and allowed to cool to ambient temperature. The mixture was diluted with ethyl acetate (40 mL), dried with magnesium sulphate, and filtered and the filtrate was concentrated at low pressure. The concentrate was placed in an ice-bath and the crystals formed were collected by filtration. The filtrate was subjected to further crystallisation (twice) and the subsequent crystals formed were collected as well. The crystals were combined and dried under vacuum to afford compound **75** as a white powder, 0.03 g, 0.21 mmol, 55 %.
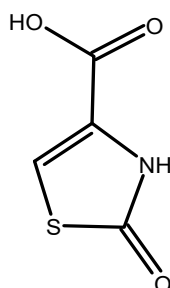
Figure 2.18: Compound **75**.

Molecular Formula: $C_4H_3NO_3S$; R_f (MeOH/DCM/Acetic acid, 1:3:0.3 %): 0.24 (single spot); melting point: 238.0 – 242.1 °C.

^{1}H NMR (400 MHz, DMSO-d_6) δ 7.30 (s, 1H, C=C<u>H</u>-S), 11.77 (s, 1H, N<u>H</u>-C=CH), 13.48 (s, 1H, COO<u>H</u>) ppm.

IR (ATR): ν = 695 (s), 735 (s, C=C), 1204 (s), 1417 (w), 1598 (s, C=C), 1710 (s, C=O), 3094 (w, O-H/N-H), 3146 (w, O-H/N-H) cm^{-1}.

2.3.19 Methyl 2-oxo-2,3-dihydrothiazole-4-carboxylate (76)

To a stirred solution of **75** (0.54 g, 3.72 mmol) in methanol (40 mL) was added concentrated hydrochloric acid (7.70 mL, 93.77 mmol, 25 eq.). The resulting mixture was heated at reflux overnight and allowed to cool to ambient temperature. The reaction solvent was removed at low pressure and the crude product was purified by flash chromatography (methanol/dichloromethane, 1:20) to afford compound **76** as an off-white solid 0.21 g, 1.32 mmol, 35 %.
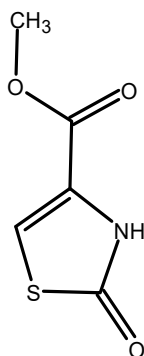
Figure 2.19: Compound **76**.

Molecular Formula: $C_5H_5NO_3S$; R_f (MeOH/DCM 1:20): 0.49 (single spot), melting point: 135.0 – 136.4 °C.

^{1}H NMR (400 MHz, DMSO-d_6) δ 3.79 (s, 3H, C<u>H$_3$</u>-O-C), 7.42 (s, 1H, C=C<u>H</u>-S), 11.97 (s, 1H, N<u>H</u>-C=CH) ppm.

IR (ATR): ν = 769 (s, C=C), 993 (s), 1188 (s, C-O), 1240 (s), 1300 (s), 1449 (m, C-H), 1580 (m, C=C), 1653 (s, C=O), 1721 (s, C=O), 2955 (w, O-H/N-H), 3050 (w, O-H/N-H), 3122 (w, O-H/N-H) cm^{-1}.

2.3.20 (S)-Methyl-1-(3-bromo-3-methyl-2-oxobutanoyl)pyrrolidine-2-carboxylate (81)

To a stirred solution of (S)-methyl pyrrolidine-2-carboxylate hydrochloride (1.00 g, 6.04 mmol, 1.3 eq.) and triethylamine (1.85 mL, 13.28 mmol, 2.9 eq.) in anhydrous dichloromethane (10 mL), at 0 ºC, was added compound **50** (corrected mass/molarity: 0.99 g, 4.64 mmol, dissolved in 5 mL dichloromethane), at a rate to maintain the reaction temperature ≤ 5 ºC. The resulting mixture was stirred at 0 ºC for 2 hours and allowed to gradually warm up to ambient temperature overnight. The mixture was diluted with dichloromethane (20 mL) and washed with 1N HCl (2x, 20 mL), a saturated aqueous solution of NaHCO$_3$ (2x, 20 mL) and a saturated aqueous solution of NaCl (20 mL) respectively, and dried with magnesium sulphate, filtered and the filtrate was collected. The filtrate was concentrated under low pressure and the crude concentrate was subjected to flash chromatography (ethyl acetate/hexane, 1:6) to afford **81** as a pale yellow oil, 0.48 g, 1.57 mmol, 34 %.
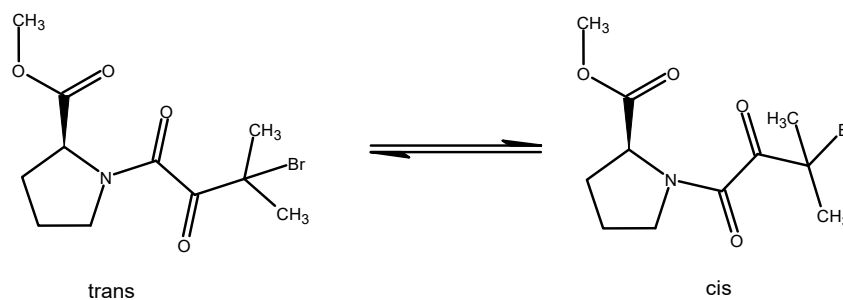
Figure 2.20: Compound **81** (*cis*/*trans*).

Molecular Formula: $C_{11}H_{16}BrNO_4$; R_f (ethyl acetate/hexane, 1:6): 0.13 (single spot).

^{1}H NMR (400 MHz, CDCl$_3$) δ (two rotamers, *cis* and *trans*, at 298 K; ratio isomers, 1:3): 1.87 (*cis* and *trans*, overlapping m, 1H, [2 x C$\underline{H}_3$]-C-Br), 1.98 (*cis* and *trans*, overlapping m, 4H, N-CH-CH$_2$-C$\underline{H}_2$-CH$_2$), 2.06 (*cis* and *trans*, overlapping m, 11H, [2 x C$\underline{H}_3$]-C-Br), 2.16 (*cis*/*trans*, overlapping m, 2H, N-CH-C$\underline{H}_2$-CH$_2$-CH$_2$), 2.28 (*cis*/*trans*, overlapping m, 2H, N-CH-C$\underline{H}_2$-CH$_2$-CH$_2$), 3.69 (*cis* and *trans*, overlapping m, 4H, N-CH-CH$_2$-CH$_2$-C$\underline{H}_2$), 3.76 (*cis* and *trans*, d, *J* = 0.9 Hz, 6H, C$\underline{H}_3$-O-CO), 4.59 (*cis* and *trans*, overlapping m, 1.5H, N-C$\underline{H}$-CH$_2$-CH$_2$-CH$_2$), 4.60 (*cis*/*trans*, dd, *J* = 8.5, 2.9 Hz, 0.5H, N-C$\underline{H}$-CH$_2$-CH$_2$-CH$_2$) ppm.

IR (ATR): υ = 1112 (w), 1174 (s, C-O ester), 1433 (w, C-H), 1641 (s, C=O amide), 1709 (s, C=O ester) cm^{-1}.

MS (+ESI) m/z = Found 306.0339 (M+H)$^+$; calculated for $C_{11}H_{17}O_4NBr$ 306.0335; 1.2 ppm; [79]Br.

2.4 **Discussion of experimental results**

Different synthetic schemes and methods were applied in the attempted syntheses of the target compound **48** as well as its precursors. The structure of the target compound/precursor was modified where the synthesis of the actual target proved impossible. Schemes 2.1 - 2.13 show the various synthetic routes involved in the formation/attempted syntheses of the respective compounds as well as the potential reaction mechanisms. The structural characterisation of the synthesised compounds by spectroscopic methods revealed the presence of unique features associated with these respective compounds while purity characterisation by TLC and melting point analysis showed no traceable impurities in most of the compounds and narrow melting point range respectively.

2.4.1 Syntheses of 52 and its precursors (Scheme 2.1)
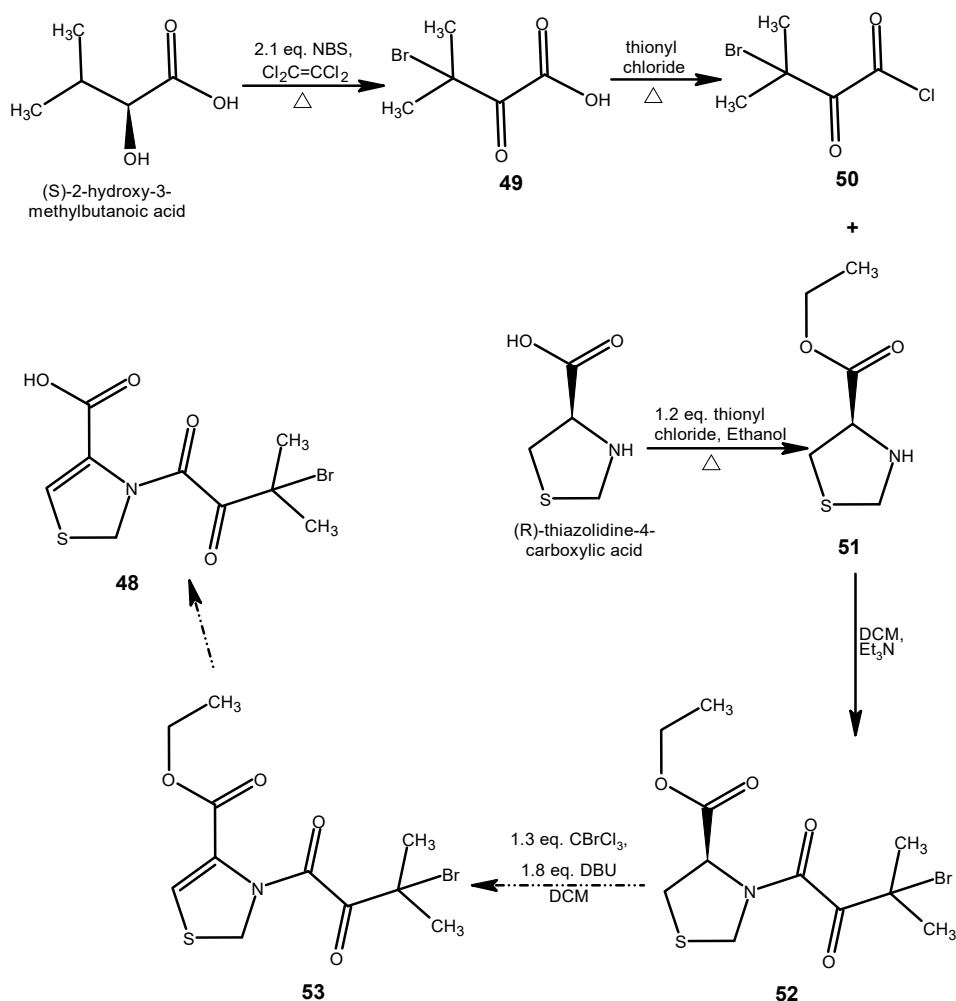
Scheme 2.1: Attempted synthesis of ethyl 3-(3-bromo-3-methyl-2-oxobutanoyl)-2,3-dihydrothiazole-4-carboxylate (**53**).

The precursor of the target compound **48** is structurally made up of two moieties, the aliphatic bromo-oxobutanoic acid and the heterocyclic thiazolidine ester. The respective moieties were prepared separately and later coupled to form the ester **52**. The aliphatic intermediate/moiety, bromo-oxobutanoic acid **49**, was prepared (Scheme 2.1) in good yield by the treatment of the (S)-2-hydroxy-3-methylbutanoic acid with the oxidising/brominating agent, N-bromosuccinimide, in an aprotic solvent (Muneeswara *et al*., 2019). Compound **49** is moisture sensitive and prone to decomposition, as evidenced by the study of Crout and Hedgecock (1979), hence partial eradication of the succinimide impurity was achieved by the vacuum filtration method. The substitution of carbon tetrachloride by tetrachloroethylene improved the crude yield of **49** and simultaneously decreased the amount of succinimide impurity in the product, possibly due to its (succinimide) poor solubility in tetrachloroethylene at low to ambient temperature (10-20 ºC).

2.4.1.1 Mechanism of N-bromosuccinimide – oxidation and substitution reactions

The N-bromosuccinimide (NBS) acts as an oxidizing agent as well as a brominating agent. It oxidizes the hydroxyl group of the (S)-2-hydroxy-3-methylbutanoic acid to the corresponding carbonyl group as well as replaces the proton attached to the tertiary carbon with bromine as judged by proton NMR and mass spectroscopy analysis. Expectedly, the proton NMR result is supported by the findings of Easton *et al*. (1988). Easton and co-workers (1988) treated N-benzoylvaline methyl ester with 2 eq. of NBS in carbon tetrachloride and the proton NMR result of the product showed the successful substitution of the proton, attached to the tertiary carbon, with bromine as well as oxidization of the N-benzoylamine group to the corresponding keto group.

A plausible reaction pathway for the transformation of (S)-2-hydroxy-3-methylbutanoic acid to compound **49** involves the oxidizing agent reacting with the hydroxyl group of the chiral carbon (Scheme 2.2), generating an unstable hypobromite intermediate that decomposes to the corresponding 3-methyl-2-oxobutanoic acid through the elimination of hydrogen bromide. An oxonium ion is generated by the protonation of the carbonyl of the 3-methyl-2-oxobutanoic acid with the concomitant release of bromine radical which attract the -CH$_3$-C**H**-CH$_3$- proton to form the enol derivative. The unsaturated carbonyl group of the enol derivative attacks the molecular bromine, which is formed from the reaction of N-bromosuccinimide with hydrogen bromide (Scheme 2.2), to give the oxonium intermediate with a C-Br bond (-CH$_3$-C**Br**-CH$_3$-). The newly released bromine radical facilitates the deprotonation of the brominated oxonium intermediate to afford the bromo-oxobutanoic acid **49** (Muneeswara *et al*., 2019). The formation of the molecular bromine, from the reaction of N-bromosuccinimide and hydrogen bromide, involves the protonation of one of the carbonyl oxygens of N-bromosuccinimide, due to the lone pair electron on the nitrogen, thus forming the corresponding unstable oxonium ion. The stabilisation of the oxonium ion is achieved by the migration of the positive charge, on the oxygen, to the neighbouring carbon, followed by the migration of the nitrogen's lone pair of electrons towards the positively charged carbon, thus generating an iminium ion with a C=N bond and a positively charged nitrogen. The positively charged iminium nitrogen would polarise the N-Br bond's electrons towards itself, generating a positively charged bromine (N$^-$ - Br $^+$). The polarisation of electrons in hydrogen bromide is towards the bromine, hence the generation of negatively charged bromine (Br$^-$) and a proton, which is the protonating agent of the N-bromosuccinimide carbonyl oxygen as earlier mentioned. The Br $^+$ of the iminium ion reacts with the Br $^-$ to form the molecular bromine (Br$_2$).
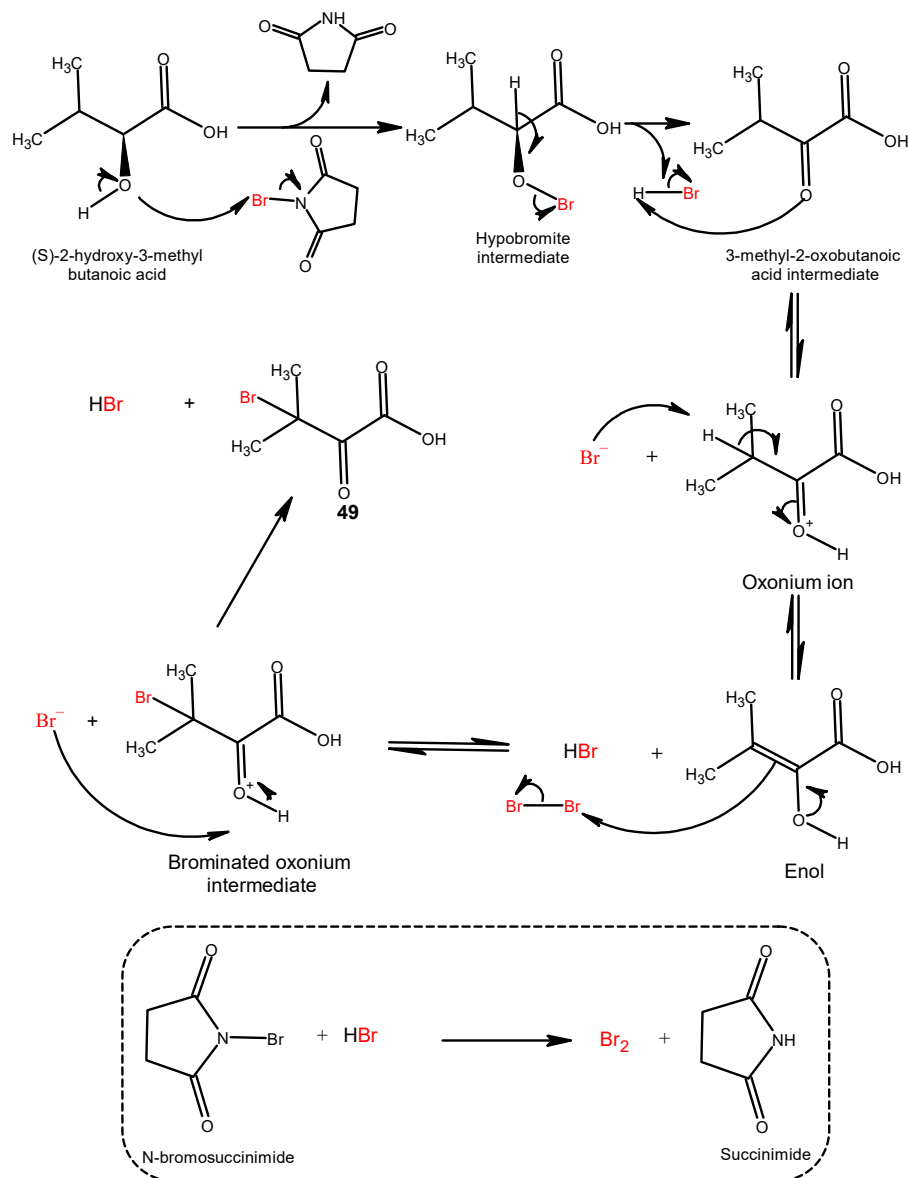
Scheme 2.2: Plausible reaction pathway for the formation of **49** (Adopted from Muneeswara *et al*., 2019).

2.4.1.2 **Conversion of carboxylic acid 49 to acid chloride 50**

R = 2-bromo-2-methyl propanoyl
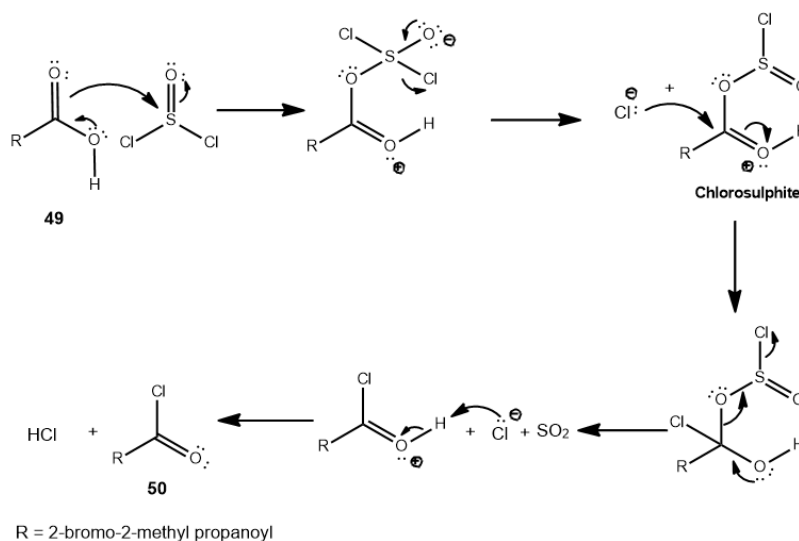
Scheme 2.3: Plausible reaction pathway for the formation of **50 (**Montalbetti and Falque, 2005; Green and Thorp, 1967).

Following the modified method of Seitz *et al*. (2016), the treatment of **49** with thionyl chloride afforded the acid chloride derivative **50** (Scheme 2.1)**,** in good yield. The plausible mechanism, for the formation of compound **50** (Scheme 2.3), involves the carboxylic acid-induced nucleophilic attack on the sulphur of the thionyl chloride (an electrophile) forming an intermediate with an O-S bond linking the carboxylic acid and the thionyl chloride. The formation of a double bond between the oxygen atom and the sulphur atom prompts a nucleophilic attack which triggers the expulsion of one of the chloride ions and the generation of a chlorosulphite intermediate with a good leaving group. The expelled chloride ion acts as a nucleophile and attacks the carbonyl electrophilic carbon of the chlorosulphite intermediate to form an unstable tetrahedral species which stabilises by the expulsion of the chlorosulphite's chloride ion and concomitant formation of sulphur dioxide. The recently expelled chloride ion acts as a base and attacks the proton attached to the carbonyl, thus forming a hydrogen chloride gas and the acid chloride **50**.

2.4.1.3 Esterification reaction - 51

The heterocyclic ester **51** was afforded, in excellent yield and purity, by thionyl chloride-induced esterification of L-4-thiazolidine carboxylic acid in ethanol (Pellegrini *et al*., 1999) (Scheme 2.1) while the initial synthetic attempt using 1.2 eq. acetyl chloride in ethanol, according to the published method of Hansen and Krogsgaard-Larsen (1980), did not yield the desired product possibly due to the insolubility of L-4-thiazolidinecarboxylic acid in acetyl chloride-ethanol mixture at varying temperatures - 0 °C, ambient and elevated temperatures.

Furthermore, having the intermediates (**49/50** and **51**) to hand, attempts were made to induce amidation of the heterocyclic ester **51**. Firstly, an effort was made to synthesise compound **52** through the coupling of compound **51** with the bromo-oxobutanoic acid **49** using 1.3 eq. of 1,1'-carbonyldiimidazole (CDI) in tetrahydrofuran (THF) at ambient temperature following the published method of Woodman *et al*., 2009. The product obtained, after aqueous workup and purification, was analysed by proton NMR. Unfortunately, the NMR spectrum was unsatisfactory as it showed a mixture of compounds and the absence of significant peaks such as the peak correlating to the aliphatic [2 x C$\underline{H}_3$]-C-Br protons but peaks correlating to the ester group (C$\underline{H}_3$-C$\underline{H}_2$-O) of the heterocyclic thiazolidine seemed to be present. The unsatisfactory outcome of the attempted CDI-mediated amidation might be due to the low reactivity of the acylimidazole species, released after the elimination of carbon dioxide, in the presence of heterocyclic thiazolidine. Secondly, in an attempt to generate a more reactive coupling-intermediate species, compound **51** was treated with **49** in anhydrous *N,N*-dimethylformamide (DMF), using 1 eq. N-(3-Dimethylaminopropyl)-N'-ethylcarbodiimide hydrochloride (EDC.HCl) in the presence of 1 eq. of 1-hydroxybenzotriazole hydrate (HOBt), at ambient temperature, in accordance with the published method by mimoto *et al*., 1999. There was no significant turnover of the starting material (compound **51**) after stirring for 2.5 days, as judged by TLC, despite the complete solubility of the reactants as well as the coupling additive, whereas the coupling of the acid chloride derivative **50** with the thiazolidine ester **51** in the presence of a base (Scheme 2.1), gave **52** in low yield (37 %) but excellent purity as judged by proton NMR, mass (MS) and infrared spectroscopy (IR) and thin layer chromatography (Zhao *et al*.,2006).

2.4.1.4 Ambiguity of ^{1}H NMR spectrum of 52 and synthesis of 55
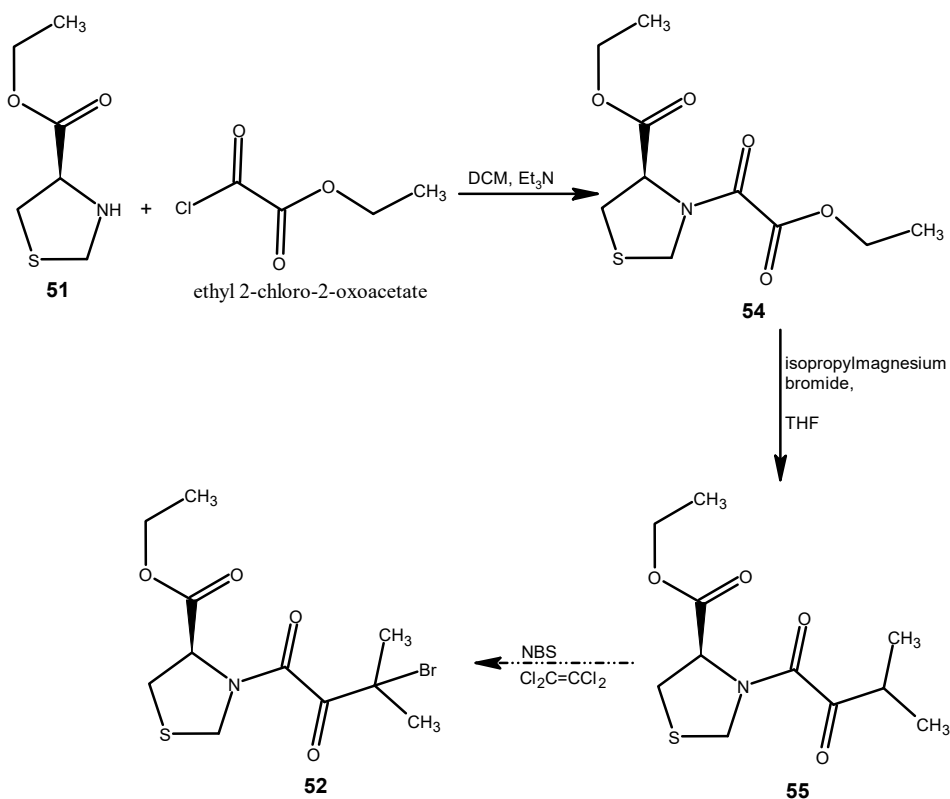
Scheme 2.4: Syntheses of (R)-ethyl 3-(3-methyl-2-oxobutanoyl)thiazolidine-4-carboxylate **55** and its precursor.

Although the IR result of **52** showed the expected functional groups were present, but the initial ^{1}H NMR characterisation, before MS analysis, was challenging due to the complexity of the ^{1}H NMR spectrum with integration of almost twice the protons of the desired compound. Based on the ambiguity of the ^{1}H NMR spectrum, especially signals correlating to -N-C$\underline{H}$-CH$_2$- and -S-C$\underline{H}_2$-N- protons respectively, it seemed there was formation of a different compound, possibly through cyclisation to give a bicyclic derivative, as a result of the presence of reactive bromo/carbonyl groups. Considering the lack of definite confirmation of the structure of **52**, based on the ambiguity of the proton NMR result, a different synthetic plan was adopted (Scheme 2.4) and **54** was obtained, in excellent yield, via acylation of compound **51** with ethyl 2-chloro-2-oxoacetate in the presence of a base, triethylamine, while the ethoxyl group of the dicarbonyl fragment of **54** was selectively substituted by isopropyl under the treatment with isopropylmagnesium bromide at -78 °C to afford **55** in moderate yield as judged by proton NMR, IR and mass spectroscopy analysis (Zhao *et al*., 2006). To our surprise **54** and **55** displayed the same ambiguity (^{1}H NMR spectrum) as compound **52,** especially at the same molecular regions -N-C$\underline{H}$-CH$_2$- and -S-C$\underline{H}_2$-N- respectively. This outcome nullifies the hypothesis of off-target product formation as a consequence of the presence of the bromo group.

2.4.2 Modification of target I - Syntheses of 58 and 59

In light of the ambiguity of the ^{1}H NMR spectra of **52**, **54** and **55** respectively especially at the -N-C$\underline{H}$-CH$_2$- and -S-C$\underline{H}_2$-N- molecular regions respectively, the methylene group (-S-C$\underline{H}_2$-N-) of the thiazolidine ring was substituted with dimethyl group, **56** (Refouvelet *et al.*, 1994; Sako *et al.*, 1992), and **57** as well as **58** were obtained (Scheme 2.5), in excellent and moderate yield respectively, via acylation of **56** with ethyl 2-chloro-2-oxoacetate in the presence of triethylamine, and isopropylmagnesium bromide treatment of the di-ethyl ester **57** respectively (Zhao *et al.*, 2006). The ^{1}H NMR spectra of **57** and **58** were straightforward with expected characteristic signals and integration respectively. Probing the reason(s) for the molecular structure-^{1}H NMR spectra variation of **54** and **55** versus **57** and **58** led to further insight into the rotational characteristics of the amide C-N bond of these compounds.
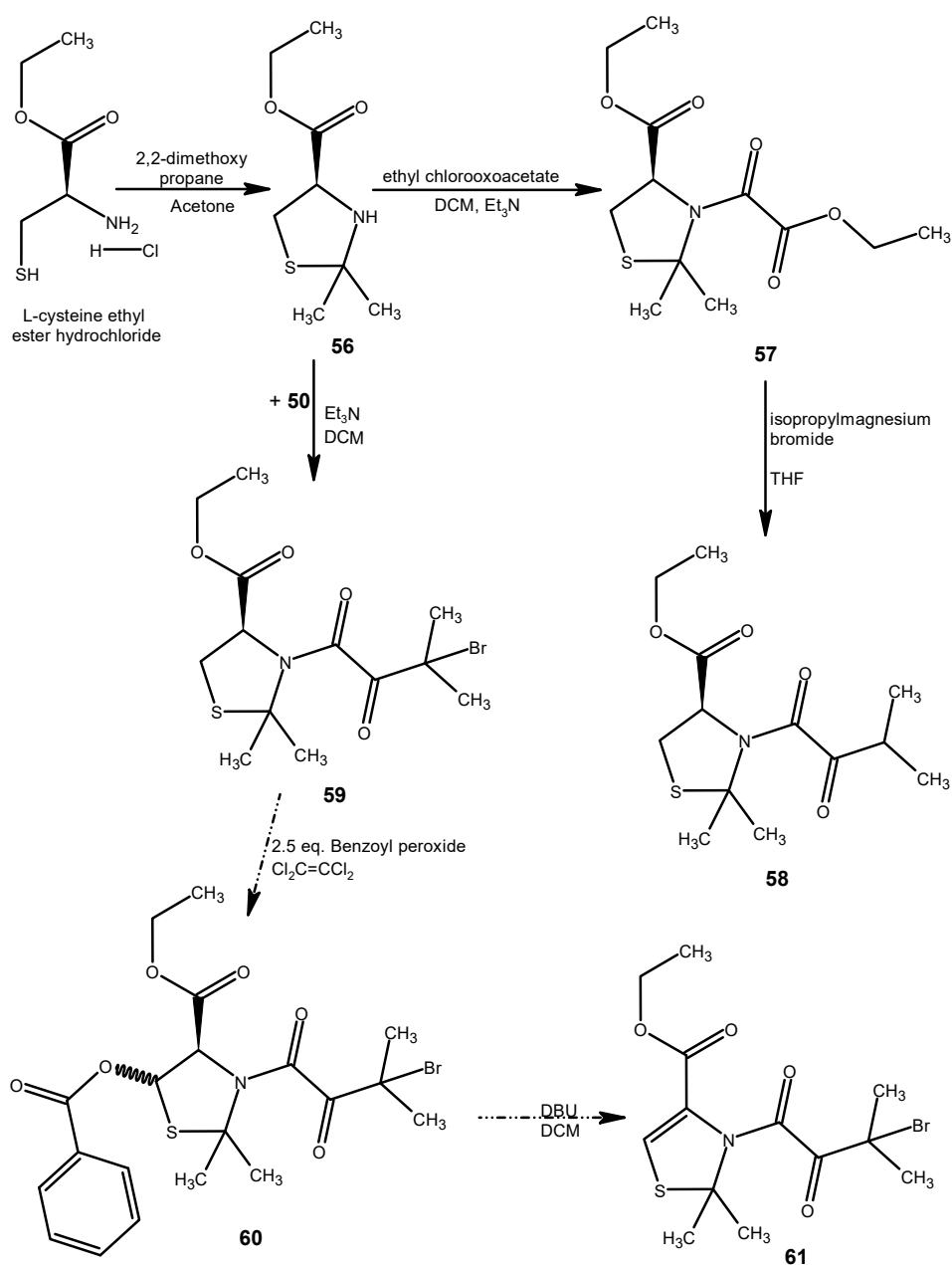
Scheme 2.5: Syntheses of (R)-Ethyl2,2-dimethyl-3-(3-methyl-2-oxobutanoyl) thiazolidine-4-carboxylate **58** and its precursors.

2.4.3 Amide bond rotation – *cis-trans* rotamers (52, 54 and 55)

$R_1 = COOCH_3, COOCH_2CH_3$

$R_2 =$

X = C, S
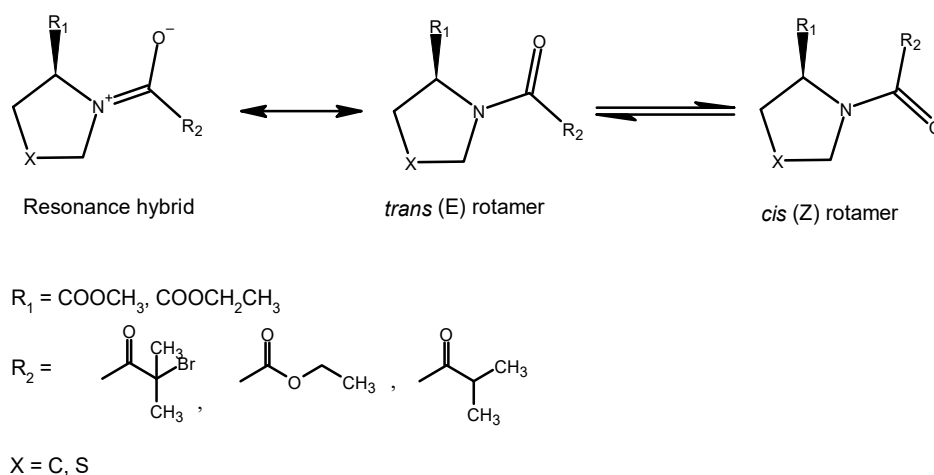
Scheme 2.6: Annotated representation of *cis-trans* isomerisation.

In contrast to a single bond, rotation about a double bond is highly restricted, hence some molecules with a double bond can exist as a pair of geometrical isomers (Perrin, 2003). For example, 2-butene exists as both Z (*cis*) and E (*trans*) isomers respectively. Interestingly, amides (Scheme 2.6) display unique characteristics as they can exist structurally in three different forms (species) with rotation about the C-N bond of one of the species (resonance hybrid) highly restricted, due to the presence of partial double bond, while the other two species (rotamers) are interconvertible as a result of rotation about the C-N bond. The partial double bond of the resonance hybrid is generated by the delocalisation of the lone pair on the nitrogen into the pi bond (C=N). Generally, *cis* (Z) secondary amides are less stable than *trans* (E) secondary amides, as a consequence of the steric repulsive interaction between the side chains which are absent in the *trans* (E) secondary amides. Although the trans conformation is more favoured (Kubyshkin and Budisa, 2017), *cis* (Z) and *trans* (E) amides interconvert rapidly at room temperature but they occur as separate species when analysed by the NMR technique (Perrin, 2003). Considering the above information, it seemed likely that the *cis* and *trans* rotamers of compounds **54** and **55** respectively exist in solution and the respective *cis/trans* rotamers are detected on the NMR time scale due to the slow *cis↔trans* interconversion of the tertiary amide rotamers, hence the duplicity of protons of compounds **54** and **55** respectively (Figures 2.5 and 2.6) (de Koning *et al.*, 2003). Theoretically, the absence of *cis-trans* isomerisation in **57** and **58** (Figures 2.8 and 2.9) may be due to the steric repulsion of the dimethyl group. However, there may be some exceptions as in the case of compounds **70** and **71** respectively (Figures 2.14 and 2.15) where the steric repulsion of the dimethyl group may not be absolute. The revelation of the *cis-trans* isomerisation of **54** and **55**, at ambient temperature, confirmed **52** (Figure 2.4) exhibits the same property with unexpected ^{1}H NMR spectrum as a consequence of the hindered rotation.

2.4.4 Coalescence formation – variable temperature ^{1}H NMR

To further validate the hypothesis that compound **52** exists as rotamers (*cis/trans*) that are detectable on the NMR time scale owing to the slow *cis↔trans* interconversion, **52** was subjected to variable temperature ^{1}H NMR analysis (DMSO) 298 - 348K (Figure 2.21), to determine if coalescence of the

signals correlating to the heterocyclic ring protons near the amide bond (-N-C$\underline{H}$-CH$_2$- and -S-C$\underline{H}_2$-N- respectively) would be formed (Huggins *et al*., 2020; Lanyon-Hogg *et al*., 2015).

The isomerisation of the rotamer species of **52** changes the environment of the protons near the amide bond (-N-C$\underline{H}$-CH$_2$- and -S-C$\underline{H}_2$-N-), through the process called a chemical exchange, such that the chemical shift of these protons differs with respect to the cis and trans configuration because these protons are in non-equivalent environment. At a low temperature of 298 K, the exchange is slow and the individual species (*cis* and *trans* rotamers) are observed in the NMR spectrum, hence the peaks at 4.98 and 4.91 ppm for -N-C$\underline{H}$-CH$_2$- protons and peaks at 4.78, 4.60 and 4.51 ppm for the -S-C$\underline{H}_2$-N- protons respectively. As the temperature progresses, it is expected that the rotational barrier would be progressively subdued and the difference in the resonance frequency (Δv)/chemical shifts of -N-C$\underline{H}$-CH$_2$- and -S-C$\underline{H}_2$-N- peaks respectively would decrease forming two overlapping broad peaks. Interestingly, at 323 K, the minor peaks at 4.91 ppm (-N-C$\underline{H}$-CH$_2$-) seemed to split without a noticeable change in chemical shift while there was an insignificant change in the chemical shift of the -S-C$\underline{H}_2$-N- protons but at 333 K, the difference between the major (4.98 ppm) and minor (4.96 ppm) peaks for -N-C$\underline{H}$-CH$_2$- protons decreases by 0.02 ppm while the peak at 4.78 ppm (-S-C$\underline{H}_2$-N-) continues to shift away from TMS (4.81 ppm) without any observable changes in other two peaks (4.60 and 4.51 ppm). At a certain temperature, called the coalescence temperature, it is expected that the two broad peaks would harmonise into a single flat-topped peak (coalescence) while above the coalescence temperature, when the rate of exchange is faster, a single sharp peak corresponding to the respective -N-C$\underline{H}$-CH$_2$- and -S-C$\underline{H}_2$-N- protons would be observed (Huggins *et al*., 2020; Lanyon-Hogg *et al*., 2015; de Koning *et al*., 2003). At 348 K, there seemed to be a gradual formation of coalescence for the -N-C$\underline{H}$-CH$_2$- peaks while such formation was not observed for the -S-C$\underline{H}_2$-N- peaks.

Unfortunately, the hypothesis of **52** existing as *cis* and *trans* rotamers, and by extension compounds **54** and **55** respectively, using variable temperature ^{1}H NMR analysis did not give a satisfactory outcome possibly because the maximum experiment temperature (348 K) was below the coalescence temperature at the field strength of the magnet (^{1}H NMR at 400 MHz).
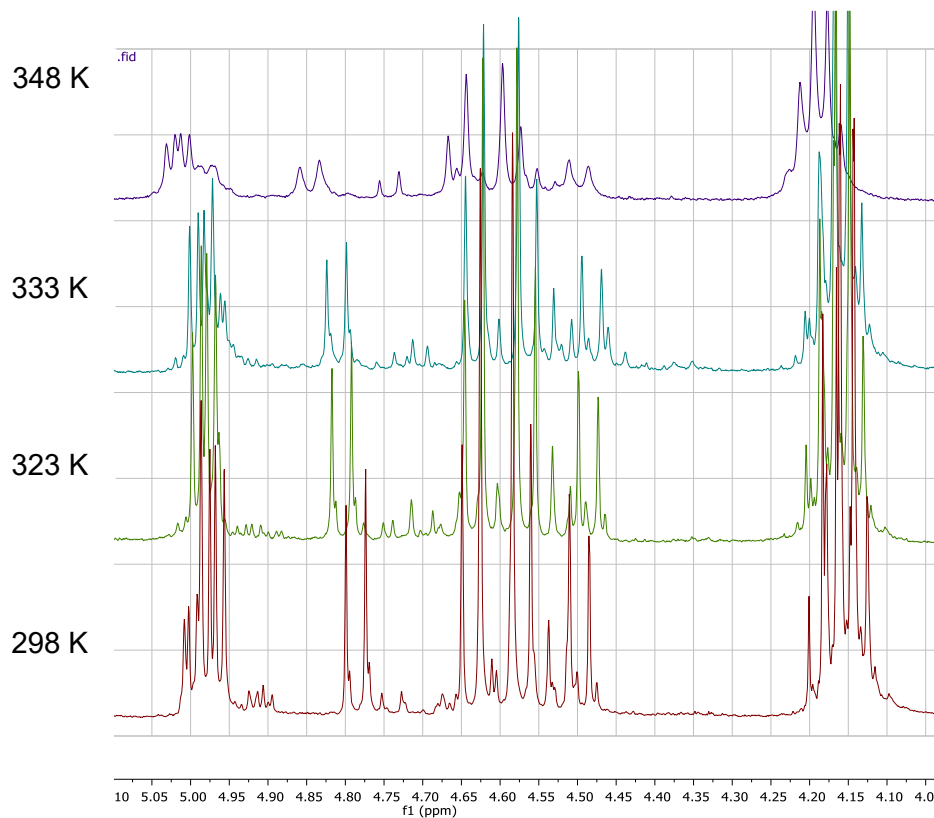
Figure 2. 21: Variable temperature ^{1}H NMR spectroscopy of **52**.

2.4.5 Attempted dehydrogenation of the thiazolidine ring in 62
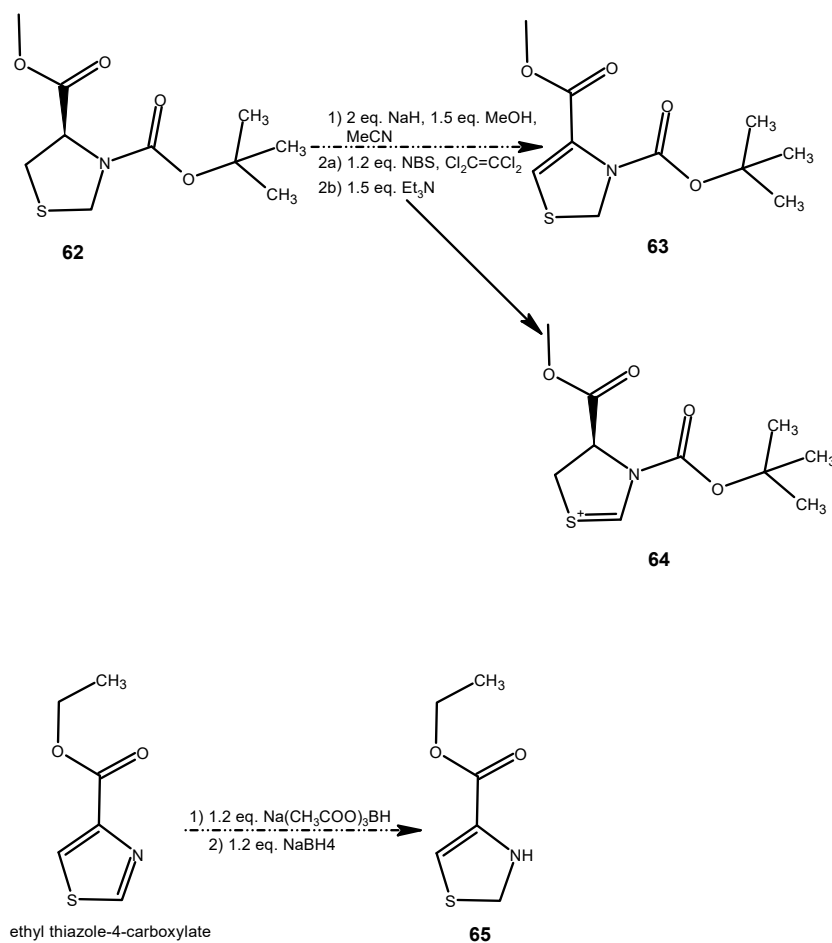
Scheme 2.7: Attempted syntheses of compounds **63** and **65**.

Following the validation that the unexpected ^{1}H NMR spectrum of **52** is consistent with its structure and the MS analysis gave the correct mass, several experiments to synthesise the bromo-dehydrothiazole carboxylate derivative **53** (Scheme 2.1), via several published methods yielded either no product or a complex mixture or off-target at best.

First, following the published method of Gracia-Victoria *et al.* (2018), **52** was treated with 1.3 eq. bromotrichloromethane (CBrCl$_3$), in dichloromethane (DCM), in the presence of 1.8 eq.1,8-diazabicyclo-[5.4.0]undec-7-ene (DBU) at 0 ºC and the reaction mixture was stirred at 0 – 8 ºC for 24 hours during which the colourless solution turned brown (Scheme 2.1). Disappointingly, there was no turnover of the starting material, as evidenced by TLC and ^{1}H NMR spectroscopy, despite repeating the experiment at 25 ºC and 35 ºC. Two possible scenarios were assumed as the reasons the reaction did not occur.

It was postulated that either the bromine was not released from CBrCl$_3$, hence there was no substitution of ring proton attached to the chiral carbon, or the bromine was released but was mopped up by the base before the substitution reaction. To validate if the bromine was released, **52** was treated with 1.3 eq. CBrCl$_3$ in DCM at the aforementioned varied temperatures for 2, 5, and 12 hours respectively before the addition of the DBU. Unfortunately, the outcome was not different from the initial experiments. This indicates that either the bromine was not released or it was released but could not substitute any ring protons under the varied experimental conditions. Similarly, there was no product formation (**63**) when DBU was substituted with 2 eq. sodium hydride (NaH) in the treatment of (R)-3-*tert*-butyl 4-methyl thiazolidine-3,4-dicarboxylate (**62**), in acetonitrile at 60 ºC, in the presence of 1.5 eq. dry methanol (Chorell *et al.*, 2007) (Scheme 2.7) while attempts to transform ethyl thiazole-4-carboxylate to ethyl 2,3-dihydrothiazole-4-carboxylate (**65**) via selective reduction of the N=C bond with 1.2 eq. sodium triacetoxyborohydride and 1.2 eq. sodium borohydride respectively (Scheme 2.7), in DMF, aqueous methanol and THF respectively, at 21 ºC, 31 ºC and 70 ºC respectively, were unsuccessful as there was no reaction as evident by TLC and proton NMR spectroscopy (Bonvicino and Hennessy, 1957).

Furthermore, the treatment of **52** and **62** respectively with 2 eq. NBS in tetrachloroethylene followed by the addition of 2 eq. triethylamine (Et$_3$N) resulted in the formation of complex mixtures, as evident by proton NMR spectroscopy, possibly due to the substitution of the two hydrogens in the ring methylene group (-CH$_2$-) by bromine (–C-Br$_2$-) and concomitant elimination of the bromine by Et$_3$N resulted in ring opening, while at lower NBS concentration of 1.2 eq. and 1.5 eq. of Et$_3$N (Schemes 2.7 and 2.8 respectively), an -S=CH-N- bond was unexpectedly formed (compounds **64** and **66** respectively), instead of the -N-C=CH- bond, as judged by proton NMR spectroscopy. This indicates that the ring -S-C<u>H$_2$</u>-N- protons are prone to halogen substitution compared to the -N-C<u>H</u>-C<u>H$_2$</u>- protons. Also, attempt to synthesise **53** (Scheme 2.8), via the treatment of **52** with 1.1 eq. benzoyl peroxide in tetrachloroethylene to obtain the benzoate analogue (**67**) that would be subjected to DBU treatment, following the published methods of Baldwin *et al.* (1975) and Allen *et al.* (1989) respectively was unsuccessful as the treatment of **52** with benzoyl peroxide gave complex mixtures as judged by proton NMR.
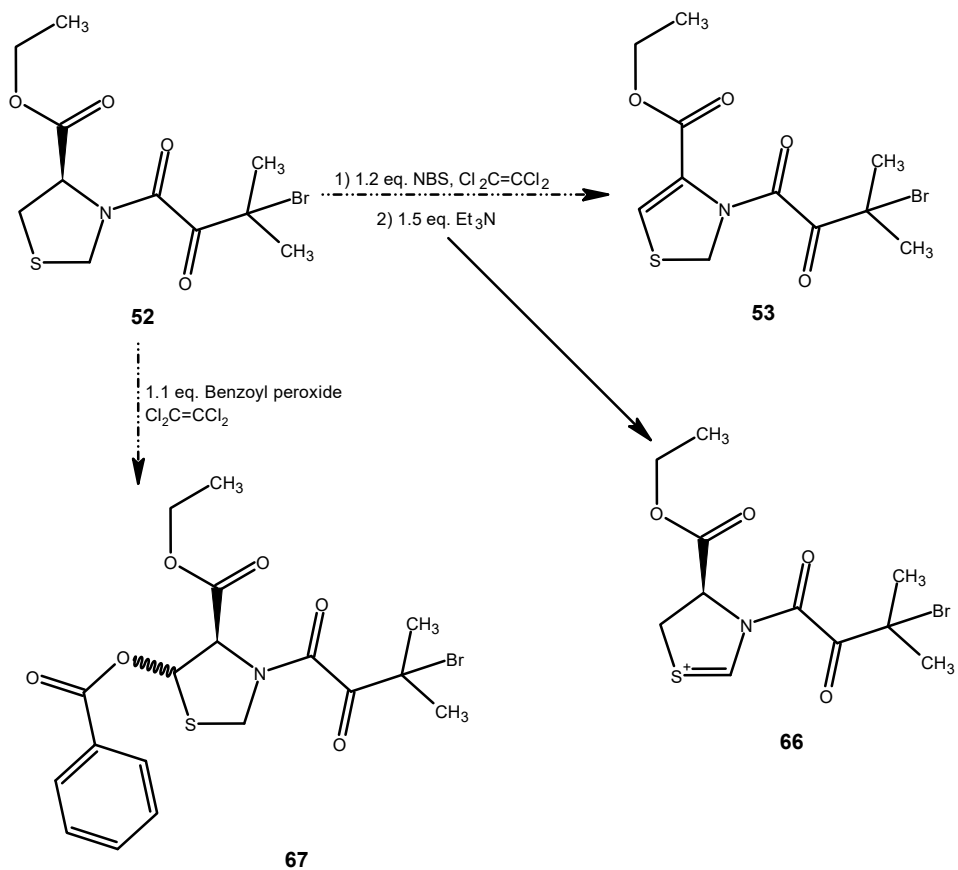
Scheme: 2.8: Attempted syntheses of **53** and **67** respectively.

2.4.6 Modification of target II – synthesis of 72
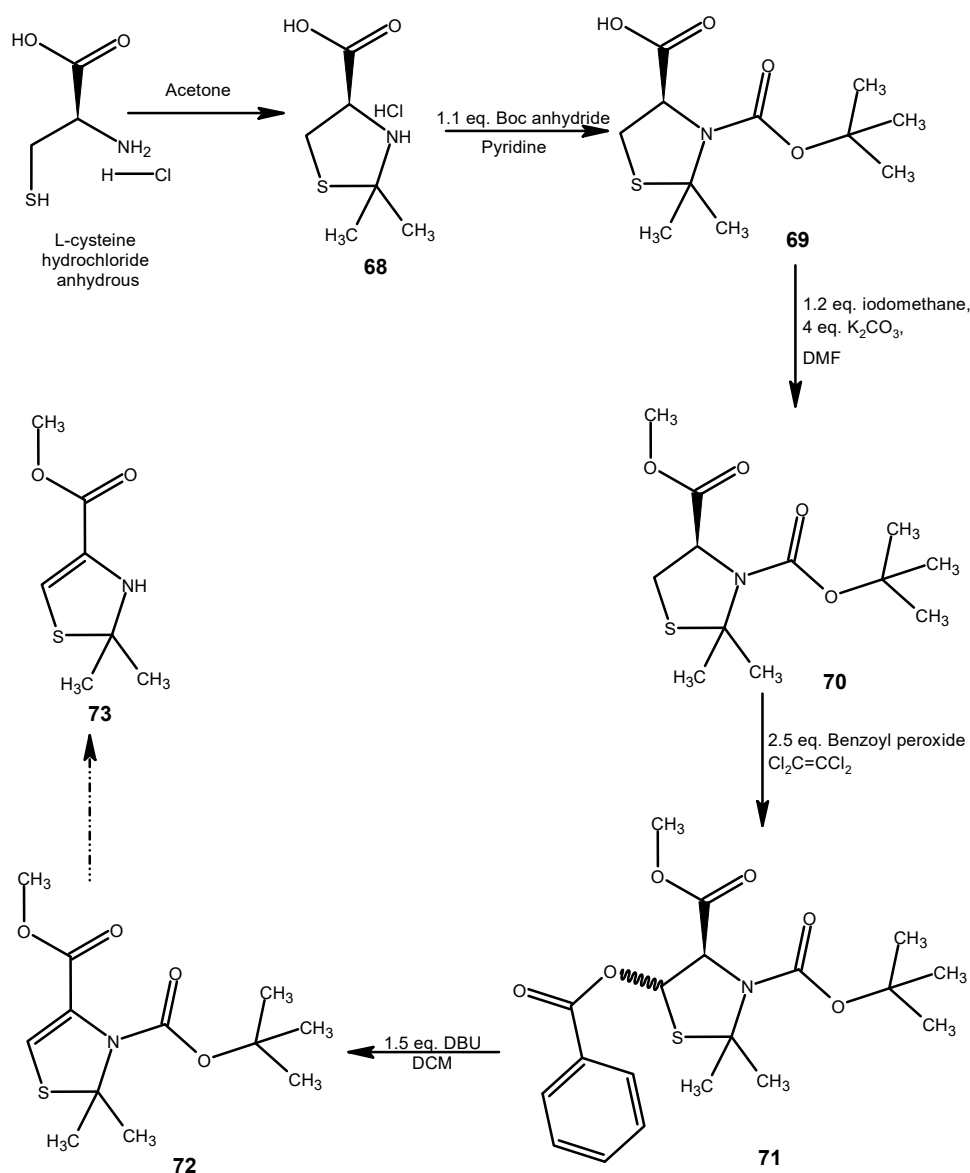
Scheme 2.9: Synthesis of 3-*tert*-butyl 4-methyl 2,2-dimethylthiazole-3,4(2H)-dicarboxylate **72** and its precursors.

As a result of the challenge in constructing -N-C=CH bond, the initial target (**52** and **48**) was modified and **59** was synthesised (Scheme 2.5), in poor yield, by acid chloride coupling of **56** with **50**. The initial attempt to synthesise **61** (-N-C=CH-) by subjecting **59** to 1.2 eq. NBS/1.5 eq. Et$_3$N treatments resulted in the formation of a charred mixture while a second trial was made by subjecting **59** to benzoyl peroxide treatment in tetrachloroethylene following the published method of Allen *et al*. (1989). Compound **59** was heated at reflux with 2.5 eq. benzoyl peroxide in the aprotic solvent, tetrachloroethylene, for 3 hours (Scheme 2.5). The crude product was diluted with ethyl acetate and subjected to aqueous work up and the potential compound (**60**) (≈70 % purity) was obtained in low yield by column chromatography. Proton NMR of the potential compound (**60**) showed substitution of one of the -N-CH-CH$_2$- protons by a benzoate group as judged by the absence of the CH$_2$ peak at 3.28 ppm and 3.35 ppm respectively with the concomitant appearance of the benzene ring (7.46, 7.59 and 8.03 ppms) and a CH peak, at 6.64 ppm, corresponding to the newly formed HC-O bond between the dimethylthiazolidine moiety and the

benzoate group. Unfortunately, the MS analysis indicates the absence of the desired product as the expected mass was not observed/detected.

Considering the MS result of **60**, a new synthetic plan (Scheme 2.9) was adopted which anchors on synthesising the dehydro-dimethylthiazole precursor **73** (–C=CH-S-) before coupling the bromo-keto fragment. Following the published protocol of Duthaler and Wyss (2011), **68** was synthesised in excellent yield by reaction of anhydrous L-cysteine hydrochloride in boiling acetone while the *N-tert*-butyloxycarbonylation treatment of **68** in pyridine afforded **69** in excellent yield (Duthaler and Wyss, 2011). The resulting product was esterified (**70**) by basic protocol (Pellegrini *et al.*, 1999) rather than the acid method due to its Boc group sensitivity to acid while the required unsaturation was introduced by treatment of **70** with 2.5 eq. benzoyl peroxide in tetrachloroethylene (Allen *et al.*, 1989; Baldwin *et al.*, 1975) and subsequent elimination of the resultant benzoate group **71** with 1.5 eq. DBU afforded the dehydro-dimethylthiazole derivative **72** using the modified method of Allen *et al.*, 1989. However, the attempt to cleave the Boc group (**73**), according to the published procedure by Suaifan *et al.*, 2006, using 10 % TFA in DCM followed by coupling (*in-situ*) of the resultant product with **50**, after the removal of the TFA, in the presence of 2 eq. Et$_3$N gave a complex mixture as judged by proton NMR possibly due to the instability of the dimethyl thiazolidine in acidic media (Rajakanthan *et al.*, 2019; Nicolaou *et al.*, 2002). Contrarily, Suaifan *et al.* (2006) reported that they were able to remove the Boc group successfully from a dimethyl thiazolidine derivative despite using 2:1 (v/v) TFA/DCM but concluded that they observed the opening of the dimethyl thiazolidine ring when they attempted to couple the deprotected dimethyl thiazolidine derivative with an activated amino acid. Considering the possible instability of **72/73** in an acidic medium, a different N-Boc deprotection method was employed. Following the method of Hwu *et al.*, 1996, **73** was heated at reflux with a catalytic amount of cerium ammonium nitrate (CAN) in acetonitrile and the progress of the reaction was monitored by TLC. Despite the resultant product showing a single spot on TLC, after purification, with an R$_f$ value different from the starting material (**73**), the proton NMR spectrum showed the absence of significant peaks such as peaks correlating to the methyl ester group and the ring -N-C=C<u>H</u>- protons respectively.

Also, N-deprotection of the Fmoc group using basic conditions such as 2 % piperazine, DBU, 50 % morpholine and 10 % diethylamine respectively have been reported to induce ring opening of the dimethyl thiazolidine derivatives as evidenced by HPLC and mass spectroscopy analysis (Wade *et al.*, 1991) while the studies of Chierici *et al.* (2005) documents the ring opening, in the attempted N-deprotection of Boc and Alloc groups of dimethyl thiazolidine derivatives, under acidic (TFA) and neutral (Pd(PPh$_3$)$_3$) conditions respectively. Considering these studies, and our experimental outcome, on the challenges of N-deprotection of dimethyl thiazolidine derivatives, using acidic, basic and neutral protocols respectively, it is likely that the limitation is not dependent on the type of protocol, rather the removal of the protective groups favours the cleavage of the ring possibly due to the dimethyl substituent.

2.4.7 Syntheses of 76 and its precursors (Scheme 2.10)
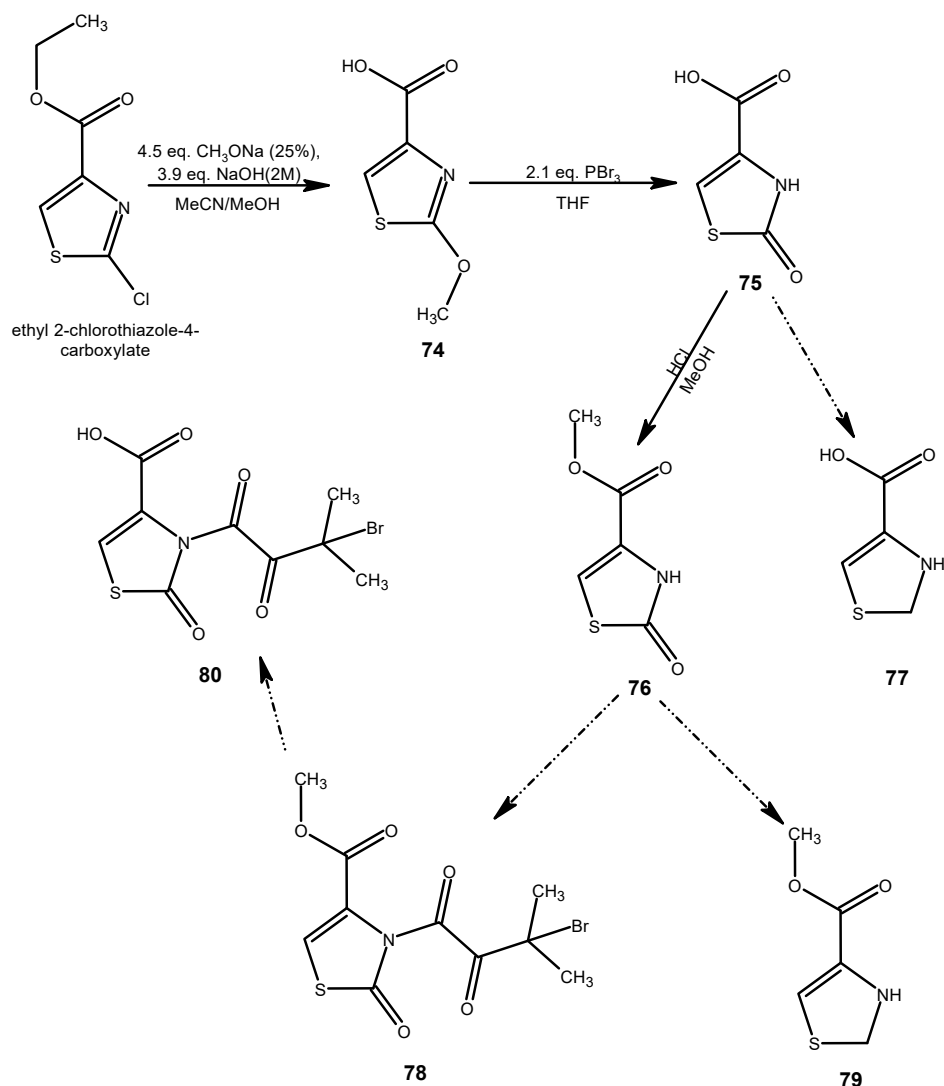
Scheme 2.10: Attempted syntheses of **77**, **78** and **79**.

The attempt to synthesise the methyl ester derivative of compound **61** through the synthesis of the methyl dihydrothiazole carboxylate **73** and couple the resultant product with compound **50** was a near success. The limitation in our approach is the instability of the heterocyclic dimethyl thiazolidine during N-deprotection under acidic (TFA) and neutral (CAN) conditions.

From our experimental trials, it was obvious that the synthesis of the methyl ester derivative of **61** through Scheme 2.9 was no longer viable due to the instability of the dimethyl thiazolidine ring, hence a new approach (Scheme 2.10) was adopted and **74** was formed by the treatment of ethyl 2-chlorothiazole-4-carboxylate with 4.5 eq. sodium methoxide (25 %) in acetonitrile/methanol (1:1). **74** was transformed to the corresponding oxo acid **75** by 2.1 eq. phosphorus tribromide treatment in tetrahydrofuran (Ané *et al*., 2002).
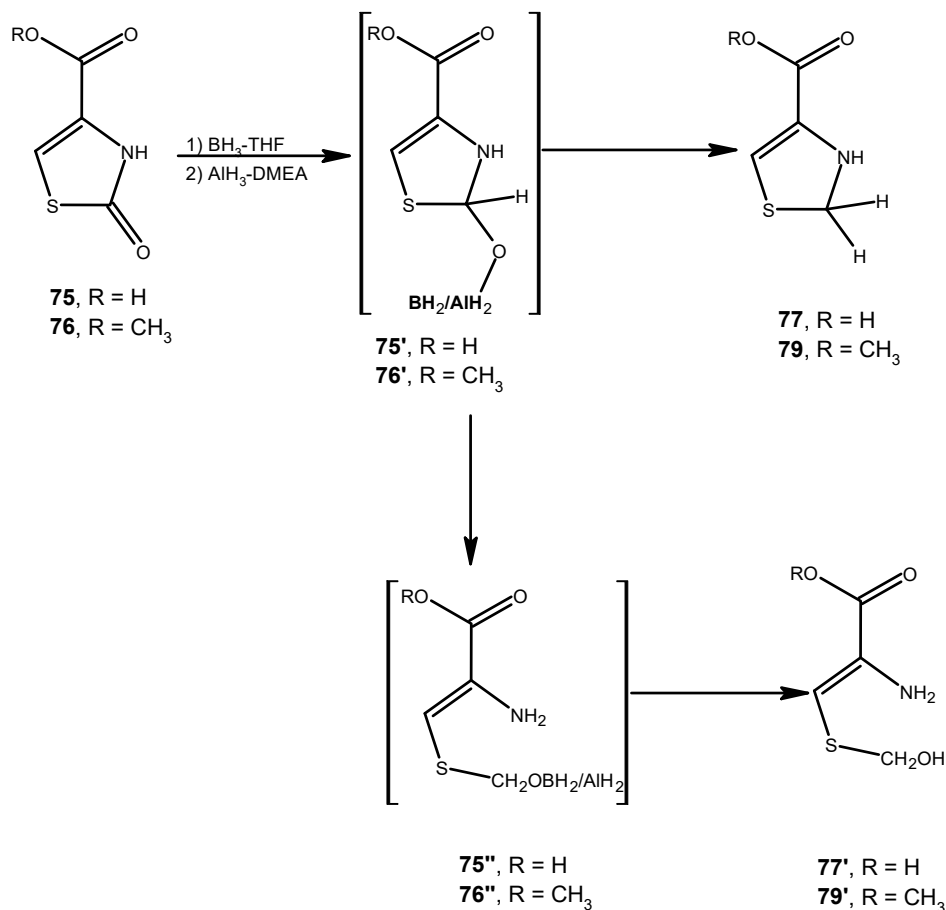
Scheme: 2.11: Potential mechanism for the attempted synthesis of **77** and **79** respectively.

The efforts to reduce the carbonyl group of **75** using a selective but less active borane-THF complex and powerful but less selective alane *N,N*-dimethylamine complex respectively were unsuccessful. First, following the published method of Jackson *et al*., 1983, 1.3 eq. borane-THF complex (1M) was added, dropwise, to a stirred solution of compound **75** in THF, under argon, at 0 °C and the resulting mixture was stirred at ambient temperature overnight. The reaction mixture (boric acid) was neutralised by 10 % aqueous sodium hydroxide solution at 5 -10 °C and subjected to extraction and purification to obtain an off-white solid which was analysed by proton NMR. The proton NMR spectrum (DMSO) indicated the possible formation of the **75**-borane complex (**75'**, Scheme 2.11). The peaks corresponding to the COO<u>H</u>, HN-C=C<u>H</u>- protons were visible while two other singlets, at 8.15 ppm (1H) and 6.54 ppm (2H) respectively, were also present. The current peaks may correlate with the S-C<u>H</u>-O-B<u>H</u>$_2$ protons (**75'**). The borane-THF complex reaction was repeated using 2 eq. borane-THF complex (1M) and the reaction mixture was heated at 50 °C for 24 hours. Unfortunately, the proton NMR spectrum was not different from the first trial. Furthermore, the reactive carboxylic acid group was protected and **76** was subjected to 1.2 eq. borane-THF complex treatment under argon at 50 °C and there was no significant turnover of starting material as judged by TLC after 24 hours. Additional 1.2 eq. borane-THF complex was added to the reaction mixture and there was still no significant progress, as judged by TLC, after heating for 3 days.

In light of the unsuccessful reduction of the carbonyl group, following the published protocol of Morales-Rios *et al*., 2002, compound **76** was treated with 1.1 eq. alane *N,N*-dimethylamine complex in toluene

(0.5M) at 0 °C under argon. The reaction mixture was quenched, with THF/water mixture (1:1), and subjected to the appropriate work to obtain a colourless liquid that was analysed by proton NMR. The proton NMR spectrum (DMSO), showed possible decomposition of the reactant as there was a complete absence of peaks correlating to the potential product or starting material but when the reaction was repeated at a lower temperature of -78 °C, TLC analysis showed turnover of starting material after 40 minutes while proton NMR (DMSO) showed a potential mixture of the alane-**76** complex (**76'**, Scheme 2.11) and the starting material. According to the proton NMR results, it is unlikely that the respective reducing agents induced ring opening of the heterocyclic oxo thiazolidine (**75''/76''** and **77'/79'** respectively) because the $\underline{H}_2$N-C=CH and S-C$\underline{H}_2$-O-**BH$_2$/AlH$_2$** or S-C$\underline{H}_2$-OH protons were not simultaneously present.

2.4.8 Imidation of compound 76

Since the reduction of the carbonyl group was unsuccessful and compound **76** is the oxo analogue of the heterocyclic ring of the target compound, attempts were made to synthesise the oxo analogue (**80**) of the target compound **48** by coupling **50** with compound **76** to obtain the ester derivative (**78**), which would be hydrolysed to the corresponding carboxylic acid **80** (Scheme 2.10). The acid chloride coupling of an amine is a bit different from the acid chloride imidation of an amide. While the mechanism is generally similar, a strong base is required for the deprotonation of the amide proton. Several trials to induce imidation of **76** using lithium diisopropylamide (LDA), n-butyllithium (n-BuLi) (Isozumi *et al.*, 2003), sodium hydride (NaH), and potassium carbonate respectively were unsuccessful as the outcome of the reaction varied between no reaction to degradation of starting material. First, the ester (**76**) was treated with 1 eq. LDA and 1 eq. n-BuLi respectively in THF at -78°C and 0°C respectively, under argon, for 10, 20 and 30 minutes respectively to form the corresponding lithium salt. The acid chloride was then treated (*in-situ*) with the **76**/LDA or **76**/n-BuLi mixture at 0°C and the respective resultant mixtures were allowed to gradually warm up to ambient temperature. According to the TLC result, there was no significant turnover of starting material with the LDA treatment at -78°C after stirring for 24 hours (ambient temperature) while LDA treatment of **76** at 0°C seemed to degrade the ester as the major peaks such as the C=CH and the ester peaks were absent. Similarly, the treatment of the ester **76** with n-BuLi at -78°C and 0°C respective resulted in the formation of mixtures of compounds with no peaks correlating to the ester group nor the C=CH protons while the treatment of **76** with 1 eq. NaH and 1.3 eq. K_2CO_3 respectively yielded no product as there was no reaction as judged by TLC and proton NMR.

2.4.9 Attempted syntheses of 82 and 84

Scheme 2.12: Attempted syntheses of **82**, **83** and **84** respectively.

Efforts were equally made to synthesise the proline analogue of **48** and compare the inhibitory activities of **48** and its proline analogue, should they be active against NDM-1. While the EDC.HCl/HOBt coupling method was unsuccessful for the synthesis of **52** (coupling of **49** with **51**), **81** was afforded, in poor yield, by either EDC.HCl/HOBt method or acid chloride coupling of **50** with (S)-methyl pyrrolidine-2-carboxylate hydrochloride. The attempts to introduce the desired unsaturation (-N-C=CH-) in the proline (**82** and **84** respectively) using CBrCl₃ and NBS/Et₃N methods respectively (Scheme 2.12), previously discussed, were unproductive. The NBS methods gave a complex mixture possibly due to the multiple substitutions of ring protons, by bromine, at different locations as a result of the non-selective mechanism of this method while there was no reaction with the CBrCl₃ method.

Scheme 2.13: Attempted synthesis of **82** through NCS-induced dehydrogenation.

Similarly, following the method by Huy *et al.*, 2011, an attempt was made to synthesise **82** (Scheme 2.13) by the treatment of (S)-methyl pyrrolidine-2-carboxylate hydrochloride with 1.1 eq. N-chlorosuccinimide in the presence of 2.2 eq. triethylamine in dichloromethane at (0 – 24 °C), followed by the dropwise addition of 2.3 eq. pyridine after stirring the initial mixture for 2.5 hours. The reaction mixture was cooled to -20 °C and a solution of 2.2 eq. **50** in DCM was added and the resultant mixture was allowed to gradually warm up to ambient temperature overnight. After appropriate workup, a pale-yellow oil (**82**) was obtained and analysed by proton NMR. The proton NMR (DMSO) showed a complex spectrum that did not correlate to the desired product or starting material. Also, efforts were made to synthesise, isolate and characterise, by proton NMR, the precursor (**86**) by the treatment of (S)-methyl pyrrolidine-2-carboxylate hydrochloride with 1.1 eq. N-chlorosuccinimide in the presence of 2.2 eq. triethylamine in dichloromethane at (0 – 24 °C). The proton NMR spectrum (CDCl₃) of **86** showed a peak correlating to succinimide (2.78 ppm), as expected, while there was absence of significant peaks such as the peak (3H, singlet) correlating to the methyl group rather 3 different peaks at 3.88, 3.83 and 3.74 ppm respectively, integrating one proton each, which are not likely to be the methyl group, were observed. In light of the challenges in constructing the double bond, **81** was subjected to ester hydrolysis, using 1M aqueous lithium hydroxide in methanol, to obtain **83** and evaluate if **83** would exhibit activity against NDM-1. Disappointingly, (S)-1-(3-hydroxy-3-methyl-2-oxobutanoyl)pyrrolidine-2-carboxylic acid was formed, instead of compound **83**, as judged by mass spectroscopy due to the substitution of the bromo group with an hydroxyl group.

Chapter 3

3.0 Bis cyclo-oxamide prodrugs and α,β-unsaturated carbonyl compounds as potential NDM-1 inhibitors.

3.1 Prodrugs

The term prodrug, introduced by Albert in 1958, is defined as a pharmacologically inert drug molecule that is converted to a pharmacologically active agent within the body by a predictable metabolic or physicochemical transformation. Prodrugs are designed and produced to circumvent challenges associated with toxicity as well as the physicochemical and pharmacokinetic properties of active drugs (Wu, 2009; Stella *et al*., 2007).

There are different types of prodrugs and they are classified by different methods. Currently, prodrugs are classified based on:

➢ the therapeutic categories. For example, antibacterial prodrugs, and anticancer prodrugs.

➢ the categories of chemical linkage. For example, ester prodrugs and glycosidic prodrugs.

➢ the functional categories or weaknesses of the active drug. For example, prodrugs for enhancing site specificity and prodrugs for improving absorption.

➢ the proposed classification - site of the conversion of the prodrug into the active drug (Wu, 2009).

3.1.1 Antibacterial prodrugs

Unfavourable pharmaceutical properties, such as poor pharmacokinetics and pharmacodynamics parameters are challenges bedevilling the development and applications of antibiotics. In recent years, scientists are exploring ways to mitigate these poor pharmaceutical properties. The antibacterial prodrug concept is one of the strategies scientists are exploring in the improvement of the pharmaceutical properties of antibiotics or potential antibiotics. Antibacterial prodrugs can be applied to either enhance the bioavailability of active antibiotics, overcome bacterial-resistant barriers or minimize drug toxicity.

3.1.1.1 Esterase-activated prodrugs

The first sets of antibacterial prodrugs (Figure 3.1) which include pivampicillin (**87**), bacampicillin (**88**) and talampicillin (**89**) were introduced into the clinics to enhance the oral bioavailability of ampicillin. They are ester analogues, of ampicillin, which are susceptible to enzymatic (esterase) hydrolysis to release the active ampicillin (Figure 3.2) (Jubeh *et al*., 2020).

87

88

89
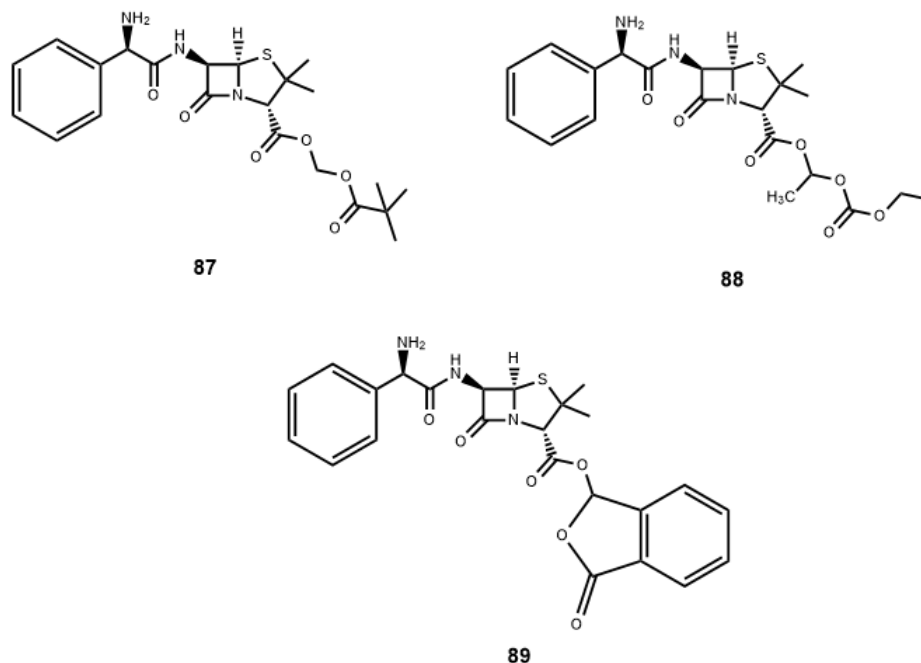
Figure 3.1: Esterase-activated prodrugs.
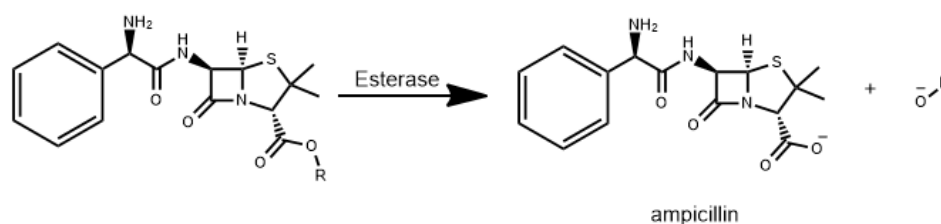
ampicillin

Figure 3.2: Activation of ampicillin.

3.1.1.2 β-lactamase-activated prodrugs

One of the resistance mechanisms of bacteria is the intracellular secretion of hydrolytic enzymes called β-lactamases (sections 1.2.3 and 1.4) which catalyse the hydrolysis of the β-lactam ring of antibiotics via cleavage of the C-N bond and render the antibiotics therapeutically irrelevant (Livermore, 2012). Antibacterial prodrugs are being developed to circumvent the antibiotic resistance associated with the secretion of β-lactamases. Scientists are exploiting the susceptibility of β-lactams to β-lactamases, especially cephalosporins, in the design of antibacterial prodrugs. The cephalosporin core can be fine-tuned into a scaffold for antibacterial prodrug with the cleavage of the C-N bond, which is associated with the loss of the leaving group at the 3'-position, as the activation point (section 1.6.1.1.2, Figure 1.10). A known or potential antibiotic can be incorporated as the leaving group, which would be released upon β-lactamase hydrolysis of the cephalosporin C-N bond. This approach enables the application of potential antibacterial molecules, which are non-selective and toxic, in the treatment of bacterial infections. The concept is selectively designed to deliver antibiotics to only pathogens that produce β-lactamases considering that the hydrolytic enzyme, which activates the release of the active antibiotics, is not produced by mammalian cells but by bacterial cells.

Recently, a novel cephalosporin-ciprofloxacin prodrug (**91**) was discovered by Evans *et al*. (2019) (Figure 3.3). The active molecule of the prodrug is ciprofloxacin (**90**), an antibiotic of the fluoroquinolone class that inhibits DNA replication in bacteria, and its host toxicity profile is well-established (Evans *et al*., 2019). To mitigate the toxicity of ciprofloxacin (**90**), Evans and co-workers reduced ciprofloxacin exposure to the host by creating an ester derivative (**91**). First, they selected a β-lactamase cleavable scaffold (cephalosporin) and modified the scaffold to reduce its bactericidal property but with the cephalosporin core retaining its good substrate property in the presence of β-lactamase. The active drug, ciprofloxacin (**90**), was attached to the cephalosporin scaffold via the carboxylic acid to give the prodrug (**91**) and such coupling abrogates the ciprofloxacin activity because the derivatisation of the carboxylic acid is associated with loss of the antibacterial activity of ciprofloxacin (**90**).
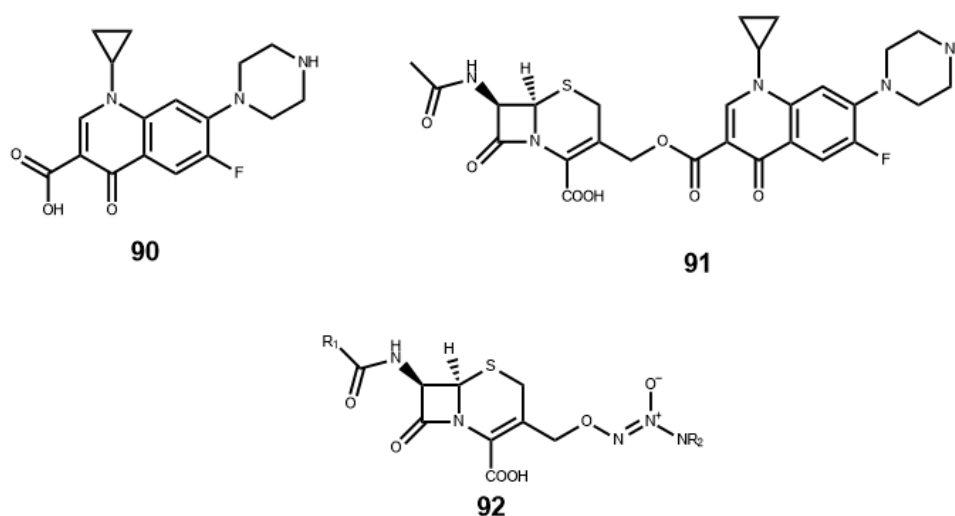
Figure 3.3: β-lactamase-activated prodrugs.

When assayed against *E. coli* producing different types of β-lactamases, **91** displayed similar inhibitory activity when compared with ciprofloxacin (**90**) whereas only minimal activity was observed when **91** was assayed against strains that did not express β-lactamases, thus confirming that the inhibitory activity of **91** is a function of β-lactamase-induced scission of the C-N bond which triggers the release of the active ciprofloxacin (**90**) in the bacteria cell.

Similarly, the above approach has been employed in the synthesis of a new class of prodrugs called cephalosporin-3'-diazeniumdiolates (C3Ds; **92**) (Jubeh *et al*., 2020). The C3Ds (Figure 3.3) are precursors of nitric oxide donors that deliver nitric oxide intracellularly (bacteria) upon scission of the C-N bond of the lactam ring.

3.2 Oxalate anion: A ligand of a metal cation and a potential inhibitor

Oxalic acid, the simplest dicarboxylic acid, was first synthesised by Scheele in 1776 (Thomas, 1808) by the oxidation of sugar with nitric acid. Different species ($H_2C_2O_4$, $HC_2O_4^-$, $C_2O_4^{2-}$) of oxalic acid exist in solution depending upon the prevailing pH as evidenced by the study by Verma *et al*. (2019) (Figure 3.4). At a lower pH,1.23, the non-ionic species is predominant while at pH ≥ 4.19 the anionic species, the conjugate base of oxalic acid, becomes dominant.

[Figure redacted]

Figure 3.4: pH-dependent ionization of oxalic acid (Verma *et al*., 2019).

Oxalate is mainly used in the alloy industry as rust removal in the treatment of metal as well as a precipitant in rare earth extraction (Riemenschneider and Tanifuji, 2011; Royen and Fortkamp, 2016). The application of oxalate in the alloy industry is due to its metal-binding property. An oxalate anion is a bidentate ligand that can bind a metal cation in two places to form a chelate. Several metals, including Zn (II) ions, tend to form oxalate compounds or complexes in the presence of oxalate anion (Krishnamurty and Harris, 1961; Perry, 2011; Rumble *et al*., 2018; William, 1972; Money and Davies, 1938).

Given that β-lactamases are produced within bacterial cells and thus far, no mammalian analogues of these enzymes have been discovered, the prodrug approach can harness bacterial resistance as a therapeutic opportunity to selectively kill antibiotic-resistant bacteria expressing β-lactamases. Also, considering that the biotransformation of β-lactamase-activated prodrug occurs within the bacterial cells, the prodrug approach can be far-reaching as it can be deployed to kill both extracellular and intracellular pathogens.

One of the advantages of zinc-dependent inhibitors is the broad-spectrum activity against the MBL family (B1-3) due to the conservation of zinc (II) ions in the three classes of Metallo-β-lactamase (section 1.4). Studies have shown that confiscation of the active site Zn (II) ions through either complexation of Zn (II) ions in the active site or removal of the Zn (II) ions resulted in the deactivation of the enzyme (Sabath and Abraham, 1966; Bergstrom *et al*., 2017; Zhang *et al*., 2017; King *et al*., 2014; Azumah *et al*., 2016; Somboro *et al*., 2015). In addition to the several zinc-dependent inhibitors discussed in section 1.6.2., oxalate anion can form water-soluble Zn (II) oxalate complex (Krishnamurty and Harris, 1961) and by extension, oxalate anion can deprive NDM-1 of its Zn (II) ions via complexation. However, one of the drawbacks of oxalate anion is the lack of selectivity which leads to host toxicity. Considering the metal-binding property of oxalate anion, it can be a classical inhibitor of NDM-1 if the molecule can be appropriately fine-tuned to mitigate the challenges of toxicity. The promiscuity of oxalate anion is associated with its metal-binding property owing to the presence of the dicarboxylic acid groups and the amidation of these groups would likely abrogate the affinity of oxalate anion for metal cations.

In the design and development of NDM-1 inhibitors, efforts to exploit the susceptibility of β-lactams to NDM-1 are gradually gaining momentum. NDM-1 degrades β-lactams antibiotics via hydrolysis of the amide bonds. The design and synthesis of the potential oxamide prodrug with an NDM-1 cleavable amide bond that would trigger the release of oxalate anion within the bacterial cell would likely reduce

the exposure of oxalate anion to the host and in turn mitigate the toxicity associated with the ligand. The released oxalate anion is expected to strip or form a complex with the Zn (II) ions in the enzyme's active site, thus denying the enzyme of its zinc ions and resulting in the abrogation of the enzyme activity.

3.3 Potential mechanism of the prodrug, bis cyclo-oxamides

The potential prodrug, bis cyclo-oxamides, is a dimer of carboxylic acid linked by an oxamide and consequently has two amide bonds. Upon binding of the prodrug to the NDM-1 active site, it is expected that the nucleophilic bridging hydroxide would hydrolyse the amide bonds to release the oxalate anion which would form a complex with the NDM-1's zinc (II) ions. Hypothetically (Figure 3.5), one or two species of zinc oxalate could be formed in the NDM-1 active site. While it is likely that the formation of a mono chelate complex(s), via complexation of one molecule of oxalate anion with one of the NDM-1's Zn (II) ions or the complexation of one molecule of oxalate anion with each of the NDM-1's Zn (II) ions respectively, may disrupt the architecture of the enzyme's active site and consequently results in the deactivation of the enzyme, it is as also possible that it may not completely abrogate the NDM-1 activity. If the latter is the case, a third/fourth oxalate anion could be generated and the newly generated oxalate anion(s) would bind to the mono chelate complex to form a bis chelate complex.
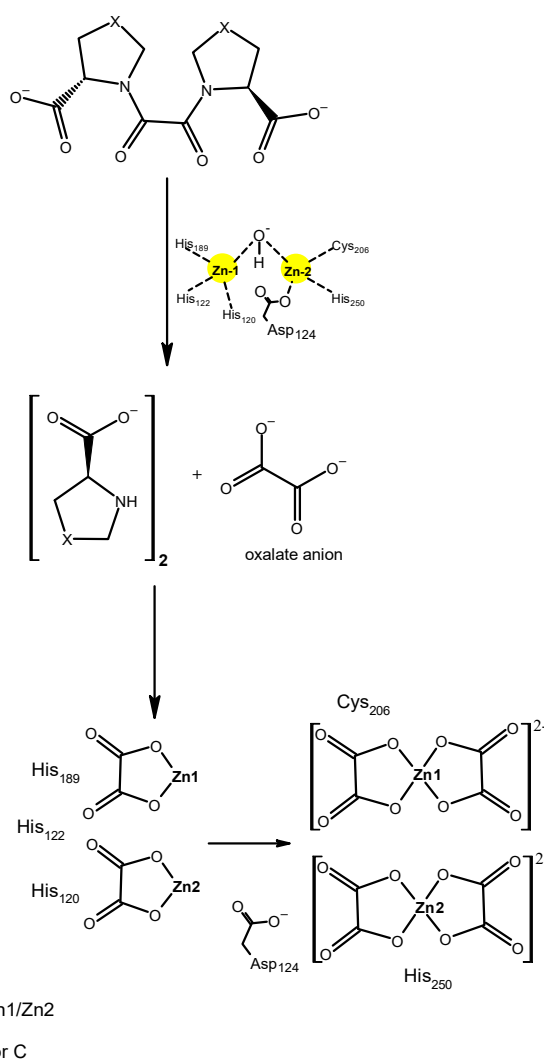
Figure 3.5: Proposed activation/inhibitory mechanism of the bis cyclo-oxamide.

3.4 Experimental methods

The general analytical method is well enumerated in chapter two, section 2.2.

The UV absorbance of the respective cyclo-oxamide-zinc chloride solutions was measured with Jenway 7205 UV-Vis spectrophotometer (198 – 400 nm) while the proton NMR results are generally reported following the format below. The below format deviates from the norms and the reason for using this format is justified in section 3.7.

Individual peak/range (ppm) (multiplicity of each peaks, total integration of all peaks [ratio of each peak], assignment of the peak(s) to molecular structure).

3.4.1 (2S,2'S)-Dimethyl-1,1'-oxalylbis(pyrrolidine-2-carboxylate) (93)

To a stirred solution of (S)-methyl pyrrolidine-2-carboxylate hydrochloride (1.00 g, 6.04 mmol) and triethylamine (1.26 mL, 9.04 mmol, 1.5 eq.) in anhydrous dichloromethane (30 mL), at 0 °C, was added oxalyl chloride (0.26 mL, 3.02 mmol, 0.5 eq., dissolved in 5 mL dichloromethane), at a rate to maintain the temperature of the mixture ≤ 5 °C. The resulting mixture was stirred at 0 °C for 2 hours and allowed to gradually warm up to ambient temperature overnight. The reaction mixture was diluted with dichloromethane (20 mL), washed with 1N aqueous HCl solution (50 mL), a saturated aqueous solution of $NaHCO_3$ (50 mL) and a saturated aqueous solution of NaCl (50 mL) respectively and dried with anhydrous magnesium sulphate, filtered and the filtrate was collected. The solvent was removed under vacuum and the residue obtained was dissolved in ethyl acetate (1 mL) followed by the addition of hexane (100 mL) and the flask was kept at 0°C for 30 minutes. The precipitate formed was collected by filtration and dried under vacuum to obtain compound **93** as a white solid, 1.18 g, 3.78 mmol, 63 %.
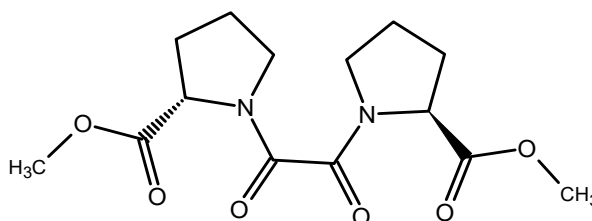
Figure 3.6: Compound **93**.

Molecular Formula: $C_{14}H_{20}N_2O_6$; R_f (ethyl acetate 100%): 0.43 (single spot); melting point: 148.7 – 150.3 °C.

^{1}H NMR (400 MHz, DMSO-d_6) δ **1.70 – 2.04, 2.14 – 2.36** (m, m respectively, total integration 8H, N-CH-[2 x C$\underline{H_2}$]-[2 x C$\underline{H_2}$]-CH_2); **3.42 – 3.52**, **3.53 – 3.58** (m, m respectively, total integration 4H, N-CH-CH_2-CH_2-[2 x C$\underline{H_2}$]); **3.63**, **3.67** (d, J = 4.3 Hz, s respectively, total integration 6H [ratio 1.0/2.2], [2 x C$\underline{H_3}$]-O-CO); **4.25, 4.41, 4.60** (dd, J = 8.4, 4.7 Hz, dd, J = 8.8, 3.6 Hz, dd, J = 8.6, 3.6 Hz, total integration 2H [ratio 1.0/2.5/1.2], N-[2 x C$\underline{H}$]-CH_2-CH_2-CH_2) ppm.

IR (ATR): $υ$ = 1172 (s, C-O ester), 1197 (s, C-O ester), 1215 (s, C-O ester), 1366 (s), 1393 (m), 1455 (w, C-H), 1637 (s, C=O amide), 1660 (s, C=O amide), 1733 (s, C=O ester), 2886 (w, C-H alkane), 2961 (w, C-H alkane) cm^{-1}.

MS (+ESI) m/z = Found 313.1399 (M+H)$^+$; calculated for $C_{14}H_{21}O_6N_2$ 313.1394; 1.6 ppm.

MS (+ESI) m/z = Found 335.1214 (M+Na)$^+$; calculated for $C_{14}H_{20}O_6N_2Na$ 335.1214; 0.1 ppm.

3.4.2 (2S,2'S)-1,1'-Oxalylbis(pyrrolidine-2-carboxylic acid) (94)

To a stirred solution of **93** (0.20 g, 0.64 mmol) in methanol (15 mL), at 15 ºC, was added an aqueous solution of sodium hydroxide (5 mL, 1N) for over 5 minutes and the resulting mixture was allowed to gradually warm up to ambient temperature (20 ºC) while the turnover of the ester was monitored by TLC (ethyl acetate 100 %). The reaction was stopped when the starting material was completely consumed. The pH of the mixture was adjusted to 3-4 using an aqueous 1N HCl solution and the desired product was extracted into ethyl acetate (2x, 30 mL). The organic portions were combined, rinsed with a saturated aqueous solution of NaCl, dried with anhydrous magnesium sulphate, filtered and the filtrate was collected. The solvent was removed at low pressure and the residue obtained was dried under vacuum to afford compound **94** as white crystals, 0.09 g, 0.32 mmol, 49 %.
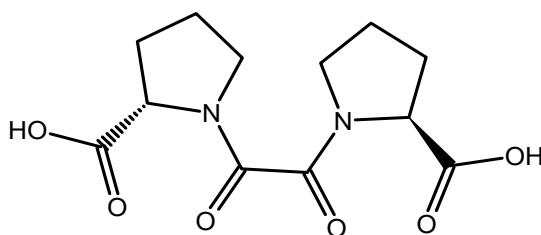
Figure 3.7: Compound **94**.

Molecular Formula: $C_{12}H_{16}N_2O_6$; R_f (dichloromethane/methanol with [0.3 % acetic acid], 1:1): 0.16 (single spot); melting point: 180.3 – 182.2 °C.

^{1}H NMR (400 MHz, DMSO-d_6) δ **1.70 – 2.05, 2.10 – 2.31** (m, m respectively, total integration 8H, N-CH-[2 x C$\underline{H}_2$]-[2 x C$\underline{H}_2$]-CH$_2$); **3.44 – 3.51**, **3.52 – 3.59** (m, m respectively, total integration 4H, N-CH-CH$_2$-CH$_2$-[2 x C$\underline{H}_2$]); **4.13, 4.29, 4.58** (dd, J = 8.3, 5.2 Hz, dd, J = 8.8, 3.4 Hz, dd, J = 8.6, 3.8 Hz, total integration 2H [ratio 1.0/2.2/1.3], N-[2 x C$\underline{H}$]-CH$_2$-CH$_2$-CH$_2$); **12.72** (s, total integration 2H, [2 x COO$\underline{H}$]) ppm.

^{13}C ATP NMR (101 MHz, DMSO-d_6) δ 22.52 ($\underline{C}H_2$), 24.57 ($\underline{C}H_2$), 29.26 ($\underline{C}H_2$), 31.00 ($\underline{C}H_2$), 46.23 ($\underline{C}H_2$), 47.19 ($\underline{C}H_2$), 47.96 ($\underline{C}H_2$), 57.93 (N-$\underline{C}$H-CH$_2$-CH$_2$-CH$_2$), 58.47 (N-$\underline{C}$H-CH$_2$-CH$_2$-CH$_2$), 59.48 (N-$\underline{C}$H-CH$_2$-CH$_2$-CH$_2$), 162.84 ($\underline{C}$=O), 163.02 ($\underline{C}$=O), 173.00 ($\underline{C}$=O), 173.64 ($\underline{C}$=O) ppm.

IR (ATR): υ = 1175, 1397 (m), 1454 (w, C-H), 1607 (s, C=O amide), 1732 (m-s, C=O carboxylic acid), 2955 (w, O-H carboxylic acid) cm^{-1}.

MS (-ESI) m/z = Found 283.0933 (M-H)$^-$; calculated for $C_{12}H_{15}O_6N_2$ 283.0936; 0.9 ppm.

3.4.3 (4R,4'R)-Diethyl 3,3'-oxalylbis(thiazolidine-4-carboxylate) (95)

To a stirred solution of **51.HCl** (2.00 g, 10.12 mmol) and N, N-diisopropylethylamine (3.52 mL, 20.23 mmol, 2 eq.) in anhydrous dichloromethane (40 mL), at 0 °C, was added oxalyl chloride (0.43 mL, 5.08 mmol, 0.5 eq., dissolved in 5 mL dichloromethane), at a rate to maintain the temperature of the mixture ≤ 5 °C. The resulting mixture was stirred at 0 °C for 2 hours and allowed to gradually warm up to ambient temperature overnight. The reaction mixture was diluted with dichloromethane (20 mL), washed with 1N aqueous HCl solution (60 mL), a saturated aqueous solution of NaHCO$_3$ (60 mL) and a saturated aqueous solution of NaCl (60 mL) respectively and dried with anhydrous magnesium sulphate, filtered

and the filtrate was collected. The solvent was removed at low pressure and the residue obtained was purified by gradient chromatography, ethyl acetate/hexane, 1, 2, 3 - 15 %, to obtain compound **95** as an off-white paste. 1.70 g, 4.52 mmol, 45 %.

Figure 3.8: Compound **95**.

Molecular Formula: $C_{14}H_{20}N_2O_6S_2$; R_f (ethyl acetate/hexane, 1:2): 0.23 (single spot); melting point: 58.5 – 62.3 °C.

^{1}H NMR (400 MHz, DMSO-d_6) δ **1.06 – 1.33** (m, total integration 6H, [2 x CH$_3$)]-CH$_2$-O), **3.19**, **3.26** (dd, J = 11.9, 4.5 Hz, m respectively, total integration 2H [ratio 1.0/1.8], N-CH-CH$_2$); **3.38**, **3.49** (m, ddd, J = 11.8, 7.1, 3.8 Hz respectively, total integration 2H [ratio 1.0/1.0], N-CH-CH$_2$); **4.02 – 4.27** (m, total integration 4H, CH$_3$-[2 x CH$_2$]-O); **4.40**, **4.52**, **4.66** (d, J = 9.9, d, J = 10, m respectively, total integration 4H [ratio 1.0/1.7/9.5], S-[2 x CH$_2$]-N); **4.87, 4.96, 5.12** (dd, J = 7.2, 4.5 Hz, dd, J = 7.4, 3.9 Hz, dd, J = 6.7, 2.1 Hz respectively, total integration 2H, [ratio 1/1.4/1.2], N-[2 x CH]-CH$_2$) ppm.

IR (ATR): ν = 1016 (s), 1180 (s, C-O ester), 1370 (s), 1388 (m), 1462 (w, C-H), 1641 (s, C=O amide), 1651 (s, C=O amide), 1673 (s, C=O amide), 1727 (s, C=O ester), 1749 (s, C=O ester), 2940 (w, C-H alkane), 2977 (w, C-H alkane) cm^{-1}.

MS (+ESI) m/z = Found 377.0838 (M+H)$^+$; calculated for $C_{14}H_{21}O_6N_2S_2$ 377.0836; 0.7 ppm.

MS (+ESI) m/z = Found 394.1099 (M+NH$_4$)$^+$; calculated for $C_{14}H_{24}O_6N_3S_2$ 394.1101; 0.5 ppm.

MS (+ESI) m/z = Found 399.0651 (M+Na)$^+$; calculated for $C_{14}H_{20}O_6N_2S_2Na$ 399.0655; 1.0 ppm.

3.4.4 (4R,4'R)-3,3'-Oxalylbis(thiazolidine-4-carboxylic acid) (96)

To a stirred solution of **95** (0.75 g, 1.99 mmol) in methanol (15 mL) at 15 °C, was added an aqueous solution of sodium hydroxide (10 mL, 1N) for over 5 minutes and the resulting mixture was allowed to gradually warm up to ambient temperature (20 °C) while the turnover of the ester was monitored by TLC (ethyl acetate/hexane, 1:2). The reaction was stopped when the starting material was completely consumed. The pH of the reaction mixture was adjusted to 3-4 using aqueous 1N HCl and the desired product was extracted into ethyl acetate (2x, 30 mL). The organic portions were combined, rinsed with a saturated aqueous solution of NaCl, dried with magnesium sulphate, filtered and the filtrate was collected. The solvent was removed at low pressure and the residue obtained was purified by flash chromatography, dichloromethane/methanol, 1:1, 0.3 % acetic acid, to afford compound **96** as a light purple paste, 0.49 g, 1.53 mmol, 77 %.

Figure 3.9: Compound **96**.

Molecular Formula: $C_{10}H_{12}N_2O_6S_2$; R_f (dichloromethane/methanol with [0.3 % acetic acid], 1:1): 0.27 (single spot); melting points: 49.3 – 77.1 °C, 95.45 – 106.7 °C, 114.8 - 116.8 °C.

^{1}H NMR (400 MHz, DMSO-d_6) δ **3.17**, **3.24** (dd, J = 11.7, 4.7 Hz, m respectively, total integration 2H [ratio 1.0/1.5], N-CH-C$\underline{H_2}$); **3.40 – 3.51** (m, total integration 2H, N-CH-C$\underline{H_2}$); **4.38**, **4.51**, **4.63** (dd, J = 19.8, 9.8 Hz, m, m respectively, total integration 4H [ratio 1.0/2.1/7.2], S-[2 x C$\underline{H_2}$]-N); **4.80, 4.87, 5.02, 5.10** (dd, J = 7.2, 4.7 Hz, dd, J = 7.5, 3.8 Hz, m, dd, J = 6.7, 2.2 Hz respectively, total integration 2H, [ratio 1/1.3/0.7/0.8], N-[2 x C$\underline{H}$]-CH$_2$); **13.22** (s, total integration 2H, [2 x COO$\underline{H}$]) ppm.

^{13}C ATP NMR (101 MHz, DMSO-d_6) δ 32.81 ($\underline{C}H_2$), 33.08 ($\underline{C}H_2$), 34.19 ($\underline{C}H_2$), 48.32 ($\underline{C}H_2$), 49.27 ($\underline{C}H_2$), 49.57 ($\underline{C}H_2$), 60.49 (N-$\underline{C}$H-CH$_2$), 61.06 (N-$\underline{C}$H-CH$_2$), 61.88 (N-$\underline{C}$H-CH$_2$), 161.64 ($\underline{C}$=O), 162.19 ($\underline{C}$=O), 170.67 ($\underline{C}$=O), 171.38 ($\underline{C}$=O) ppm.

IR (ATR): υ = 1167, 1378 (m), 1455 (w, C-H), 1614 (s, C=O amide), 1727 (m-s, C=O carboxylic acid), 2929 (w, O-H carboxylic acid) cm^{-1}.

MS (-ESI) m/z = Found 319.0061 (M-H)$^-$; calculated for $C_{10}H_{11}O_6N_2S_2$ 319.0064; 0.9 ppm.

MS (-ESI) m/z = Found 159.0003 (M-2H)$^{2-}$; calculated for $C_{10}H_{10}O_6N_2S_2$ 158.9996; 4.6 ppm.

3.4.5 (4R,4'R)-Diethyl-3,3'-oxalylbis(2,2-dimethylthiazolidine-4-carboxylate) (97)

To a stirred solution of **56** (1.00 g, 5.28 mmol) and triethylamine (0.74 mL, 5.28 mmol) in anhydrous dichloromethane (30 mL), at 0 °C, was added oxalyl chloride (0.23 mL, 2.64 mmol 0.5 eq., dissolved in 5 mL dichloromethane), at a rate to maintain the temperature of the mixture ≤ 5 °C. The resulting mixture was stirred at 0 °C for 2 hours and allowed to gradually warm up to ambient temperature overnight. The reaction mixture was diluted with dichloromethane (20 mL), washed with 1N aqueous HCl solution (50 mL), a saturated aqueous solution of NaHCO$_3$ (50 mL) and a saturated aqueous solution of NaCl (50 mL) respectively and dried with anhydrous magnesium sulphate, filtered and the filtrate was collected. The solvent was removed at low pressure and the residue obtained was purified by flash chromatography, ethyl acetate/hexane, 1:2, to afford compound **97** as white crystals 0.16 g, 0.37 mmol, 7 %.
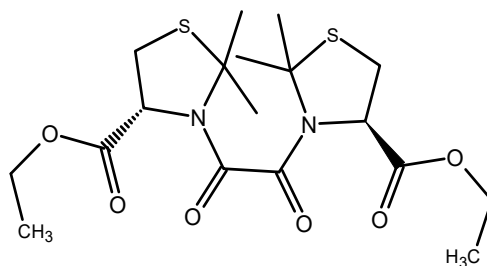
Figure 3.10: Compound **97**.

Molecular Formula: $C_{18}H_{28}N_2O_6S_2$; R_f (ethyl acetate/hexane, 1:2): 0.48 (single spot); melting point: 161.2 – 162.9 °C.

^{1}H NMR (400 MHz, DMSO-d_6) δ **1.10 – 1.30** (m, total integration 6H, [2 x C$\underline{H}_3$]-CH$_2$-O); **1.71 – 1.95** (m, total integration 12H, C-[2 x (C$\underline{H}_3$)$_2$]); **3.16, 3.23** (dd, J = 12.3, 1.0 Hz, m respectively, total integration 2H [ratio 1.0/0.8], N-CH-C$\underline{H}_2$); **3.50, 3.57** (m, ddd, J = 12.3, 6.8, 5.2 Hz respectively, total integration 2H [ratio 1.0/3.8], N-CH-C$\underline{H}_2$); **3.99 – 4.26** (overlapping m, total integration 4H, CH$_3$-[2 x C$\underline{H}_2$]-O); **4.71, 4.96, 5.01** (d, J = 6.1 Hz, dd, J = 7.2, 1.8, d, J = 5.9 Hz respectively, total integration 2H, [ratio 1.0/0.4/0.5], N-[2 x C$\underline{H}$]-CH$_2$) ppm.

IR (ATR): v = 1025 (m), 1194 (s, C-O ester), 1321 (s), 1356 (m), 1374 (m, C-H), 1388 (m, C-H), 1425 (w, C-H), 1650 (s, C=O amide), 1666 (s, C=O amide), 1673 (s, C=O amide), 1737 (s, C=O ester), 1757 (s, C=O ester), 2934 (w, C-H alkane), 2981 (w, C-H alkane) cm^{-1}.

MS (+ESI) m/z = Found 433.1464 (M+H)$^+$; calculated for $C_{18}H_{29}O_6N_2S_2$ 433.1462; 0.6 ppm.

MS (+ESI) m/z = Found 455.1276 (M+Na)$^+$; calculated for $C_{18}H_{28}O_6N_2S_2Na$ 455.1281; 1.1 ppm.

3.4.6 (4R,4'R)-3,3'-Oxalylbis(2,2-dimethylthiazolidine-4-carboxylic acid) (98)

To a stirred solution of **97** (0.10 g, 0.27 mmol) in methanol (10 mL) at 15 ºC, was added an aqueous solution of sodium hydroxide (5 mL, 1N) for over 5 minutes and the resulting mixture was allowed to gradually warm up to ambient temperature (20 ºC) while the turnover of the ester was monitored by TLC (ethyl acetate/hexane, 1:2). The pH of the reaction mixture was adjusted to 3-4 using aqueous 1N HCl and the desired product was extracted into ethyl acetate (2x, 30 mL). The organic portions were combined, rinsed with a saturated solution of NaCl, dried with anhydrous magnesium sulphate, filtered and the filtrate was collected. The solvent was removed at low pressure and the residue obtained was purified by flash chromatography, methanol/dichloromethane, 1:3, 0.3 % acetic acid, to obtain **98** as a white solid, 0.07 g, 0.16 mmol, 61 %.
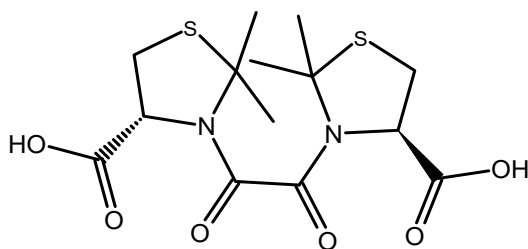
Figure 3.11: Compound **98**.

Molecular Formula: $C_{14}H_{20}N_2O_6S_2$; R_f (dichloromethane/methanol with [0.3 % acetic acid], 3:1): 0.36 (single spot); melting point: 179.3 – 181.6 °C.

^{1}H NMR (400 MHz, DMSO-d_6) δ **1.68 – 1.99** (m, total integration 12H, C-[2 x (C$\underline{H}_3$)$_2$]); **3.12 – 3.26** (m, total integration 2H, N-CH-C$\underline{H}_2$); **3.39, 3.54** (m, ddd, J = 14.9, 12.4, 6.8 Hz respectively, total integration 2H [ratio 1/1.5], N-CH-C$\underline{H}_2$); **4.62, 4.88, 5.03, 5.13** (m, dd, J = 7.3, 2.3 Hz, dd, J = 6.2, 1.3 Hz, m respectively, total integration 2H, [ratio 1.0/0.4/0.2/0.4], N-[2 x C$\underline{H}$]-CH$_2$), 12.81 (s, total integration 2H, [2 x COO$\underline{H}$]) ppm.

^{13}C ATP NMR (101 MHz, DMSO-d_6) δ 27.26 (C-$\underline{C}H_3$), 27.87 (C-$\underline{C}H_3$), 29.01 (C-$\underline{C}H_3$), 29.75, 31.34 (C-$\underline{C}H_3$), 32.48 ($\underline{C}H_2$), 65.89 (N-$\underline{C}H$-CH$_2$), 66.09 (N-$\underline{C}H$-CH$_2$), 71.18 ($\underline{C}$-(CH$_3$)$_2$), 73.35 ($\underline{C}$-(CH$_3$)$_2$), 161.18 ($\underline{C}$=O), 161.45 ($\underline{C}$=O), 162.08 ($\underline{C}$=O), 170.78 ($\underline{C}$=O), 171.08 ($\underline{C}$=O) ppm.

IR (ATR): v = 1204 (m-s), 1354 (m), 1432 (w, C-H), 1632 (s, C=O amide), 1652 (s, C=O amide), 1720 (m-s, C=O carboxylic acid), 2973 (w, O-H carboxylic acid) cm^{-1}

MS (-ESI) m/z = Found 375.0689 (M-H)$^-$; calculated for C$_{14}$H$_{19}$O$_6$N$_2$S$_2$ 375.0690; 0.3 ppm.

MS (-ESI) m/z = Found 187.0315 (M-2H)$^{2-}$; calculated for C$_{14}$H$_{18}$O$_6$N$_2$S$_2$ 187.0309; 3.4 ppm.

3.4.7 (R)-Ethyl-2,2-diethylthiazolidine-4-carboxylate (99)

To a stirred solution of L-cysteine ethyl ester hydrochloride (3.0 g, 16.16 mmol) and triethylamine (2.25 mL, 16.16 mmol) in toluene (50 mL) was added 3-pentanone (2.23 mL, 21.00 mmol, 1.3 eq.) and the resulting mixture was heated at reflux overnight. The mixture was allowed to cool and the reaction solvent was removed at low pressure while the residue obtained was neutralized with a saturated aqueous solution of NaHCO$_3$. The desired product was extracted into dichloromethane (3x, 30 mL) and the organic portions were combined, dried with anhydrous magnesium sulphate, filtered and the filtrate was collected. The solvent was removed at low pressure and the residue obtained was dried under vacuum to afford compound **99** as a yellow oil, 2.91 g, 13.39 mmol, 83 %, which was used in the next step without further purification.
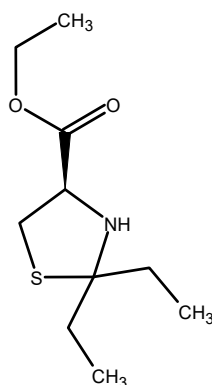
Figure 3.12: Compound **99**.

Molecular Formula: C$_{10}$H$_{19}$NO$_2$S; R$_f$ (ethyl acetate/hexane, 1:5): 0.40 (single spot).

^{1}H NMR (400 MHz, DMSO-d_6) δ 0.83 (t, J = 7.3 Hz, 3H, C-CH$_2$-C$\underline{H}_3$), 0.92 (t, J = 7.4 Hz, 3H, C-CH$_2$-C$\underline{H}_3$), 1.22 (t, J = 7.1 Hz, 3H, C$\underline{H}_3$-CH$_2$-O), 1.63 (dd, J = 14.3, 7.2 Hz, 1H, C-C$\underline{H}_2$-CH$_3$), 1.72 (ddd, J = 14.0, 7.2, 5.6 Hz, 2H, C-C$\underline{H}_2$-CH$_3$), 1.84 (dt, J = 14.7, 7.3 Hz, 1H, C-C$\underline{H}_2$-CH$_3$), 2.72 (d, J = 12.0 Hz, 1H, N$\underline{H}$-CH-CH$_2$), 2.85 (dd, J = 10.3, 8.5 Hz, 1H, NH-CH-C$\underline{H}_2$), 3.21 (dd, J = 10.3, 6.8 Hz, 1H, NH-CH-C$\underline{H}_2$), 4.03 (ddd, J = 12.0, 8.5, 6.8 Hz, 1H, NH-C$\underline{H}$-CH$_2$), 4.15 (m, 2H, CH$_3$-C$\underline{H}_2$-O) ppm.

IR (ATR): v = 1025 (m), 1174 (s, C-O ester), 1220 (s), 1370 (w-m), 1458 (w, C-H), 1736 (s, C=O ester), 2936 (w, C-H alkane), 2967 (w, C-H alkane), 3300 (w, N-H) cm^{-1}.

3.4.8 (4R,4'R)-Diethyl-3,3'-oxalylbis(2,2-diethylthiazolidine-4-carboxylate) (100)

To a stirred solution of **99** (0.50 g, 2.30 mmol) and N, N-diisopropylethylamine (0.80 mL, 4.60 mmol, 2 eq.) in anhydrous dichloromethane (10 mL), at 0 °C, was added oxalyl chloride (0.10 mL, 1.15 mmol, 0.5 eq. dissolved in 5 mL dichloromethane), at a rate to maintain the temperature of the mixture ≤ 5 °C. The resulting mixture was stirred at 0 °C for 3 hours and allowed to gradually warm up to ambient temperature overnight. The reaction mixture was diluted with dichloromethane (20 mL), washed with 1N aqueous HCl solution (2x, 40 mL), a saturated aqueous solution of NaHCO$_3$ (2x, 40 mL) and a saturated aqueous solution of NaCl (40 mL) respectively and dried with anhydrous magnesium sulphate, filtered and the filtrate collected. The solvent was removed at low pressure and the residue obtained was purified by gradient chromatography, ethyl acetate/hexane solvent mixture 5 – 20 %, to obtain compound **99** as a dark yellow oil, 0.04 g, 0.08 mmol, 4 %.
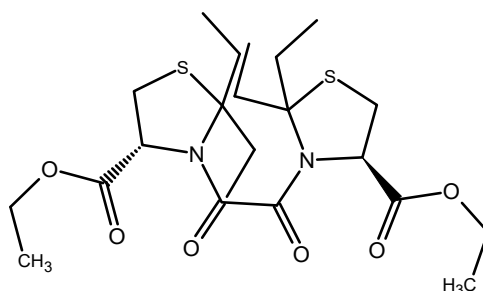
Figure 3.13: Compound **100**.

Molecular Formula: C$_{22}$H$_{36}$N$_2$O$_6$S$_2$; R$_f$ (ethyl acetate/hexane, 1:5): 0.34 (single spot).

^{1}H NMR (400 MHz, DMSO-d_6) δ **0.76 – 0.89, 0.94** (m, td, J = 7.4, 5.0 Hz, respectively, total integration 12H, C-(CH$_2$)$_2$-[2 x (C$\underline{H}_3$)$_2$]), **1.20** (t, J = 7.2 Hz, total integration 6H, [2 x C$\underline{H}_3$]-CH$_2$-O); **1.93**, **2.31** (dd, , J = 14.2, 7.2 Hz, m respectively, total integration 8H, [ratio 1.0/2.6], C-[2 x (C$\underline{H}_2$)$_2$]-(CH$_3$)$_2$), **3.09** (d, J = 12.3 Hz, total integration 2H, N-CH-C$\underline{H}_2$), **3.46** (dd, J = 12.3, 7.0 Hz, total integration 2H, N-CH-C$\underline{H}_2$); **3.99 – 4.11** (m, total integration 2H, CH$_3$-C$\underline{H}_2$-O); **4.12 – 4.22** (m, total integration 2H, CH$_3$-C$\underline{H}_2$-O); **4.86** (d, J = 6.8 Hz, total integration 2H, N-[2 x C$\underline{H}$]-CH$_2$) ppm.

IR (ATR): ν = 1014 (m), 1199 (s, C-O ester), 1240 (m), 1370 (w), 1409 (w, C-H), 1674 (s, C=O amide), 1738 (s, C=O ester), 2941 (w, C-H alkane), 2975 (w, C-H alkane) cm^{-1}.

MS (+ESI) m/z = Found 489.2093 (M+H)$^+$; calculated for C$_{22}$H$_{37}$O$_6$N$_2$S$_2$ 489.2088; 1.1 ppm.

MS (+ESI) m/z = Found 511.1901 (M+Na)$^+$; calculated for C$_{22}$H$_{36}$O$_6$N$_2$S$_2$Na 511.1907; 1.2 ppm.

3.4.9 (4R)-Ethyl-2-benzylthiazolidine-4-carboxylate (101)

To a stirred solution of L-cysteine ethyl ester hydrochloride (3.50 g, 18.85 mmol) in water/ethanol (56 mL, 25:3) was added phenylacetaldehyde (2.32 mL, 19.79 mmol, 1.05 eq.) and the resulting mixture was stirred at ambient temperature (25 °C) for 12 hours. The mixture was diluted with dichloromethane (50 mL) and neutralized with saturated sodium hydrogen carbonate solution (20 mL) under stirring. The organic layer was separated, and the aqueous portion was further extracted with dichloromethane (2x, 50 mL). The organic portions were combined, dried with anhydrous magnesium sulphate, filtered and

the filtrate collected. The solvent was removed at low pressure and the residue obtained was purified by gradient chromatography, ethyl acetate/hexane: 5,10, 15 & 20 %, to obtain compound **101** as a pale-yellow oil, 3.22 g, 12.81 mmol, 68 %, which was used in the next step without further purification.
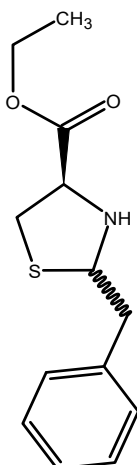
Figure 3.14: Compound **101**.

Molecular Formula: $C_{13}H_{17}NO_2S$; Rf (ethyl acetate/hexane 1:3) = 0.23 (single spot).

^{1}H NMR (400 MHz, DMSO-d_6) δ 1.20 (dt, J = 10.3, 7.1 Hz, 6H, C$\underline{H}_3$-CH$_2$-O), 2.82 (overlapping m, 2H, NH-CH-C$\underline{H}_2$), 2.95 (overlapping m, 2H, CH-C$\underline{H}_2$-C$_6$H$_5$), 3.15 (overlapping m, 5H, N$\underline{H}$-CH-C$\underline{H}_2$, CH-C$\underline{H}_2$-C$_6$H$_5$), 3,44 (m, 1H, N$\underline{H}$-CH-CH$_2$), 3.81 (ddd, J = 12.3, 9.0, 6.9 Hz, 1H, NH-C$\underline{H}$-CH$_2$), 4.13 (dq, J = 22.1, 7.1 Hz, 4H, CH$_3$-C$\underline{H}_2$-O), 4.24 (ddd, J = 8.8, 7.0, 5.0 Hz, 1H, C$\underline{H}$-CH$_2$-C$_6$H$_5$), 4.65 (ddd, J = 12.2, 7.2, 6.3 Hz, 1H, NH-C$\underline{H}$-CH$_2$), 4.80 (dt, J = 10.1, 7.0 Hz, 1H, C$\underline{H}$-CH$_2$-C$_6$H$_5$), 7.28 (m, 10H, CH-CH$_2$-C$_6$$\underline{H}_5$) ppm.

IR (ATR): ν = 698 (s, C=C phenyl), 752 (m, C=C phenyl), 1028 (m), 1156 (s, C-O ester), 1188 (s), 1372 (w-m), 1453 (w, C-H), 1495 (w, C-H), 1732 (s, C=O ester), 2933 (w, C-H alkane), 2974 (w, C-H alkane), 3295 (w, N-H) cm^{-1}.

3.4.10 (4R,4'R)-Diethyl-3,3'-oxalylbis(2-benzylthiazolidine-4-carboxylate) (102)

To a stirred solution of **101** (1.00 g, 3.98 mmol) and N, N-diisopropylethylamine (1.04 mL, 5.97 mmol, 1.5 eq.) in anhydrous dichloromethane (20 mL), at 0 °C, was added oxalyl chloride (0.17 mL, 1.99 mmol, 0.5 eq. dissolved in 5 mL dichloromethane), at a rate to maintain the temperature of the mixture ≤ 5 °C. The resulting mixture was stirred at 0 °C for 2 hours and allowed to gradually warm up to ambient temperature overnight. The reaction mixture was diluted with dichloromethane (20 mL), washed with 1N aqueous HCl solution (2x, 40 mL), a saturated aqueous solution of NaHCO$_3$ (2x, 40 mL) and a saturated aqueous solution of NaCl (40 mL) respectively and dried with anhydrous magnesium sulphate, filtered and the filtrate was collected. The solvent was removed and the residue obtained was purified by gradient chromatography, ethyl acetate/hexane, 5 – 20 %, to obtain compound **102** as an off-white amorphous solid, 0.66 g, 1.19 mmol, 30 %.
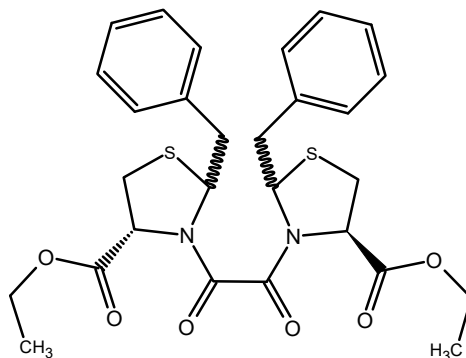
Figure 3.15: Compound **102** (mixture of diastereomers).

Molecular Formula: $C_{28}H_{32}N_2O_6S_2$; R_f (ethyl acetate/hexane, 1:3): 0.21 (single spot); melting point: 37.1 – 38.8 °C.

IR (ATR): v = 698 (s, C=C phenyl), 1021 (m), 1180 (s, C-O ester), 1363 (w), 1453 (w, C-H), 1635 (s, C=O amide), 1738 (s, C=O ester), 2935 (w, C-H alkane), 2979 (w, C-H alkane) cm^{-1}.

MS (+ESI) m/z = Found 557.1783 (M+H)$^+$; calculated for $C_{28}H_{33}O_6N_2S_2$ 557.1775; 1.5 ppm.

MS (+ESI) m/z = Found 574.2037 (M+NH$_4$)$^+$; calculated for $C_{28}H_{36}O_6N_3S_2$ 574.2040; -0.5 ppm.

MS (+ESI) m/z = Found 579.1585 (M+Na)$^+$; calculated for $C_{28}H_{32}O_6N_2S_2Na$ 579.1594; -1.6 ppm.

3.4.11 (4R,4'R)-3,3'-Oxalylbis(2-benzylthiazolidine-4-carboxylic acid) (103)

To a stirred solution of **102** (0.60 g, 1.08 mmol) in a 1,4-dioxane-water (30 mL 4;2) was added lithium hydroxide monohydrate (0.14 g, 3.34 mmol, 3.10 eq.) and the resulting mixture was stirred at ambient temperature (25 ºC) overnight. The solvent was removed at low pressure while the water portion was neutralized with 3M HCl to pH 3-4 and the crude product was extracted into ethyl acetate (3x, 40 mL). The organic portions were combined, dried with anhydrous magnesium sulphate, filtered and the filtrate was collected. The solvent was removed and the residue obtained was purified by gradient chromatography, methanol/dichloromethane 2, 4---20 %, 0.3 % acetic acid), to obtain an off-white paste which was further purified by crystallization (hexane) to afford compound **103** as an off-white solid 0.34 g, 0.68 mmol, 63 %.
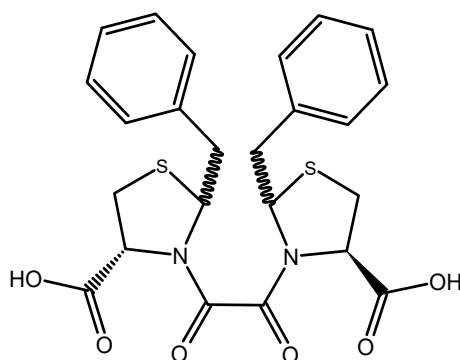
Figure 3.16: Compound **103** (mixture of diastereomers).

Molecular Formula: $C_{24}H_{24}N_2O_6S_2$; R_f (dichloromethane/methanol with [0.3 % acetic acid], 1:1): 0.53 (streak/smear), melting point: 121.2 – 124.2 °C.

^{13}C ATP NMR (101 MHz, DMSO-d_6) δ 31.01 (C$\underline{H}_2$), 33.08 (C$\underline{H}_2$), 41.39 (C$\underline{H}_2$), 42.59 (C$\underline{H}_2$), 62.36 (C$\underline{H}$), 63.22 (C$\underline{H}$), 63.97 (C$\underline{H}$), 65.82 (C$\underline{H}$), 66.92 (C$\underline{H}$), 67.78 (C$\underline{H}$), 127.28 (ArC$\underline{H}$), 128.85 (ArC$\underline{H}$), 129.65 (ArC$\underline{H}$), 130.00 (ArC$\underline{H}$), 137.27 (Ar$\underline{C}$-CH$_2$), 137.59 (Ar$\underline{C}$-CH$_2$), 137.81 (Ar$\underline{C}$-CH$_2$), 138.17 (Ar$\underline{C}$-CH$_2$), 160.68 ($\underline{C}$=O), 161.54 ($\underline{C}$=O), 161.95 ($\underline{C}$=O), 162.16 ($\underline{C}$=O), 171.00 ($\underline{C}$=O), 171.12 ($\underline{C}$=O), 171.52 ($\underline{C}$=O) ppm.

IR (ATR): v = 698 (s, C=C phenyl), 750 (m, C=C phenyl), 1178 (m), 1370 (m), 1454 (w, C-H), 1634 (s, C=O amide), 1724 (m-s, C=O carboxylic acid), 3028 (w, O-H carboxylic acid) cm^{-1}.

MS (-ESI) m/z = Found 499.1001 (M-H)$^-$; calculated for $C_{24}H_{23}O_6N_2S_2$ 499.1003; 0.4 ppm.

MS (-ESI) m/z = Found 249.0462 (M-2H)$^{2-}$; calculated for $C_{24}H_{22}O_6N_2S_2$ 249.0465; 1.3 ppm.

3.4.12 (R)-Ethyl-5-thia-8-azaspiro[3.4]octane-7-carboxylate (104)

To a stirred solution of L-cysteine ethyl ester hydrochloride (2.0 g, 10.77 mmol) and triethylamine (1.50 mL, 10.77 mmol) in toluene (30 mL) was added cyclobutanone (0.80 mL, 10.77 mmol) and the resulting mixture was heated at reflux overnight. The mixture was allowed to cool and the reaction solvent was removed at low pressure while the residue obtained was neutralized (pH 7) with a concentrated aqueous solution of NaHCO$_3$. The desired product was extracted into dichloromethane (3x, 30 mL) and the organic portions were combined, dried with anhydrous magnesium sulphate, filtered and the filtrate was collected. The solvent was removed and the residue obtained was dried under vacuum to obtain compound **104** as a yellow oil, 1.82 g, 9.04 mmol, 84 %, which was used in the next step without further purification.
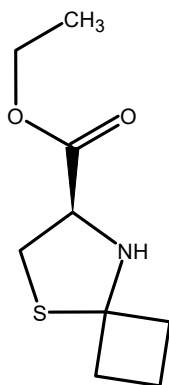
Figure 3.17: Compound **104**.

Molecular Formula: $C_9H_{15}NO_2S$; R_f (ethyl acetate: hexane 1:3): 0.33 (single spot).

^{1}H NMR (400 MHz, DMSO-d_6) δ 1.23 (t, J = 7.1 Hz, 3H, C$\underline{H}_3$-CH$_2$-O), 1.78 (m, 1H, S-C-CH$_2$-CH$_2$-C$\underline{H}_2$-NH), 1.89 (dt, J = 10.6, 8.3 Hz, 1H, S-C-CH$_2$-CH$_2$-C$\underline{H}_2$-NH), 2.20 (m, 2H, S-C-CH$_2$-C$\underline{H}_2$-CH$_2$-NH), 2.38 (m, 2H, S-C-C$\underline{H}_2$-CH$_2$-CH$_2$-NH), 2.93 (dd, J = 10.1, 8.3 Hz, 1H, NH-CH-C$\underline{H}_2$), 3.20 (dd, J = 10.1, 6.6 Hz, 1H, NH-CH-C$\underline{H}_2$), 3.32 (1H, overlapped with H$_2$O peak), 3.83 (ddd, J = 11.6, 8.3, 6.6 Hz, 1H, NH-C$\underline{H}$-CH$_2$), 4.15 (m, 2H, CH$_3$-C$\underline{H}_2$-O) ppm.

IR (ATR): v = 811 (m), 1021 (m), 1159 (s, C-O ester), 1217 (m), 1329 (m), 1369 (w-m), 1445 (w, C-H), 1732 (s, C=O ester), 2934 (w, C-H alkane), 2980 (w, C-H alkane), 3294 (w, N-H) cm^{-1}.

3.4.13 Ethyl-(7R)-8-[2-[(7R)-7-ethoxycarbonyl-5-thia-8-azaspiro[3.4]octan-8-yl]-2-oxo-acetyl]-5-thia-8-azaspiro[3.4]octane-7-carboxylate (105)

To a stirred solution of **104** (0.50 g, 2.48 mmol) in anhydrous dichloromethane (10 mL), at -5 °C, was added N, N-diisopropylethylamine (0.65 mL, 3.73 mmol, 1.5 eq.) and oxalyl chloride (0.11 mL, 1.24 mmol, 0.5 eq. dissolved in 2 mL dichloromethane), at a rate to maintain the temperature of the mixture ≤ 3 °C. The resulting mixture was stirred at 0 - 10 °C for 5 hours. The reaction mixture was diluted with dichloromethane (10 mL), washed with 1N aqueous HCl solution (2x, 30 mL), a saturated aqueous solution of $NaHCO_3$ (2x, 30 mL) and a saturated aqueous solution of NaCl (30 mL) respectively and dried with anhydrous magnesium sulphate, filtered and the filtrate was collected. The solvent was removed and the residue obtained was purified by gradient chromatography ethyl acetate/hexane, 5, 10 – 25 % to obtain compound **105** as a white paste 0.20 g, 0.44 mmol, 18 %.
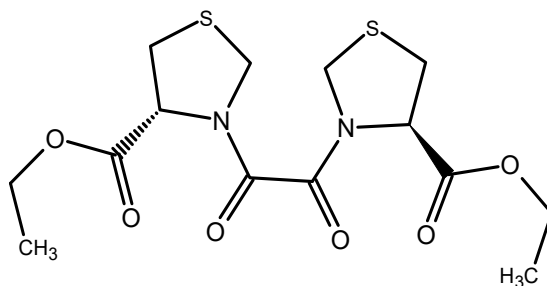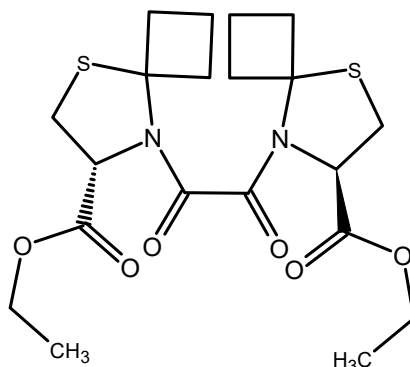

Figure 3.18: Compound **105**.

Molecular Formula: $C_{20}H_{28}N_2O_6S_2$; R_f (ethyl acetate: hexane 1:3): 0.31 (single spot); melting point: 75.5 – 78.4 °C.

^{1}H NMR (400 MHz, DMSO-d_6) δ **1.08 − 1.39** (m, total integration 6H, [2 x C$\underline{H_3}$]-CH$_2$-O); **1.66 − 2.03, 2.05 – 2.37** (m, m, respectively, total integration 12H, C-[2 x C$\underline{H_2}$]-CH$_2$-CH$_2$-N, C-CH$_2$-[2 x C$\underline{H_2}$]-CH$_2$-N, C-CH$_2$-CH$_2$-[2 x C$\underline{H_2}$]-N); **3.18**, **3.42**, **3.57** (d, J = 12.0 Hz, m, m respectively, total integration 4H, [ratio 1.0/1.1/0.5], N-CH-[2 x C$\underline{H_2}$]); **3.94 − 4.28** (m, total integration 4H, CH$_3$-[2 x C$\underline{H_2}$]-O); **4.76 − 4.95**, **5.05** (m respectively, total integration 2H, N-[2 x C$\underline{H}$]-CH$_2$) ppm.

IR (ATR): υ = 1021 (m), 1186 (s, C-O ester), 1286 (w), 1363 (w), 1429 (w, C-H), 1632 (s, C=O amide), 1655 (s, C=O amide), 1732 (s, C=O ester), 2949 (w, C-H alkane) cm^{-1}.

MS (+ESI) m/z = Found 457.1468 (M+H)$^+$; calculated for $C_{20}H_{29}O_6N_2S_2$ 457.1462; 1.4 ppm.

MS (+ESI) m/z = Found 474.1726 (M+NH$_4$)$^+$; calculated for $C_{20}H_{32}O_6N_3S_2$ 474.1727; 0.2 ppm.

MS (+ESI) m/z = Found 479.1278 (M+Na)$^+$; calculated for $C_{20}H_{28}O_6N_2S_2Na$ 479.1281; 0.6 ppm.

3.4.14 (7R,7'R)-8,8'-(1,2-dioxoethane-1,2-diyl)di(5-thia-8-azaspiro[3.4]octane-7-carboxylic acid) (106)

To a stirred solution of **105** (0.43 g, 0.94 mmol) in a 1,4-dioxane-water mixture (30 mL 4:2) was added lithium hydroxide monohydrate (0.12 g, 2.83 mmol, 3 eq.) and the resulting mixture was stirred at ambient temperature (25 ºC) overnight. The solvent was removed at low pressure while the water portion was neutralized with 1M HCl to pH 3-4 and the crude product was extracted into ethyl acetate

(3x, 40 mL). The organic portions were combined, dried with anhydrous magnesium sulphate, filtered and the filtrate collected. The solvent was removed at low pressure and the residue obtained was purified by crystallization (hexane) to afford compound **106** as an off-white solid, 0.15 g, 0.37 mmol, 40 %.
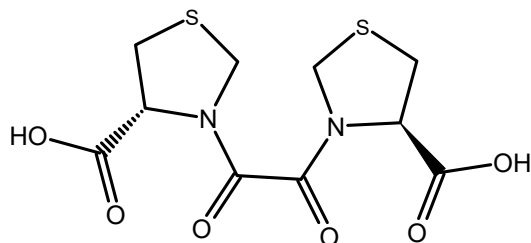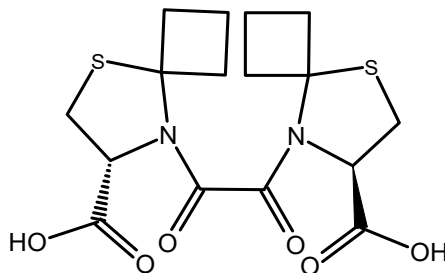

Figure 3.19: Compound **106**.

Molecular Formula: $C_{16}H_{20}N_2O_6S_2$; R_f (dichloromethane/methanol with [0.3 % acetic acid], 1:1): 0.29 (single spot); melting point: 168.9 – 170.8 °C.

^{1}H NMR (400 MHz, DMSO-d_6) δ **1.62 – 2.00, 2.14** (m, d, J = 11.4 Hz respectively, total integration 12H, C-[2 x C$\underline{H}_2$]-CH$_2$-CH$_2$-N, C-CH$_2$-[2 x C$\underline{H}_2$]-CH$_2$-N, C-CH$_2$-CH$_2$-[2 x C$\underline{H}_2$]-N); **3.29** (4H, overlapped with H$_2$O peak, N-CH-[2 x C$\underline{H}_2$]); **4.70**, **4.81**, **5.01**, **5.12** (d, J = 6.0 Hz, dd, J = 7.2, 3.9 Hz, dd, J = 5.1, 2.7 Hz, dd, J = 5.1, 2.2 Hz respectively, total integration 2H [ratio 1.0/1.1/1.3/0.9], N-[2 x C$\underline{H}$]-CH$_2$); **13.03** (s, total integration 2H, [2 x COO$\underline{H}$]) ppm.

^{13}C ATP NMR (101 MHz, DMSO-d_6) δ 32.27 ($\underline{C}$H$_2$), 34.88 ($\underline{C}$H$_2$), 35.52 ($\underline{C}$H$_2$), 36.60 ($\underline{C}$H$_2$), 37.29 ($\underline{C}$H$_2$), 64.73 (N-$\underline{C}$H-CH$_2$), 65.26 (N-$\underline{C}$H-CH$_2$), 73.98 ($\underline{C}$-(CH$_2$)$_3$), 74.12 ($\underline{C}$-(CH$_2$)$_3$), 161.86 ($\underline{C}$=O), 162.59 ($\underline{C}$=O), 170.95 ($\underline{C}$=O), 171.45 ($\underline{C}$=O) ppm.

IR (ATR): ν = 1190 (m), 1359 (m), 1434 (w, C-H), 1635 (s, C=O amide), 1730 (m-s, C=O carboxylic acid), 2946 (w, O-H carboxylic acid) cm^{-1}.

MS (-ESI) m/z = Found 399.0696 (M-H)$^{-}$; calculated for $C_{16}H_{19}O_6N_2S_2$ 499.1003; 0.4 ppm.

MS (-ESI) m/z = Found 421.0508 (M-2H+Na)$^{-}$; calculated for $C_{16}H_{18}O_6N_2S_2Na$ 421.0509; 0.3 ppm.

3.4.15 **(R)-Ethyl-1-thia-4-azaspiro[4.4]nonane-3-carboxylate (107)**

To a stirred solution of L-cysteine ethyl ester hydrochloride (2.0 g, 10.77 mmol) and triethylamine (1.50 mL, 10.77 mmol) in toluene (30 mL) was added cyclopentanone (0.95 mL, 10.77 mmol) and the resulting mixture was heated at reflux overnight. The mixture was allowed to cool and the reaction solvent was removed at low pressure while the residue obtained was neutralized (pH 7) with a concentrated aqueous solution of NaHCO$_3$. The desired product was extracted into dichloromethane (3x, 30 mL) and the organic portions were combined, dried with anhydrous magnesium sulphate, filtered and the filtrate was collected. The solvent was removed and the residue was dried under vacuum to afford compound **107** as a yellow oil, 1.98 g, 9.20 mmol, 85 %, which was used in the next step without further purification.
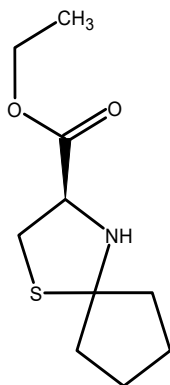
Figure 3.20: Compound **107**.

Molecular Formula: $C_{10}H_{17}NO_2S$; R_f (ethyl acetate: hexane 1:3): 0.33 (single spot).

^{1}H NMR (400 MHz, DMSO-d_6) δ 1.23 (t, J = 7.1 Hz, 3H, C$\underline{H_3}$-CH$_2$-O), 1.56 – 1.79 (m, 5H, S-C-CH$_2$-C$\underline{H_2}$-C$\underline{H_2}$-C$\underline{H_2}$-NH), 1.80 – 1.90 (m, 1H, S-C-CH$_2$-C$\underline{H_2}$-CH$_2$-CH$_2$-NH), 1.92 – 2.05 (m, 2H, S-C-C$\underline{H_2}$-CH$_2$-CH$_2$-CH$_2$-NH), 2.95 (dd, J = 10.1, 8.3 Hz, 1H, NH-CH-C$\underline{H_2}$), 3.08 (d, J = 12.3 Hz, 1H, N$\underline{H}$-CH-CH$_2$), 3.27 (dd, J = 10.1, 7.0 Hz, 1H, NH-CH-C$\underline{H_2}$), 3.94 (ddd, J = 12.2, 8.6, 6.9 Hz, 1H, NH-C$\underline{H}$-CH$_2$), 4.16 (dq, J = 7.1, 1.0 Hz, 2H, CH$_3$-C$\underline{H_2}$-O) ppm.

IR (ATR): υ = 796 (m), 1025 (m), 1162 (s, C-O ester), 1222 (m), 1333 (m), 1369 (w-m), 1445 (w, C-H), 1733 (s, C=O ester), 2961 (w, C-H alkane), 3301 (w, N-H) cm^{-1}.

3.4.16 Ethyl-(3R)-4-[2-[(3R)-3-ethoxycarbonyl-1-thia-4-azaspiro[4.4]nonan-4-yl]-2-oxo-acetyl]-1-thia-4-azaspiro[4.4]nonane-3-carboxylate (108)

To a stirred solution of **107** (0.50 g, 2.32 mmol) in anhydrous dichloromethane (10 mL), at -5 °C, was added N, N-diisopropylethylamine (0.61 mL, 3.48 mmol, 1.5 eq.) and oxalyl chloride (0.10 mL, 1.16 mmol, 0.5 eq. dissolved in 2 mL dichloromethane), at a rate to maintain the temperature of the mixture ≤ 3 °C. The resulting mixture was stirred at 0 - 10 °C for 5 hours. The reaction mixture was diluted with dichloromethane (10 mL), washed with 1N aqueous HCl solution (2x, 30 mL), a saturated aqueous solution of NaHCO$_3$ (2x, 30 mL) and a saturated aqueous solution of NaCl (30 mL) respectively and dried with anhydrous magnesium sulphate, filtered and the filtrate was collected. The solvent was removed and the residue obtained was purified by gradient chromatography ethyl acetate/hexane, 5, 10 – 25 % to obtain compound **108** as a white solid, 0.08 g, 0.17 mmol, 7 %.
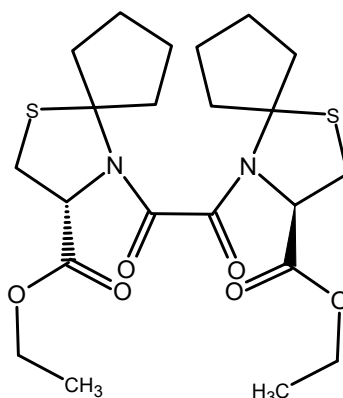
Figure 3.21: Compound **108.**

Molecular Formula: $C_{22}H_{32}N_2O_6S_2$; R_f (ethyl acetate/hexane 1:3): 0.33 (single spot); melting point: 128.0 – 131.3 °C.

^{1}H NMR (400 MHz, DMSO-d_6) δ **1.10 – 1.31** (m, total integration 6H, [2 x C$\underline{H_3}$]-CH$_2$-O); **1.60, 1.80, 2.56, 2.77** (dd, J = 15.0, 8.0 Hz, m, m, dd, J = 12.8, 7.8 Hz respectively, total integration 16H, [ratio 1.0/1.9/overlapped with DMSO//0.7], C-[2 x C$\underline{H_2}$]-CH$_2$-CH$_2$-CH$_2$-N, C-CH$_2$-[2 x C$\underline{H_2}$]-CH$_2$- CH$_2$-N, C-CH$_2$- CH$_2$-[2 x C$\underline{H_2}$]-CH$_2$-N, C-CH$_2$- CH$_2$-CH$_2$-[2 x CH$_2$]-N); **3.20**, **3.47** (m, dd, J = 12.3, 6.3 Hz respectively, total integration 4H, [ratio 1.0/0.7], N-CH-[2 x C$\underline{H_2}$]); **3.95 – 4.29** (m, total integration 4H, CH$_3$-[2 x C$\underline{H_2}$]-O); **4.76**, **4.98**, **5.11**, **5.65** (m, dd, J = 7.1, 2.6 Hz, d, J = 5.6 Hz, dd, J = 6.2, 2.4 Hz respectively, total integration 2H, [ratio 1.0/0.3/0.3/0.3], N-[2 x C$\underline{H}$]-CH$_2$) ppm.

IR (ATR): υ = 1027 (m), 1181 (s, C-O ester), 1196 (s, C-O ester), 1281 (w), 1328 (m), 1359 (m), 1374 (w), 1437 (w, C-H), 1645 (s, C=O amide), 1660 (s, C=O amide), 1741 (s, C=O ester), 2868 (w, C-H alkane), 2955 (w, C-H alkane) cm^{-1}.

MS (+ESI) m/z = Found 485.1777 (M+H)$^+$; calculated for $C_{22}H_{33}O_6N_2S_2$ 485.1775; 0.5 ppm.

MS (+ESI) m/z = Found 502.2033 (M+NH$_4$)$^+$; calculated for $C_{22}H_{36}O_6N_3S_2$ 502.2040; 1.4 ppm.

MS (+ESI) m/z = Found 507.1587 (M+Na)$^+$; calculated for $C_{22}H_{32}O_6N_2S_2Na$ 507.1594; 1.4 ppm.

3.5 Spectrophotometric determination of chelating property of bis cyclo-oxamides

To an ethanolic solution of zinc (II) chloride (0.02 mL, 14.67 mM) was added an ethanolic solution of bis cyclo-oxamide (0.01 mL, 2 mg/mL) and the volume of the resulting solution was made up to 3 mL using ethanol. The experiment was repeated with a fixed amount of zinc (II) chloride (0.02 mL) but varying amounts of cyclo-oxamide (0.02, 0.03, 0.04, 0.05 and 0.06 mL respectively). The UV absorbance of the respective cyclo-oxamide-zinc chloride solutions was measured, at ambient temperature, after 0.5- and 10-minutes incubation periods respectively.

Table 3.1: Shows the molarity of the respective cyclo-oxamides and zinc chloride as well as their respective molar ratios

		$ZnCl_2$	oxamide						
$ZnCl_2$	Experimental vol. (mL)	0.01	0.00	0.02	0.02	0.02	0.02	0.02	0.02
	Final conc. (mg/mL)	0.007	0.000	0.013	0.013	0.013	0.013	0.013	0.013
	Molarity (mM)	0.050	0.0	0.100	0.100	0.100	0.100	0.100	0.100
94	Experimental vol. (mL)	0.0	0.01	0.01	0.02	0.03	0.04	0.05	0.06
	Final conc. (mg/mL)	0.000	0.007	0.007	0.013	0.020	0.027	0.033	0.040
	Molarity (mM)	0.0	0.025	0.025	0.046	0.070	0.095	0.116	0.141
	Molar ratio (**94/ZnCl₂**)			**0.25**	**0.46**	**0.70**	**0.95**	**1.2**	**1.41**
96	Experimental vol. (mL)	0.0	0.01	0.01	0.02	0.03	0.04	0.05	0.06
	Final conc. (mg/mL)	0.000	0.007	0.007	0.013	0.020	0.027	0.033	0.040
	Molarity (mM)	0.000	0.022	0.022	0.041	0.062	0.084	0.103	0.125
	Molar ratio (**96/ZnCl₂**)			**0.22**	**0.41**	**0.62**	**0.84**	**1.03**	**1.25**
98	Experimental vol. (mL)	0.0	0.01	0.01	0.02	0.03	0.04	0.05	0.06
	Final conc. (mg/mL)	0.000	0.007	0.007	0.013	0.020	0.027	0.033	0.040
	Molarity (mM)	0.0	0.019	0.019	0.035	0.053	0.072	0.088	0.106
	Molar ratio (**98/ZnCl₂**)			**0.19**	**0.35**	**0.53**	**0.72**	**0.88**	**1.06**
103	Experimental vol. (mL)	0.0	0.01	0.01	0.02	0.03	0.04	0.05	0.06
	Final conc. (mg/mL)	0.000	0.007	0.007	0.013	0.020	0.027	0.033	0.040
	Molarity (mM)	0.0	0.014	0.014	0.026	0.040	0.054	0.066	0.080
	Molar ratio (**103/ZnCl₂**)			**0.14**	**0.26**	**0.40**	**0.54**	**0.66**	**0.80**
106	Experimental vol. (mL)	0.0	0.01	0.01	0.02	0.03	0.04	0.05	0.06
	Final conc. (mg/mL)	0.000	0.007	0.007	0.013	0.020	0.027	0.033	0.040
	Molarity (mM)	0.0	0.017	0.017	0.032	0.050	0.067	0.082	0.100
	Molar ratio (**106/ZnCl₂**)			**0.17**	**0.32**	**0.50**	**0.67**	**0.82**	**1.0**

3.6 **Discussion of experimental results**

Three respective reaction steps were employed in the syntheses of the bis cyclo-oxamides. First, the monocyclic esters were synthesised, where applicable, by treatment of L-cysteine ester hydrochloride with the appropriate aldehyde/ketone. Thereafter, the mono esters were treated with 0.5 eq. of oxalyl chloride to afford the respective dimer esters which were transformed into the corresponding carboxylic acid via hydrolysis.

3.6.1 Syntheses of monocyclic esters

(S)-Methyl pyrrolidine-2-carboxylate hydrochloride was used as purchased while compound **51** was afforded by the esterification of L-4-thiazolidine carboxylic acid (Scheme 2.1) (Pellegrini *et al*., 1999). The thiazolidine derivatives **56**, **99**, **101**, **104** and **107** were synthesised by the treatment of L-cysteine ethyl ester hydrochloride with the appropriate aldehyde/ketone (Ratner and Clarke, 1937; Refouvelet *et al*., 1994; Sako *et al*., 1992; Yang *et al*., 2021; Zhao *et al*., 2018). The formation of the thiazolidine ring is a consequence of the reaction of electrophilic carbonyl compounds with the nucleophilic aminothiols and it has been reported to proceed through an addition-elimination sequence to generate an unstable iminium cation which undergoes rapid cyclisation to form a stable thiazolidine ring (Chen *et al*., 2016; Kallen, 1971; Nagasawa *et al*., 1982). There are two plausible pathways in the formation of the thiazolidine ring (Scheme 3.1). First, the five-membered ring can be formed by nucleophilic addition of the amine to the aldehyde/ketone to form a carbinolamine which undergoes condensation to the corresponding Schiff base which is then protonated to give an iminium ion. The unstable iminium ion cyclises rapidly with the neighbouring sulfhydryl group to give the heterocyclic thiazolidine ring. Alternatively, the ring can be formed via the initial attack on the aldehyde/ketone by the sulphur atom to form hemithioacetal which undergoes similar condensation to give the unstable sulphonium ion intermediate that cyclises with the neighbouring amine to generate the thiazolidine ring (Chen *et al*., 2016; Kallen, 1971; Nagasawa *et al*., 1982).

Considering the formation of thiazolidine from cysteine and aldehyde/ketone involves an equilibrium, the methylene group at position C-2 plays a significant role towards the stability of the ring and as such, the substitution of the methylene with alkyl groups would decrease the stability of the heterocyclic ring. According to Butvin *et al*., 1999, the bulkier the C-2 substituents, the faster the decomposition of the heterocyclic ring.
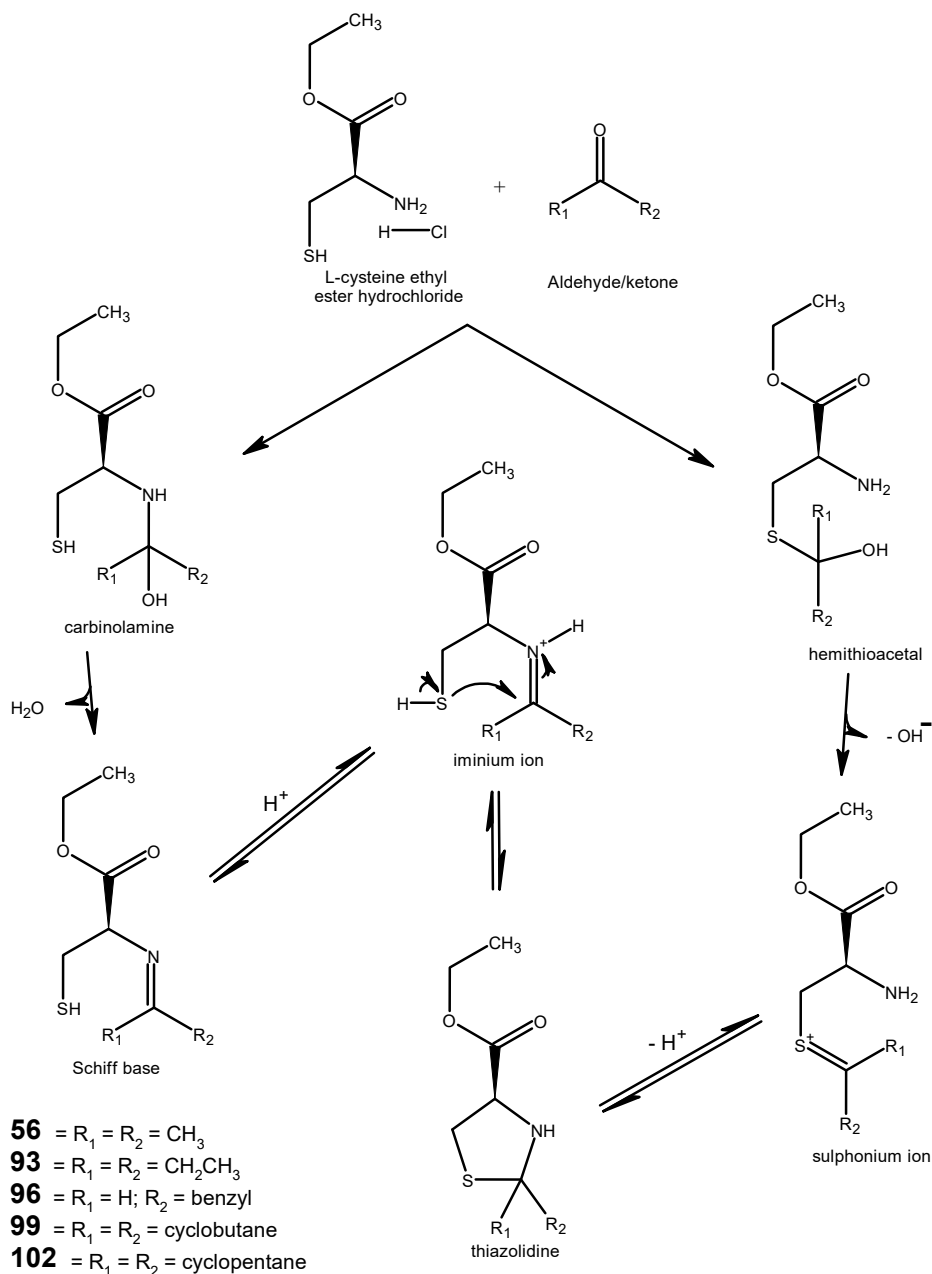
Scheme 3.1: Plausible reaction pathway for the formation of thiazolidine derivatives.

56 = $R_1 = R_2 = CH_3$
93 = $R_1 = R_2 = CH_2CH_3$
96 = $R_1 = H$; $R_2 = $ benzyl
99 = $R_1 = R_2 = $ cyclobutane
102 = $R_1 = R_2 = $ cyclopentane

3.6.2 Syntheses of dimeric esters and carboxylic acids

93 = $R_1 = R_2 = H_2$; $R_3 = CH_3$; X = C
95 = $R_1 = R_2 = H_2$; $R_3 = CH_2CH_3$; X = S
97 = $R_1 = R_2 = CH_3$; $R_3 = CH_2CH_3$; X = S
100 = $R_1 = R_2 = R_3 = CH_2CH_3$; X = S
102 = $R_1 = H$; $R_2 = $ benzyl; $R_3 = CH_2CH_3$; X = S
105 = $R_1 = R_2 = $ cyclobutane; $R_3 = CH_2CH_3$; X = S
108 = $R_1 = R_2 = $ cyclopentane; $R_3 = CH_2CH_3$; X = S
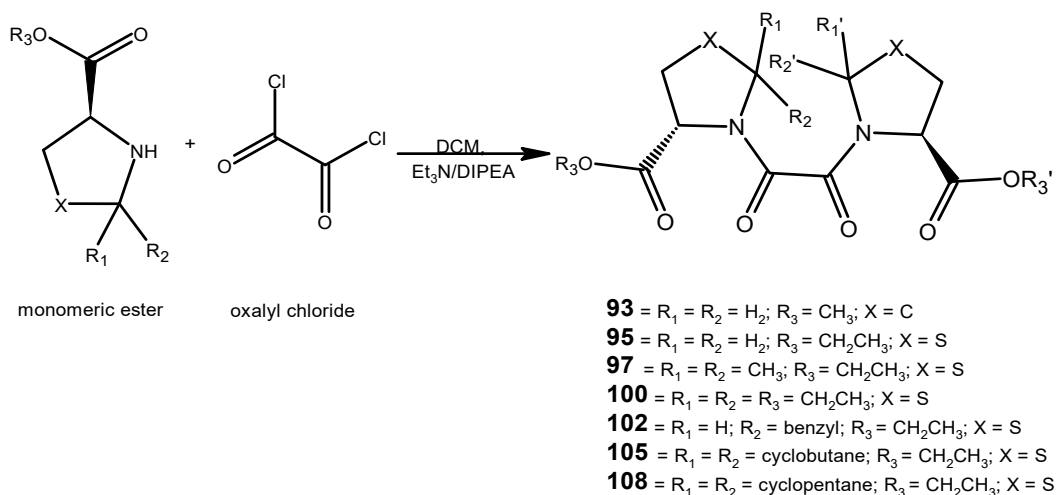
Scheme 3.2: Syntheses of dimeric esters

The respective dimeric esters, **93**, **95**, **97**, **100**, **102**, **105** and **108**, were afforded, in good to poor yield, by coupling of the respective monomeric amines with 0.5 eq. of oxalyl chloride in the presence of a base (Scheme 3.2). The yields were significantly poor, especially the dimeric esters with C-2 dialkyl/cyclo substitutions. There are three plausible reasons for the poor yields. First, the disappointing yields of the dimeric esters may be due to the instability of the C-2 substituted dimer due to the bulkiness of the C-2 substituents (Butvin *et al.*, 1999). Secondly, the instability of the di-amides (esters), especially the aliphatic substituted analogues, in an acidic medium might also account for the poor yield (Chierici *et al.*, 2005) while the steric factor owing to the C-2 substituents can as well reduce the reaction rate and consequently leads to less product formation. In an attempt to mitigate the presumed acid instability of the C-2 substituted thiazolidine analogue (**100**), excess base was used in the coupling reaction and the reaction was steadily monitored by TLC. Unfortunately, there was no improvement in the yield. The heterocyclic ring seems to decompose, possibly, into the corresponding cysteine ester which can favourably react with oxalyl chloride in the presence of a base.

Considering the very low yield, possibly due to the instability of the ring, **100** and **108** were discontinued and the other esters were hydrolysed to the corresponding carboxylic acids in the presence of an inorganic base to afford the final respective compounds (Scheme 3.3). Characterisation of the final dicarboxylic acids by spectroscopic methods (NMR, IR and MS) validate the formation of the desired product while most of the final compounds (dicarboxylic acids) showed single spot and narrow melting range when characterisation by thin-layer chromatography and melting analysis. Compound **96** displaced an unusual melting point profile, with varying melting points and a wide melting point range, despite showing a single spot on TLC. The melting of the crystals, observed at 49.3 – 77.1 °C, seemed to result in the formation of a secondary crystal structure that had a melting point range of 95.45 – 106.7 °C. Surprisingly the secondary crystal structure seemed to give rise to a pseudo-crystal structure which turned complete liquid at 114.8 – 116.8 °C. There could be different reasons for the unusual melting point profile for compound **96**. First, the unusual melting point profile could be due to the presence of impurities. However, while it is possible, it is also unlikely that impurities could be the cause of the unusual melting point profile considering that compound **96** showed a single spot on the TLC. Secondly, compound **96** could be heat labile and as a consequence can be converted structurally into different compound(s), with higher melting points, upon heating, hence the formation of secondary and pseudo crystal structures observed during melting point analysis.
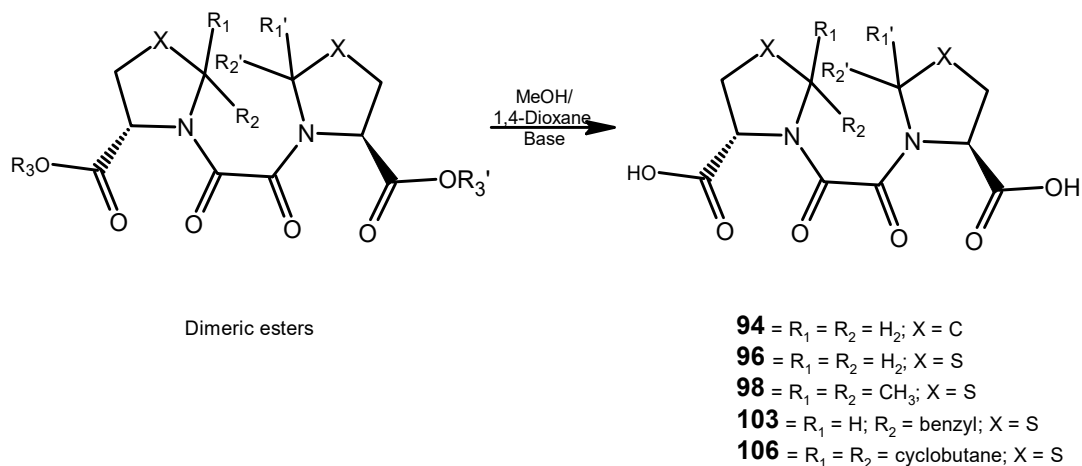
Scheme 3.3: Syntheses of dicarboxylic acids (bis cyclo-oxamides).

Below the reaction scheme:

Dimeric esters

94 = R₁ = R₂ = H₂; X = C
96 = R₁ = R₂ = H₂; X = S
98 = R₁ = R₂ = CH₃; X = S
103 = R₁ = H; R₂ = benzyl; X = S
106 = R₁ = R₂ = cyclobutane; X = S

3.7 Amide bond rotation - *cis-trans* rotamers: The implication on ^{1}H NMR multiplicity of bis cyclo-oxamides

Considering the unique characteristic of amide bonds, with respect to free and restricted rotations, monoamides can exist structurally in three different forms (resonance hybrid, *cis* and *trans* rotamers) and these forms have implications on the proton NMR spectrum (see section 2.4.3). At 298 K, the restricted rotation about the C-N bond persists owing to the delocalisation of the lone pair on the nitrogen into the pi bond (C=N), hence the interconversion of the *cis* and *trans* rotamers is slow and the rotamers become visible on the NMR time scale. The protons of the respective rotamers, especially the protons near the amide bond, differ in chemical shifts because the protons of the respective species are in a non-equivalent environment, hence the ambiguity of the ^{1}H proton spectrum.

Given the ^{1}H proton NMR (spectrum) complexity of the monoamides, it is expected that the complexity would be worse with diamides such as bis cyclo-oxamides. The bis cyclo-oxamides can likely exist structurally in 6 different forms/species with two of the species having restricted rotation about the C-N bond and four potential rotamers with free rotation about the C-N bond but with the trans conformation more favoured (Kubyshkin and Budisa, 2017). That is, the rotamers would be likely visible, at 298K, on the NMR time scale owing to the slow interconversion. As expected, at 298K, ^{1}H NMR spectra of the dimeric esters and acids respectively were very complex, as the signal of most of the protons splits into multiple peaks and sometimes overlapped with each other, possibly because of the restricted rotation about the C-N bond. In light of this, the ^{1}H NMR was reported differently using the general format stated in section 3.4. The protons of compounds **102** and **103** could not be assigned, according to the format stated in section 3.4, due to the complexity of the respective spectrum which emanates from multiple overlapping peaks. The multiple overlapping peaks observed in the proton NMR spectra can be attributed to the respective compounds (**102** and **103**) existing as rotamers as well as a mixture of diastereomers.

3.8 Protein-ligand docking studies

To investigate the potential binding mode of the respective bis cyclo-amides, Eshtiwi, A. (visiting research fellow, Aston University, 2022) conducted protein-ligand docking studies and obtained a

crystal structure of the respective bis cyclo-amides complexed with NDM-1 (Table 3.2). The respective ligand-NDM-1 complexes showed several conserved interactions which are enumerated below.

➢ In all ligand-NDM-1 crystal structures, the NDM-1 zinc ions were sandwiched by the two carboxylate groups of the respective ligands via polar interactions with the carboxylate oxygen atoms. The interaction of the carboxylate of substrate with the NDM-1 zinc ions has been reported by Linciano *et al*., 2019.

➢ In all ligand-NDM-1 crystal structures, one of the carboxylates interacts with Lys211 (184) and ASN 220 (193) residues respectively via polar interactions (salt bridge, hydrogen bonding and attractive charges respectively). The observed interactions with Lys211 (184) and ASN 220 (193) residues respectively align with the findings of Linciano *et al*., 2019.

➢ In most of the ligand-NDM-1 crystal structures, a metal-acceptor bond is formed between the enzyme's zinc ions and the oxygen atoms of the carboxylates and oxo moiety respectively. Dicarboxylic acids are potential chelating agents which can form a metal complex in the presence of a metal ion such as zinc ions.

➢ In all ligand-NDM-1 crystal structures, except for compound **98**-NDM-1 complex, the carbonyl oxygen of the oxo moiety forms a hydrogen bond with a water molecule

➢ In all ligand-NDM-1 crystal structures, the ring system (proline, thiazolidine, benzene and cyclobutane respectively) interacts with NDM-1 active site hydrophobic residues.

Table 3.2: Protein-ligand docking complexes of respective bis cyclo-amides complexed with NDM-1.

Ligand	Bis cyclo-amide-NDM-1 complexes (2D diagram)
94	
96	

98	
103	
106	
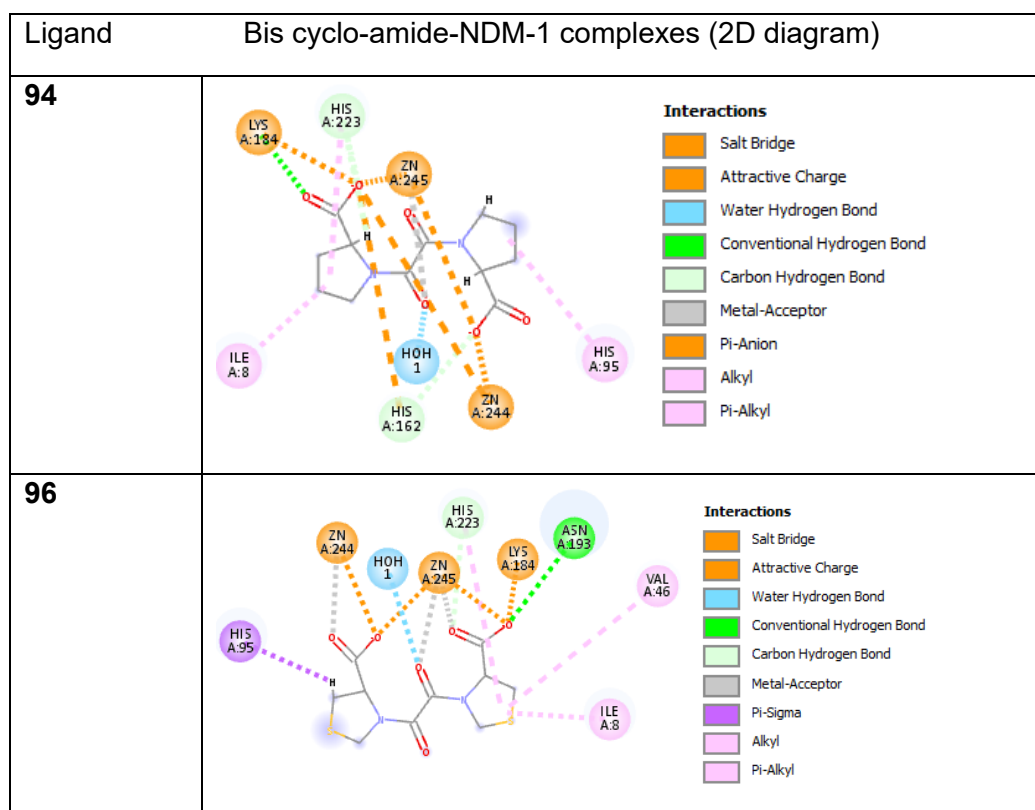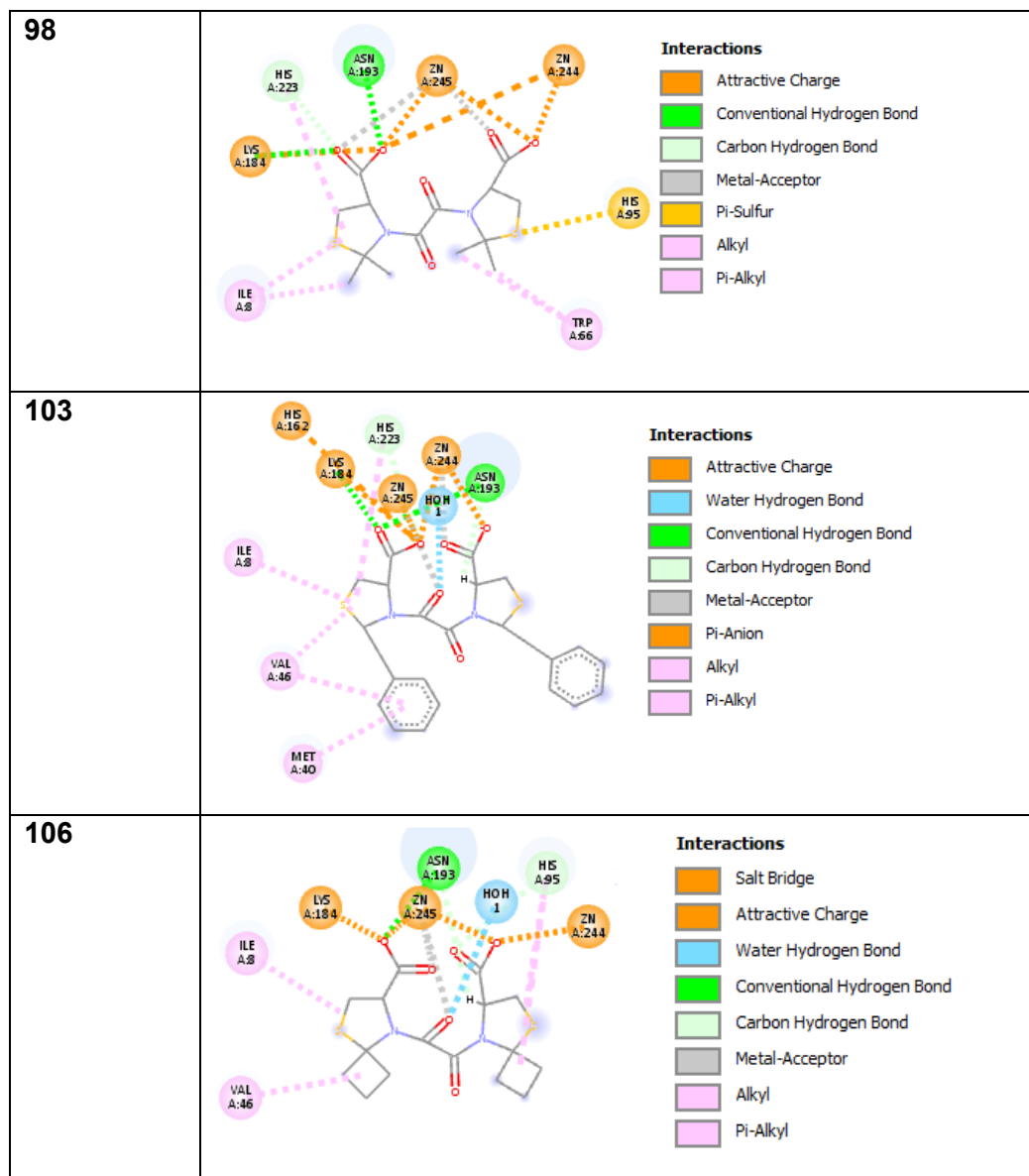
3.9 Chelation potential of bis-cyclo-oxamides

Metal-binding molecules are highly promiscuous in the human body due to a lack of selectivity over metalloenzymes and as a consequence, they are bad drug candidates. Theoretically, the final compounds, bis cyclo-oxamides, can be potential ligands due to the presence of oxygen, nitrogen and sulphur atoms as well as the dicarboxylic acid functional groups in the molecule. Preliminary UV studies were undertaken to determine if the bis cyclo-oxamides possess metal-binding properties using zinc (II) chloride, with a λ_{max} of 198 nm (Trivedi *et al*., 2017), as a source of metal ions. A fixed concentration, zinc (II) chloride was treated with varying amounts of respective bis cyclo-oxamides, in ethanol with a final volume of 3 mL, (Table 3.1), and the respective solutions were scanned after 0.5- and 10-minute incubation periods respectively in the UV region (198 – 400 nm). The respective bis cyclo-oxamides were used as positive controls while ethanol was used as blank. If the bis cyclo-oxamides possess metal-binding properties, it is expected that they would form respective complexes, with the zinc ion, which would have maximum absorption (λ_{max}) at a certain UV wavelength. Also, if there is complete utilisation of the bis cyclo-oxamides in the formation of respective zinc-complexes, the λ_{max} of the free

bis cyclo-oxamides would disappear but if the bis cyclo-oxamides are in excess, the absorbance value, which is a function of the concentration, of free bis cyclo-oxamides in the scanned solution, would decrease accordingly after the formation of the respective complexes. The scanned solutions were monitored for these changes.

3.9.1 Spectrophotometric detection of Zn (II)-bis cyclo-oxamide complex
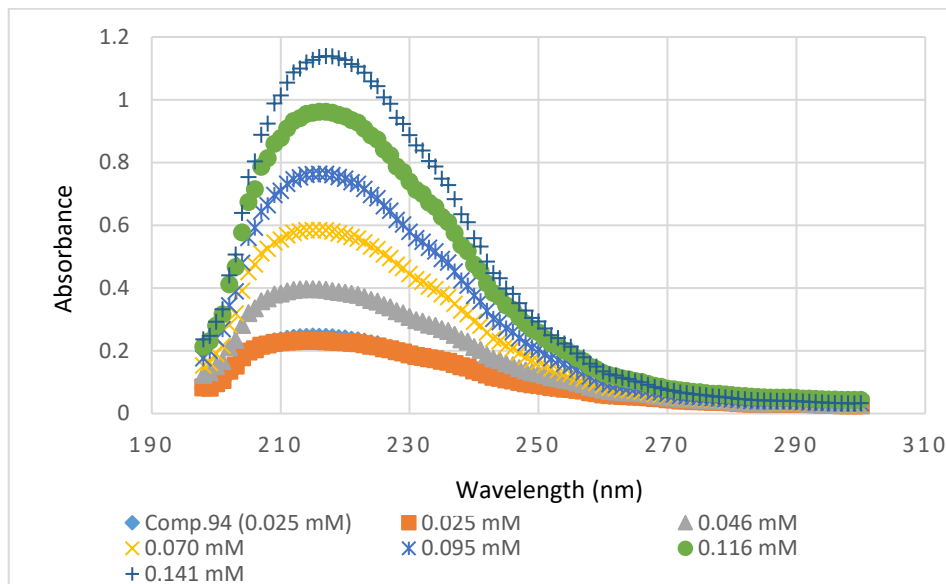
Figure 3.22: UV spectrum of zinc ions at a fixed concentration of 0.10 mM with varying concentrations of compound **94** at 0.5 minutes incubation period.

The bis cyclo-oxamide-$ZnCl_2$ samples were prepared according to the procedure stated in section 3.5 and the respective bis cyclo-oxamide-$ZnCl_2$ solutions were analysed spectrophotometrically. Table 3.1 shows the molarities of zinc (II) chloride and the respective bis cyclo-oxamide solutions as well as their respective molar ratios.

It should be noted that the concentrations reported here onward are the final concentrations of the respective bis cyclo-oxamides and the zinc (II) chloride respectively.

First, a known concentration of the respective bis cyclo-oxamides was measured and their respective λ_{max} was discovered to be similar (around 220 nm) (Figures 3.22 – 3.31). Thereafter, a known concentration of zinc (II) chloride (0.10 mM) was treated with varying concentrations (low to high molarity) of the respective bis cyclo-oxamides in ethanol and the absorbance was measured after 0.5- and 10-minutes incubation periods respectively.
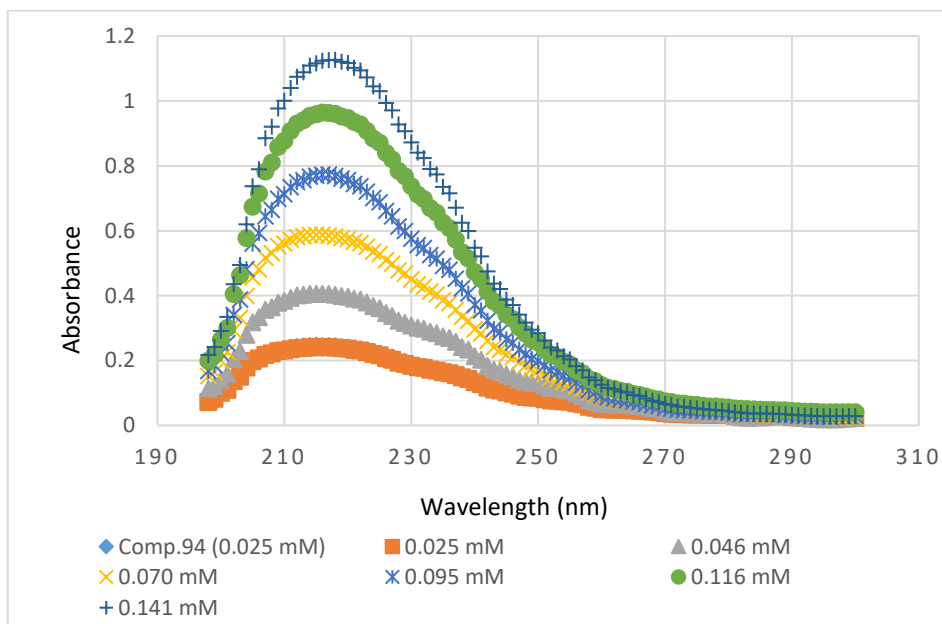
Figure 3:23: UV spectrum of zinc ions at a fixed concentration of 0.10 mM with varying concentrations of compound **94** at 10 minutes incubation period.

The spectrophotometric results showed that besides the λ_{max} of the pure bis cyclo-oxamides (220 nm), no new λ_{max} was observed, after 0.5- and 10-minute incubation periods respectively, when the zinc (II) chloride was treated with varying molarity of the respective bis cyclo-oxamides (Figures 3.22 – 3.31). Also, the absorbance of a known concentration of the respective bis cyclo-oxamides was monitored in the presence and absence of 0.10 mM of the zinc (II) chloride respectively. According to the UV results (Figures 3.22 – 3.31), there was no reduction in the absorbance of the potential ligands, despite the presence of the zinc ions in the solution, when compared with the respective controls. Expectedly, it was observed that the absorbance and molar ratio (Figure 3.32) were a function of the concentration of bis cyclo-oxamides and they increased with increasing concentration of ligands. In addition, the shoulder of the absorbance peaks broadens as the concentration of the potential ligand increases.

Considering the spectrophotometric results, it is unlikely that the bis cyclo-oxamides possess metal-binding properties and as a consequence, the off-target effects and toxicity associated with the binding of essential human metalloenzymes are potentially reduced.
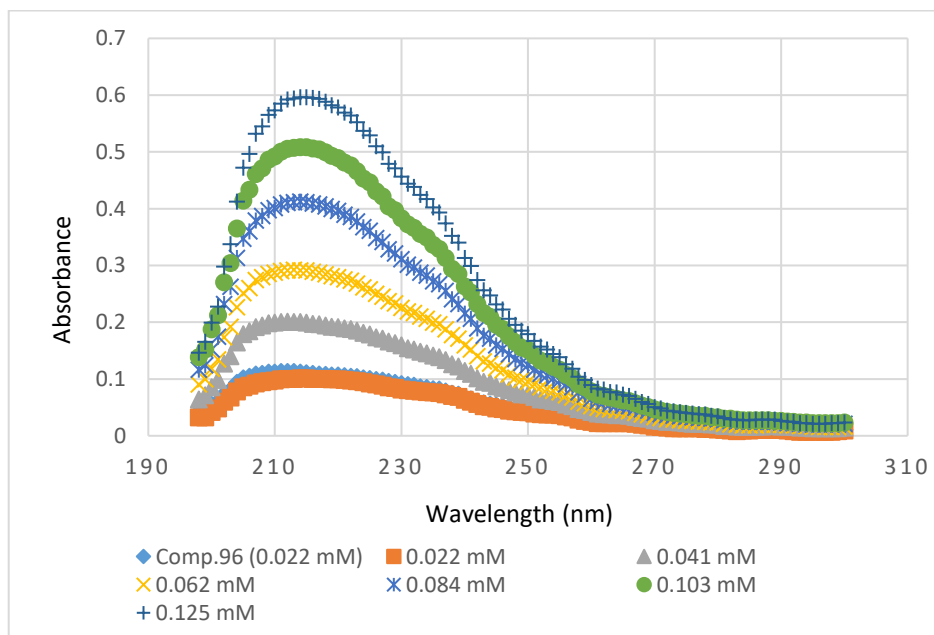
Figure 3.24: UV spectrum of zinc ions at a fixed concentration of 0.10 mM with varying concentrations of compound **96** at 0.5 minutes incubation period.
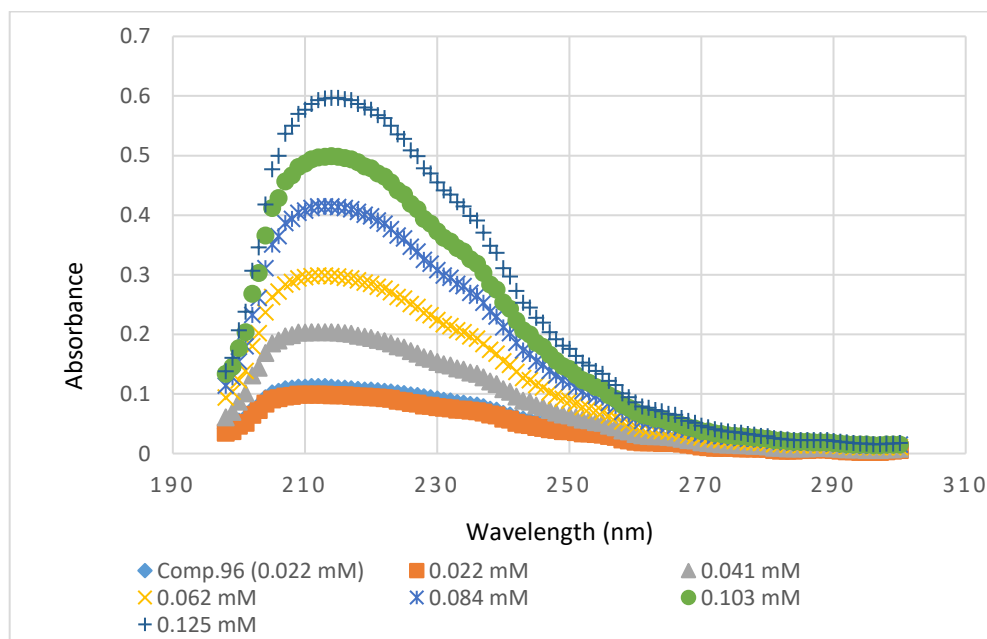
Figure 3:25: UV spectrum of zinc ions at a fixed concentration of 0.10 mM with varying concentrations of compound **96** at 10 minutes incubation period.
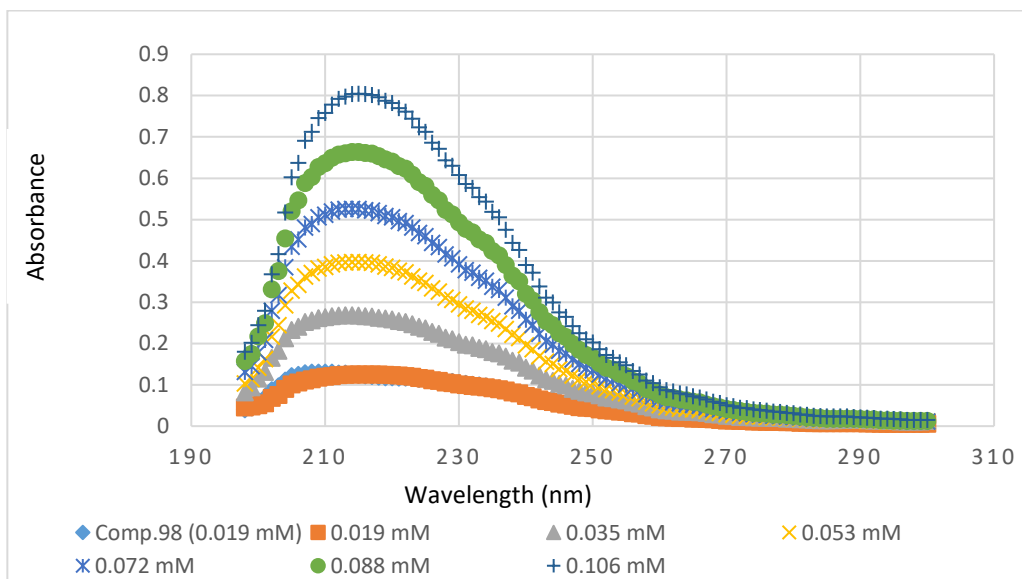
Figure 3.26: UV spectrum of zinc ions at a fixed concentration of 0.10 mM with varying concentrations of compound **98** at 0.5 minutes incubation period.
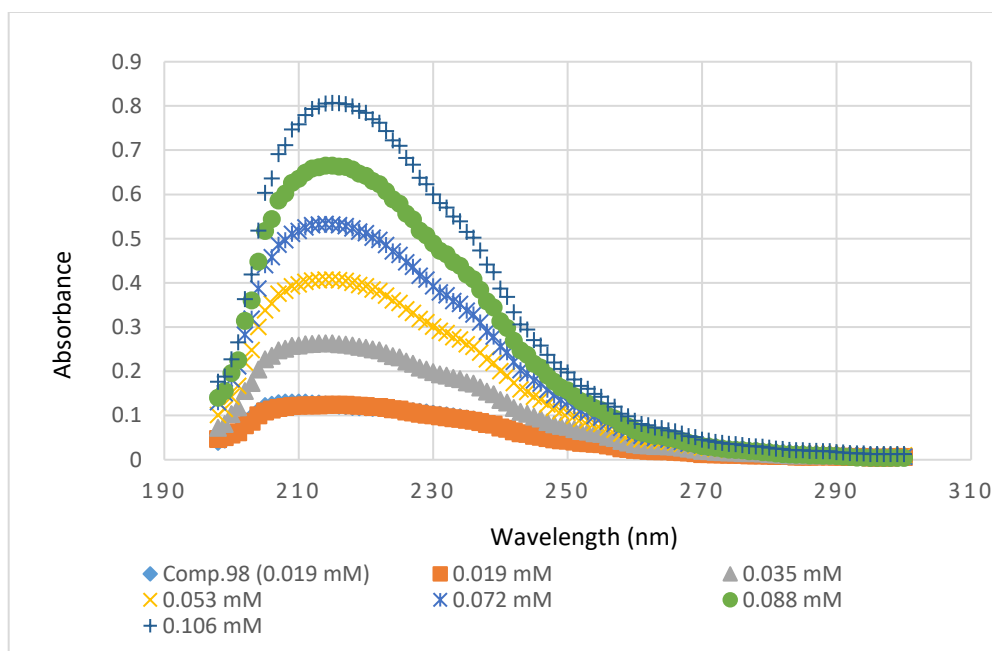
Figure 3.27: UV spectrum of zinc ions at a fixed concentration of 0.10 mM with varying concentrations of compound **98** at 10 minutes incubation period.
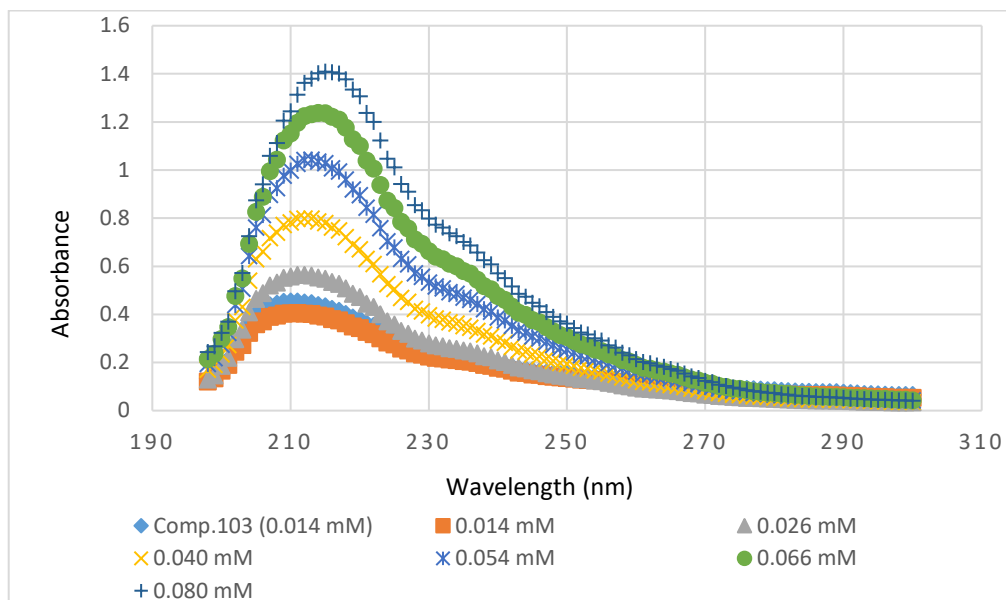
Figure 3.28: UV spectrum of zinc ions at a fixed concentration of 0.10 mM with varying concentrations of compound **103** at 0.5 minutes incubation period.
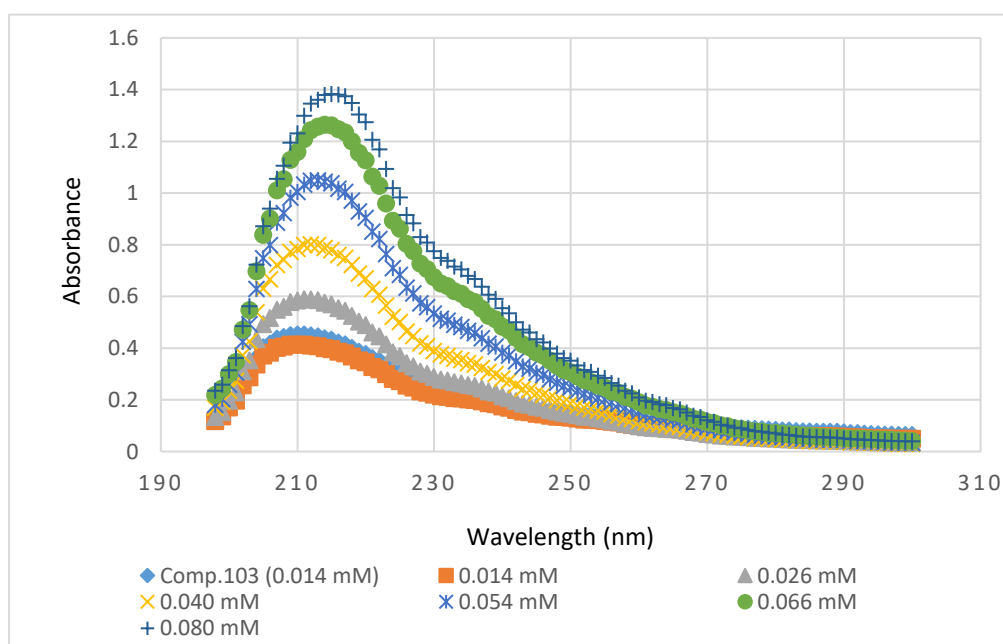
Figure 3.29: UV spectrum of zinc ions at a fixed concentration of 0.10 mM with varying concentrations of compound **103** at 10 minutes incubation period.
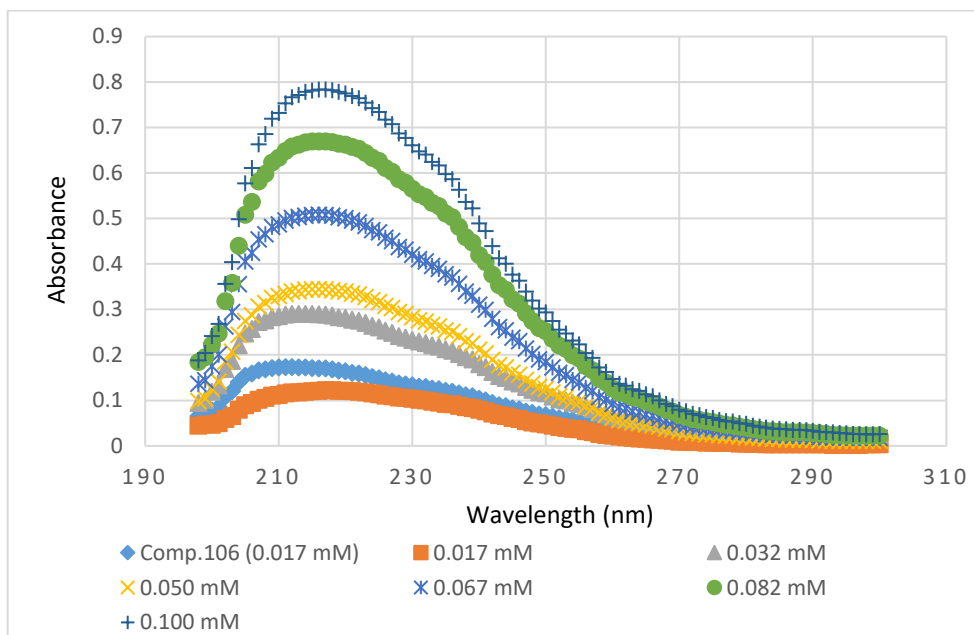
Figure 3.30: UV spectrum of zinc ions at a fixed concentration of 0.10 mM with varying concentrations of compound **106** at 0.5 minutes incubation period.
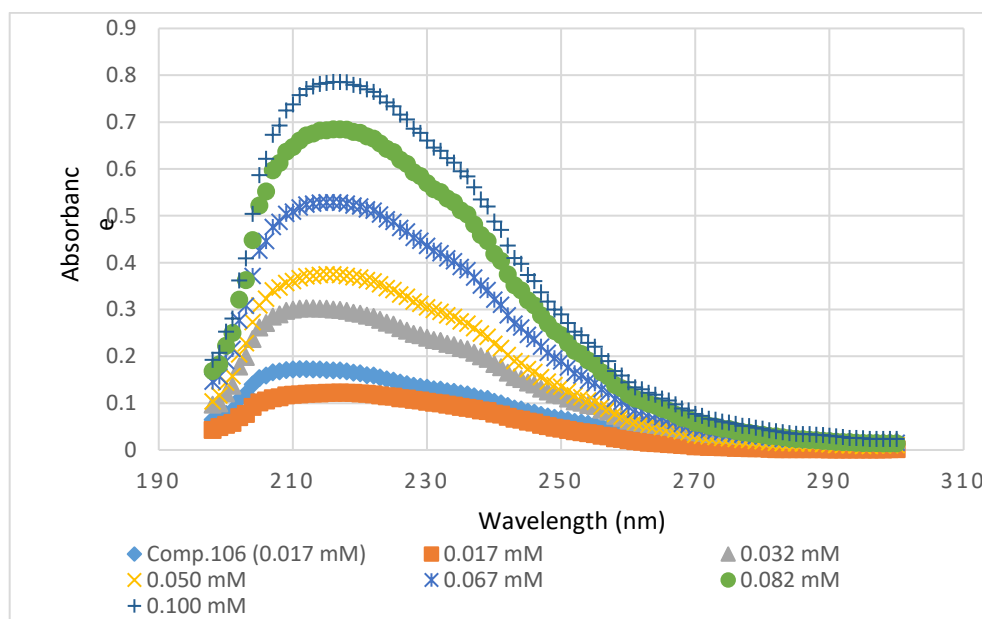
Figure 3:31: UV spectrum of zinc ions at a fixed concentration of 0.10 mM with varying concentrations of compound **106** at 10 minutes incubation period.
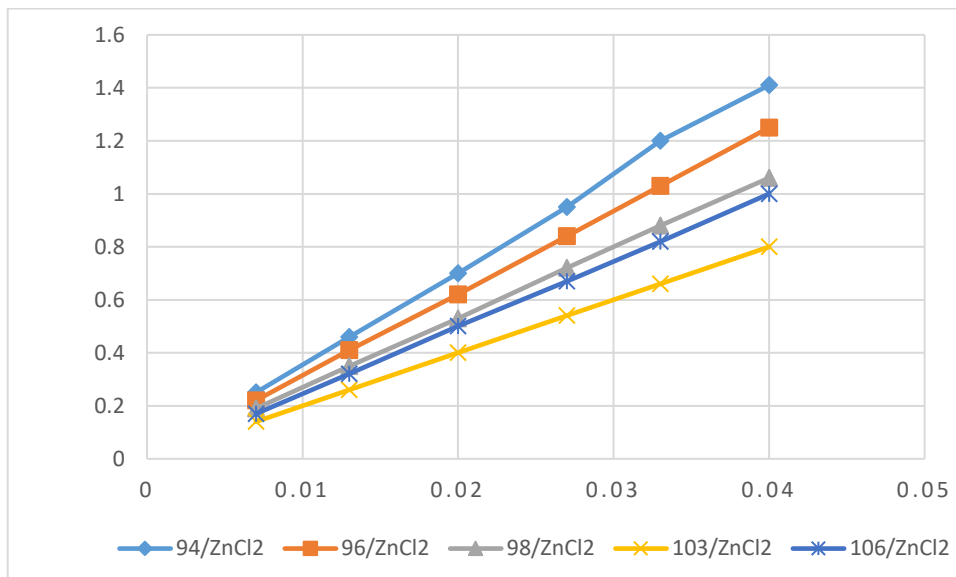
Figure 3:32: A plot of the molar ratio of ligand/ZnCl$_2$ against the concentration of potential ligand

3.10 α,β-unsaturated carbonyl compounds as potential NDM-1 inhibitors

Considering the structural and catalytic composition of the NDM-1 active site, studies have shown that the active site amino residues, Lys211 and Cys208 respectively, are essential for the activity of the enzyme (Thomas *et al*., 2014; Mercuri *et al*., 2004; Zervosen *et al*., 2001) and these residues possess reactive groups that are potent nucleophiles. The functional side chain amino group and the thiol group of NDM-1 Lys and Cys residues are nucleophilic and are susceptible to covalent modification, via Michael addition, in the presence of a suitable electrophile such as α,β-unsaturated carbonyl compounds.

Michael addition occurs due to the electronegativity of the oxygen atom of an α,β-unsaturated carbonyl compound. The electronegative oxygen atom withdraws electrons from the β-carbon, making it electron-deficient and electrophilic (Scheme 3.4) (Baker *et al*., 2007). The electrophilic β-carbon, of the α,β-unsaturated carbonyl compound, is attacked by a nearby nucleophile to generate a resonance-stabilized enolate ion which undergoes protonation at the α-carbon to give the saturated Michael addition product (Baker *et al*., 2007). The formation of the Michael addition product would likely abrogate the amino nucleophile's functionality and consequently lead to the irreversible deactivation of the enzyme (Ghosh *et al*., 1996).
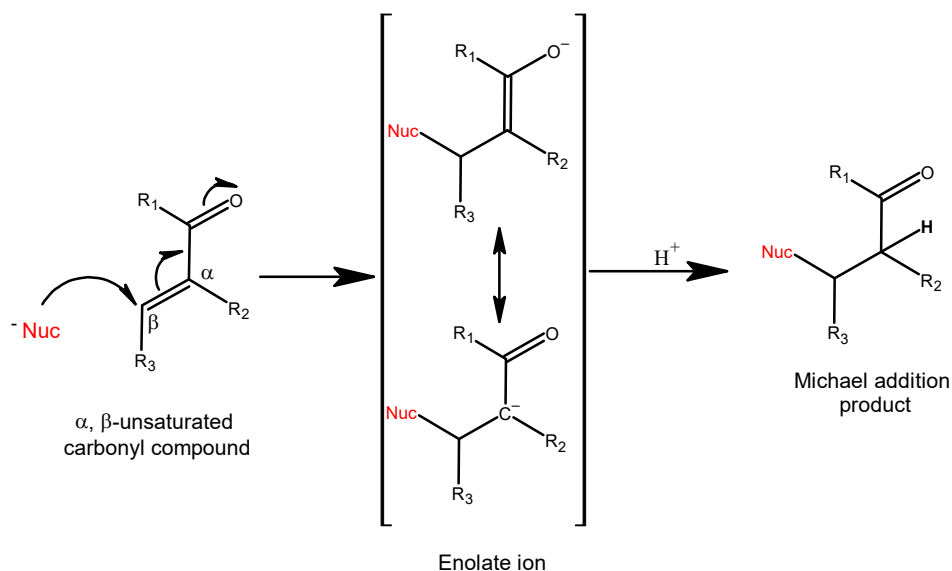
Scheme 3.4: Annotated representation of Michael addition reaction (Baker *et al*., 2007).

There are two hypothetical inhibition profiles for compound **110** (Figure 3.33). While it is possible that the α,β-unsaturated amide (**110**) would be attacked by the Lys211 nucleophile in the NDM-1 active site, it is also likely that the NDM-1 nucleophilic bridging hydroxide may induce amide hydrolysis that would result in the generation of the electrophile, α,β-unsaturated carboxylate, which is as also susceptible to Michael addition by the Lys211 nucleophile. Figure 3.33 shows a diagrammatic representation of the potential covalent modification of the NDM-1 Lys211 residue. Likewise, the Cys208 residue can potentially be modified covalently via the formation of an S-C bond with the α,β-unsaturated amide or α,β-unsaturated carboxylate.
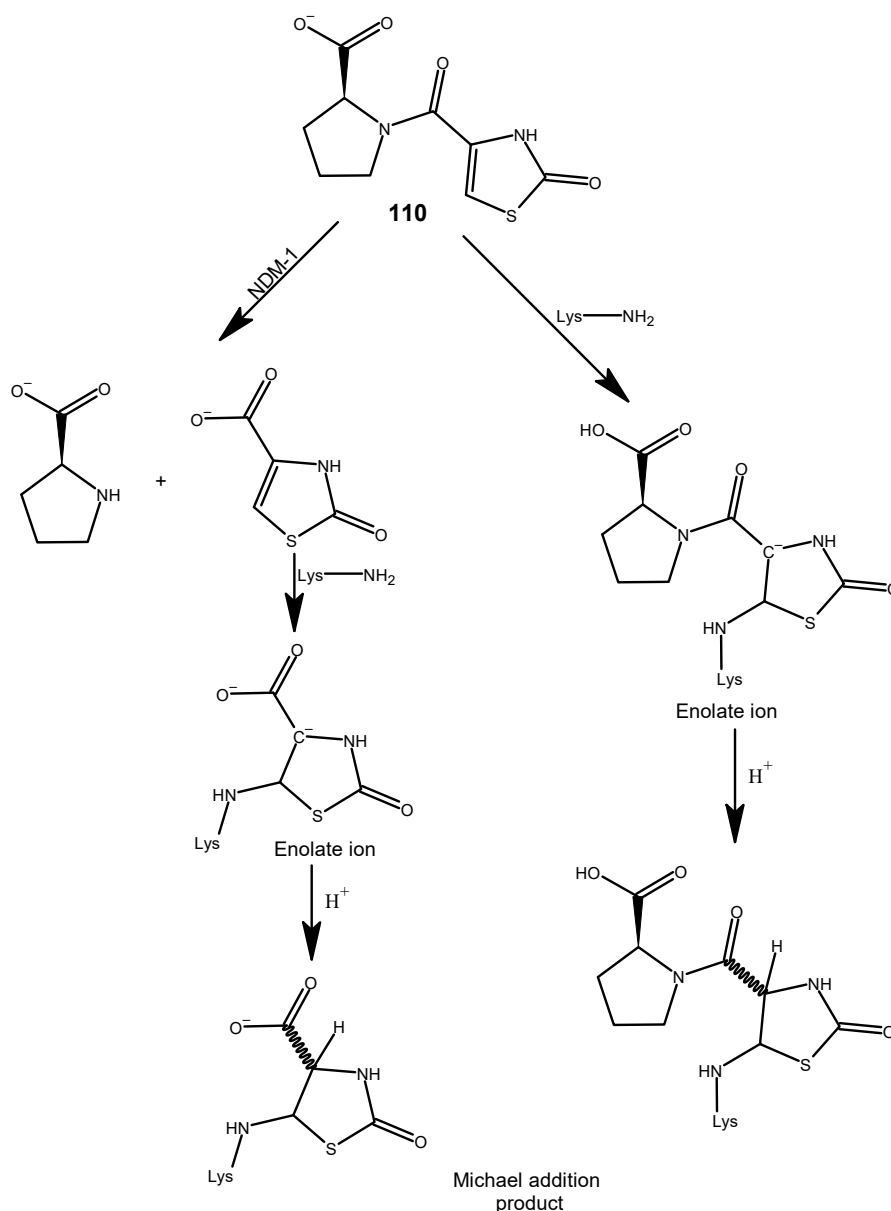
Figure 3.33: Hypothetical inhibition mechanism of compound **110**.

3.11 Experimental methods

The general analytical methods enumerated in chapter two, section 2.2, were applied in the preparation of α,β-unsaturated carbonyl compounds.

3.11.1 (S)-methyl 1-(2-oxo-2,3-dihydrothiazole-4-carbonyl)-pyrolidine-2-carboxylate (109)

To a stirred solution of (S)-methyl pyrrolidine-2-carboxylate hydrochloride (1.00 g, 6.04 mmol) in dry *N,N*-dimethylformaldehyde (20 mL) was added *N,N*-diisopropylethylamine (3.16 mL, 18.11 mmol, 3 eq.), 1-(3-dimethylaminopropyl)-3-ethylcarbodiimide hydrochloride (1.50 g, 7.85 mmol, 1.3 eq.), 1-hydroxybenzotriazole hydrate (0.63 g, 4.83 mmol, 0.8 eq.) and **75** (0.88 g, 6.04 mmol) and the resulting mixture was stirred at ambient temperature (21 °C) overnight. The mixture was diluted with ethyl acetate (40 mL), washed with 1N HCl (40 mL) and a saturated aqueous solution of NaCl (40 mL) respectively, dried with anhydrous magnesium sulphate, filtered, concentrated and purified by gradient chromatography (dichloromethane/methanol, 1, 2, 3 – 10 %) to obtain compound **109** as pale yellow paste, 0.62 g, 2.42 mmol, 40 %.
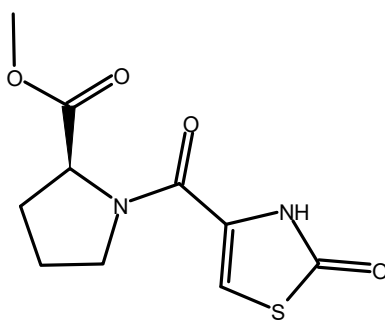
Figure 3.34: Compound **109**

Molecular Formula: $C_{10}H_{12}N_2O_4S$, R_f (dichloromethane/methanol, 15:1): 0.44 (single spot).

^{1}H NMR (400 MHz, DMSO-d_6) δ 1.93 (m, 3H, N-CH-C<u>H</u>$_2$-C<u>H</u>$_2$-CH$_2$), 2.22 (m, 1H, N-CH-CH$_2$-C<u>H</u>$_2$-CH$_2$), 3.39 (q, J = 7.0 Hz, 1H, N-CH-CH$_2$-CH$_2$-C<u>H</u>$_2$), 3.64 (s, 3H, C<u>H</u>$_3$-O-CO), 3.78 (d, J = 6.7 Hz, 1H, N-CH-CH$_2$-CH$_2$-C<u>H</u>$_2$), 4.43 (dd, J = 8.4, 5.1 Hz, 1H, N-C<u>H</u>-CH$_2$-CH$_2$-CH$_2$), 7.15 (s, 1H, NH-C=C<u>H</u>), 11.57 (s, 1H, N<u>H</u>-C=CH) ppm.

IR (ATR): v = 1171 (m, C-O ester), 1393 (m), 1444 (m, C-H), 1613 (m, C=C), 1667 (m, C=O amide), 1740 (w, C=O ester), 2953 (w, C-H alkane), 3143 (w, C-H alkene) cm^{-1}.

MS (+ESI) m/z = Found 257.0593 (M+H)$^+$; calculated for $C_{10}H_{13}O_4N_2S$ 257.0591; 1.0 ppm.

MS (+ESI) m/z = Found 279.0410 (M+Na)$^+$; calculated for $C_{10}H_{12}O_4N_2SNa$ 279.0410; 0.0 ppm.

3.11.2 (S)-1-(2-oxo-2,3-dihydrothiazole-4-carbonyl)pyrrolidine-2-carboxylic acid (110)

To a stirred solution of **109** (0.31 g, 1.21 mmol) in methanol (10 mL), at 10-15 ºC, was added aqueous solution of lithium hydroxide monohydrate (20 mL, 2 N) for over 5 minutes. The resulting mixture was allowed to gradually warm up to ambient temperature (20 ºC) and the progress of the reaction was monitored by TLC. The pH of the reaction mixture was adjusted to 3-4 using aqueous 1N HCl and the crude product was extracted with ethyl acetate (2x, 30 mL). The organic portions were combined, rinsed with a saturated aqueous solution of sodium chloride, dried with magnesium sulphate, filtered, concentrated and purified by gradient chromatography (dichloromethane/methanol, 2, 4, 6 – 20% in 0.3 % acetic acid) to obtain compound **110** as an off-white solid, 0.17 g, 0.70 mmol, 58 %.
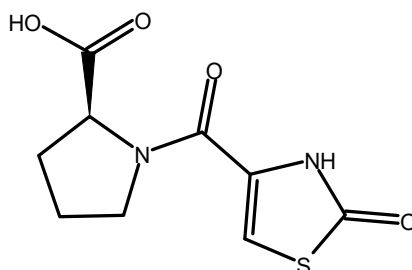
Figure 3.35: **110** (*cis* and *trans* rotamers).

Molecular Formula: $C_9H_{10}N_2O_4S$, R_f (dichloromethane/methanol, 2:1, 0.3 % acetic acid): 0.28 (single spot), melting point: 145.2 – 147.9 °C.

¹H NMR (400 MHz, DMSO-*d₆*) δ (two rotamers, *cis* and *trans*, at 298 K): 1.92 (m, total integration 3H, N-CH-C$\underline{H}_2$-CH₂-CH₂), 2.10, 2.21 (d, *J* = 5.9 Hz, ddd, *J* = 15.4, 10.0, 6.4 Hz, total integration 1H, [ratio 1.0/1.5], N-CH-CH₂-C$\underline{H}_2$-CH₂), 3.48, 3.76 (d, *J* = 8.8 Hz, q, *J* = 6.7 Hz respectively, total integration 2H [ratio 1.0/1.92], N-CH-CH₂-CH₂-C$\underline{H}_2$), 4.36, 4.65 (dd, *J* = 8.4, 5.0 Hz, s respectively, total integration 1H [ratio 1.0/0.4], N-C$\underline{H}$-CH₂-CH₂-CH₂), 6.80, 7.12 (s, s respectively, total integration 1H [1.0/2.1], NH-C=C$\underline{H}$), 11.55 (s, total integration 1H, N$\underline{H}$-C=CH), 12.76 (s, total integration 1H, COO$\underline{H}$) ppm.

¹³C ATP NMR (101 MHz, DMSO-*d₆*) δ 25.42 ($\underline{C}$H₂), 28.83 ($\underline{C}$H₂), 49.03 ($\underline{C}$H₂), 60.31 (N-$\underline{C}$H), 109.34, 128.66 (N-C=$\underline{C}$H), 129.36 (N-C=$\underline{C}$H), 129.55 (N-$\underline{C}$=CH), 157.61, ($\underline{C}$=O), 170.89 ($\underline{C}$=O), 173.37 ($\underline{C}$=O) ppm.

IR (ATR): v = 1191 (m), 1226 (m), 1389 (m), 1445 (m, C-H), 1613 (s, C=C), 1712 (s, C=O), 3156 (w, C-H alkene) cm⁻¹.

MS (-ESI) m/z = Found 241.0290 (M-H)⁻; calculated for $C_9H_9O_4N_2S$ 241.0289; 0.6 ppm.

MS (-ESI) m/z = Found 263.0108 (M-2H+Na)⁻; calculated for $C_9H_8O_4N_2SNa$ 263.0108; 0.0 ppm.

3.12 Discussion of experimental results

The synthesis of the final compound involved two steps, coupling and hydrolysis respectively (Scheme 3.5). First, the amide (**109**) was synthesised in moderate yield by EDC-induced coupling via activation of the carboxylic acid in the presence of HOBt hydrate (Scheme 3.6) and characterisation by spectroscopic methods confirms the formation of the desired compound. The EDC reacts with the carboxylic acid group, of compound **75**, to form an O-acylisourea ester whose carbonyl carbon is susceptible to attack by the hydroxy group of HOBt. The HOBt attack on the O-acylisourea ester results in the displacement of the isourea moiety with the concomitant formation of reactive benzotriazole ester (Chan and Cox, 2007). The O-benzotriazole moiety, of the benzotriazole ester, is readily displaced by the nucleophilic attack from the amino group of the proline ester, thus, resulting in the formation of an amide bond with the carboxyl group of **75** while the hydroxybenzotriazole is regenerated as a by-product (Chan and Cox, 2007).

The second synthetic step involves hydrolysis of the synthesised compound (**109**) to the corresponding carboxylic acid (**110**) using an aqueous solution of an inorganic base in methanol.
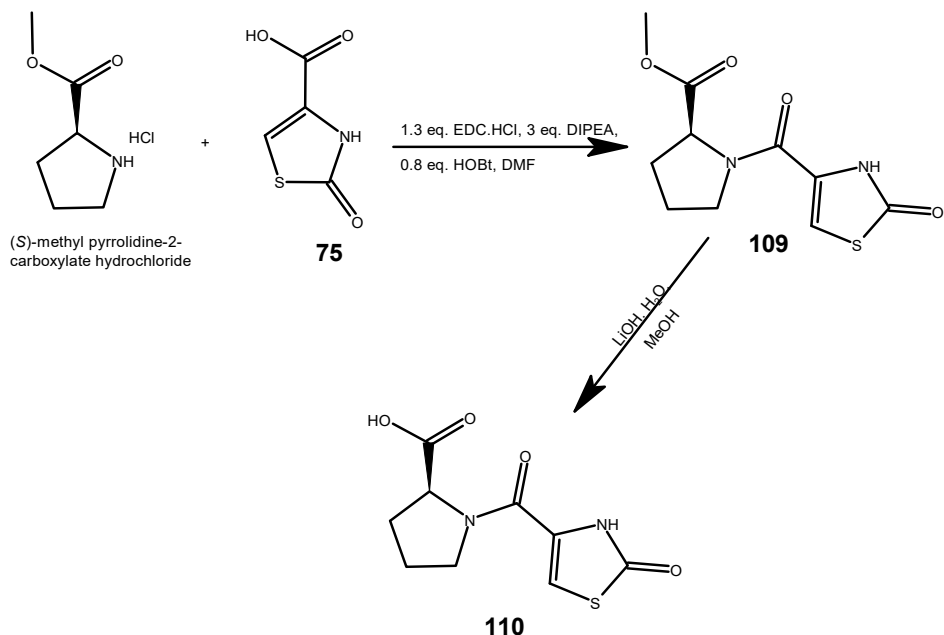
Scheme 3.5: Syntheses of compounds **109** and **110**.
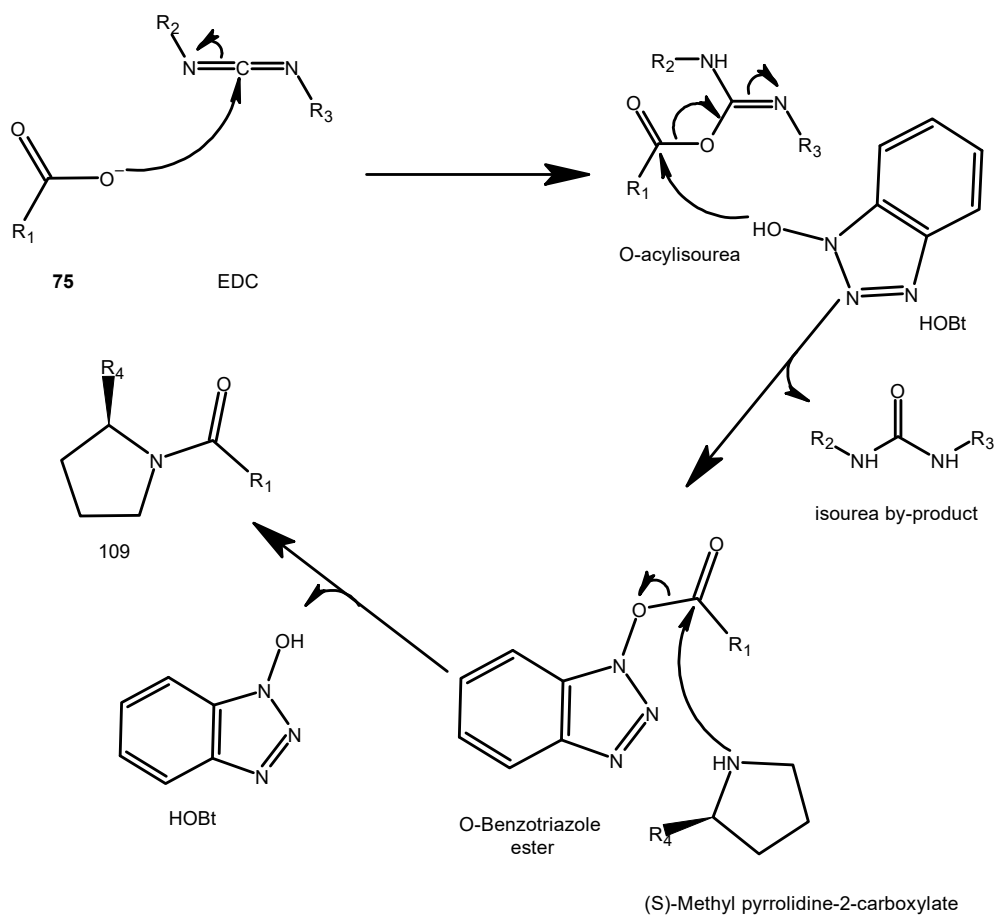
R_1 = thiazole-2(3*H*)-one
R_2 = CH_2CH_3
R_3 = $CH_2CH_2CH_2NH$- (2 x CH_3)
R_4 = $COOCH_3$

Scheme 3.6: Reaction pathway of compound **75** with (S)-methyl pyrrolidine-2-carboxylate in the presence of EDC.HCl/HOBt (Chan and Cox, 2007).

Furthermore, protein-ligand docking studies conducted by Eshtiwi, A. showed that compound **110** has the potential to form several non-covalent interactions with the enzyme active site (Figure 3.36). The carboxylate binds the loop 10 residues (Lys211(184) and ASN220(193)), both zinc ions and histidine residue respectively via polar interactions while the proline moiety seems to interact with the enzyme's hydrophobic residues. Also, the cyclic amide oxygen hydrogen bond with Asp124 (97) while the acyclic amide oxygen intercalates Zn2 and a water molecule.
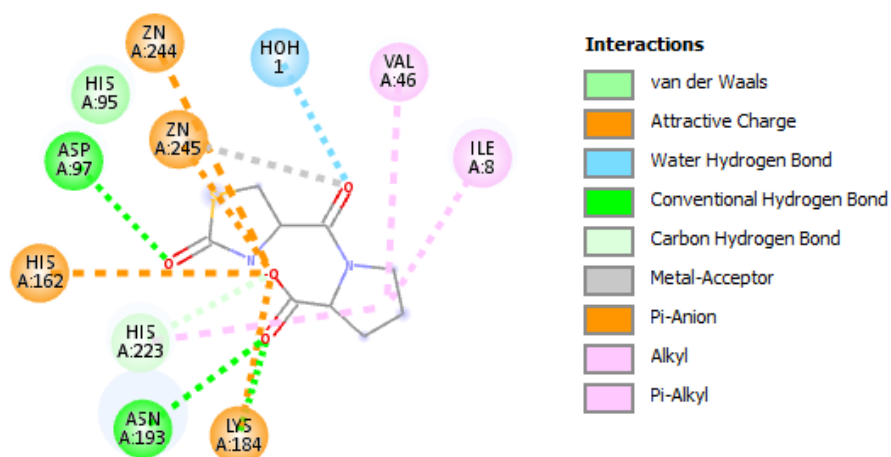
Figure 3.36: Compound **110**-NDM-1 complex (2D diagram).

Chapter 4

4.1 Biological Evaluation: Inhibitory potential of bis cyclo-oxamides and α,β-unsaturated carbonyl compound against NDM-1 activity

The application and frequent use of β-lactam antibiotics have resulted in the emergence and dissemination of highly efficient resistance mechanisms, such as the secretion of β-lactamase, in clinically relevant bacterial pathogens (Bonomo, 2017). The increased susceptibility of commonly used β-lactam antibiotics to bacterial strains harbouring β-lactamase(s) is an increasing threat to public healthcare (WHO, 2012). The discovery and application of clinically relevant β-lactamase inhibitor(s) would erode the threat of β-lactamase associated pathogens to public healthcare. However, the ability to detect, identify and quantify β-lactamase(s) is crucial in the biological research and discovery of potential inhibitors of β-lactamase enzymes (Pala *et al*., 2020). Several screening techniques for *in vitro* and *in vivo* detection and estimation of β-lactamases have been reported (Viswanatha *et al*., 2008; van Berkel *et al*, 2013) and these techniques are either qualitative or quantitative. One of the prerequisites for the screening of β-lactamase activity is the application of a suitable substrate. Generally, an appropriate enzyme substrate for this purpose consists of two main substructures which include:

➢ the recognition/binding moiety, which is recognised by the target enzyme and essential for the binding of the substrate and

➢ the signal-generating substructure, which produces a detectable and measurable signal(s) after the enzymatic reaction (Pala *et al*., 2020).

Substrates for the screening β-lactamase activity can be categorised based on the type of signal that is generated following the enzymatic reaction and they include

➢ fluorogenic substrates (Gao *et al*., 2003; Rukavishnikov *et al*., 2011; Zhang *et al*., 2013; Klingler *et al*., 2015).

➢ chromogenic substrates such as (6R,7R)-3-[(3-carboxy-4-nitrophenyl)sulfanylmethyl]-8-oxo-7-[(2-thiophen-2-ylacetyl)-amino]-5-thia-1-azabicyclo[4.2.0]oct-2-ene-2-carboxylic acid (CENTA) (Jones *et al*., 1982a), pyridine-2-azo-*p*-dimethylanaline cephalosporin (PADAC) (Jones *et al*., 1982b), cephalothin (Jones *et al*., 1982b) and nitrocefin (Shannon and Phillips, 1980).

➢ luminescent probes (Yao *et al*., 2007, Pala *et al*., 2020)

➢ penams, such as penicillin V. The hydrolysed product of penicillin V can be detected by thin layer chromatography.

4.2 Fluorogenic and chromogenic substrates

Most of the chromogenic and fluorogenic substrates employed in screening β-lactamase activity are cephalosporin-based substrates and their principle of action are similar (Pala *et al*., 2020; van Berkel *et al*, 2013). The cephalosporin scaffold is of important interest in the development of β-lactamase substrate owing to its cleavable amide bond as well as its potential leaving group at position 3' which serves as an anchor for the linkage of the suitable fluorogenic/chromogenic substituents.

4.2.1 Fluorogenic substrates

Concerning the fluorogenic substrates, the cleavage of the amide bond initiates the release of the fluorochrome (Figure 4.1), which is excited by a given wavelength of incident light (photon). The excited state decays rapidly to the ground state with concomitant emission of a fluorescence signal (photon) that can be detected and measured fluorometrically at the emission wavelength (Guilbault, 1990). Different cephalosporin-based fluorogenic substrates have been synthesised via the conjugation of different coumarin derivatives to respective cephalosporin scaffolds. 4-Methylumbelliferone (4-MU, compound **111**) (Figure 4.2) is one of the widely used fluorescent moieties (Rajapaksha *et al.*, 2019) and its derivatives were first employed in the 70s for the detection of bacterial enzymes.

112: R_1 = Bn, R_2 = R3 =H, n = 0, X = O
113: R_1 = Bn, R_2 = R3 =H, n = 1, X = O
114: R_1 = Bn, R_2 = OMe, R3 =H, n = 0, X = O
115: R_1 = Bn, R_2 = R3 =H, n = 2, X = O
116: R_1 = Bn, R_2 = H, R3 =CH_3, n = 0, X = S
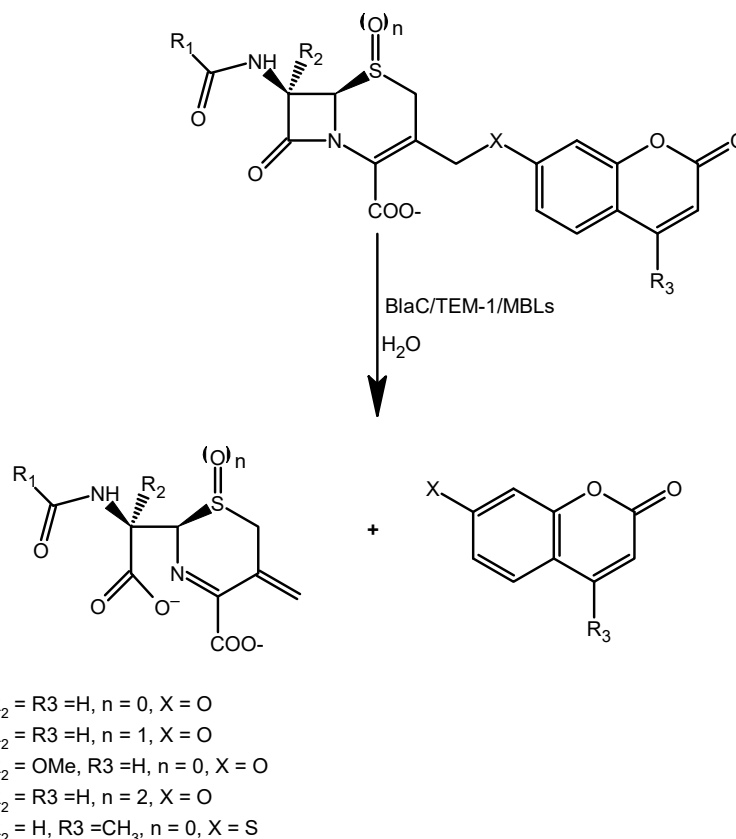
Figure 4.1: β-lactamase induced release of fluorophore (Xie *et al.*, 2012; van Berkel *et al.*, 2013).

Xie *et al.* (2012) reported the development of fluorogenic probes for the early detection of BlaC, an enzyme that is naturally expressed and secreted by the pathogen *tubercle bacilli*, as early detection of the enzyme is essential for improved treatment regimen of tuberculosis. The cephalosporin-based fluorogenic substrates enabled sensitive and selective detection of BlaC in the presence of its class A analogue, TEM-1 β-lactamase. The main difference between the two class A enzymes results from residue 164, which is an arginine in TEM-1 and an alanine in BlaC. Arginine (164) plays a central role in the molecular dynamics of the substrate-specificity loop, in TEM-1, because it is associated with the formation of three additional salt bridges. However, the alanine mutation (BlaC) results in the loss of these stabilizing salt bridges in BlaC, which ultimately enhances the flexibility of the BlaC substrate-specificity loop, relative to that of TEM-1, in the hydrolysis of bulkier substrates. Xie and colleagues (2012) synthesised several umbelliferone-based probes with bulky groups at the 7-position on the lactam ring and evaluated their selectivity profiles for BlaC over TEM-1. While compounds **112** and **113**

showed no remarkable selectivity profile, compound **114** showed a distinct selectivity profile for BlaC over TEM-1 owing to its methoxyl group which provided the optimum hydrolytic rate for the release of the fluorophore (Figure 4.2).

112: R_1 = Bn, R_2 = R_3 =H, n = 0, X = O
113: R_1 = Bn, R_2 = R_3 =H, n = 1, X = O
114: R_1 = Bn, R_2 = OMe, R_3 =H, n = 0, X = O
115: R_1 = Bn, R_2 = R_3 =H, n = 2, X = O
116: R_1 = Bn, R_2 = H, R_3 =CH$_3$, n = 0, X = S
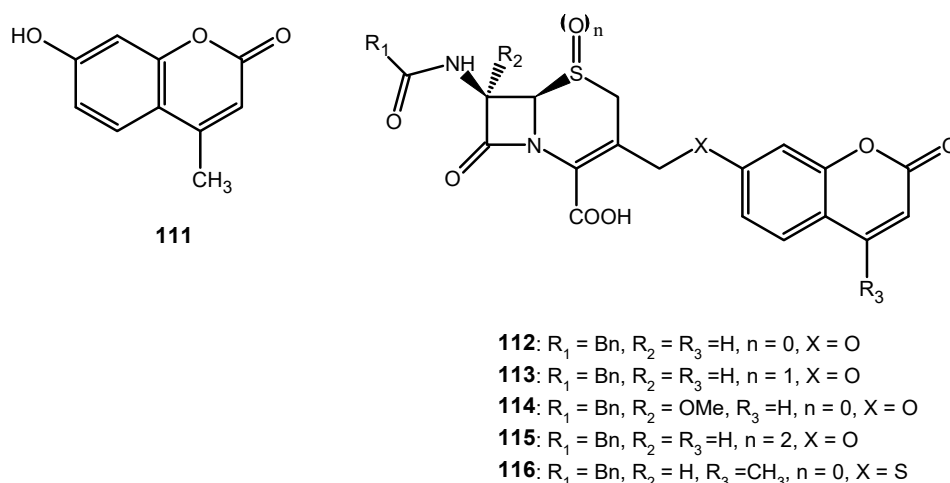
Figure 4.2: Structure of β-lactamase fluorogenic substrates

Following the outcome of BlaC cephalosporin-based fluorogenic substrates study by Xie *et al.* (2012), analogues of compound **113** (**115** and **116**) were synthesised and evaluated, along with compound **112** and other chromogenic substrates, against a panel of Metallo-β-lactamases (NDM-1, VIM-2, IMP-1, SPM-1 and BcII) in order to compare their kinetic parameters (van Berkel *et al.*, 2013). The studies revealed that compounds **113** and especially **115** are highly sensitive and efficient fluorogenic substrates for the screening of the five Metallo-β-lactamases owing to their high K_{cat}/K_M values which is an indicator of the respective enzyme kinetic efficiency. Interestingly, for NDM-1 specifically, it was observed that the oxidation of the dihydrothiazine sulphur seemed to enhance the K_{cat}/K_M value for compounds **115** and **113** by up to 20- and 3-folds respectively when compared with the K_{cat}/K_M value of compound **112**.

4.2.2 Chromogenic substrates

Concerning cephalosporin-based chromogenic substrates, the hydrolysis of the amide bond, induced by enzymatic action, initiates the release of the chromogen which generates detectable signals that can be measured spectrophotometrically at the appropriate wavelength (Pala *et al.*, 2020; van Berkel *et al*, 2013; Bebrone *et al.*, 2001). Several β-lactamase assay platforms have employed cephalosporin-based chromogenic substrates.

Schindler and Huber (1980) developed one of the oldest cephalosporin-based chromogenic substrates, PADAC (**117**) (Figure 4.3). The substrate (**117**) has a distinct colour change from purple to clear yellow with changes in λ$_{max}$ from ca. 570 nm to ca. 465 nm following the scission of the beta-lactam ring by β-lactamase. Schindler and Huber (1982) also synthesised the analogue of PADAC (**117**), CENTA (**118**), a cephalosporin-based chromogenic substrate, by substituting the dimethyl-4-(pyridin-2-yldiazenyl)aniline substituent with 5-mercapto-2-nitrobenzoic acid. CENTA (**118**) is a β-lactamase-labile chromogenic substrate that changes from light yellow (λ$_{max}$ ca. 340 nm) to chrome yellow (λ$_{max}$ ca. 405 nm) following the hydrolysis of the β-lactam ring and expulsion of the C-3' leaving group (Bebrone *et*

al., 2001). Upon discovery of nitrocefin (**120**), its β-lactamase sensitivity was compared with that of PADAC (**117**) using different β-lactamase-producing bacteria (Jones *et al*., 1982b). The *in vitro* studies showed that the substrate, PADAC (**117**), has reduced β-lactamase susceptibility compared to nitrocefin (**120**) but has a better stability profile in biological fluids, such as human serum and broth culture media respectively. A similar β-lactamase substrate susceptibility study was carried out using PADAC (**117**), CENTA (**118**), cephalothin (**119**) and nitrocefin (**120**) respectively (Jones *et al*., 1982a). The susceptibility of the substrates, with the C-3' leaving group, to β-lactamase, was compared with that of nitrocefin in an *in vitro* study using different β-lactamase-producing bacteria. The findings revealed that CENTA (**118**) displayed promising characteristics, over cephalothin (**119**), as a potential diagnostic substrate while nitrocefin (**120**), as expected, proved to be a better substrate for early detection of β-lactamase-producing clinical isolates compared to CENTA (**118**).

117

118

119

120
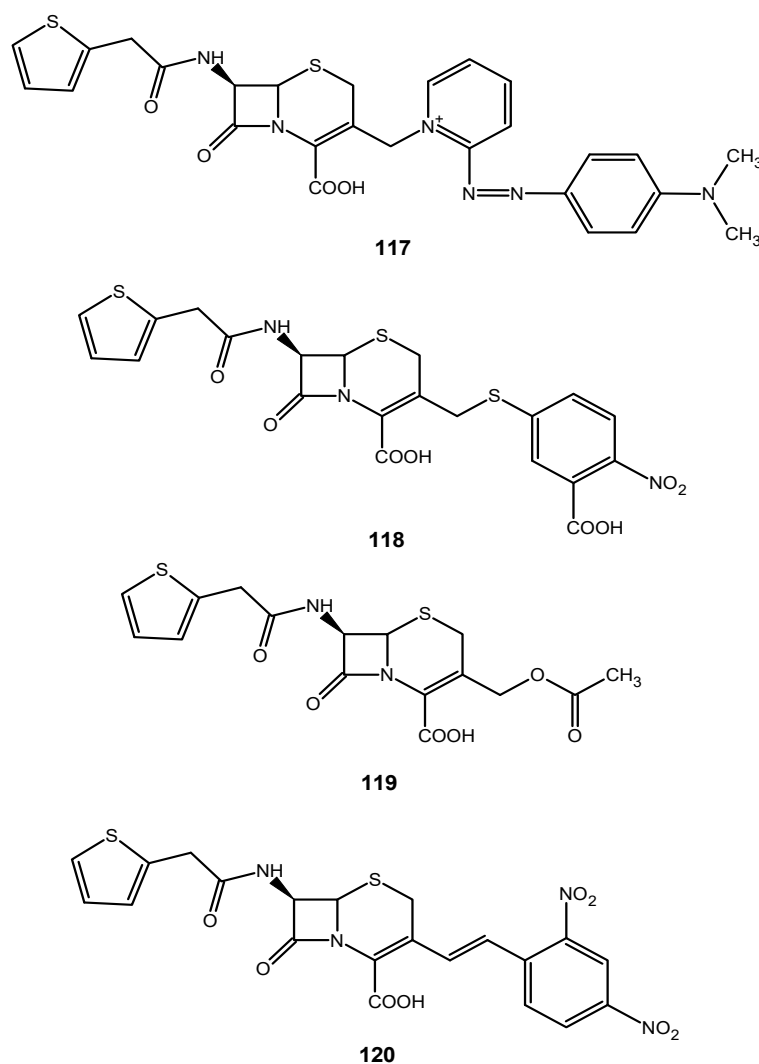
Figure 4.3: Structures of β-lactamase chromogenic substrates.

Nitrocefin (**120**) is a widely used chromogenic substrate for the screening of β-lactamase activity due to its sensitivity and reliability (O'Callaghan *et al*., 1972). Besides its sensitivity and reliability, nitrocefin (**120**) is uniquely different from the other chromogenic substrates as the leaving group bond is replaced by an alkene group. Generally, most cephalosporins have maximum absorption at ca. 237 nm and ca. 260 nm owing to the thienyl-acetyl-7-acyl group and the β-lactam ring respectively but nitrocefin (**120**)

was discovered to have an extra absorption maximum at 386 nm in addition to maximum absorption at 237 nm and ca. 260 nm respectively (O'Callaghan *et al*., 1972). Considering that compounds related to dinitrostyrene have λ_{max} around ca. 320 nm, O'Callaghan *et al.* (1972) attributed the extra λ_{max} of nitrocefin (386 nm) to the dinitrostyrene substituent and stipulated that the bathochromic shift (320 nm to 386 nm) is due to the conjugation of the dihydrothiazine ring with the dinitrostyryl group in addition to the conjugation in the β-lactam ring. Nitrocefin (**120**) generates yellow colour in solution with a λ_{max} of 386 nm but following β-lactamase action, the colour changes to red with a λ_{max} of 482 nm. Unlike PADAC, CENTA, the release of its chromogen is not associated with the expulsion of a leaving group (O'Callaghan *et al.,* 1972). Despite the sensitivity of nitrocefin in detecting β-lactamase in bacterial strains, O'Callaghan *et al*. (1972) discovered that it is unstable in biological fluids such as serum, hence its applications *in vivo* studies are limited.

4.3 Luminogenic probes

The luminogenic-based assay is a new technique with better superiority to fluorogenic and chromogenic-based assays and it does not depend on an external light source for excitation. The emission of light from luminogenic substrates is a consequence of the presence of an enzyme, atoms, molecules or metabolites (Pala *et al*., 2020; Yao *et al*., 2007; Chen *et al*., 2017; Hananya and Shabat, 2019). Generally, there are two types of luminescence probes for screening β-lactamase activity and they are bioluminescence probes and chemiluminescence probes.

4.3.1 Bioluminescence probes

Bioluminescence is a natural phenomenon that is associated with the emission of light generated by a biological reaction within various living organisms such as insects, bacteria and marine organisms (Li *et al*., 2013; Pala *et al*., 2020). One of the most studied bioluminescent systems is the firefly luciferin–luciferase reaction, where the bioluminescence is produced by an oxidative transformation of the substrate, luciferin (**121**), into an excited state intermediate by the enzyme luciferase, in the presence of oxygen, ATP and Mg^{2+} cofactors, (Li *et al*., 2013; Yao *et al*., 2007) followed by relaxation of the excited intermediate back to the ground state. The mechanism involves the formation of luciferyl adenylate (Figure 4.4), following the reaction of firefly-luciferin (**121**) with ATP, which oxidises and cyclises to the corresponding dioxetanone intermediate with concomitant expulsion of AMP. The decarboxylation of dioxetanone anion generates the excited state/light emitter oxyluciferin. A luminescent light, with a peak intensity range of 530 to 640 nm which can be captured with a sensitive charge-coupled device (CCD), is produced following the relaxation of the excited oxyluciferin to the ground state (Fraga *et al*., 2004; Branchini *et al*., 2015; Pala *et al*., 2020; Li *et al*., 2013).

[Figure redacted]

Figure 4.4: The pathway for firefly bioluminescence emission (Li *et al*., 2013).

Scientists are exploring this natural phenomenon in the development of luminogenic-based assay. Yao and colleagues (2007) designed and developed a cephalosporin-based bioluminescence substrate, Bluco (**122**), for imaging β-lactamase activity *in vivo*. Bluco (**122**) was developed by the coupling of the 6-hydroxy group of synthesised D-luciferin to the C-3' position of the cephalosporin through an ether bond while the stability of the conjugate was enhanced by the oxidation of the dihydrothiazine sulfide group to the corresponding sulfoxide (Figure 4.5). Bluco (**122**) is a poor substrate for luciferase but a good substrate of β-lactamase. β-lactamase prompts the scission of the amide bond, of Bluco (**122**), resulting in tautomerisation of the double in the dihydrothiazine ring and subsequent release of the luciferin substituent (**121**) upon the cleavage of the ether bond (Figure 4.5). The free luciferin (**121**) is oxidised in the presence of the luciferase resulting in the generation of luminescent light that is captured by a suitable CCD. Bluco (**122**) is mainly applied in *in vivo* studies, however, its fluorogenic feature, with pre-β-lactamase maximum fluorescence emission of 440 nm and post-β-lactamase maximum emission of 540 nm respectively, can be employed in the measurement of its hydrolysis kinetics in the presence of β-lactamase (Yao *et al*., 2007).

[Figure redacted]

Figure 4.5: The structure of Bluco and the pathway for bioluminescent emission of activated Bluco (Yao *et al.*, 2007).

4.3.2 Chemiluminescence probe

While bioluminescence is associated with an enzymatic reaction, chemiluminescence is a non-enzymatic process that is characterised by the emission of light due to a chemical reaction. In chemiluminescence, a high-energy intermediate is produced as a result of a chemical reaction and in the presence of oxygen or hydrogen peroxide, the energetic intermediate returns to the ground state emitting a luminescence signal in the process (Chen *et al.*, 2017; Hananya and Shabat, 2019).

The adamantane-1,2-dioxetane derivative (**123**) was amongst the first chemiluminescence probes introduced by Schaap over two decades ago (Figure 4.6) (Pala *et al.*, 2020). The chemiluminogenic process of compound **123** involves the deprotection of its hydroxyl group by enzymatic action, followed by deprotonation of the newly formed phenol-dioxetane intermediate at an alkaline pH 10. The deprotonated phenolate decomposes, generating an excited phenolate species via a chemiexcitation phenomenon. The relaxation of the excited phenolate species to the ground state is accompanied by the emission of luminescence that can be captured by a suitable device (Figure 4.6) (Pala *et al.*, 2020). The four-membered ring peroxide, which is structurally similar to the luciferin intermediate, and the adamantanylene substituent are not associated with the chemiluminescence properties of the compound **123** rather the four-membered ring peroxide is associated with the decarboxylation of the phenolate-dioxetane intermediate while the adamantanylene substituent confers stability to the molecule (Pala *et al.*, 2020).

[Figure redacted]

Figure 4.6: The pathway for chemiluminescent emission of adamantane-1,2-dioxetane (**123**) (Pala *et al*., 2020).

Despite the chemiluminescence properties of the adamantane-1,2-dioxetane derivatives, the *in vitro* and *in vivo* application of these probes in biological systems is challenging owing to the water-associated quenching of the luminescence. However, the chemiluminescence quenching in water was suppressed by introducing an electron-withdrawing acrylic substituent into the ortho position on the phenoxy-dioxetane moiety (**124**) (Hananya *et al*., 2016; Hananya and Shabat, 2017; Hananya and Shabat, 2019).

Considering compound **123** as a potential probe for enzyme activity screening, Das *et al*. (2020) exploited the chemiluminescence properties of **123** in developing the first carbapenem-based chemiluminescence probe (**124**) for the screening of bacterial resistance, associated with carbapenemases (Figure 4.7). Das *et al*. (2020) developed the carbapenem-based chemiluminescence probe by coupling the adamantane-dioxetane-based luminophore to a carbapenem core through a 4-hydroxymethylphenyl linker and evaluated the mechanism of the probe (**124**) by monitoring its hydrolysis and fragmentation profiles in the presence of a known carbapenemase (SPM-1) in a PBS buffer at physiological pH 7.4, using RP-HPLC and mass spectroscopy respectively. Furthermore, they evaluated the chemiluminescence profile of the probe (**124**) by suspending colonies of live bacteria-producing carbapenemases (IMP-2 and KPC-2) in PBS buffer at physiological pH 7.4 and measured the light emission in the presence of the carbapenem-based probe (**124**) over time. According to their findings, compound **124** enabled the detection and measurement of carbapenemase activities owing to the strong chemiluminescence output of the PBS-bacterial suspension. The hydrolysis and fragmentation studies of the probe (**124**) in the presence of SPM-1 in addition to the chemiluminescence study, indicate that the potential mechanism of the carbapenem-based probe (**124**) in the detection and measurement of carbapenemase activities involves the generation of the phenolate-dioxetane, with

concomitant elimination of the carbapenem moiety, following carbapenemase-induced cleavage of the amide bond (Figure 4.7). The phenolate-dioxetane facilitates the generation of the excited benzoate species via a chemiexcitation phenomenon while the decay of the excited benzoate species to the ground state is accompanied by the emission of a chemiluminescence signal (bright green light) which correlates to the carbapenemase activity.

To consolidate the reliability of the carbapenem-based probe (**124**), Das *et al*. (2020) evaluated its ability to detect live bacteria-producing carbapenemases, IMP-2 and KPC-2, in the presence and absence of a Metallo-β-lactamase inhibitor (EDTA) and a serine-β-lactamase (3-aminophenylboronic acid) respectively. The results showed that in the absence of the respective inhibitors, the probe was able to detect carbapenemase activity while in the presence of the respective inhibitors, the probe detected insignificant or no carbapenemase activity.

The carbapenem-based probe (**124**) is unique and essential in the selective detection of carbapenemase activity over regular β-lactamase activity.

[Figure redacted]

Figure 4.7: The structure of compound **124** and the pathway for chemiluminescent emission of activated adamantane-1,2-dioxetane (Das *et al*., 2020; Pala *et al*., 2020).

4.4 Thin layer chromatography (TLC)-based assay

A highly sensitive, efficient and reliable substrate is essential for the biological evaluation of potential β-lactamase inhibitors. However, cost and commercial availability are also important factors when considering the type of substrate for inhibitory studies. The susceptibility of most penams to β-lactamase has been exploited by Lopeman *et al*. (2020) in the development of a novel TLC-based assay. Lopeman *et al*. (2020) applied the new technique in the screening of *Mycobacterium abscessus* β-lactamase (Bla*Mab*) activity by monitoring the hydrolytic profile of penicillin V potassium salt (**125**) in the presence of the Bla*Mab* along with a positive control which contains only the substrate, penicillin V (Figure 4.8). After 10 minutes incubation period, an aliquot of the respective mixtures was spotted on an aluminium-backed silica gel plate (60 F_{254}, Merck). The plate was dried and subjected to Thin-layer Chromatography analysis using a suitable mobile phase. Once dried, the plate was visualised with an aqueous solution of potassium permanganate ($KMnO_4$). According to their findings, the retention factor (R_f) of the spot that contains the enzyme and the substrate was significantly lowered when compared with the positive control. This indicates that the enzyme, Bla*Mab*, hydrolysed substrate, penicillin V, to the corresponding penicilloic acid product which has a lower R_f value. The TLC-based assay was further validated by incubating the Bla*Mab* with penicillin V in the presence of known inhibitors, relebactam and avibactam respectively, along with the appropriate control. The TLC result showed no turnover of the substrate (penicillin V) when compared with the positive control because the respective inhibitors abrogated the activity of the enzyme.

Penicillin V potassium salt (125)   **Penicilloic acid V**
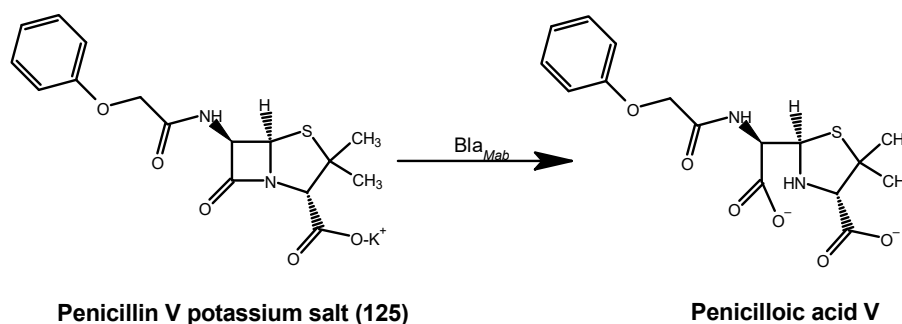
Figure 4.8: The structure of penicillin V potassium salt (**125**) and the hydrolysis of the penam by Bla*Mab* (Lopeman *et al*., 2020).

The substrates for fluorogenic, chromogenic and luminogenic-based assays are expensive, where they are commercially available but the substrate for the TLC-based assay is relatively cheap. Although the TLC-based assay is qualitative and inferior to the fluorogenic, chromogenic and luminogenic-based assays, it can be employed for preliminary inhibitory studies of potential β-lactamase inhibitors. Where potential compounds display a positive inhibitory profile, fluorogenic, chromogenic or luminogenic-based assays can be employed for in-depth inhibitory studies.

4.5 *In vitro* inhibitory studies of cyclo-oxamides against NDM-1

The first batch of the synthesised bis cyclo-oxamides (compounds **94**, **96** and **98**) were screened for their respective inhibitory potential against NDM-1 using the TLC-based assay. Preliminary UV-based inhibitory screening of the first and second batches of the bis cyclo-oxamides (compounds **103** and

106) as well as the α,β-unsaturated carbonyl compound (**110**) was also evaluated against NDM-1 using the chromogenic substrate, nitrocefin (rapid nitrocefin test).

4.5.1 Materials and Methods

Penicillin V potassium salt and nitrocefin were purchased from Biosynth Carbosynth Ltd. while the penicilloic acid V and precoated silica gel plates (60 F_{254}, Merck) were purchased from Scientific Laboratory Supplies and Merck respectively. The PBS buffer tablets (1x) were purchased from Melford while the recombinant enzyme, NDM-1, suspended in PBS buffer, was purchased from RayBiotech Life, Inc. Lastly, the UV-start microplate (96 wells) was purchased from Greiner Bio-One Ltd.

For the TLC-based assay, the visualisation of the TLC plate was achieved with an aqueous solution of potassium permanganate ($KMnO_4$) while for the UV-based assay, hydrolysis of nitrocefin was monitored by BMG Labtech FLUOstar Omega microplate reader.

4.5.2 Method I (TLC-based assay)

To a well containing the recombinant NDM-1 (10 µL, 3.94 µM), was added the potential inhibitor (10 µL, 2 mg/mL) and the resulting mixture was incubated for 5 minutes at ambient temperature (17 - 20 °C). Penicillin V potassium salt (10 µL, 10.30 mM) was added to the NDM-1-inhibitor mixture and the resulting mixture was incubated for additional 20 minutes at the same ambient temperature. The test samples were prepared and analysed along with positive and negative controls. 1 µL of the respective reaction mixtures was spotted on a precoated silica gel plate. The plate was dried and subjected to Thin-layer Chromatography (TLC) using ethyl acetate:water:acetic acid (3:1:1, v/v/v) as the mobile phase. Once dried, the plate was visualised with an aqueous solution of $KMnO_4$.

Table 4.1: Shows the preparation of the TLC-based assay samples along with the controls.

	Vol. (µL)	1	2	3	4	5	6	7	8	9
NDM-1	10		x				x	X		x
Potential Inhibitor	10			x			x	X		
Penicillin V	10				x	x		X		x
Penicilloic acid V	10								x	
Boiled NDM-1	10					x				
PBS Buffer		x	x	x	x	x	x	X	x	x
PBS Buffer		30	20	20	20	10	10	0	20	10
Total volume (µL)		30	30	30	30	30	30	30	30	30

4.5.3 Method II (UV-based assay)

To a well containing the PBS buffer (75 µL) and the recombinant NDM-1 (10 µL, 0.358 µM) was added the potential inhibitor (5 µL, 2 mg/mL) and the resulting mixture was incubated for 5 minutes. Nitrocefin (10 µL, 0.968 mM) was added to the NDM-1-inhibitor mixture. The test samples were prepared and analysed along with positive and negative controls. The hydrolysis profile of nitrocefin, in the presence of the respective potential inhibitors, was monitored by the FLUOstar Omega microplate reader.

Table 4.2: Shows the preparation of the UV-based assay samples along with the controls.

Vol. in µL	Nitroc-efin	94	96	98	103	106	110	Oxalic acid	NDM-1
NDM-1	-	10	10	10	10	10	10	10	10
Inhibitor	-	5	5	5	5	5	5	5	5
PBS	90	75	75	75	75	75	75	75	75
Substrate	10	10	10	10	10	10	10	10	10
Final Vol.	100	100	100	100	100	100	100	100	100

4.6 Discussion

The results of the TLC- and the UV-based assays are discussed in sections 4.6.1 and 4.6.2 respectively. It should be noted that all concentrations reported here onward are final concentrations of the enzyme, substrate and potential inhibitors respectively. Also, penicillin V potassium salt would be referred to as penicillin V from here onward.

4.6.1 TLC-based assay

First, the optimum NDM-1 concentration and incubation period required for the complete turnover of the penicillin V (3.42 mM) were evaluated. Also, the hydrolytic profile of penicillin V (3.42 mM), in the presence of varying NDM-1 concentrations (0.11 µM, 0.36 µM, 0.97 µM and 1.33 µM respectively), was monitored for 10, 15 and 20 minutes respectively. 1.33 µM was observed to be the optimum enzyme (NDM-1) concentration for the complete hydrolysis of the substrate (3.42 mM) to the corresponding penicilloic acid V after an incubation period of not less than 20 minutes. Below the optimum enzyme-substrate incubation period (20 minutes), only partial hydrolysis of penicillin V was observed as evidenced by the presence of two components – one corresponding to the hydrolysed product (penicilloic acid V) and the other component with a higher R_f corresponding to the unhydrolysed penicillin V.

Most of the bis cyclo-oxamides were not soluble in water, hence they were dissolved in ethanol. Considering the potential compounds were ethanolic solutions, the effect of ethanol on NDM-1 was also evaluated prior to the inhibitory studies. 1.33 µM of the enzyme (NDM-1) was pre-incubated with 20 % and 40 % ethanol respectively for initial 5 minutes, followed by an incubation period of 20 minutes upon the addition of the substrate to the NDM-1-ethanol mixture. The enzyme displayed its hydrolytic property against the substrate (3.42 mM) despite the presence of ethanol (20 % and 40 % respectively) when compared with the positive control that contains only the substrate.

4.6.1.1 TLC-based assay hypothesis

Following the confirmation of the optimum conditions for the enzyme activity and substrate susceptibility, samples for the TLC-based inhibitory studies were prepared according to method I and Table 4.1. To monitor if PBS would produce visualisable components on the TLC plate when visualised with an aqueous solution of $KMnO_4$, 1 μL of PBS (spot 1) was analysed along with the respective test samples (Table 4.1). Also, the stability of the potential inhibitors (spot 3) and penicillin V (spot 4) in the presence of the PBS buffer was respectively examined while spot 4 also served as a positive control for the test sample (spot 7) as it contains only the substrate. The susceptibility of bis cyclo-oxamides to NDM-1 (spot 6) was similarly evaluated. As stated in section 3.3, the potential mechanism of the bis cyclo-oxamide prodrug involves NDM-1-induced hydrolysis of the amide bond to release the oxalate anion that is expected to form a complex with the NDM-1 zinc ions. Considering the potential mechanism of the prodrug, it is expected that spot 6 would produce component(s) with distinct R_f values from that of the prodrug (spot 3) after the TLC analysis. Two negative controls (spots 8 and 9) were also prepared and analysed along with the test sample (spot 7). It is expected that in the presence of the NDM-1, the substrate would be hydrolysed to the corresponding acid (spot 9). The formation of the penicilloic acid, resulting from the hydrolysis of penicillin V, was validated with a standard control (penicilloic acid V; spot 8) and it is expected that the components of spots 8 and 9 would have the same R_f values.
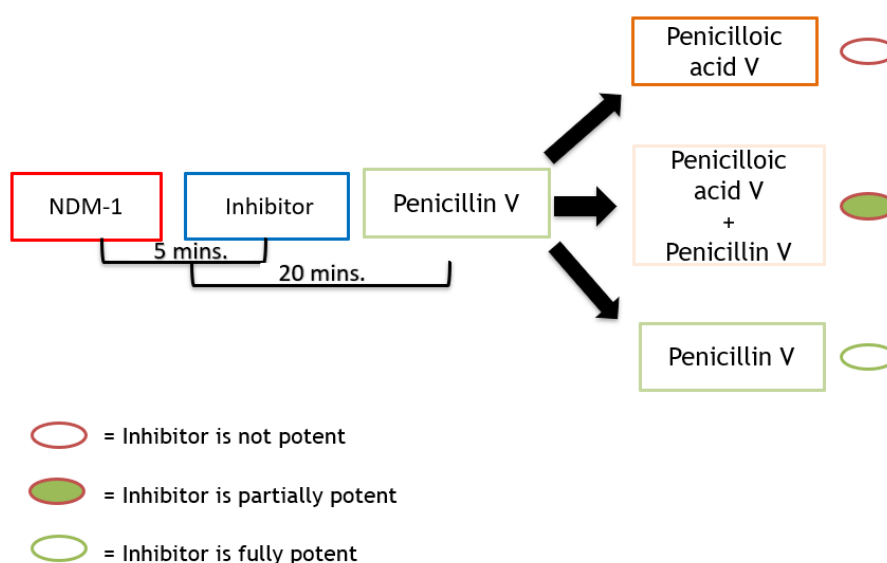
Figure 4.9: Possible outcomes of the inhibitory potential of compounds **94**, **96** and **98**

With respect to spot 7, three different scenarios were possible depending on the inhibitory potential of the respective bis cyclo-oxamide prodrugs (Figure 4.9). If oxalate anion is potent, following the biotransformation of the prodrug, it will deactivate the enzyme after the initial (pre) incubation period such that added substrate, penicillin V, would remain chemically stable, hence the penicillin V, along with the proline/thiazolidine monomers, would be visible on the TLC plate following the visualisation with $KMnO_4$ but if the oxalate anion is not potent, the substrate would be hydrolysed and the penicilloic acid V, along with the proline/thiazolidine monomers, would be observed on the TLC plate while if there

is partial inhibition of the enzyme, a mixture of penicillin V and the penicilloic acid V, along with the proline/thiazolidine monomers, would be observed on the TLC plate.

4.6.1.2 TLC-based assay experimental outcome

Based on the experimental outcome of the inhibitory potential of compound **94** (Figure 4.10), the PBS buffer did not produce a visible component on the TLC plate (spot 1) when visualised with $KMnO_4$ while the substrate remained stable (spot 4) in the presence of PBS buffer throughout the incubation period. Unfortunately, the susceptibility of compound **94** to NDM-1 (spot 6) as well as its stability in the presence of PBS buffer (spot 3) could not be determined because the prodrug was not visualisable with $KMnO_4$. However, the inhibitory potential of compound **94** was determined by evaluating the effect of the enzyme on the substrate in the presence of the potential inhibitor. Spot 7 showed two components which indicate a mixture of two compounds. The component with a higher R_f value is the unhydrolysed penicillin V as its R_f correlates with that of the positive control (spot 4) while the component with lower R_f is the penicilloic acid V as its R_f correlates with the negative controls (spots 8 and 9). This indicates that 2.36 mM of compound **94** partially inhibited 1.33 µM of NDM-1 activity, hence at this concentration, compound **94** is a partial inhibitor of the enzyme.

	Vol. (µl)	1	2	3	4	5	6	7	8	9
NDM-1	10		x				x	X		x
Potential Inhibitor	10			x			x	X		
Penicillin V	10				x	x		X		x
Hydrolysed Penicillin V	10								x	
Boiled NDM-1	10					x				
PBS Buffer		x	x	x	x	x	x	X	x	x
PBS Buffer		30	20	20	20	10	10	0	20	10
Total volume		30	30	30	30	30	30	30	30	30

Concentration: NDM-1 = 1.33 µM, Penicillin V = 3.42 mM, Compound **94** = 2.36 mM
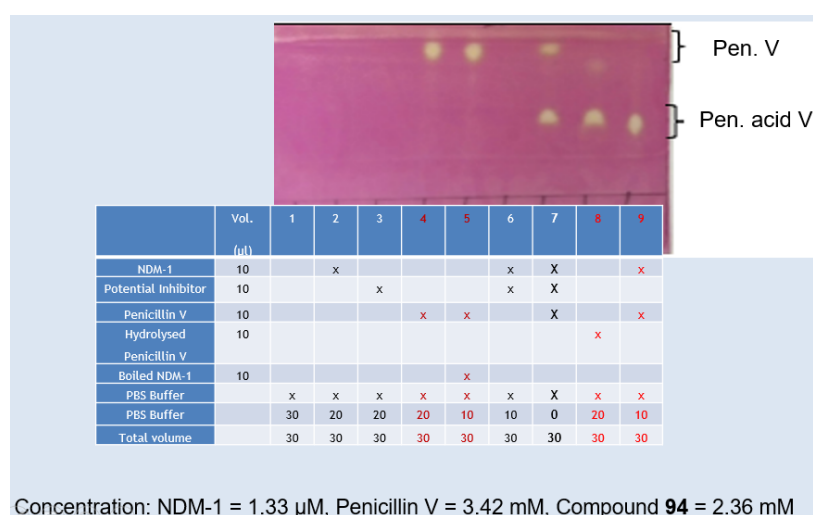
Figure 4.10: TLC-based assay of the inhibitory potential of compound **94**

Similarly, the inhibitory potential of compound **96** was evaluated (Figure 4.11). As earlier confirmed, the PBS buffer showed no visualisable component (spot 1) while the substrate remained stable (spot 4) in the presence of PBS buffer throughout the incubation period. Interestingly, the susceptibility of compound **96** to NDM-1 (spot 6) and its stability in the presence of PBS buffer (spot 3) were determined. Compound **96** was stable in the presence of PBS as evidenced by the presence of a single component (spot 3) but contrary to our expectation, the prodrug seemed insusceptible to NDM-1 as evidenced by the presence of a single component in spot 6, which has an R_f value similar to spot 3. Contrary to compound **94**, 2.09 mM of **96** completely blocked NDM-1 activity (spot 7) such that the substrate remained stable. Irrespective of the non-biotransformation of the potential prodrug, to release the active agent (oxalate anion), compound **96** seemed to display full inhibitory potential against the enzyme.

Remarkably, it indicates that the bis cyclo-oxamide (**96**) is an NDM-1 inhibitor in its own right rather than a prodrug and the findings negate the initial hypothesis pertaining to the inhibitory mechanism of bis cyclo-oxamides (section 3.3).

	Vol. (µl)	1	2	3	4	5	6	7	8	9
NDM-1	10		x				x	X		x
Potential Inhibitor	10			x			x	X		
Penicillin V	10				x	x		X		x
Hydrolysed Penicillin V	10								x	
Boiled NDM-1	10					x				
PBS Buffer		x	x	x	x	x	x	X	x	x
PBS Buffer		30	20	20	20	10	10	0	20	10
Total volume		30	30	30	30	30	30	30	30	30

Concentration: NDM-1 = 1.33 µM, Penicillin V = 3.42 mM, Compound **96** = 2.09 mM
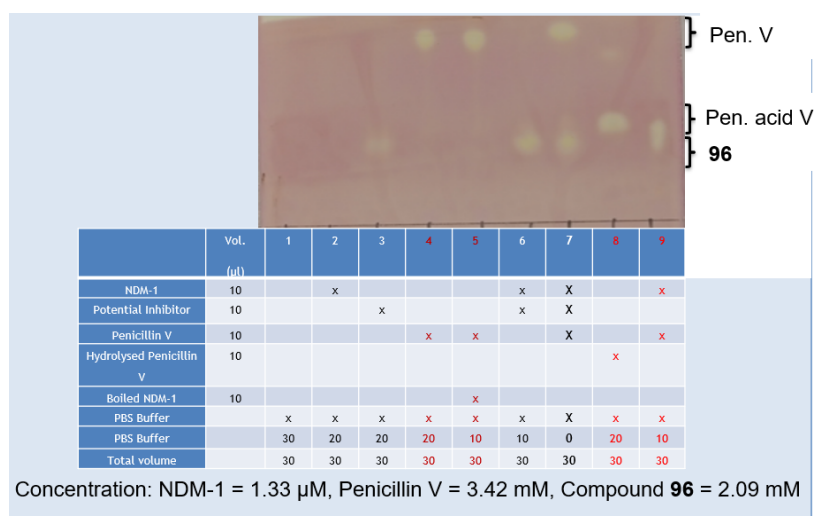
Figure 4.11: TLC-based assay of the inhibitory potential of compound **96**

Compound **98** displaced a similar inhibitory profile as **96** (Figure 4.12). Similarly, the amide hydrolysis of the **98** by NDM-1 was not observed (spot 6) and 1.78 mM of compound **98** terminated the activity of the enzyme.

	Vol. (µl)	1	2	3	4	5	6	7	8	9
NDM-1	10		x				x	X		x
Potential Inhibitor	10			x			x	X		
Penicillin V	10				x	x		X		x
Hydrolysed Penicillin V	10								x	
Boiled NDM-1	10					x				
PBS Buffer		x	x	x	x	x	x	X	x	x
PBS Buffer		30	20	20	20	10	10	0	20	10
Total volume		30	30	30	30	30	30	30	30	30

Concentration: NDM-1 = 1.33 µM, Penicillin V = 3.42 mM, Compound **98** = 1.78 mM
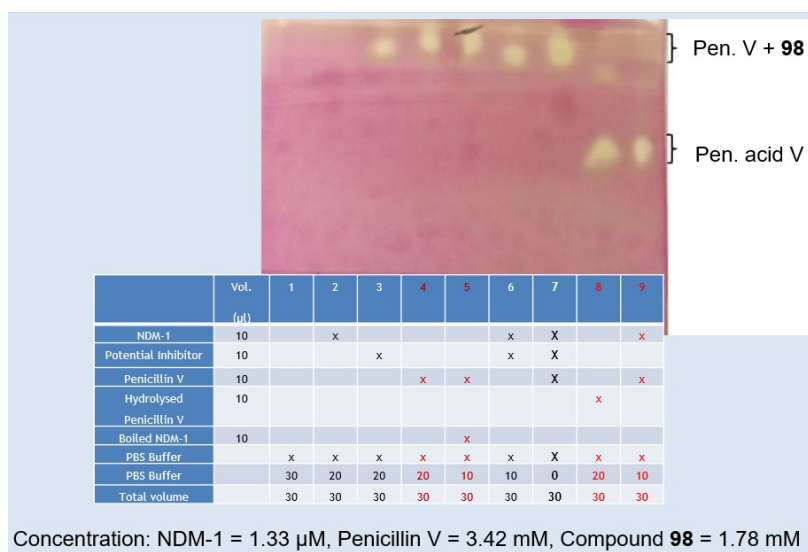
Figure 4.12: TLC-based assay of the inhibitory potential of compound **98**

It should be noted that while it is possible that compounds **96** and **98** behaved as NDM-1 inhibitors in their right, it is also likely that the inhibition is a result of NDM-1 associated production of oxalate anion but the hydrolysis of the potential prodrugs (**96** and **98**) occur at a nanomolecular/micromolecular amount which is not detectable on the TLC scale.

The potential prodrugs were more than 1000-fold (in molar concentration) higher than the enzyme and the TLC results showed that two of the compounds (**96** and **98** respectively) are potent inhibitors of NDM-1 at the respective experimental concentrations (final) but when the respective concentrations were reduced by 0.5-fold, compounds **96** and **98** displaced partial inhibitory profiles which indicate that the respective bis cyclo-oxamides are concentration dependent inhibitors.

4.6.2 UV-based assay (rapid nitrocefin test)

Nitrocefin is a chromogenic β-lactamase substrate that undergoes distinctive colour change from yellow (λ_{max} = 390 nm) to red (λ_{max} = 486 nm) as the amide bond in the β-lactam ring is hydrolysed by β-lactamase.

Nitrocefin can be employed for the screening of potential β-lactamase inhibitors based on changes in maximum absorbance which can be monitored spectrophotometrically at the appropriate wavelength.

Following the outcome of the TLC-based assay, a second batch of the bis cyclo-oxamides (compounds **103** and **106**) and the α, β-unsaturated carbonyl compound (**110**) were synthesised and their potential inhibitory properties, along with the first batch of bis cyclo-oxamides (compounds **94**, **96** and **98**), were evaluated by the UV-based assay (rapid nitrocefin test).

First, the chromogenic substrate, nitrocefin was prepared by dissolving 1 mg of nitrocefin in 100 μL DMSO, followed by the addition of 1900 μL PBS buffer (1x). Thereafter, the optimum enzyme (NDM-1) concentration and incubation period required for the turnover of 0.097 mM of nitrocefin was determined prior to the assay. 0.097 mM of the substrate was incubated with varying concentrations (0.004 μM, 0.007 μM, 0.018 μM, 0.036 μM) of the enzyme for 5, 10 and 15 minutes respectively and the turnover of the substrate was monitored spectrophotometrically. 0.036 μM of the enzyme completely hydrolysed the substrate within 5 minutes incubation period as evidenced by changes in maximum absorbance from 390 nm (nitrocefin) to 486 nm (hydrolysed product) (Figure 4.13).
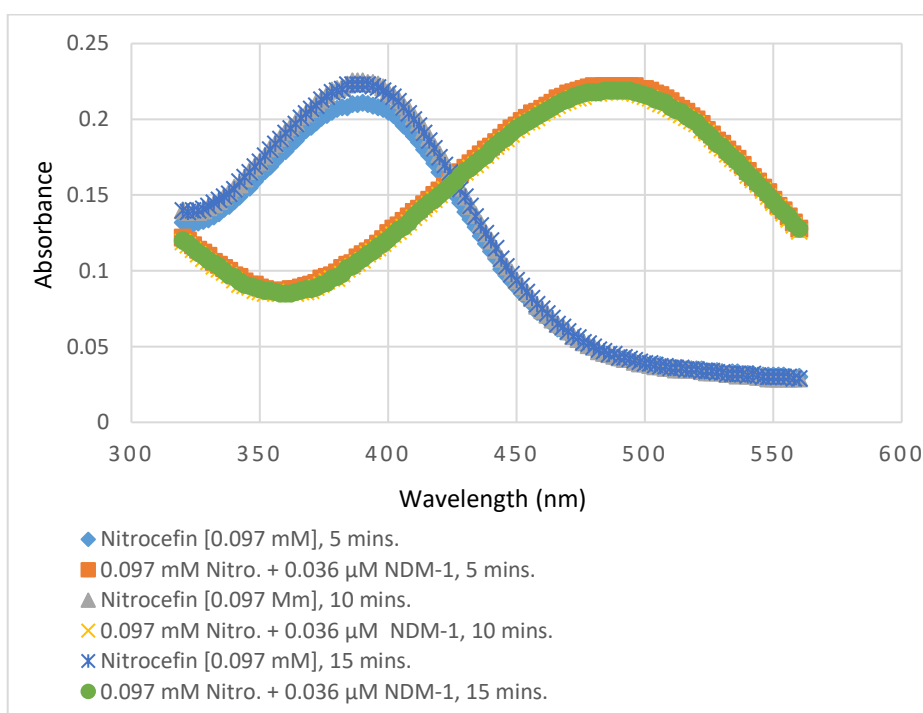
Figure 4.13: UV spectrum of the turnover rate of nitrocefin (0.097 mM) in the presence of 0.036 μM NDM-1.

Similar to the TLC-based assay, the effect of ethanol on the NDM-1 enzyme was also evaluated. 0.036 µM of NDM-1 was pre-incubated with varying percentages of ethanol (5 %, 10 % and 15 % respectively) for 5 minutes, followed by a further 5 minutes incubation period upon the addition of the substrate. The test samples were prepared and analysed along with positive (0.097 mM nitrocefin) and negative (0.097 mM nitrocefin + 0.036 µM NDM-1) controls respectively. The UV spectrum showed that the enzyme hydrolysed the substrate optimally in the presence of 5 % ethanol when compared with the negative control (0.097 mM Nitro. + 0.036 µM NDM-1), whereas at 10 % and 15 % ethanol respectively, a decrease in the formation of the hydrolysed product was observed (Figure 4.14). It indicates that the ethanol (10 % and 15 % respectively) did not completely abrogate the activity of the enzyme but possibly lowered the efficiency of the enzyme which in turn decreased the rate at which it hydrolyses the substrate.
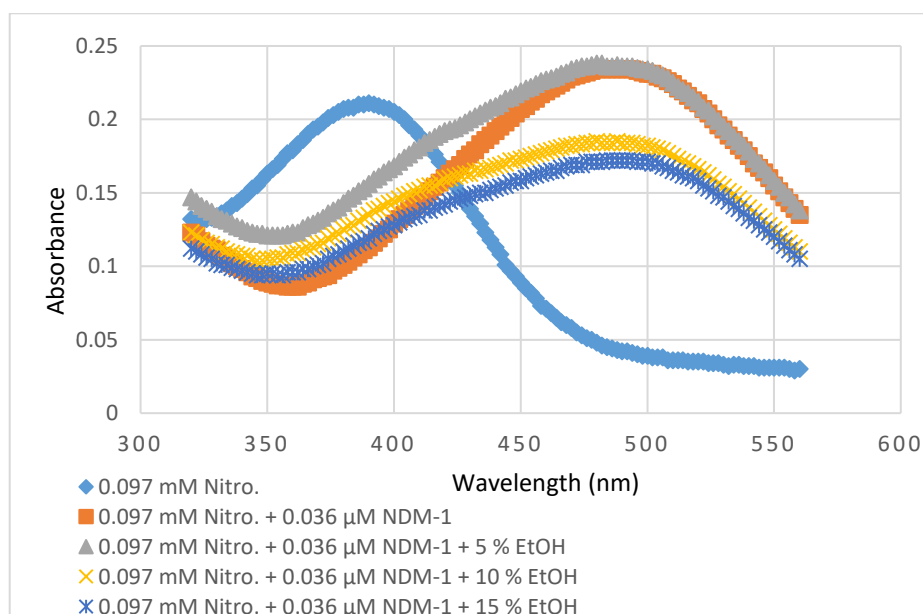
Figure 4.14: UV spectrum of the NDM-1 (0.036 µM) hydrolysis of nitrocefin (0.097 mM) in the presence of 5 %, 10 % and 15 % ethanol.

Following the evaluation of the optimum enzyme concentration and incubation period respectively as well as the optimum percentage of ethanol required, samples for the inhibitory study of the bis cyclo-oxamides (**94**, **96**, **98**, **103** and **106**) and the α, β-unsaturated carbonyl compound (**110**) respectively as well as oxalic acid were prepared according to method II and Table 4.2, along with the positive (contains only substrate) and negative (contains substrate and enzyme) controls. The preliminary UV-based screening of oxalic acid was to determine NDM-1 sensitivity to the chelating agent.

0.1 mg/mL of the respective inhibitor, whose molarity varies as a result of their respective molecular weight, was pre-incubated with respective 0.036 µM of the enzyme in 75 µL PBS buffer (1x) for five minutes, followed by a further five minutes incubation period upon the addition of 0.097 mM of nitrocefin to the respective wells. Unfortunately, at the experimental concentration which was more than 5,000-fold higher than the enzyme concentration, none of the potential inhibitors (**94**, **96**, **98**, **103**, **106** and **110** respectively) prevented the catalysis of the substrate by the enzyme, as evidenced by the changes in the λ_{max} of nitrocefin (390 nm) to that of the hydrolysed product (486 nm) when compared with the positive control, thus indicating that the compounds did not abrogate the activity of the enzyme (Figures

4.15 and 4.16). Interestingly, the preliminary investigation also revealed the inhibitory potential of oxalic acid as the enzyme catalysis of the substrate seemed abated, in the presence of oxalic acid, when compared with the negative control (Figure 4.16). The unexpectedly high absorbance of the oxalic acid sample (around 320 – 360 nm) might be due to the presence of oxalic acid which has a λ_{max} peak with a broad shoulder ending around 325 - 350 nm depending on the prevailing concentration (Lund Myhre and Nielsen, 2004).
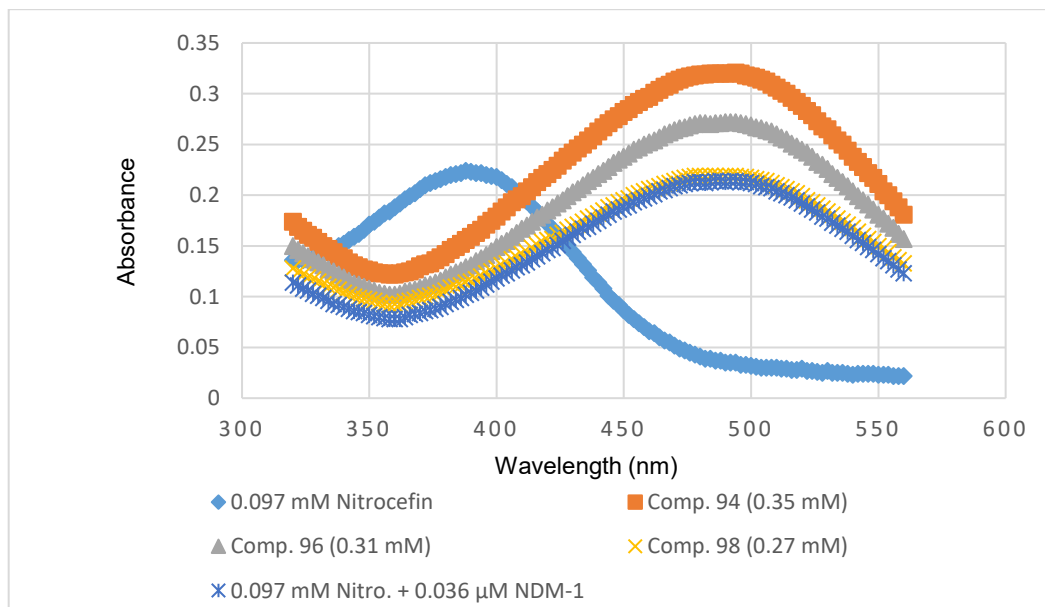
Figure 4.15: UV-based assay of the inhibitory potential of compounds **94**, **96** and **98** respectively.
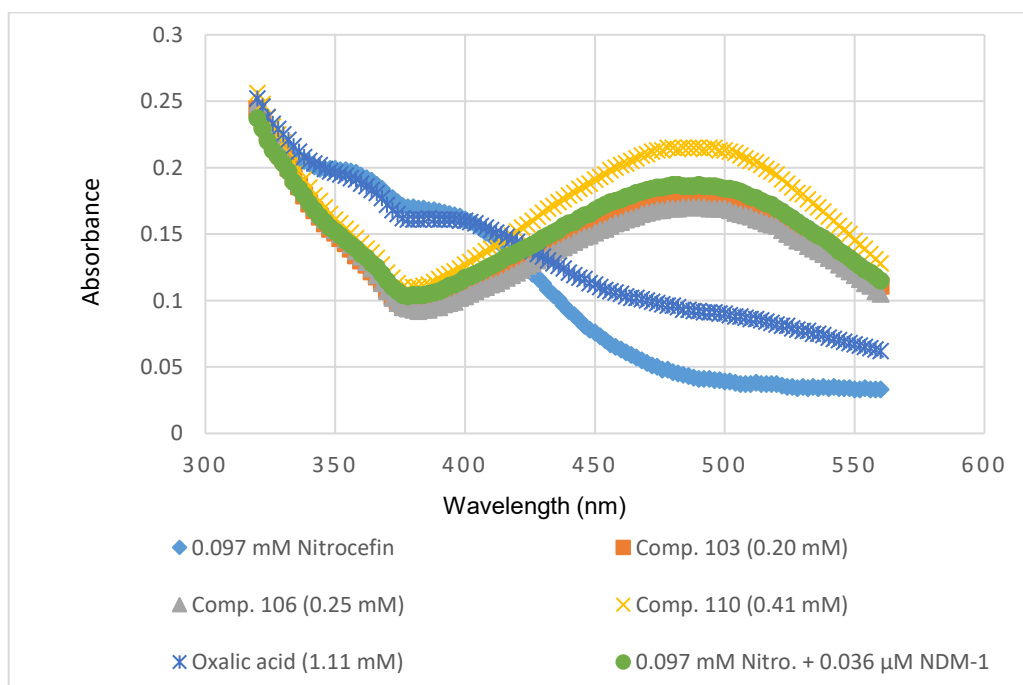
Figure 4.16: UV-based assay of the inhibitory potential of compounds **103**, **106**, **110** and oxalic acid respectively.

Unfortunately, the result of the UV-based assay (rapid nitrocefin test) is in contrast with the TLC-based assay especially the results of compounds **94**, **96** and **98**. The plausible reasons for this contrast are enumerated below.

➢ TLC-based assay - The effect of ethanol on NDM-1 was evaluated and the result showed that the enzyme was still active at 40 % ethanol as it was able to hydrolyse substrate on the TLC scale. The partial inhibition profile of compound **94** also confirms the activity of the enzyme in the presence of ethanol (33 %). If the enzyme was denatured by ethanol (33 %), there would not have been a partial turnover of the substrate during the inhibitory assay of compound **94**.

➢ The TLC assay is a qualitative screening method and cannot reveal to what extent the enzyme was active. However, the evaluation of the effect of ethanol on the enzyme using the UV-based method showed that indeed ethanol can impede the efficiency of the enzyme in the catalysis of the substrate. Also, it should be highlighted that the enzyme concentration for the TLC-based assay was up to 37-fold higher than that of the UV-based assay and this difference could account for the activity of the enzyme in the presence of 33 % ethanol considering that enzymes are may be more stable in concentrated solutions than in diluted solution.

➢ TLC-based assay - Considering the UV evaluation of the effect of ethanol on the enzyme, it is likely that the ethanol did not abrogate the activity of the enzyme but reduced the efficiency of the enzyme such that compounds **96** and **98** deactivated a less efficient enzyme, hence there was no turnover of penicillin V to the corresponding penicilloic acid V.

While it is likely that some of the prodrugs may possess inhibitory activity against NDM-1 as judged by TLC, validatory TLC and UV inhibitory studies, in the absence of ethanol, are required to validate the inhibitory activity of the potential prodrugs that have shown positive results on the TLC scale.

Chapter 5

5.0 *Mycobacterium abscessus*: Chemical synthesis and biological evaluation of potential Bla$_{Mab}$ inhibitors.

5.1 *Mycobacterium abscessus*

Mycobacterium abscessus (*Mab*), a nontuberculous Mycobacterium with three subspecies (*Mab. abscessus, Mab. bolletii, and Mab. Massiliense*) (Sassi and Drancourt, 2014), is known to cause various pathological conditions such as skin and soft tissue infections. *Mab* is also associated with lung infection in patients with chronic lung diseases, such as cystic fibrosis (CF) (Esther *et al*., 2010; Medjahed et al., 2010). *Mab* is an environmental Mycobacterium (dust, soil and water) which can contaminate products such as medical devices and medications (CDC, 2010).

Mab-associated infections are difficult to eradicate, especially infections that are associated with lung(s) disease which have a cure rate of less than 50 % (Jarand *et al*., 2011; Esther *et al*., 2010). The current lung infection therapy for the treatment of *Mab* infection in patients with cystic fibrosis, developed by the US Cystic Fibrosis Foundation and European Cystic Fibrosis Society (Floto *et al*., 2016), involves the use of macrolide (clarithromycin or azithromycin), aminoglycoside (amikacin) and β-lactam antibiotics (cefoxitin or imipenem). The role of β-lactam antibiotics as part of the treatment regimen is to inhibit the enzyme, transpeptidase, which is responsible for the final cross-linking of one stem peptide to the adjacent stem peptide during bacterial cell wall biosynthesis. Studies have shown that the stem peptides in *Mab* are cross-linked by both L, D-transpeptidase (3→3 linkage, major) and D, D-transpeptidase (4→3 linkage, minor) (Figure 1.2) (Lavollay *et al*., 2011; Mattoo *et al.,* 2017; Kumar *et al*., 2017a). These transpeptidases have a distinct affinity for the different classes of β-lactam antibiotics, with D,D-transpeptidase susceptible to all β-lactam antibiotics while L,D-transpeptidase are preferentially inhibited by carbapenems and, to a lesser extent, by cephalosporins (Kumar *et al*., 2017 a, b). Despite the classic functionality of β-lactam antibiotics, especially the carbapenems, their therapeutic effect against *Mab* is dwindling due to the development of *Mab* resistance. *Mab* develops resistance to this class of antibiotics through the secretion of hydrolases, generally called β-lactamase, which degrade the β-lactam antibiotics via amide hydrolysis of the lactam ring (Floto *et al*., 2016).

Considering the susceptibility of β-lactam antibiotics to *Mab-associated* β-lactamase, the absence of a β-lactamase inhibitor in the current lung infection therapy might be responsible for poor treatment outcomes of *Mab* infections in patients with cystic fibrosis.

5.2 *Mycobacterium abscessus* β-lactamase (Bla$_{Mab}$)

One of the preferential mechanisms through which bacteria develop resistance against β-lactam antibiotics is the secretion of diverse hydrolytic enzymes generally called β-lactamases. β-lactamases are profiled into classes A, B, C and D respectively (see section 1.4) based on the conserved amino acid sequence and the active site catalytic residues (Bush and Jacoby, 2010). Currently, two types of β-lactamases, with minimal variation, have been identified in *Mab* and they include

- Bla*Mab* and
- Bla*Mmas* (produced by *Mab. Massiliense* in addition to Bla*Mab*; Glu38 and Thr140 in Bla*Mab* are replaced by Val38 and Ala140 in Bla*Mmas*)

Despite insufficient scientific publications on the specific architecture and catalytic mechanism of Bla*Mab* and Bla*Mmas*, some studies have revealed that both enzymes are Class A hydrolases, based on the conserved active site residues, with 50% and 52% sequence identity with KPC-2 and SFC-1 respectively (Ramirez *et al.*, 2017).

[Figure redacted]

Figure 5.1: 3D models of β-lactamases from *Mycobacterium abscessus* (Bla*Mab*) and *Mycobacterium massiliense* (Bla*Mmas*) (Ramirez *et al.*, 2017).

Using KPC-2 as a reference (Figure 5.1), the active site is embedded in a cleft generated by two subdomains (α/αβ) and it consists of the catalytic serine, S70, acylation water, deacylation water (that is triggered via interaction with E166 and N170 as well as S70), oxyanion hole (formed by the backbone nitrogen atoms of S70 and T237), conserved lysine residues (K73 and K234) as well as Asn 132 (N132) (Ke *et al.*, 2007).

5.3 Catalytic activity of Bla*Mab*

Several penams are good substrates of Bla*Mab*, hence their poor efficacy in the treatment of Bla*Mab*-induced infection. Substrate hydrolysis by this class of enzyme involves the controversial Glu166 or Lys73 activation of the active site S70, followed by the nucleophilic attack on the β-lactam carbonyl carbon by the activated S70 (Figure 5.1A) which results in the formation of transient tetrahedral intermediate (Figure 5.2B) that is stabilised by the scission of the amide bond to form the corresponding stable acyl-enzyme intermediate (Figure 5.2C). E166 and N170 trigger de-acylation/hydrolytic water molecule for the second nucleophilic attack of acyl-enzyme intermediate (carbonyl carbon) (Figure 5.2D) to form an unstable tetrahedral intermediate (Figure 5.2E), which decomposes to the corresponding hydrolysed β-lactam and the free enzyme respectively (Figure 5.2F) (Minasov *et al.*, 2002; Ke *et al.*, 2007).

[Figure redacted]

Figure 5.2: Hydrolytic pathway of β-lactam in the presence of Class A enzyme (Minasov *et al*., 2002).

Bla$_{Mab}$ displays broad spectrum activity against several β-lactam antibiotics, with high efficiency against penams (except temocillin), first- and second-generation cephalosporins (except cefoxitin) but low efficiency against carbapenems. Cefoxitin and imipenem are highly insusceptible to Bla$_{Mab}$ hydrolysis, hence their use in *Mab* lung infection therapy (Ramirez *et al*., 2017; Soroka *et al*., 2014). Contrary to the imipenem insusceptibility to Bla$_{Mab}$, Bla$_{Mmas}$ seems to display moderate activity against the carbapenem (imipenem) (Ramirez *et al*., 2017). The catalytic difference might be due to the slight amino acid variation between the two *Mab* enzymes.

5.3.1 Activation of nucleophilic serine (S70)

The activation of the active site serine, by a catalytic base that accepts the proton from the active site S70 residue, is a prerequisite for nucleophilic attack of the β-lactam carbonyl carbon. However, the identity of the base has been a subject of controversy. Mutagenesis and crystallographic studies of class A enzymes have identified two distinct residues, Glu116 and Lys73 respectively, as the potential catalytic base. The Lys73 unprotonated amino group (side-chain) and the carboxylate of Glu166 respectively are postulated as the base required for the activation of S70 (Gibson *et al*.,1990; Lamotte-Brasseur *et al*., 1991; Strynadka *et al*., 1992). The hypotheses such as the low pK_a of the Lys73 amino group (side-chain) owing to its unprotonated state, reduced enzyme activity associated with the substitution of Lys73 residue and the formation of hydrogen bond between the Lys73 nitrogen atom (side-chain amino group) and the oxygen atom (hydroxyl group) of S70 respectively, support Lys73 as the catalytic base required for activation of the active site S70. However, the NMR study of the active-site lysine residue of wild-type TEM-1 contradicts the initial postulation of low pK_a associated with the Lys73 side-chain amino group (Damblon *et al*., 1996). Contrary to the initial postulation, the pK_a of the Lys73 unprotonated amino group (side-chain) is >10 making it unlikely for Ly73 to be a proton acceptor during catalysis (Damblon *et al*., 1996).

Considering the high pK_a of the Lys73 amino group (side-chain), Glu116 was suggested to be a better candidate (catalytic base) owing to the protonation of its carboxyl group and also the reduced enzyme activity associated with the substitution of the Glu116 residue (Minasov *et al*., 2002).

However, the possibility of direct proton transfer between Glu166 carboxylate oxygen and the S70 hydroxyl group remains controversial owing to the long distance between the two groups. While it is unlikely that there is direct proton transfer between the two groups, a conserved water molecule bridging the two side chains likely offers a possible relay for this transfer (Damblon *et al*., 1996).

Despite strong evidence supporting Glu166 as the catalytic base, recent publications still postulate Lys73 as the catalytic base.

5.4 Bla$_{Mab}$ inhibitors

The clinical challenge of β-lactamase (*staphylococcal penicillinase*) prompted the successful development of first-generation inhibitors. However, the hydrolytic enzyme has evolved over the years with more than 2,000 naturally occurring β-lactamases that have been profiled into four classes and each class possesses a distinct amino acid sequence and enzymatic profile (Abraham and Chain 1988; Bonomo, 2017). Considering the dynamic nature of the hydrolytic enzyme, new-generation inhibitors are being developed because the first-generation inhibitors are becoming clinically insignificant in combatting infections associated with bacterial harbouring sophisticated β-lactamase.

5.4.1 First generation β-lactam inhibitors of Bla$_{Mab}$

Several studies on the inhibitory activity of the first generation β-lactam inhibitors, clavulanic acid (**126**), sulbactam (**127**) and tazobactam (**128**) (Figure 5.3), revealed these compounds are susceptible Bla$_{Mab}$ (Soroka *et al*., 2014; Ramirez *et al*., 2017) whereas clavulanic acid is insusceptible to BlaC (class A β-lactamase that shares 48% sequence identity with Bla$_{Mab}$) of *Mycobacterium tuberculosis* (Wang *et al*., 2006) possibly due to the substitution of the active site asparagine (Bla$_{Mab}$) with glycine (Bla C) at position 132 (Soroka *et al*., 2015; Soroka *et al*., 2017). Asn132, as part of the conserved β-lactam binding motif (Ser-Asp-**Asn**) of class A β-lactamase, plays an essential role in stabilising clavulanate at Bla$_{Mab}$ active site via hydrogen bonding of its side chain nitrogen atom with the carbonyl oxygen of the carboxyl group whereas substitution of this residue with glycine, (Ser-Asp-**Gly**), leads to loss of the hydrogen bonding and consequently results in poor BlaC-clavulanate hydrolysis. The active site residue substitution accounts for the differential sensitivity of Bla$_{Mab}$ and BlaC towards clavulanic acid (Soroka *et al*., 2015; Shimamura *et al*., 2002).

126   **127**   **128**
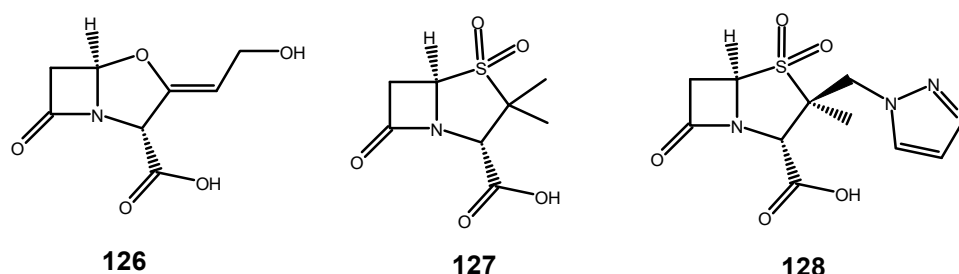
Figure 5.3: First Generation β-lactam Inhibitors.

Soroka *et al*. (2015) conducted a structure-assisted site-directed mutagenesis of BlaC where the Ser-Asp-**Gly** binding motif was converted to Bla$_{Mab}$'s binding motif (Ser-Asp-**Asn**) to validate the differential sensitivity of Bla$_{Mab}$ and BlaC, respectively, towards clavulanic acid.

According to the finding, the mutant enzyme, with the Ser-Asp-**Asn** binding motif, hydrolysed clavulanic acid. The hydrolysis of clavulanic acid by the mutant enzyme involves the initial activation of the active site serine (S70) by the Lys73 (Figure 5.4A), followed by nucleophilic attack on the β-lactam carbonyl carbon by the activated S70 (Figure 5.4A) which resulted in the cleavage of the β-lactam ring that prompted the rupture of the five-membered heterocyclic ring (Figures 5.4B and C) with the concomitant formation of an acyclic imine intermediate (Figure 5.4C). The acyclic imine undergoes rapid decarboxylation and isomerisation to form a stable acyl-enzyme, *α-β-trans* enamine (Figures 5.4D and E), while the hydrolysis of the acyl-enzyme resulted in the liberation of the enzyme and the degraded β-lactam (Figure 5.4F).

[Figure redacted]

Figure 5.4: Pathway of clavulanate hydrolysis by mutant BlaC (Soroka *et al*., 2015).

5.4.2 New generation non-β-lactam inhibitors

Novel non-β-lactam inhibitors are being developed in light of the susceptibility of the first generation β-lactam inhibitors to pathogens harbouring advanced β-lactamase. Recent *in vitro* and *in vivo* studies have shown that the new generation non-β-lactam inhibitors, vaborbactam (**27**), compounds **28**, **29** and **30**, taniborbactam (**31**) (phase III) (Figure 1.19; section 1.6.2.1.2), avibactam (**129**) and relebactam (**130**) (Figure 5.5), improved the efficacy of β-lactam antibiotics against *Mab*-induced infections by blocking the activity of Bla$_{Mab}$ (Kaushi *et al*., 2019; Liu *et al*., 2019; Krajnc *et al*., 2019; Brem *et al*., 2016). Avibactam and relebactam function via an acylation-deacylation mechanism (Krishnan *et al*., 2015) while compounds **27**, **28**, **29**, **30** and **31** are dual action inhibitors that function as transition state analogues (Kaushi *et al*., 2019; Liu *et al*., 2019; Krajnc *et al*., 2019; Brem *et al*., 2016) and their mechanism is well reviewed in section 1.6.2.1.2 (Figure 1.18).

129 **130**
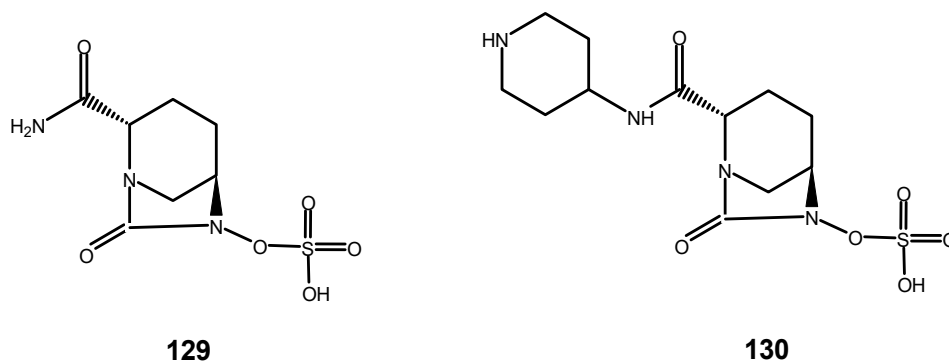
Figure 5.5: Non-β-lactam Inhibitors.

The combination of avibactam with piperacillin, imipenem, amoxicillin, ceftaroline and carbapenems respectively, significantly restored piperacillin activity against *Mab* in an *in vivo Galleria mellonella* model (Meir *et al*., 2018), potentiate imipenem and amoxicillin activities against *Mab* in macrophages (*in vitro*) and zebrafish (*in vivo*) (Dubée *et al*., 2015a; Lefebvre *et al*., 2017), enhanced the activity of ceftaroline against *Mab* in clinical isolates (Dubée *et al*., 2015b) and remarkably reduced carbapenems (several) MICs to therapeutic concentrations in clinical isolates producing Bla$_{Mab}$ (Kaushik *et al*., 2017) respectively. Similarly, the combination of relebactam with carbapenems (including imipenem and meropenem) and cephalosporins (including cefepime, ceftaroline, and cefuroxime) showed a similar positive trend against clinical isolates expressing Bla$_{Mab}$ (Kaushik *et al*., 2019; Lopeman *et al*., 2020).

5.5 Avibactam and relebactam inhibition mechanisms

Avibactam, a novel β-lactamase inhibitor that lacks the β-lactam core, is known to inhibit class A, class C and some class D β-lactamases. When combined with β-lactam antibiotics that are susceptible to class A and C enzymes, avibactam restores the efficacy of these β-lactam antibiotics against transpeptidase by deactivating the hydrolytic enzyme. Avibactam blocks the activity of β-lactamase via a distinct mechanism – a covalent-reversible reaction (Krishnan *et al*., 2015).

[Figure redacted]

Figure 5.6: Pathway for avibactam inhibition of serine-β-lactamase (KPC-2) (Krishnan *et al*., 2015).

According to simulation studies, avibactam binds covalently with the active site S70 of KPC-2 (an analogue of Bla*Mab*) with its urea carbonyl oxygen, amide group and sulphate portion interacting with the enzyme's active site oxyanion hole (formed by the backbone nitrogen atoms of S70 and T237), the N132 residue and the S130, T237, T235 residues respectively (Krishnan *et al*., 2015). The potential inhibitory mechanism of avibactam involves the activation of the S70 by a catalytic base (Glu116 or Lys73), followed by nucleophilic attack on the urea carbonyl carbon resulting in the scission of the amide bond with concomitant acylation of the S70 (acyl-enzyme) (Figures 5.6A and B). Interestingly, the newly formed acyl-enzyme is prone to deacylation through the re-cyclisation of the four-membered ring and the regeneration of the potent avibactam that can initiate subsequent acylation cycles as opposed to hydrolysis and turnover (Krishnan *et al*., 2015; King *et al*., 2015).

Unfortunately, a slow KPC-2 resistance mechanism, possibly conferred by the hydrogen bond interaction of S130 residue with avibactam, has been reported. This involves the slow removal of the sulphonic group of avibactam resulting in the formation of hydroxamic acid/imine (Figures 5.6C and D). The imine intermediate hydrolyses to the keto derivative (Figure 5.6E), which is further hydrolysed to release the enzyme with concomitant formation of a new carboxylate group, that is prone to decarboxylation (Figure 5.6 F) (Krishnan *et al*., 2015).

While investigating the therapeutic potential of amoxicillin in combination with imipenem-relebactam against *Mab*, Lopeman *et al*., 2020 conducted molecular docking simulations (*in silico*) of relebactam against Bla$_{Mab}$ to determine the mechanism/binding mode of relebactam inhibition of Bla$_{Mab}$. The docking showed that the relebactam probably forms a relatively stable complex in the Bla$_{Mab}$ active site via several binding interactions such as the polar interactions between the sulphate group and Lys74, Lys233, Ser 131 and Thr234 residues respectively while hydrophobic interaction was observed between the relebactam central piperidine ring and Trp106 (Figure 5.7). Furthermore, they observed that the urea carbonyl group of relebactam was well positioned for nucleophilic attack by the hydroxyl group of the active site serine (S70), resulting in possible cleavage of the urea ring with simultaneous acylation of the nucleophilic serine (S70).

[Figure redacted]

Figure 5.7: Molecular modelling (*in silico*) showing the potential relebactam-Bla$_{Mab}$ interaction (Lopeman *et al*., 2020).

5.6 β-lactam Bla$_{Mab}$ inhibitors

Given the broad-spectrum activity and catalytic prowess of Bla$_{Mab}$, there is a need for new *Mab* lung infection therapy guidelines that will accommodate the use of Bla$_{Mab}$ inhibitors in addition to the current treatment regimen. The addition of a Bla$_{Mab}$ inhibitor to the current treatment regimen would likely improve treatment outcomes of *Mab* infection in patients with chronic pulmonary diseases.

The inhibitory potential of non-β-lactam inhibitors against Bla$_{Mab}$ enzyme is well documented while none of the current β-lactam inhibitors (clavulanic acid, sulbactam and tazobactam; Figure 5.3) is therapeutically active against Bla$_{Mab}$, hence the search for potent β-lactam-Bla$_{Mab}$ inhibitors. In the search for potent Bla$_{Mab}$ inhibitors, a commercially available bicyclic carboxylic compound (compound **132**), an analogue of penams, was discovered to be active against Bla$_{Mab}$ (Jonathan Cox, Aston University). The inhibitory activity of compound **132** against Bla$_{Mab}$ is the rationale for the synthesis of novel or existing analogues of the lead compound. The structural activity relationship of **132** may lead to the discovery of analogues with remarkable activity against the Bla$_{Mab}$ enzyme.

132
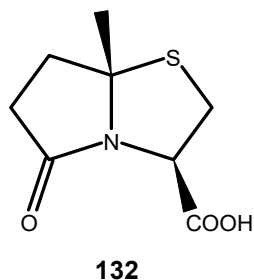
Figure 5.8: Structure of the lead compound (**132**).

5.7 Experimental methods

The general analytical method is well enumerated in chapter two, section 2.2.

5.7.1 (3R,7aS)-Ethyl 7a-methyl-5-oxohexahydropyrrolo[2,1-b] thiazole-3-carboxylate (131)

To a stirred solution of levulinic acid (9.00 g, 77.51 mmol) in dry toluene (75 mL) was added L-cysteine ethyl ester hydrochloride (14.39 g, 77.51 mmol) and the resulting mixture was heated at reflux, under Dean–Stark condition, for 24 hours. The mixture was allowed to cool (ambient temperature) and was washed with distilled water (3 x 30 mL), dried with anhydrous magnesium sulphate, filtered and the filtrate was collected. The toluene was removed at low pressure and the residue obtained was dried under vacuum to afford compound **131** as an amber-coloured oil, 11.40 g, 49.72 mmol, 64 %, which was used in the next step without further purification.

Figure 5.9: Structure of compound **131**

Molecular Formula: $C_{10}H_{15}NO_3S$; R_f (methanol/ethyl acetate, 1:1): 0.83 (single spot).

^{1}H NMR (400 MHz, CDCl$_3$) δ 1.30 (t, J = 7.1 Hz, 3H, CH$_3$-CH$_2$-O), 1.69 (s, 3H, S-C(CH$_3$)-CH$_2$), 2.28 (ddd, J = 13.3, 9.6, 5.0 Hz, 1H, S-C(CH$_3$)-CH$_2$), 2.45 (ddd, J = 13.4, 9.9, 7.0 Hz, 1H, S-C(CH$_3$)-CH$_2$), 2.57 (ddd, J = 17.1, 9.9, 5.0 Hz, 1H, CH$_2$-CO-N), 2.79 (ddd, J = 16.8, 9.6, 7.0 Hz, 1H, CH$_2$-CO-N), 3.52 (dd, J = 11.8, 8.8 Hz, 1H, N-CH-CH$_2$), 3.63 (dd, J = 11.8, 5.7 Hz, 1H, N-CH-CH$_2$), 4.24 (m, 2H, CH$_3$-CH$_2$-O), 5.04 (dd, J = 8.8, 5.7 Hz, 1H, N-CH-CH$_2$) ppm.

IR (ATR): v = 1188 (s, C-O, ester), 1368 (m, C-H), 1448 (m, C-H), 1704 (s, C=O), 2976 (w, C-H) cm^{-1}.

5.7.2 (3R,7aS)-7a-Methyl-5-oxohexahydropyrrolo[2,1-b]thiazole-3-carboxylic acid (132)

To a stirred solution of **131** (1.00 g, 4.36 mmol) in methanol/water (20 mL; 4:2) was added lithium hydroxide monohydrate (0.92 g, 21.85 mmol, 5 eq.). The resulting mixture was stirred at ambient temperature (20 ℃) and the turnover of the ester was monitored by TLC. The reaction was stopped when the starting material was completely consumed. The pH of the mixture was adjusted to 2 - 3 using

a 4N aqueous solution of HCl and the desired compound was extracted into ethyl acetate (3 x 20 mL). The organic portions were combined, washed with a saturated aqueous solution of NaCl (20 mL), dried with anhydrous magnesium sulphate, filtered and the filtrate was collected. The solvent was removed at low pressure and the residue obtained was dried under vacuum to afford compound **132** as a white solid, 0.81 g, 4.02 mmol, 92 %.

Figure 5.10: Structure of lead compound **132.**

Molecular Formula: $C_8H_{11}NO_3S$; R_f (methanol/ethyl acetate, 1:1): 0.38 (single spot); melting point: 180.9 – 183.1 ºC.

^{1}H NMR (400 MHz, CDCl$_3$) δ 1.72 (s, 3H, S-C(C$\underline{H}_3$)-CH$_2$), 2.32 (ddd, J = 13.2, 9.3, 3.8 Hz, 1H, S-C(CH$_3$)-C$\underline{H}_2$), 2.50 (ddd, J = 13.3, 9.9, 8.6 Hz, 1H, S-C(CH$_3$)-C$\underline{H}_2$), 2.66 (ddd, J = 17.5, 9.9, 3.8 Hz, 1H, C$\underline{H}_2$-CO-N), 2.90 (dddd, J = 18.1, 9.4, 8.7, 0.8 Hz, 1H, C$\underline{H}_2$-CO-N), 3.59 (dd, J = 12.3, 8.6 Hz, 1H, N-CH-C$\underline{H}_2$), 3.75 (m, 1H, N-CH-C$\underline{H}_2$), 4.91 (ddd J = 8.2, 7.3, 0.7 Hz, 1H, N-C$\underline{H}$-CH$_2$) ppm.

^{13}C ATP NMR (101 MHz, CDCl$_3$) δ 30.14 ($\underline{C}$H$_3$), 32.62 ($\underline{C}$H$_2$), 33.81 ($\underline{C}$H$_2$), 35.91 ($\underline{C}$H$_2$), 58.47 (S-$\underline{C}$(CH$_3$)-CH$_2$), 78.39 (N-$\underline{C}$H-CH$_2$), 172.07 ($\underline{C}$=O), 177.06 ($\underline{C}$=O) ppm.

IR (ATR): $υ$ = 1201 (s), 1394 (m, C-H), 1640 (s, C=O), 1738 (s, C=O), 2557 (w) 2921 (w), 2959 (w) cm^{-1}.

MS (-ESI) m/z = Found 200.0387 (M-H)$^-$; calculated for $C_8H_{10}O_3NS$ 200.0387; 0.1 ppm.

5.7.3 (3*R*,7a*S*)-7a-Methyl-5-oxohexahydropyrrolo[2,1-*b*][1,3]thiazole-3-carboxamide (133)

To a hydrothermal synthesis reactor containing a solution of **131** (1.00 g, 4.36 mmol) in dry tetrahydrofuran (5 mL) was added excess ammonium hydroxide (6.00 mL, 154.39 mmol, 35.4 eq.). The reactor was sealed and the resulting mixture was stirred at 40 ºC for 6 days. The mixture was allowed to cool and the solvent (THF) was removed at low pressure while the residue obtained was dissolved in ethyl acetate (10 mL). The organic solution was washed with a saturated aqueous solution of NaCl (2 x 5 mL), dried with anhydrous magnesium sulphate, filtered and the filtrate was collected. The filtrate was concentrated, distilled water (10 mL) was added and the flask was kept at 0°C overnight. The precipitate formed was collected by vacuum filtration, rinsed with chilled distilled water (4 mL) and dried under vacuum to obtain compound **133** as a white solid, 0.28 g, 1.40 mmol, 32 %.

Figure 5.11: Structure of compound **133**.

Molecular Formula: $C_8H_{12}N_2O_2S$; R_f (methanol/ethyl acetate, 1:1): 0.79 (single spot); melting point: 171.2 – 174.3 ºC.

^{1}H NMR (400 MHz, CDCl3) δ 1.68 (s, 3H, S-C(CH3)-CH2), 2.27 (ddd, J = 13.5, 9.7, 5.0 Hz, 1H, S-C(CH3)-CH2), 2.50 (ddd, J = 13.5, 10.2, 7.3 Hz, 1H, S-C(CH3)-CH2), 2.66 (ddd, J = 17.6, 10.2, 5.0 Hz, 1H, CH2-CO-N), 2.82 (ddd, J = 17.6, 9.6, 7.2, 0.7 Hz, 1H, CH2-CO-N), 3.44 (dd, J = 12.3, 8.8 Hz, 1H, N-CH-CH2), 4.00 (dd, J = 12.3, 7.2 Hz, 1H, N-CH-CH2), 4.79 (ddd, J = 8.8, 7.2, 0.6 Hz, 1H, N-CH-CH2), 5.39 (s, 1H, CO-NH2), 6.62 (s, 1H, CO-NH2) ppm.

^{13}C ATP NMR (101 MHz, DMSO-d_6) δ 30.61 (CH3), 31.99 (CH2), 32.51 (CH2), 36.25 (CH2), 59.38 (S-C(CH3)-CH2), 78.77 (N-CH-CH2) ppm.

IR (ATR): v = 1075 (m), 1345 (m, C-H), 1393 (m, C-H), 1688 (s, C=O), 2974 (w, C-H), 3228 (m, N-H) cm^{-1}.

MS (ESI) m/z = Found 201.0692 (M+H)$^+$; calculated for $C_8H_{13}O_2N_2S$ 201.0692; 0.1 ppm.

MS (ESI) m/z = Found 223.0511 (M+Na)$^+$; calculated for $C_8H_{12}O_2N_2SNa$ 223.0512; 0.3 ppm.

5.7.4 (3R,9bS)-Ethyl 5-oxo-2,3,5,9b-tetrahydrothiazolo[2,3-a]isoindole-3-carboxylate (134)

To a stirred solution of L-cysteine ethyl ester hydrochloride (2.23 g, 12.01 mmol) and triethylamine (1.67 mL, 12.01 mmol) in dry toluene (50 mL) was added 2-carboxybenzaldehyde (1.98 g, 13.21 mmol). The resulting mixture was heated at reflux, under Dean-Stark condition, for 24 hours. The mixture was allowed to cool (ambient temperature) and the toluene was removed at low pressure. Ethyl acetate (30 mL) was added to the flask and the precipitate formed was separated by vacuum filtration. The filtrate was washed with a saturated aqueous solution of NaHCO3 (2 x 30 mL) and a saturated aqueous solution of NaCl (30 mL) respectively, dried with anhydrous magnesium sulphate, filtered and the filtrate was collected. The ethyl acetate was removed at low pressure and the residue obtained was dried under vacuum to obtain compound **134** as an amber-coloured oil, 2.94 g, 11.17 mmol, 93 %, which was used in the next step without further purification.
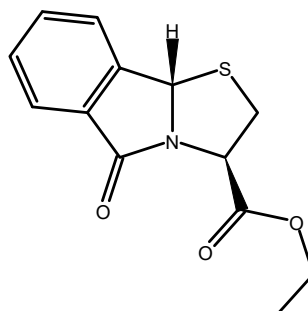
Figure 5.12: Structure of compound **134.**

Molecular Formula: $C_{13}H_{13}NO_3S$; R_f (methanol/ethyl acetate, 1:1): 0.85 (single spot).

^1H NMR (400 MHz, CDCl$_3$) δ 1.35 (t, J = 7.1 Hz, 3H, C$\underline{H_3}$-CH$_2$-O), 3.64 (m, 2H, N-CH-C$\underline{H_2}$), 4.31 (dq, J = 7.1, 1.9, Hz, 2H, CH$_3$-C$\underline{H_2}$-O), 5.27 (ddd, J = 7.5, 4.4, 0.6 Hz, 1H, N-C$\underline{H}$-CH$_2$), 6.12 (s, 1H, S-C($\underline{H}$)-C), 7.53 (m, 2H, C$\underline{H}$-C$\underline{H}$-CH-C), 7.63 (td, J = 7.5, 1.2 Hz, 1H, CH-CH-C$\underline{H}$-C), 7.85 (dt, J = 7.5, 1.0 Hz, 1H, C$\underline{H}$-C-CO) ppm.

IR (ATR): v = 1023 (m-s), 1190 (s, C-O, ester), 1385 (m, C-H), 1614 (w, C=C), 1703 (s, C=O), 2981 (w, C-H) cm^{-1}.

5.7.5 (3*R*,9b*S*)-5-Oxo-2,3,5,9b-tetrahydro[1,3]thiazolo[2,3-*a*]isoindole-3-carboxylic acid (135)

To a stirred solution of **134** (0.60 g, 2.28 mmol) in methanol/water (20 mL; 4:2) was added lithium hydroxide monohydrate (0.48 g, 11.39 mmol, 5 eq.). The resulting mixture was stirred at ambient temperature (24 ºC) and the turnover of the ester was monitored by TLC. The reaction was stopped when the starting material was completely consumed. The pH of the mixture was adjusted to 2-3 using a 4N aqueous solution of HCl and the desired compound was extracted into ethyl acetate (2 x 20 mL). The organic portions were combined and washed with a saturated aqueous solution of NaCl (20 mL), dried with anhydrous magnesium sulphate, filtered and the filtrate was collected. The solvent was removed at low pressure and the residue obtained was dried under vacuum to afford compound **135** as a white solid, 0.45 g, 1.91 mmol, 84 %.
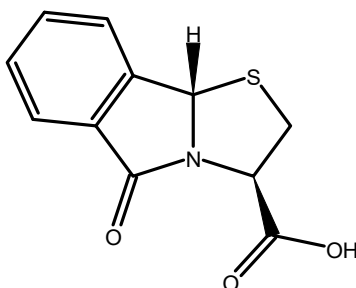
Figure 5.13: Structure of compound **135**.

Molecular Formula: $C_{11}H_9NO_3S$; R_f (methanol/ethyl acetate, 1:1): 0.51 (single spot); melting point: 118.6 – 121.4 ºC.

^1H NMR (400 MHz, DMSO-d_6) δ 3.60 (dd, J = 11.4, 4.8 Hz, 1H, N-CH-C$\underline{H_2}$), 3.73 (dd, J = 11.4, 7.8 Hz, 1H, N-CH-C$\underline{H_2}$), 5.01 (dd, J = 7.7, 4.8 Hz, 1H, N-C$\underline{H}$-CH$_2$), 6.16 (s, 1H, S-C($\underline{H}$)-C), 7.59 (dd, J = 7.5, 6.2, 2.3 Hz, 1H, CH-CH-C$\underline{H}$-C), 7.70 (dd, J = 6.3, 1.2 Hz, 2H, C$\underline{H}$-C$\underline{H}$-CH-C), 7.70 (m, 1H, C$\underline{H}$-C-CO) ppm.

^{13}C ATP NMR (101 MHz, DMSO-d_6) δ 57.92, 66.34 (N-$\underline{C}$H-CH$_2$), 124.59 ($\underline{C}$H), 130.06 ($\underline{C}$H), 130.54 (CH-$\underline{C}$-CO), 131.40 ($\underline{C}$H), 133.65 ($\underline{C}$H), 145.19 (CH-CH-CH-$\underline{C}$), 169.86 (C=O), 171.62 (C=O) ppm.

IR (ATR): v = 1195 (m-s), 1388 (m, C-H), 1644 (m-s, C=C), 1706 (s, C=O), 2924 (w, O-H) cm^{-1}.

MS (-ESI) m/z = Found 234.0232 (M-H)$^-$; calculated for $C_{11}H_8O_3NS$ 234.0230; 0.7 ppm.

5.7.6 (3*R*,9b*S*)-5-Oxo-2,3,5,9b-tetrahydro[1,3]thiazolo[2,3-*a*]isoindole-3-carboxamide (136)

To a stirred solution **135** (0.05 g, 0.21 mmol) in dry tetrahydrofuran (5 mL) was added 1,1-carbonyldiimidazole (CDI) (0.10 g, 0.64 mmol, 3 eq.) and the resulting mixture was stirred at ambient temperature for 10 minutes. Excess ammonium hydroxide solution (0.13 mL, 3.40 mmol, 16 eq.) was

added to the **136**-CDI solution and the mixture was stirred at ambient temperature (25 ℃) overnight. The THF was removed at low pressure and the residue obtained was dissolved in ethyl acetate (20 mL). The solution was washed saturated aqueous solution of NaCl (2 x 20 mL), dried with anhydrous magnesium sulphate, filtered and the filtrate was collected. The solvent was removed at low pressure and the residue obtained was dried under vacuum to afford compound **136** as a white solid, 0.02 g, 0.09 mmol, 40 %.
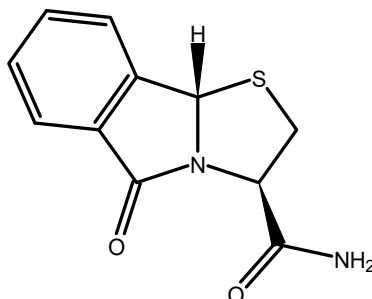
Figure 5.14: Structure of compound **136**.

Molecular Formula: $C_{11}H_{10}N_2O_2S$; R_f (methanol/ethyl acetate, 1:1): 0.77 (single spot); melting point: 98.4 – 102.5 ℃.

^{1}H NMR (400 MHz, DMSO-d_6) δ 3.66 (dd, J = 12.2, 7.6 Hz, 1H, N-CH-C<u>H</u>$_2$), 4.05 (dd, J = 12.2, 7.4 Hz, 1H, N-CH-C<u>H</u>$_2$), 4.85 (m, 1H, N-C<u>H</u>-CH$_2$), 5.49 (s, 1H, CON<u>H</u>$_2$), 5.97 (s, 1H, S-C(<u>H</u>)-C), 6.89 (s, 1H, CON<u>H</u>$_2$), 7.55 (m, 2H, C<u>H</u>-C<u>H</u>-CH-C), 7.65 (dd, J = 7.5, 1.2 Hz, 1H, CH-CH-C<u>H</u>-C), 7.86 (d, J = 7.6, 1H, C<u>H</u>-C-CO) ppm.

^{13}C ATP NMR (101 MHz, DMSO-d_6) δ 40.61 (N-CH-<u>C</u>H$_2$), 58.72, 66.92 (N-<u>C</u>H-CH$_2$), 124.30 (<u>C</u>H), 130.92 (CH-<u>C</u>-CO), 133.54 (<u>C</u>H), 145.26 (CH-CH-CH-<u>C</u>), 170.29 (C=O), 171.67 (C=O) ppm.

5.7.7 (3R,9bS)-Ethyl 9b-methyl-5-oxo-2,3,5,9b-tetrahydrothiazolo[2,3-*a*]isoindole-3-carboxylate (137)

To a stirred solution of L-cysteine ethyl ester hydrochloride (2.26 g, 12.17 mmol) and triethylamine (1.70 mL, 12.17 mmol) in dry toluene (50 mL) was added 2-acetylbenzoic acid (2.00 g, 12.17 mmol). The resulting mixture was heated at reflux, under Dean-Stark condition, for 24 hours. The mixture was allowed to cool (ambient temperature) and the toluene was removed at low pressure. Ethyl acetate (30 mL) was added to the flask and the precipitate formed was separated by vacuum filtration. The filtrate was washed with a saturated aqueous solution of NaHCO$_3$ (2 x 30 mL) and a saturated aqueous solution of NaCl (30 mL) respectively, dried with anhydrous magnesium sulphate, filtered and the filtrate was collected. The ethyl acetate was removed at low pressure and the residue obtained was dried under vacuum to afford compound **137** as an amber-coloured oil, 3.0 g, 10.82 mmol, 89 %, which was used in the next step without further purification.
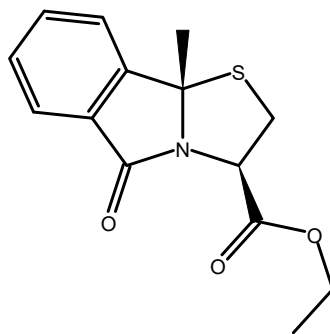
Figure 5.15: Structure of compound **137**.

Molecular Formula: $C_{14}H_{15}NO_3S$; R_f (methanol/ethyl acetate, 1:1): 0.92 (single spot).

^{1}H NMR (400 MHz, CDCl$_3$) δ 1.34 (t, J = 7.1 Hz, 3H, C<u>H</u>$_3$-CH$_2$-O), 1.97 (s, 3H, S-C(C<u>H</u>$_3$)-C), 3.84 (dd, J = 11.8, 8.7 Hz, 1H, N-CH-C<u>H</u>$_2$), 3.94 (dd, J = 11.8, 6.4, Hz, 1H, N-CH-C<u>H</u>$_2$), 4.30 (m, 2H, CH$_3$-C<u>H</u>$_2$-O), 5.15 (dd, J = 8.7, 6.4 Hz, 1H, N-C<u>H</u>-CH$_2$), 7.51 (m, 2H, C<u>H</u>-C<u>H</u>-CH-C), 7.63 (td, J = 7.5, 1.2 Hz, 1H, CH-CH-C<u>H</u>-C), 7.81 (dt, J = 7.6, 1.0 Hz, 1H, C<u>H</u>-C-CO) ppm.

IR (ATR): υ = 1203 (m, C-O ester), 1337 (m, C-H), 1611 (w, C=C), 1704 (s, C=O), 2980 (w, C-H) cm^{-1}.

5.7.8 (3R,9bS)-9b-Methyl-5-oxo-2,3,5,9b- tetrahydrothiazolo[2,3-*a*] isoindole-3-carboxylic acid (138)

To a stirred solution of **137** (1.50 g, 5.41 mmol) in methanol/water (20 mL; 4:2) was added lithium hydroxide monohydrate (0.91g, 21.68 mmol, 4 eq.). The resulting mixture was stirred at ambient temperature (24 ºC) and the turnover of the ester was monitored by TLC. The reaction was stopped when the starting material was completely consumed. The pH of the mixture was adjusted to 2-3 using a 4N aqueous solution of HCl and the desired compound was extracted into ethyl acetate (2 x 20 mL). The organic portions were combined and washed with a saturated aqueous solution of NaCl (20 mL), dried with anhydrous magnesium sulphate, filtered and the filtrate was collected. The solvent was removed at low pressure and the residue obtained was dried under vacuum to afford compound **138** as a white solid, 1.04 g, 4.17 mmol, 77 %.
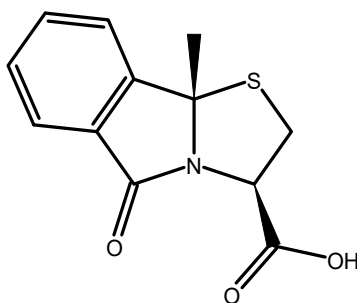
Figure 5.16: Structure of compound **138**.

Molecular Formula: $C_{12}H_{11}NO_3S$; R_f (methanol/ethyl acetate, 1:1): 0.52 (single spot); melting point: 140.8 – 142.1 ºC.

^{1}H NMR (400 MHz, DMSO-d_6) δ 1.91 (s, 3H, S-C(C<u>H</u>$_3$)-C), 3.91 (m, 2H, N-CH-C<u>H</u>$_2$), 4.93 (dd, J = 8.5, 7.0 Hz, 1H, N-C<u>H</u>-CH$_2$), 7.59 (dd, J = 7.3, 1.2 Hz, 1H, CH-CH-C<u>H</u>-C), 7.73 (m, 2H, C<u>H</u>-C<u>H</u>-CH-C), 7.77 (m, 1H, C<u>H</u>-C-CO) ppm.

^{13}C ATP NMR (101 MHz, DMSO-d_6) δ 27.97 (S-C(C$\underline{H}_3$)-C), 40.61 (N-CH-C$\underline{H}_2$), 58.26, 77.61 (N-$\underline{C}$H-CH$_2$), 123.0 ($\underline{C}$H), 124.28 ($\underline{C}$H), 129.0 (CH-$\underline{C}$-CO), 130.08 ($\underline{C}$H), 133.97 ($\underline{C}$H), 149.29 (CH-CH-CH-$\underline{C}$), 169.86 (C=O), 172.50 (C=O) ppm.

IR (ATR): υ = 1371 (m, C-H), 1660 (m, C=C), 1747 (s, C=O), 2930 (w), 2976 (w) cm^{-1}.

MS (-ESI) m/z = Found 248.0389 (M-H)$^-$; calculated for $C_{12}H_{10}O_3NS$ 248.0387; 0.9 ppm.

5.7.9 (3*R*,9b*S*)-9b-Methyl-5-oxo-2,3,5,9b-tetrahydro[1,3]thiazolo[2,3-*a*]isoindole-3-carboxamide (139)

To a stirred solution of **138** (0.20 g, 0.80 mmol) in dry tetrahydrofuran (3 mL) was added 1,1-carbonyldiimidazole (CDI) (0.39 g, 2.41 mmol, 3 eq.) and the resulting mixture was stirred at ambient temperature for 10 minutes. Excess ammonium hydroxide (0.50 mL, 12.84 mmol, 16 eq.) was added to the **138**-CDI solution and the mixture was stirred at ambient temperature overnight. The THF was removed at low pressure and the residue obtained was dissolved in ethyl acetate (20 mL). The solution was washed with a saturated aqueous solution of NaCl (2 x 20 mL), dried with anhydrous magnesium sulphate, filtered and the filtrate was collected. The ethyl acetate was removed at low pressure and the residue obtained was dried under vacuum to afford compound **139** as a white solid, 0.10 g, 0.42 mmol, 50 %.
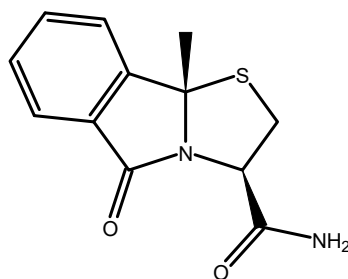
Figure 5.17: Structure of compound **139**.

Molecular Formula: $C_{12}H_{12}N_2O_2S$; R_f (methanol/ethyl acetate, 1:1): 0.86 (single spot); melting point: 128.9 – 132.1 ºC.

^{1}H NMR (400 MHz, CDCl$_3$) δ 1.97 (s, 3H, s, S-C(C$\underline{H}_3$)-C), 3.77 (dd, J = 12.4, 8.6 Hz, 1H, N-CH-C$\underline{H}_2$), 4.29 (dd, J = 12.4, 7.9 Hz, 1H, N-CH-C$\underline{H}_2$), 4.88 (dd, J = 8.6, 7.9 Hz, 1H, N-C$\underline{H}$-CH$_2$), 5.68 (s, 1H, CON$\underline{H}_2$), 6.82 (s, 1H, CON$\underline{H}_2$), 7.54 (m, 2H, C$\underline{H}$-C$\underline{H}$-CH-C), 7.67 (td, J = 7.5, 1.2 Hz, 1H, CH-CH-C$\underline{H}$-C), 7.82 (dt, J = 7.6, 1.0 Hz, 1H, C$\underline{H}$-C-CO) ppm.

^{13}C ATP NMR (101 MHz, CDCl$_3$) δ 27.89 (S-C(C$\underline{H}_3$)-C), 38.36 (N-CH-C$\underline{H}_2$), 58.80, 122.05 ($\underline{C}$H), 124.70 ($\underline{C}$H), 128.91 (CH-$\underline{C}$-CO), 129.59 ($\underline{C}$H), 133.62 ($\underline{C}$H), 148.94 (CH-CH-CH-$\underline{C}$), 171.71 (C=O) ppm.

IR (ATR): υ = 1331 (m, C-H), 1610 (m, C=C), 1673 (s, C=O), 3186 (w), 3383 (w, N-H) cm^{-1}.

MS (ESI) m/z = Found 249.0694 (M+H)$^+$; calculated for $C_{12}H_{13}O_2N_2S$ 249.0692; 0.7 ppm.

MS (ESI) m/z = Found 271.0513 (M+Na)$^+$; calculated for $C_{12}H_{12}O_2N_2SNa$ 271.0512; 0.5 ppm.

5.7.10 (3S,7aR)-Ethyl 7a-methyl-5-oxohexahydropyrrolo[2,1-*b*]thiazole-3-carboxylate (140)

To a stirred solution of D-cysteine ethyl ester hydrochloride (0.50 g, 2.67 mmol) and triethylamine (0.37 mL, 2.67 mmol) in dry toluene (20 mL) was added levulinic acid (0.31 g, 2.67 mmol) and the resulting mixture was heated at reflux, under Dean-Stark condition, for 24 hours. The mixture was allowed to

cool (ambient temperature) and the toluene was removed at low pressure. Ethyl acetate (20 mL) was added to the flask and the precipitate formed was separated by vacuum filtration and the filtrate was collected. The filtrate was washed with a saturated aqueous solution of NaHCO$_3$ (2 x 20 mL) and a saturated aqueous solution of NaCl (20 mL) respectively, dried with anhydrous magnesium sulphate, filtered and the filtrate was collected. The solvent was removed at low pressure and the residue obtained was dried under vacuum to afford compound **140** as an amber-coloured oil, 0.26 g, 1.13 mmol, 42 %, which was used in the next step without further purification.
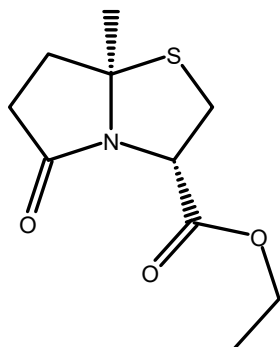
Figure 5.18: Structure of compound **140**.

Molecular Formula: C$_{10}$H$_{15}$NO$_3$S; R$_f$ (methanol/ethyl acetate, 1:1): 0.87 (single spot).

^{1}H NMR (400 MHz, CDCl$_3$) δ 1.23 (t, J = 7.1 Hz, 3H, C$\underline{H}_3$-CH$_2$-O), 1.63 (s, 3H, S-C(C$\underline{H}_3$)-CH$_2$), 2.21 (ddd, J = 13.4, 9.6, 7.1 Hz, 1H, S-C(CH$_3$)-C$\underline{H}_2$), 2.39 (ddd, J = 13.4, 9.9, 7.1 Hz, 1H, S-C(CH$_3$)-C$\underline{H}_2$), 2.51 (ddd, J = 17.2, 9.9, 5.0 Hz, 1H, C$\underline{H}_2$-CO-N), 2.73 (ddd, J = 16.8, 9.6, 7.1 Hz, 1H, C$\underline{H}_2$-CO-N), 3.46 (dd, J = 11.8, 8.8 Hz, 1H, N-CH-C$\underline{H}_2$), 3.56 (dd, J = 11.8, 5.7 Hz, 1H, N-CH-C$\underline{H}_2$), 4.17 (m, 2H, CH$_3$-C$\underline{H}_2$-O), 4.97 (dd, J = 8.8, 5.8 Hz, 1H, N-C$\underline{H}$-CH$_2$) ppm.

5.7.11 (3S,7aR)-7a-methyl-5-oxohexahydropyrrolo[2,1-b][1,3]thiazole-3-carboxylic acid (141)

To a stirred solution of **140** (0.21 g, 0.92 mmol) in methanol/water (12 mL; 4:2) was added lithium hydroxide monohydrate (0.09 g, 2.11 mmol, 2.3 eq.). The resulting mixture was stirred at ambient temperature (23 °C) and the turnover of the ester was monitored by TLC. The reaction was stopped when the starting material was completely consumed. The pH of the mixture was adjusted to 2-3 using a 1N aqueous solution of HCl and the desired compound was extracted into ethyl acetate (2 x 10 mL). The organic portions were combined and washed with a saturated aqueous solution of NaCl (10 mL), dried with anhydrous magnesium sulphate, filtered and the filtrate was collected. The solvent was removed at low pressure and the residue obtained was dried under vacuum to afford **141** as a white solid, 0.16 g, 0.80 mmol, 87 %.
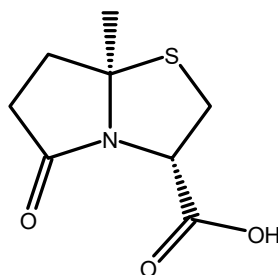
Figure 5.19: Structure of compound **141**.

Molecular Formula: $C_8H_{11}NO_3S$; R_f (methanol/ethyl acetate, 1:1): 0.5 (single spot); melting point: 164.3 – 168.1 ºC.

^{1}H NMR (400 MHz, DMSO-d_6) δ 1.61 (s, 3H, S-C(C$\underline{H_3}$)-CH$_2$), 2.25 (m, 1H, S-C(CH$_3$)-C$\underline{H_2}$), 2.37 (m, 2H, S-C(CH$_3$)-C$\underline{H_2}$; C$\underline{H_2}$-CO-N), 2.76 (m, 1H, C$\underline{H_2}$-CO-N), 3.55 (m, 2H, N-CH-C$\underline{H_2}$), 4.82 (dd, J = 8.5, 6.1 Hz, 1H, N-C$\underline{H}$-CH$_2$), 13.08 (s, 1H, COO$\underline{H}$) ppm.

^{13}C ATP NMR (101 MHz, CDCl$_3$) δ 30.63 ($\underline{C}H_3$), 31.78 ($\underline{C}H_2$), 33.06 ($\underline{C}H_2$), 36.05 ($\underline{C}H_2$), 58.63 (S-$\underline{C}$(CH$_3$)-CH$_2$), 78.54 (N-$\underline{C}$H-CH$_2$), 172.20 ($\underline{C}$=O), 176.32 ($\underline{C}$=O) ppm.

IR (ATR): v = 1201 (s), 1395 (m, C-H), 1641 (s, C=O), 1738 (s, C=O), 2910 (w), 2975 (w) cm^{-1}.

MS (-ESI) m/z = Found 200.0388 (M-H)$^-$; calculated for $C_8H_{10}O_3NS$ 200.0387; 0.6 ppm.

5.7.12 (3S,9bR)-ethyl 5-oxo-2,3,5,9b-tetrahydrothiazolo[2,3-a]isoindole-3-carboxylate (142)

To a stirred solution of D-cysteine ethyl ester hydrochloride (0.53 g, 2.85 mmol) and triethylamine (0.40 mL, 2.85 mmol) in dried toluene (20 mL) was added 2-carboxybenzaldehyde (0.43 g, 2.85 mmol). The resulting mixture was heated at reflux, under Dean-Stark condition, for 24 hours. The mixture was allowed to cool (ambient temperature) and the toluene was removed at low pressure. Ethyl acetate (15 mL) was added to the flask and the precipitate formed was separated by vacuum filtration. The filtrate was washed with a saturated aqueous solution of NaHCO$_3$ (2 x 20 mL) and a saturated aqueous solution of NaCl (20 mL) respectively, dried with anhydrous magnesium sulphate, filtered and the filtrate was collected. The solvent was removed at low pressure and the residue obtained was dried under vacuum to afford compound **142** as an amber-coloured oil, 0.50 g, 1.90 mmol, 67 %, which was used in the next step without further purification.
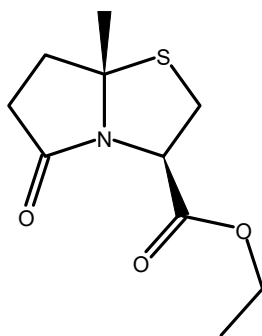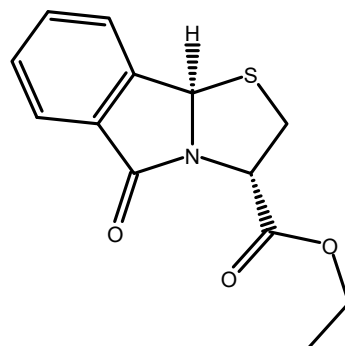

Figure 5.20: Structure of compound **142**.

Molecular Formula: $C_{13}H_{13}NO_3S$; R_f (methanol/ethyl acetate, 1:1): 0.89 (single spot).

^{1}H NMR (400 MHz, CDCl$_3$) δ 1.27 (t, J = 7.1 Hz, 3H, C$\underline{H_3}$-CH$_2$-O), 3.57 (m, 2H, N-CH-C$\underline{H_2}$), 4.22 (dd, J = 7.1, 1.9, Hz, 2H, CH$_3$-C$\underline{H_2}$-O), 5.18 (ddd, J = 7.5, 4.4, 0.6 Hz, 1H, N-C$\underline{H}$-CH$_2$), 6.03 (s, 1H, S-C($\underline{H}$)-C), 7.44 (m, 2H, C$\underline{H}$-C$\underline{H}$-CH-C), 7.54 (td, J = 7.4, 1.2 Hz, 1H, CH-CH-C$\underline{H}$-C), 7.75 (dt, J = 7.5, 1.0 Hz, 1H, C$\underline{H}$-C-CO) ppm.

5.7.13 (3S,9bR)-5-oxo-2,3,5,9b-tetrahydrothiazolo[2,3-a]isoindole-3-carboxylic acid (143)

To a stirred solution of **142** (0.42 g, 1.60 mmol) in methanol/water (20 mL; 4:2) was added lithium hydroxide monohydrate (0.20 g, 4.79 mmol, 3 eq.). The resulting mixture was stirred at ambient temperature (21 ºC) and the turnover of the ester was monitored by TLC. The reaction was stopped when the starting material was completely consumed. The pH of the mixture was adjusted to 2-3 using

a 4N aqueous solution of HCl and the desired compound was extracted into ethyl acetate (2 x 10 mL). The organic portions were combined and washed with a saturated aqueous solution of NaCl (10 mL), dried with anhydrous magnesium sulphate, filtered and the filtrate was collected. The solvent was removed at low pressure and the residue obtained was dried under vacuum to afford compound **143** as a white solid, 0.24 g, 1.02 mmol, 64 %.
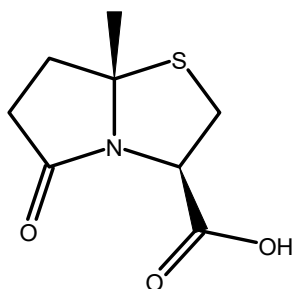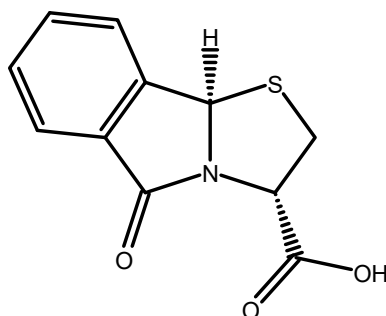

Figure 5.21: Structure of compound **143**.

Molecular Formula: $C_{11}H_9NO_3S$; R_f (methanol/ethyl acetate, 1:1): 0.56 (single spot); melting point: 125.9 – 128.3 ºC.

^{1}H NMR (400 MHz, DMSO-d_6) δ 3.60 (dd, J = 11.4, 4.9 Hz, 1H, N-CH-C<u>H</u>$_2$), 3.74 (dd, J = 11.4, 7.8 Hz, 1H, N-CH-C<u>H</u>$_2$), 5.02 (dd, J = 7.7, 4.9 Hz, 1H, N-C<u>H</u>-CH$_2$), 6.16 (s, 1H, S-C(<u>H</u>)-C), 7.60 (ddd, J = 8.1, 6.3, 2.2 Hz, 1H, CH-CH-C<u>H</u>-C), 7.70 (dd, J = 6.4, 1.3 Hz, 2H, C<u>H</u>-C<u>H</u>-CH-C), 7.75 (d, J = 7.6 Hz, 1H, C<u>H</u>-C-CO) ppm.

^{13}C ATP NMR (101 MHz, DMSO-d_6) δ 40.61 (N-CH-<u>C</u>H$_2$), 57.92, 66.34 (N-<u>C</u>H-CH$_2$), 124.60 (<u>C</u>H), 130.06 (<u>C</u>H), 130.54 (CH-<u>C</u>-CO), 133.65 (<u>C</u>H), 145.20 (CH-CH-CH-<u>C</u>), 169.87 (C=O), 171.62 (C=O) ppm.

IR (ATR): υ = 1229 (m-s), 1393 (m, C-H), 1645 (m-s, C=C), 1745 (s, C=O), 2924 (w, O-H) cm^{-1}.

MS (-ESI) m/z = Found 234.0232 (M-H)$^-$; calculated for $C_{11}H_8O_3NS$ 234.0230; 0.7 ppm.

5.7.14 (3S,9bR)-ethyl 9b-methyl-5-oxo-2,3,5,9b-tetrahydrothiazolo[2,3-a]isoindole-3-carboxylate (144)

To a stirred solution of D-cysteine ethyl ester hydrochloride (0.70 g, 3.77 mmol) and triethylamine (0.53 mL, 3.77 mmol) in dry toluene (20 mL) was added 2-acetylbenzoic acid (0.62 g, 3.77 mmol). The resulting mixture was heated at reflux, under Dean-Stark condition, for 24 hours. The mixture was allowed to cool (ambient temperature) and the toluene was removed at low pressure. Ethyl acetate (30 mL) was added to the flask and the precipitate formed was separated by vacuum filtration. The filtrate was washed with a saturated aqueous solution of NaHCO$_3$ (2 x 20 mL) and a saturated aqueous solution of NaCl (20 mL) respectively, dried with anhydrous magnesium sulphate, filtered and the filtrate was collected. The ethyl acetate was removed at low pressure and the residue obtained was dried under vacuum to afford compound **144** as an amber-coloured oil, 0.55 g, 1.98 mmol, 53 %, which was used in the next step without further purification.
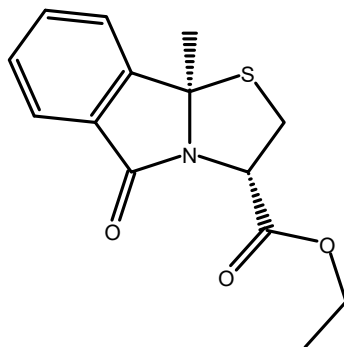
Figure 5.22: Structure of compound **144**.

Molecular Formula: $C_{14}H_{15}NO_3S$; R_f (methanol/ethyl acetate, 1:1): 0.80 (single spot).

^{1}H NMR (400 MHz, CDCl₃) δ 1.27 (t, J = 7.1 Hz, 3H, C<u>H</u>₃-CH₂-O), 1.90 (s, 3H, S-C(C<u>H</u>₃)-C), 3.76 (dd, J = 11.8, 8.7 Hz, 1H, N-CH-C<u>H</u>₂), 3.86 (dd, J = 11.9, 6.4, Hz, 1H, N-CH-C<u>H</u>₂), 4.23 (m, 2H, CH₃-C<u>H</u>₂-O), 5.07 (dd, J = 8.7, 6.4 Hz, 1H, N-C<u>H</u>-CH₂), 7.44 (m, 2H, C<u>H</u>-C<u>H</u>-CH-C), 7.55 (td, J = 7.5, 1.2 Hz, 1H, CH-CH-C<u>H</u>-C), 7.74 (dt, J = 7.6, 1.0 Hz, 1H, C<u>H</u>-C-CO) ppm.

5.7.15 (3S,9bR)-9b-methyl-5-oxo-2,3,5,9b-tetrahydrothiazolo[2,3-*a*]isoindole-3-carboxylic acid (145)

To a stirred solution of **144** (0.55 g, 1.98 mmol) in methanol/water (20 mL; 4:2) was added lithium hydroxide monohydrate (0.25 g, 5.95 mmol, 3 eq.).

The resulting mixture was stirred at ambient temperature (23 ⁰C) and the turnover of the ester was monitored by TLC. The reaction was stopped when the starting material was completely consumed. The pH of the mixture was adjusted to 2-3 using a 4N aqueous solution of HCl and the desired compound was extracted into ethyl acetate (2 x 10 mL). The organic portions were combined and washed with a saturated aqueous solution of NaCl (10 mL), dried with anhydrous magnesium sulphate, filtered and the filtrate was collected. The solvent was removed at low pressure and the residue obtained was dried under vacuum to afford compound **145** as a white solid, 0.38 g, 1.52 mmol, 77 %.
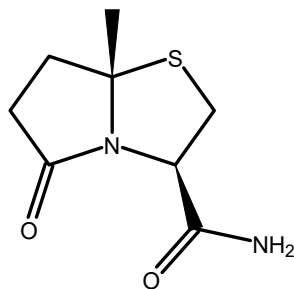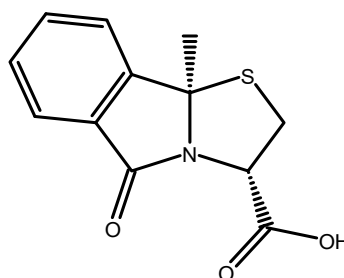

Figure 5.23: Structure of compound **145**.

Molecular Formula: $C_{12}H_{11}NO_3S$; R_f (methanol/ethyl acetate, 1:1): 0.59 (single spot); melting point: 164.0 – 167.8 ⁰C.

^{1}H NMR (400 MHz, DMSO-*d₆*) δ 1.91 (s, 3H, S-C(C<u>H</u>₃)-C), 3.96 (m, 2H, N-CH-C<u>H</u>₂), 4.93 (dd, J = 8.5, 7.0 Hz, 1H, N-C<u>H</u>-CH₂), 7.60 (m, 1H, CH-CH-C<u>H</u>-C), 7.73 (m, 2H, C<u>H</u>-C<u>H</u>-CH-C), 7.78 (m, 1H, C<u>H</u>-C-CO) ppm.

^{13}C ATP NMR (101 MHz, DMSO-d_6) δ 28.00 (S-C($\underline{C}$H$_3$)-C), 40.61 (N-CH-$\underline{C}$H$_2$), 58.11, 77.62 (N-$\underline{C}$H-CH$_2$), 123.02 ($\underline{C}$H), 124.29 ($\underline{C}$H), 129.00 (CH-$\underline{C}$-CO), 130.10 ($\underline{C}$H), 134.00 ($\underline{C}$H), 149.29 (CH-CH-CH-$\underline{C}$), 169.88 (C=O), 172.02 (C=O) ppm.

IR (ATR): ν = 1201 (m), 1393 (m, C-H), 1643 (m, C=C), 1737 (s, C=O), 2930 (w), 2976 (w) cm^{-1}.

MS (-ESI) m/z = Found 248.0389 (M-H)$^-$; calculated for C$_{12}$H$_{10}$O$_3$NS 248.0387; 0.9 ppm.

5.8 Discussion of experimental results

The ring system, the functional group and the chirality of the lead compound (**132**) were varied. The bicyclic and tricyclic analogues, with carboxylic acid and amide functional groups respectively, and their respective enantiomers were synthesised by cyclisation reaction to afford the respective precursors (esters) while the precursors were subjected to hydrolysis to give the corresponding carboxylic acid. The respective amides were synthesised by either direct treatment of the ester with ammonium hydroxide or via activation of the carboxylic acid with 1,1'-carbonyldiimidazole followed by *in situ* treatment of the activated species with ammonium hydroxide. Identity characterisation by spectroscopic methods (^{1}H and ^{13}C- NMR, IR, MS) confirmed the formation of respective compounds while purity characterisation by TLC and melting point analysis indicates most of the synthesised compounds are pure.

5.8.1 Bicyclic and tricyclic esters

The treatment of L/D-cysteine ethyl ester hydrochloride with levulinic acid, 2-carboxylbenzaldehyde, and 2-acetylbenzoic acid afforded the bicyclic and tricyclic esters (compounds **131**, **134** and **137**) and their respective enantiomers (compounds **140**, **142** and **144**) in excellent yield and purity as judged by proton NMR and IR (Scheme 5.1) (Danton *et al*., 2019; Allin *et al*., 2000a, b).
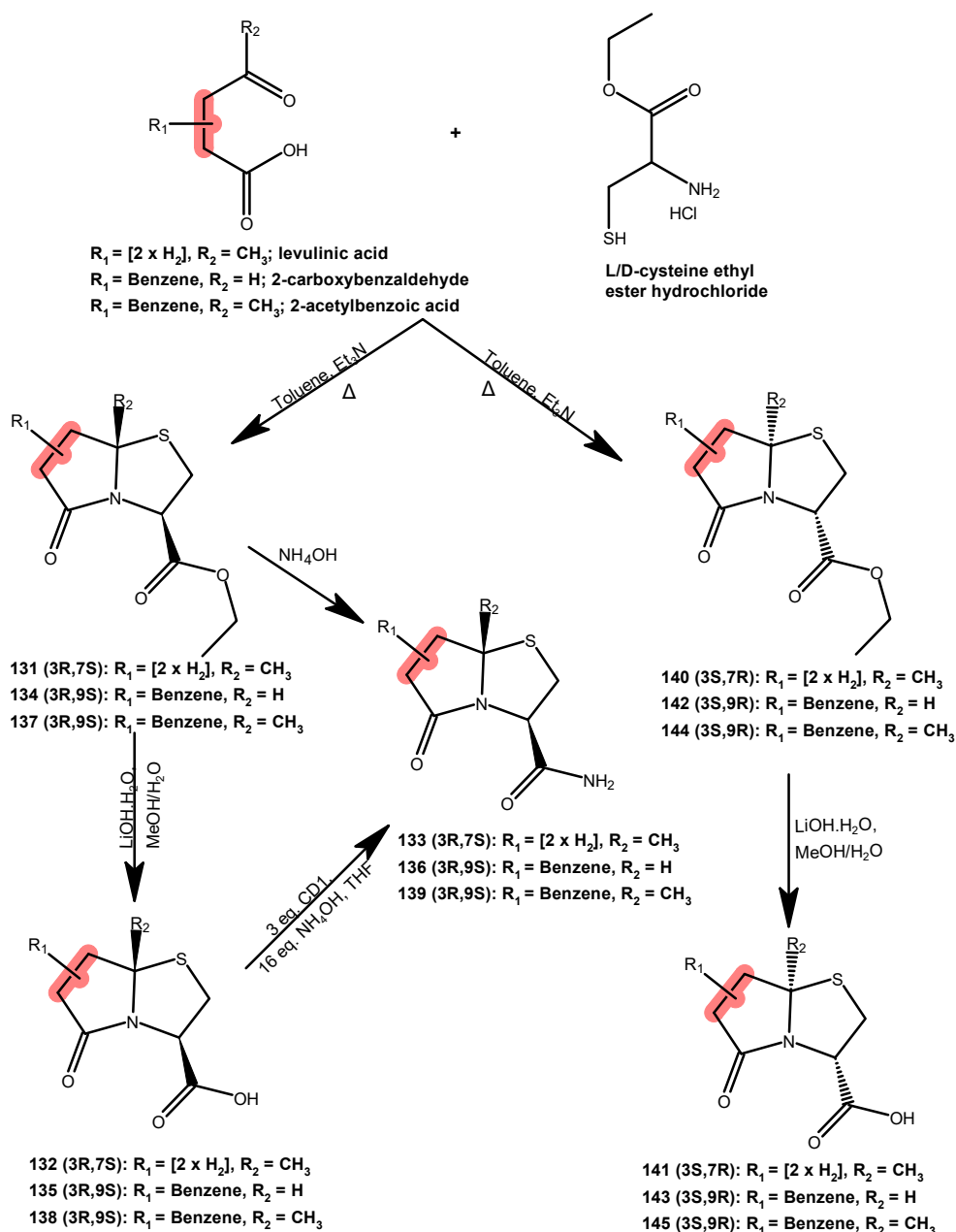
Scheme 5.1: Syntheses of the lead compound (**132**) and its bicyclic and tricyclic analogues.

The formation of these *N,S* heterocyclic esters (Scheme 5.2) proceed through nucleophilic addition of the amino group of cysteine ester to the aldehyde/ketone functional group, resulting in the formation of carbinolamine intermediate which undergoes condensation to the corresponding Schiff base that is then protonated to give an unstable iminium ion (see section 3.6.1). The unstable iminium ion cyclises rapidly with the neighbouring sulfhydryl group to give the thiazolidine intermediate which readily

undergoes condensation via the reaction of the carboxylic acid of the aldehyde/ketone (levulinic acid, 2-acetylbenzoic acid and 2-carboxybenzaldehyde respectively) with the secondary amine of the newly formed thiazolidine to yield the bicyclic or tricyclic esters (Oliver *et al*., 1958; Chen *et al*., 2016; Kallen, 1971; Nagasawa *et al*., 1982).
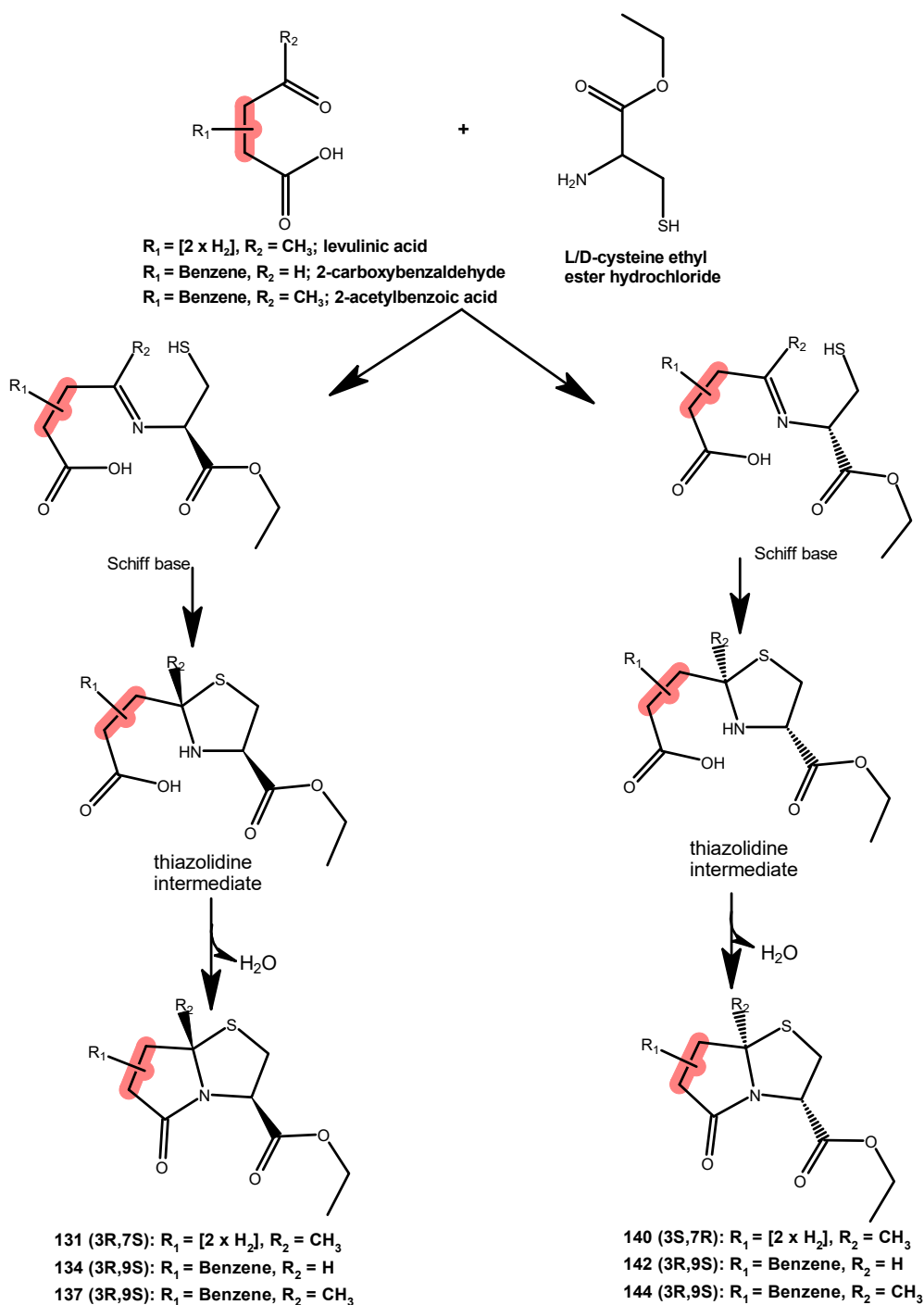
Scheme 5.2: Pathway for the formation of the *N,S* heterocyclic ester.

The proton NMR characterisation confirms the formation of esters. The proton NMR spectrum revealed the presence of major groups such as the ester group while the chemical shift of the C3 proton seems to be deshielded possibly due to the presence of electronegative oxygen atoms and neighbouring amide bonds respectively. The fusion of the benzene ring to the bicyclic esters resulted in the loss of the pyrrolidinone protons with the concomitant appearance of peaks

corresponding to the benzene protons. Also, the IR characterisation of the bicyclic and tricyclic esters showed key absorption bands corresponding to C-H, C=O and C=C (aromatic region, tricyclic esters) respectively while purity characterisation by TLC showed single distinct spot which, indicate the formation of new pure compounds.

The proton NMR and IR results are consistent with the data from published articles (Table 5.1) and the spectroscopic results also align with the factors that influence chemical shifts and wavenumbers as specified by Watson, 2012.

Table 5.1: Comparison between data from literature and experimental results

Compound No.	Reference	Comments
131	Danton *et al*., 2019	The ^{1}H NMR and IR data of **131** are consistent with the data from the literature
134	Allin *et al*., 2000a; Pinho e Melo *et al*., 2004	Pinho e Melo *et al*., 2004 used methyl ester instead of ethyl group. Besides this variation, ^{1}H NMR and IR data of **134** correlate with the data from both literature
137	Allin *et al*., 2000a; Pinho e Melo *et al*., 2004; Danton *et al*., 2019	The ^{1}H NMR and IR data of **137** are consistent with the data from the literature
140	Novel	
142	No literature	
144	Allin *et al*., 2000a	The ^{1}H NMR and IR data of **144** are consistent with the data from the literature but the literature-assigned configuration is wrong

The attempts to synthesise the analogue of **137** by substituting the methyl group attached to the chiral carbon with a benzene ring were unsuccessful. Following the published method of Allin *et al*. (2000a), the treatment of L-cysteine ethyl ester with an equimolar concentration of 2-benzoylbenzoic acid, in the presence of a base, resulted in the formation of complex mixtures as judged by TLC and proton NMR. The variation of reaction conditions such as solvent (methanol, ethanol) to enhance the solubility of the reactants did not yield positive outcomes.

5.8.1.1 Chirality of the bicyclic and tricyclic esters

The bicyclic and tricyclic esters are single diastereomers with two chiral centres. It is expected that the configuration at C3 should mimic the configuration of the cysteine ethyl ester considering that the ester is the precursor of the thiazolidine ring. The configuration of L-cysteine ethyl ester hydrochloride is R while that of D-cysteine ethyl ester hydrochloride is S. Hence, the configuration at C3, for compounds synthesised from L-cysteine ester, is expected to be R while compounds

synthesised from D-cysteine ester would be an S configuration. The new chiral centre, at C7 for bicyclic compounds and C9 for tricyclic compounds respectively, is not an extension from the reactant(s) rather it is formed following the cyclisation of the iminium ion to the corresponding thiazolidine ring. Oliver *et al.*, 1958 reported the direct synthesis of compound **135** following the reaction of 2-carboxybenzaldehyde with cysteine hydrochloride in the presence of pyridine. However, the C3 and C9 configurations were not mentioned. Similarly, Allin *et al.*, 2000a documented the synthesis of compounds **134** and **137** respectively from L-cysteine ethyl ester. Unfortunately, the stereochemistry, especially at C3 was wrongly assigned. Allin *et al.*, 2000a reported the stereochemistry of the compounds (**134** and **137**) as (3S,9bR). The compounds were derived from L-cysteine ethyl ester which has an R configuration. Hence, it is expected that the C3 configuration of the compounds should be R and not S. Also, Allin *et al.*, 2000b, synthesised the enantiomeric pairs of compounds **134** and **137** (**142** and **144**) respectively from D-cysteine ethyl ester but the configuration was also wrongly assigned as (3R,9bR) in contrast to the stereochemistry of the precursor amino acid moiety.

Pinho e Melo *et al.,* (2003/2004) undertook an X-ray crystallography study on the methyl derivatives of compounds **134** and **137** respectively and their findings validate the R configuration at C3 (Pinho e Melo *et al.*, 2003; Pinho e Melo *et al.*, 2004). Interestingly the studies also revealed the configuration of the new chiral centre (C7/C9) as S. Considering the X-ray crystallography study by Pinho e Melo *et al.*, 2004, the treatment of L-cysteine ethyl ester hydrochloride with the respective ketone/aldehyde afforded a single diastereomeric bicyclic and tricyclic esters with (3R, 7aS) and (3R, 9bS) configurations respectively while the treatment of D-cysteine ethyl ester hydrochloride with the respective ketone/aldehyde is likely to generate the bicyclic and tricyclic analogues with (3S, 7aR) and (3S, 9bR) configurations respectively. While the configuration at C3 is likely to be S owing to the configuration of the precursor D-cysteine ethyl ester, the R configuration at C7 (bicyclic) and C9 (tricyclic) is tentative and subject to confirmation by X-ray/NMR studies.

5.8.2 Bicyclic and tricyclic carboxylic acids

The treatment of the respective heterocyclic esters with an inorganic base afforded the corresponding carboxylic acids in excellent yield and good purity as judged by TLC, melting point analysis and spectroscopic techniques (MS, ^{1}H and ^{13}C-NMR, IR).

The elimination of the ethyl group did not significantly alter the chemical shifts of the protons when compared with the ester. TLC showed a single distinct spot for the carboxylic acid, with lower R_f values compared with the respective esters. There was no significant variation in the ^{1}H-, ^{13}C-NMR, IR and R_f values when the R, S series were compared with the S, R pairs but there were slight variations when the respective melting points were compared. The variation in melting point might be due to solvent content or impurities that are not detectable on the TLC scale. IR characterisation of the respective carboxylic acids showed essential wavenumbers corresponding to C-H, O-H, C=O and C=C (aromatic region, tricyclic compounds) respectively while ^{13}C NMR showed several characteristic peaks with a unique peak at ≥ 168 corresponding to the carbonyl carbon. The absence of the ethyl protons, the

reduced R_f values (compared to esters) and the change in physical state (oil to solid) confirm the transformation of the esters while the MS results validate the formation of respective carboxylic acids.

Table 5.2: Comparing data from literature and experimental results

	132	**135**	**138**	**141, 143 and 145**
Reference	Baldwin and Christie, 1978	Pinho e Melo *et al*., 2004	Pinho e Melo *et al*., 2004[y]; Danton *et al*., 2019[z]	No literature
Found ^{1}H NMR	Consistent with literature	Consistent with literature	Consistent with literature	
Found IR	Consistent with literature	N/A	N/A	
Literature mp	193.0-194.5	156.1-157.9	162.3-164.9[y]; 193-195[z]	
Found mp	180.9-183.1	118.6-121.4	140.8-142.1	
Literature MS	N/A	(M^+-H): 249	N/A	
Found MS	$(M-H)^-$: 200	$M-H)^-$: 234	$M-H)^-$: 248	

The spectroscopy results (^{1}H NMR and IR) of compounds **132**, **135** and **138** respectively agree with the spectroscopic data from the respective literature (Table 5.2). The reported higher mass (249) of compound **135** is due to the methylation of the carboxylic acid with diazomethane before the MS analysis (Pinho e Melo *et al*., 2004). The melting point values were not consistent with our experimental result (Table 5.2). This variation was also observed when data from published articles were compared (compound **138**). These inconsistencies, in melting points, may be attributed to the impurities/residual solvents in the samples or may be due to the different methods employed in determining the melting point. it seems there are no published articles for the S, R series (compounds **141**, **143**, **145**). However, the S, R spectroscopic results are consistent with the R, S series.

The attempt to innovate one-pot synthesis of the lead compound (**132**) by treating methyl levulinate with L-cysteine in ethanol in the presence of p-toluenesulphonic monohydrate (Baldwin and Christie, 1978) resulted in the formation of two compounds as judged by TLC. The two compounds were separated and characterised by proton NMR. The proton NMR results revealed the formation of the desired compound (**132**) in low yield and its ethyl ester derivative (**131**). The formation of **131** may be due to the esterification of the L-cysteine which becomes the reactant for the formation of the bicyclic product. It is also possible that the bicyclic carboxylic acid was formed and the acid was esterified in the presence of ethanol.

5.8.3 Bicyclic and tricyclic amides

The bicyclic amide (**133**) was synthesised, in low yield, by direct amidation of the ester **131** in the presence of excess concentrated ammonium hydroxide solution. Considering the low reactivity of the bicyclic ester, the tricyclic amides were synthesised, in good yield, via CDI-mediated activation of the carboxylic acids (**135** and **138** respectively) to afford the reactive acyl imidazole intermediate that

reacted with the ammonium hydroxide to afford the corresponding amides (compounds **136** and **139** respectively).

Table 5.3: Data from literature and experimental results

	133	136	139
Reference	Novel	Novel	Novel
Literature mp	N/A	N/A	N/A
Found mp	171.2-174.3	98.4-102.5	128.9-132.1
Literature MS	N/A	N/A	N/A
Found MS	(M+H)$^+$: 201		(M+H)$^+$: 249

The bicyclic and tricyclic amides are novel compounds and structural characterisation by spectroscopic methods (^{1}H-, ^{13}C-NMR, IR and MS) validates their formation while TLC and melting point analyses revealed the respective amides as pure compounds with increased R_f values and decreased melting point range when compared to the respective carboxylic acids.

5.8.4 Hydroxamic and oxyamine derivatives

The attempts to synthesise the hydroxamic acid (**145**) and oxyamine (**147**) derivatives through the substitution of the carboxylic with R-CONHOH and R-COONH$_2$ groups, respectively, were unsuccessful (Figure 5.24). The synthetic plan for the synthesis of the hydroxamic acid derivative involved the initial activation of the carboxylic acid to the acid chloride derivative which would then to be treated with hydroxylamine hydrochloride to afford the desired hydroxamic acid derivative. Following the published protocol of Das *et al*., 2019, the conversion of compound **132** to the acid chloride derivative was challenging owing to the instability of the ring in acidic conditions. The treatment of the carboxylic acid with 1.5 eq. thionyl chloride, in DCM, resulted in the decomposition of the bicyclic ring. Similarly, the treatment of compound **132** with 2.5 eq. of oxalyl chloride in the presence of DMF, also induced the decomposition of the bicyclic ring.

In an attempt to synthesise oxyamine derivative (**147**), the carboxylic acid (**132**) was treated with the coupling agent CDI, in the presence of N-Boc-hydroxylamine, to generate reactive species that would react, *in situ,* with the N-Boc-hydroxylamine to afford the *tert-butyl* carbamate (**146**) (Figure 5.24) that would be subjected to TFA treatment to generate the desired oxyamine. Unfortunately, there was no formation of the *tert-butyl* carbamate (**146**) as judged by proton NMR. According to the proton NMR, peaks corresponding to bicyclic ring protons were present, however there was no consistent peak corresponding to the Boc group protons.
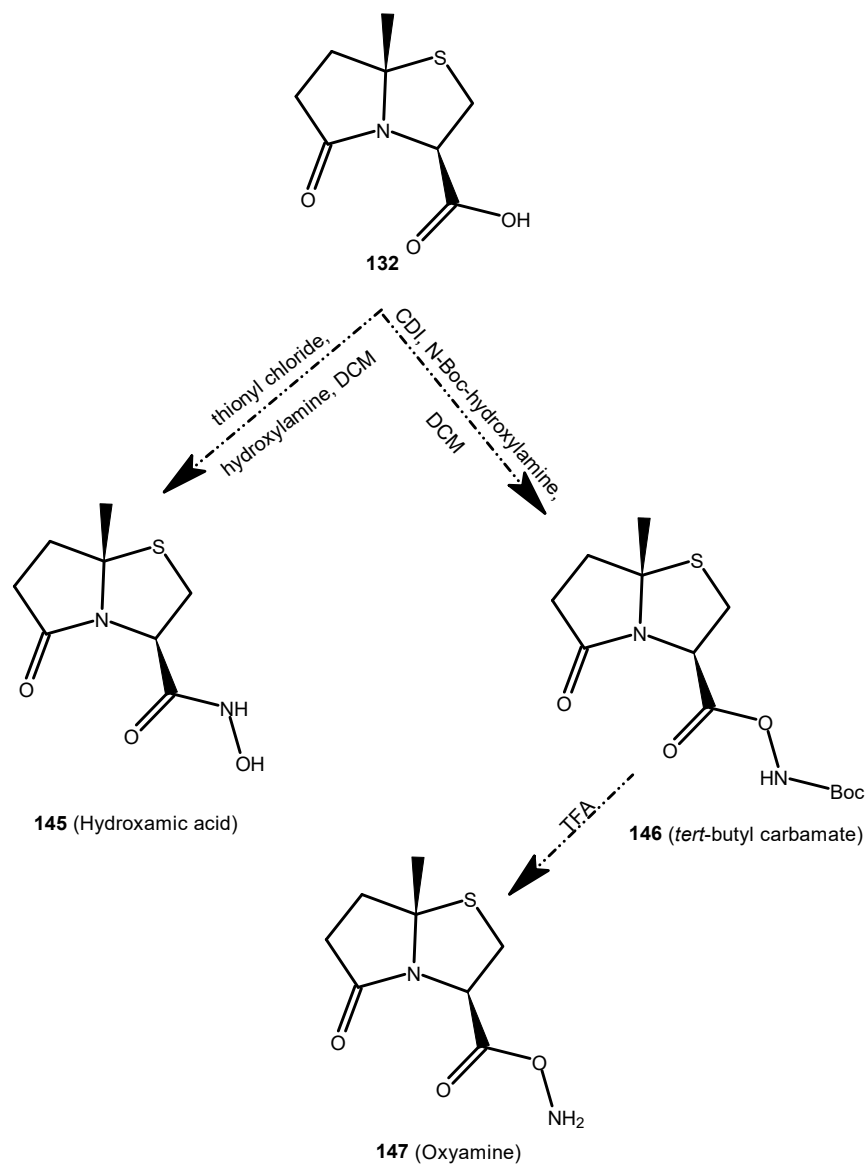
Figure 5.24: Attempted synthesis of hydroxamic acid and oxyamine derivatives.

5.9 *In vitro* inhibitory studies of potential bicyclic and tricyclic inhibitors against Bla$_{Mab}$

The final compounds (carboxylic acids and amides) were screened for their respective inhibitory potential against the enzyme Bla$_{Mab}$ using the TLC-based assay with penicillin V potassium salt as the substrate. The inhibitory study of these compounds was done by the microbiology team (Jonathan Cox and James Harrison, Aston University).

5.9.1 Materials and methods

Penicillin V potassium salt was purchased from Biosynth Carbosynth Ltd. while the precoated silica gel plates (60 F$_{254}$, Merck) were purchased from Merck respectively. The recombinant enzyme, Bla$_{Mab}$, was expressed and purified by the biology team (Jonathan Cox and James Harrison, Aston University). The visualisation of the TLC plate was achieved with an aqueous solution of potassium permanganate (KMnO$_4$).

5.9.2 Methods

To a well containing the recombinant Bla$_{Mab}$ (10 µL, 0.01 mg/mL), was added the potential inhibitor (10 µL, 2 mg/mL) and the resulting mixture was incubated for 5 minutes at ambient temperature (17 - 20 °C). Penicillin V potassium salt (10 µL, 10.30 mM) was added to the Bla$_{Mab}$-inhibitor mixture and the resulting mixture was incubated for additional 10 minutes at the same ambient temperature. The test samples were prepared and analysed along with positive and negative controls. 1 µL of the respective reaction mixtures was spotted on a pre-coated silica gel plate. The plate was dried and subjected to Thin-layer Chromatography (TLC) using ethyl acetate:water:acetic acid (3:1:1, v/v/v) as the mobile phase. The plate was dried following the TLC analysis and visualised with an aqueous solution of KMnO$_4$.

Table 5.4: Shows the preparation of samples along with the controls.

	Vol. (µL)	1	2	3	4	5	6	7	8
Bla$_{Mab}$	10		x				x	X	x
Potential Inhibitor	10			x			x	X	
Penicillin V	10				x	x		X	x
Penicilloic acid V	10								
Boiled NDM-1	10					x			
Tris HCl Buffer		x	x	x	x	x	x	X	x
Tris HCl Buffer		30	20	20	20	10	10	0	10
Total volume (µL)		30	30	30	30	30	30	30	30

5.10 Discussion

The concentrations reported here onward are the final concentrations of the enzyme, substrate and potential inhibitors respectively.

Before the inhibitory assay, the optimum Bla$_{Mab}$ concentration and incubation period required for the complete turnover of the penicillin V (1.33 mg/mL = 3.42 mM) were established to be 0.003 mg/mL and 10 minutes respectively (see section 4.6.1).

5.10.1 TLC-based assay hypothesis

Samples for the TLC-based inhibitory studies were prepared according to Table 5.4. Considering the Bla$_{Mab}$ enzyme was suspended in 25 mM Tris HCl (pH 7), 100 mM NaCl buffer, 1 µL of the buffer (spot 1) was analysed along the respective test samples to determine and monitor potential visualisable components of the buffer. The stability of potential inhibitors (spot 3) and penicillin V (spot 4) in the presence of Tris HCl buffer were also evaluated while spot 4 also served as a positive control for the test sample (spot 7). The negative control (spot 8) was also prepared and analysed along with the test sample (spot 7). It is expected that in the presence of the Bla$_{Mab}$, the substrate would be hydrolysed to the corresponding penicilloic acid V with a lower R$_f$ value.
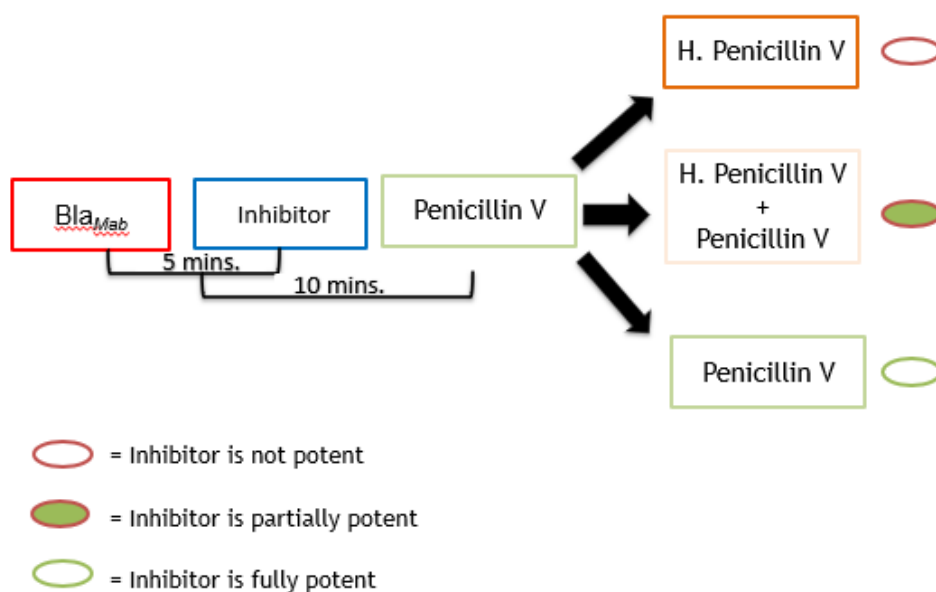
Figure 5.25: Possible outcomes of the inhibitory potential of potential inhibitors.

Concerning spot 7, the three different scenarios illustrated in Figure 5.25 are possible depending on the inhibitory potential of the respective bicyclic and tricyclic thiazolidine inhibitors. If a potential inhibitor is potent, it will deactivate the enzyme after the pre-incubation period such that added substrate, penicillin V, would remain chemically stable, hence the penicillin V would be visible on the TLC plate following the visualisation with KMnO$_4$ but if the substrate is hydrolysed to the corresponding penicilloic acid V following the incubation period, it indicates that the potential inhibitor is not potent against the Bla$_{Mab}$ enzyme. However, if there is partial inhibition of the enzyme, a mixture of penicillin V and penicilloic acid V would be observed on the TLC plate following the visualisation.

5.10.2 TLC-based assay experimental outcome

Following the inhibitory assay, it was observed that the Tris HCl buffer produced a visualisable component on the TLC plate but with a very low R_f value. Also, the potential inhibitors and penicillin V were stable in the presence of the Tris HCl buffer (spots 3 and 4).

Jonathan Cox's group also evaluated the antimicrobial properties of the potential inhibitors against Gram-negative bacteria using a solid media disc diffusion assay. Table 5.5 Summarises the results of the inhibitory and antimicrobial assays of the potential inhibitors.

Table 5.5: Summary of inhibitory and antimicrobial results.

Compound No.	Structure	Molarity (mM)[a]	Inhibitory activity	Antimicrobial activity
133		3.35	Negative	Negative
135		2.85	Negative	Negative
136		2.86	Negative	Negative
138		2.69	Negative	Negative
139		2.70	Negative	Limited activity observed
141		3.33	Negative	Limited activity observed
143		2.85	Negative	Negative
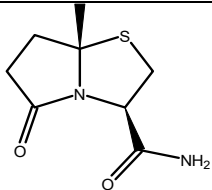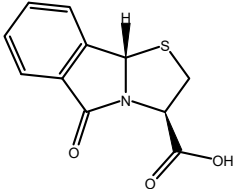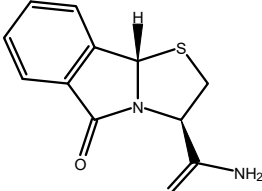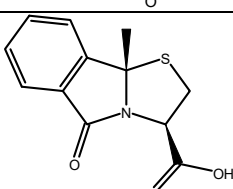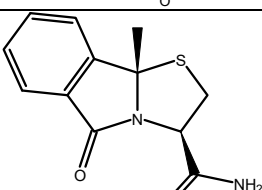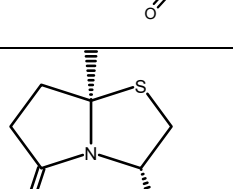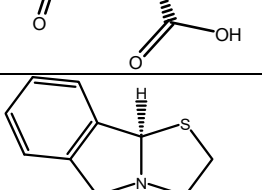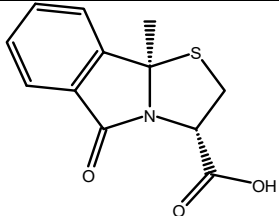
| 145 | | 2.69 | Negative | Negative |

a = molar concentrations (the respective compounds) for the inhibitory studies

Unfortunately, at the respective molar concentrations (Table 5.5), none of the bicyclic and tricyclic acids/amides prevented the turnover of 3.42 mM penicillin V in the presence of 0.003 mg/mL Bla$_{Mab}$. The result indicates that the compounds lack inhibitory properties against Bla$_{Mab}$ at the experimental concentration. Interestingly, **139** and **141** displayed minimal antimicrobial activity against some Gram-negative bacteria.

Conclusion

The key research findings in relation to the aim and objectives of the study are summarised in this section. In addition, the section highlights the value and contribution of the study and also enumerates its limitation and propose opportunities for future research.

The discovery of antibiotics revolutionised public health positively but it can be argued that its application in clinical settings came with a hefty price that has promulgated the development of antibiotic resistance which is associated with a high mortality rate. Microbial defence via β-lactamases is one of the current bacterial drug resistance mechanisms and New Delhi Metallo-β-lactamase 1 (NDM-1) is recognised as one of the most notorious β-lactamases that destroys nearly all of the most commonly used β-lactam antibiotics. NDM-1 is considered a global menace and bacteria harbouring the enzyme are associated with life-threatening infections. Despite the disease burden associated with NDM-1, there are no clinically significant inhibitors for this enzyme. Considering the absence of clinically useful NDM-1 inhibitors and the need to prevent an NDM-associated infection pandemic, this study aimed to develop small molecules as potential inhibitors for NDM-1 through chemical synthesis and biological evaluation.

Three inhibitory concepts for NDM-1 inhibition were developed and three classes of small molecules were designed based on these concepts. The three classes of small molecules include ketene-generating monocyclic compounds, bis cyclo-oxamide prodrugs and α,β-unsaturated carbonyl compounds respectively.

The attempts to synthesise the monocyclic compound (**48**) were futile. The unsuccessful dehydrogenation of the thiazolidine ring (**52**), N-deprotection of the dimethyl derivative (**72**), decarbonylation of the oxo derivative (**75** and **76**) and imidation of oxo derivative (**76/78**) respectively were the limiting steps in the attempted syntheses of compound **48** and its dimethyl/oxo analogues (**61/80**) respectively. While the ethyl ester precursor of **48** was successfully obtained via acid chloride coupling, the attempted dehydrogenation of the thiazolidine ring (**52**), at the C3-C4 position, was problematic due to the presence of a second methylene group (S-<u>CH$_2$</u>-N) whose protons were prone to halogen substitution compared to the proton attached to the chiral carbon (C4). However, the substitution of the second methylene group with a dimethyl group and a carbonyl group respectively afforded the desired dihydrothiazole ring but the attempted N-deprotection of the dimethyl derivative and decarbonylation of the oxo derivative respectively likely resulted in the decomposition of the heterocyclic ring. Furthermore, the attempted synthesis of the oxo analogue (**80**) was also disappointing due to the instability of the dihydrothiazole ring in the presence of strong bases such as LDA and n-BuLi respectively. The studies indicate that the attempted construction of the scaffold was the primary challenge. Choosing or constructing a different NDM-1 hydrolysable scaffold such as cephalosporin could have enabled the successful synthesis of small molecules containing the ketene-generating fragment. However, this was not done owing to time constraints.

Following the unsuccessful synthesis of **48** and its analogues, a different concept for the inhibition of NDM-1, which allows the systematic and selective delivery of the chelating agent, oxalate anion, to the

NDM-1 active site, was developed. The chelating property of the oxalate moiety was masked with a potential NDM-1 hydrolysable scaffold through a coupling reaction. The treatment of proline/thiazolidine monomeric esters with oxalyl chloride afforded the dimeric esters (bis cyclo-oxamide esters), in moderate to poor yield due to the instability of the thiazolidine ring, especially the CH_2 substituted derivatives while basic hydrolysis of the ester yielded the corresponding carboxylic acid. The bis cyclo-oxamide prodrugs stand a chance to be a potential broad-spectrum inhibitor against Metallo-β-lactamases (B1-3) owing to their conserved zinc (II) ions in their active site.

Equally, a third concept for NDM-1 inhibition was developed by the synthesis of α,β-unsaturated carbonyl compound (**110**) as a potential inhibitor based on the composition of the NDM-1 active site. The NDM-1 active site contains important nucleophilic amino residues such as Lys211, which are prone to covalent modification via Michael addition. Biological modification of these residues by small molecules may abrogate their functionalities in the enzyme's active site and consequently results in the deactivation of the enzyme.

Identity characterisation of monocyclic precursors of **48**, the bis cyclo-oxamide prodrugs and the α,β-unsaturated carbonyl compound was achieved by spectroscopic methods (^{1}H-NMR, ^{13}C-NMR, IR and Mass spectroscopy respectively). However, there are drawbacks associated with the use of ^{1}H NMR for the characterisation of the monocyclic precursor of **48** (**52**), the bis cyclo-oxamide prodrugs and the α,β-unsaturated carbonyl compound (**110**) owing to restricted rotation of the amide bond which slows the *cis-trans* interconversion and results in complexity and multiplicity of protons, especially with the bis cyclo-oxamide prodrugs which have two amide bonds. Also, the purity characterisation of most of the solid compounds gave a positive result. However, the melting point result of compound **96** was unusual. It seemed compound **96** is heat labile and undergoes heat-induced transformation to a new compound with a different melting point.

The protein-ligand docking study showed that key moieties of the bis cyclo-oxamides, such as the carboxylate, oxo moiety and the ring system, have the potential to make polar and hydrophobic interactions, respectively, with residues in the NDM-1 active site that are essential to the mechanism of the enzyme. Similarly, protein-ligand docking study of α,β-unsaturated carbonyl compound (**101**) showed that the carboxylate group and the proline moiety displayed potential interactions with the loop 10 residues (Lys211(184) and Asn220(193)) and the substrate binding loop 3 hydrophobic residues (Val73(46)) respectively.

Considering that the bis cyclo-oxamides are dicarboxylic acids, they can display undesired chelating properties. However, spectrophotometric studies on the chelating properties of the bis cyclo-oxamides indicated that the dimeric compounds do not display chelating properties and by extension, they are unlikely to display off-target toxicity.

The inhibitory potential of the bis cyclo-oxamides and the α,β-unsaturated carbonyl compound against NDM-1 were evaluated by TLC-based assay, using penicillin V potassium salt as the substrate, and rapid nitrocefin test respectively. The TLC-based assay of the first batch of the bis cyclo-oxamides showed that the prodrugs were not likely transformed by the enzyme to release oxalate anion as the compounds remained chemically stable in the presence of NDM-1 contrary to the postulated inhibitory

mechanism. Surprisingly, the inhibitory studies showed that compounds **96** and **98** respectively were inhibitors of NDM-1 in their own right rather than acting as prodrugs.

Unfortunately, when all the bis cyclo-oxamides and the α,β-unsaturated carbonyl compound (**110**) were assayed by the UV method (rapid nitrocefin test), none of the compounds displayed inhibitory activities against the NDM-1 enzyme. While the contradicting result may be attributed to the effect of ethanol considering that the compounds were solubilised in ethanol, it is also likely that the difference may be attributed to the high enzyme concentration used for the TLC-based assay (1.33 µM) compared to the concentration of the enzyme in the UV-based assay (0.036 µM). Despite the disappointing result, a rapid nitrocefin test confirmed NDM-1 sensitivity in presence of oxalic acid. Oxalate anion potentiated the inhibition of NDM-1 such that the turnover of the nitrocefin substrate was impeded in the presence of 1.11 mM of oxalic acid. The sensitivity of NDM-1 to oxalic acid indicates the potential of the prodrug concept. However, the findings showed that the proline and thiazolidine ring are not suitable scaffolds for the prodrug concept and, by extension perhaps the same for the ketene-generating concept, considering that these scaffolds are not hydrolysed by the NDM-1 enzyme. Perhaps, using known NDM-1 hydrolysable scaffolds, such as cephalosporins, as carriers of the oxalate anion may be beneficiary to the development of this concept.

Besides NDM-1, other β-lactamases are notorious for promulgating antibiotic resistance and aggravating pathological conditions. One of such β-lactamases is the β-lactamase from *Mycobacterium abscessus* which is termed Bla*Mab*. *Mab* is known to aggravate lung diseases, especially in patients with cystic fibrosis. Despite *Mab* produces Bla*Mab*, the current lung infection therapy for the treatment of *Mab* infection in patients with cystic fibrosis does not include an inhibitor for Bla*Mab* and the lack of Bla*Mab* inhibitor as part of the treatment regimen may be responsible for poor treatment outcome of *Mab* infections in patients with cystic fibrosis. It is likely that the addition of Bla*Mab* inhibitor to the current treatment regimen (macrolide, aminoglycoside and β-lactam antibiotics) would likely improve the treatment outcome of *Mab* infections in patients with cystic fibrosis. While the first generation β-lactam inhibitors are susceptible to Bla*Mab* hydrolysis, the non-β-lactam inhibitors such as transition state analogues, avibactam and relebactam respectively, are potent inhibitors of Bla*Mab*. A recent in-house screening of several compounds for their inhibitory activity against Bla*Mab* flagged up a commercially available bicyclic lactam as a potential inhibitor (**132**) of Bla*Mab*. Bicyclic and tricyclic analogues of the lead compound (**132**) were synthesised and their inhibitory potential against Bla*Mab* was evaluated. The bicyclic and tricyclic analogues and their enantiomeric pairs were afforded by the cyclisation reaction of L/D-cysteine ester with the corresponding keto acid/aldehyde, followed by hydrolysis and/or amidation reaction. Structural characterisation by spectroscopic methods affirmed the formation of all desired final compounds. Attempts to equally synthesise the hydroxamic acid and oxyamine derivatives were unsuccessful. The limiting step for the hydroxamic acid derivative was attributed to the instability of the bicyclic ring under acid chloride treatment while that of the oxyamine derivative is a consequence of the non-activation of the carboxylic acid of the lead compound in the presence of CDI.

Unfortunately, the inhibitory studies of bicyclic and tricyclic carboxylic acid and amide and their respective enantiomeric pair (carboxylic acid) showed that none of these analogues displayed inhibitory activity against Bla$_{Mab}$ at the respective tested concentrations. The bioisosteric replacement of the carboxylic functional group and the methylene groups with an amide group and a benzene ring respectively resulted in the loss of biological activity of the lead compound. However, antimicrobial studies showed some of the compounds (**139** and **141** respectively) displayed limited antimicrobial activity against some Gram-negative bacteria. Perhaps, the limited antimicrobial properties of the above compounds can be exploited in the development of antibiotics via structural activity relationship studies. Conclusively, this study has highlighted the clinical challenges associated with β-lactamase and developed concepts for the inhibition of two types of β-lactamases (NDM-1 and Bla$_{Mab}$ respectively) through the development of small molecules as potential inhibitors. While the limitations are clearly obvious, the study has shown that the concepts, especially the prodrug concept, are viable in the development of broad-spectrum β-lactamase inhibitors.

List of References

Abboud, M. I., Kosmopoulou, M., Krismanich, A. P., Johnson, J. W., Hinchliffe, P., Brem, J., Claridge, T. D. W., Spencer, J., Schofield, C. J. and Dmitrienko, G. I. (2018). Cyclobutanone mimics of intermediates in metallo-β-lactamase catalysis. *Chemistry - A European Journal*, *24*(22), 5734–5737.

Abraham, E. P. and Chain, E. (1940). An enzyme from bacteria able to destroy penicillin. *Nature*, *146*(3713), 837–837.

Albert, A. (1958). Chemical aspects of selective toxicity. *Nature*, *182*(4633), 421–423.

Alexander Fleming. Discovery and development of penicillin - landmark. Retrieved January 13, 2023, from https://www.acs.org/education/whatischemistry/landmarks/flemingpenicillin.html.

Allen, N. E., Boyd, D. B., Campbell, J. B., Deeter, J. B., Elzey, T. K., Foster, B. J., Hatfield, L. D., Hobbs, J. N. Jr, Hornback, W. J., Hunden, D. C., Jones, N. D., Kinnick, M. D., Morin, J. M. Jr., Munme,J. E., Swartzendruber, J. K. and Vogt, D. G. (1989). Molecular modeling of γ-lactam analogues of β-lactam antibacterial agents: Synthesis and biological evaluation of selected penem and carbapenem analoques. *Tetrahedron*, *45*(7), 1905–1928.

Allin, S. M., Vaidya, D. G., Page, M. I., Slawin, A. M. Z. and Smith, T. (2000b). Highly diastereoselective synthesis and template manipulation of the thiazolo[2,3-a]isoindolin-1-one ring system. *Tetrahedron Letters*, *41*(13), 2219–2222.

Allin, S. M., Vaidya, D. G., Page, M. I. and Slawin, A. M. (2000a). Highly diastereoselective synthesis of 2,3-dihydro-9bh- thiazolo[2,3-a]isoindolin-5-ones. *Arkivoc*, *2000*(2), 151–157.

Amaral, L., Martins, A., Spengler, G. and Molnar, J. (2014). Efflux pumps of Gram-negative bacteria: What they do, how they do it, with what and how to deal with them. *Frontiers in Pharmacology*, *4*, 168.

Ané, A., Prestat, G., Thiam, M., Josse, S., Pipelier, M., Pradère, J. P. and Dubreuil, D. (2002). Synthesis of Thiaazaheterocycle nucleoside analogues. *Nucleosides, Nucleotides and Nucleic Acids*, *21*(4-5), 335–360.

Antibacterial agents in clinical development - world health organization. Retrieved January 9, 2023, from https://apps.who.int/iris/bitstream/handle/10665/258965/WHO-EMP-IAU-2017.11-eng.pdf?sequence=1.

Antibiotic resistance threats in the United States, 2019. Retrieved January 9, 2023, from https://stacks.cdc.gov/view/cdc/82532.

Arshad, M., Mahmood, S. F., Khan, M., and Hasan, R. (2020). Covid-19, misinformation, and antimicrobial resistance. *BMJ*, m4501. http://doi.org/10.1136/bmj.m4501.

Azumah, R., Dutta, J., Somboro, A. M. Ramtahal, M., Chonco, L., Parboosing, R., Bester, L. A., Kruger, H. G., Naicker, T., Essack, S. Y. and Govende, T. (2016). *In vitro* evaluation of metal chelators as potential metallo-beta-lactamase inhibitors. *Journal of Applied Microbiology*, *120*(4), 860–867.

Babic, M., Hujer, A. and Bonomo, R. (2006). What's new in antibiotic resistance? focus on beta-lactamases. *Drug Resistance Updates*, *9*(3), 142–156.

Baker, L. M. S., Baker, P. R. S, Golin-Bisello, F., Schopfer, F. J., Fink, M., Woodcock, S. R., Branchaud, B. P., Radi, R. and Freeman, B. A. (2007). Nitro-Fatty Acid reaction with glutathione and cysteine. *Journal of Biological Chemistry*, *282*(42), 31085–31093.

Baldwin, J. E., Au, A., Christie, M., Haber, S. B. and Hesson, D. (1975). Stereospecific conversion of peptides into beta-lactams. *Journal of the American Chemical Society*, *97*(20), 5957–5958.

Baldwin, J. E., and Christie, M. A. (1978). Stereospecific synthesis of penicillins. Stereoelectronic control in the conversion of a peptide into a penicillin. *Journal of the American Chemical Society*, *100*(14), 4597–4599.

Bauer, D. J. (1965). Chemoprophylaxis of smallpox and treatment of vaccinia gangrenosa with 1-methylisatin 3-thiosemicarbazone. *Antimicrobial Agents and Chemotherapy*, 5, 544 − 547.

Bebrone, C., Moali, C., Mahy, F., Rival, S., Docquier, J. D., Rossolini, G. M., Fastrez, J., Pratt, R. F., Frere, J.-M., and Galleni, M. (2001). CENTA as a chromogenic substrate for studying β-lactamases. *Antimicrobial Agents and Chemotherapy*, *45*(6), 1868–1871.

Bergstrom, A., Katko, A., Adkins, Z., Hill, J., Cheng, Z., Burnett, M., Yang, H., Aitha, M., Mehaffey, M. R., Brodbelt, J. S., Tehrani, K. H. M. E., Martin, N. I., Bonomo, R. A., Page, R. C., Tierney, D. L., Fast, W., Wright, G. D. and Crowder, M. W. (2017). Probing the interaction of Aspergillomarasmine A with metallo-β-lactamases NDM-1, VIM-2, and IMP-7. *ACS Infectious Diseases*, *4*(2), 135 − 145.

Bonomo, R. A. (2017). β-lactamases: A focus on current challenges. *Cold Spring Harbor Perspectives in Medicine*, *7*(1), a025239.

Bonvicino, G. E. and Hennessy, D. J. (1957). The action of Borohydrides on Thiamin in aqueous medium1-3. *Journal of the American Chemical Society*, *79*(23), 6325 − 6328.

Branchini, B. R., Behney, C. E., Southworth, T. L., Fontaine, D. M., Gulick, A. M., Vinyard, D. J. and Brudvig, G. W. (2015). Experimental support for a single electron-transfer oxidation mechanism in Firefly bioluminescence. *Journal of the American Chemical Society*, *137*(24), 7592–7595.

Brem, J., Cain, R., Cahill, S., McDonough, M. A., Clifton, I. J., Jiménez-Castellanos, J.-C., Avison, M. B., Spencer, J., Fishwick, C. W. G. and Schofield, C. J. (2016). Structural basis of metallo-β-lactamase, serine-β-lactamase and penicillin-binding protein inhibition by cyclic boronates. *Nature Communications*, *7*, 12406.

Bush, K. (2010). β-Lactam antibiotics: Penicillins. *Antibiotic and Chemotherapy*, 200 − 225.

Bush, K. (2013). Proliferation and significance of clinically relevant β-lactamases. *Annals of the New York Academy of Sciences*, *1277*(1), 84 − 90.

Bush, K. and Bradford, P. A. (2016). β-lactams and β-lactamase inhibitors: An overview. *Cold Spring Harbor Perspectives in Medicine*, *6*(8).

Bush, K. and Jacoby, G. A. (2010). Updated Functional Classification of β-lactamases. *Antimicrobial Agents and Chemotherapy*, *54*(3), 969 − 976.

Büttner, D., Kramer, J. S., Klingler, F. M., Wittmann, S. K., Hartmann, M. R., Kurz, C. G., Kohnhäuser, D., Weizel, L., Brüggerhoff, A., Frank, D., Steinhilber, D., Wichelhaus, A. A., Pogoryelov, D. and Proschak, E. (2018). Challenges in the development of a thiol-based broad-spectrum inhibitor for metallo-β-lactamases. *ACS Infectious Diseases*, *4*(3), 360 − 372.

Butvin, P., Al-Ja'afreh, J., Svetlik, J. and Havranek, E. (1999). Solubility, stability, and dissociation constants of (2RS, 4R)-2-substituted thiazolidine-4-carboxylic acids in aqueous solutions. *Chemical Papers*, *53*(5), 315 − 322.

Carfi, A., Duée, E., Paul-Soto, R., Galleni, M., Frère, J.-M. and Dideberg, O. (1998). X-ray structure of the ZnII β-lactamase from *Bacteroides fragilis* in an orthorhombic crystal form. *Acta Crystallographica Section D Biological Crystallography*, *54*(1), 47–57.

Carfi, A., Pares, S., Duée, E., Galleni, M., Duez, C., Frère, J. M. and Dideberg, O. (1995). The 3-D structure of a zinc metallo-beta-lactamase from bacillus cereus reveals a new type of protein fold. *The EMBO Journal*, *14*(20), 4914–4921.

Chan, L. C. and Cox, B. G. (2007). Kinetics of amide formation through carbodiimide/*n*-hydroxybenzotriazole (HOBt) couplings. *The Journal of Organic Chemistry*, *72*(23), 8863–8869.

Chen, A. Y., Thomas, P. W., Stewart, A. C., Bergstrom, A., Cheng, Z., Miller, C., Bethel, C. R., Marshall, S. H., Credille, C. V., Riley, C. L., Page, R. C., Bonomo, R. A., Crowder, M. W., Tierney, D. L., Fast, W. and Cohen, S. M. (2017). Dipicolinic acid derivatives as inhibitors of New Delhi Metallo-β-lactamase-1. *Journal of Medicinal Chemistry*, *60*(17), 7267 − 7283.

Chen, G., Jin, M., Du, P., Zhang, C., Cui, X., Zhang, Y., Wang, J., Jin, F., She, Y., Shao, H., Wang, S. and Zheng, L. (2017). A review of enhancers for chemiluminescence enzyme immunoassay. *Food and Agricultural Immunology*, *28*(2), 315–327.

Chen, N. H., Djoko, K. Y., Veyrier, F. J. and McEwan, A. G. (2016). Formaldehyde stress responses in bacterial pathogens. *Frontiers in Microbiology*, 7, 257.

Chen, Y., Shoichet, B. and Bonnet, R. (2005). Structure, function, and inhibition along the reaction coordinate of CTX-m β-lactamases. *Journal of the American Chemical Society*, *127*(15), 5423–5434.

Cheng, B., Zhong, J. P., Wu, F. X., Li, G. L., Ruan, Q. X., Luo, G. and Jiang, H. (2019). EBSELEN protects rat hearts against myocardial ischemia-reperfusion injury. *Experimental and Therapeutic Medicine*. 17(2), 1412-1419.

Chierici, S., Figuet, M., Dettori, A. and Dumy, P. (2005). Thiazolidines to lock *Cis* Xaa-Pro amide bond: New synthetic approach. *Comptes Rendus Chimie*, *8*(5), 875–880.

Chiou, J., Wan, S., Chan, K. F., So, P. K., He, D., Chan, E. W. C., Chan, T. H., Wong, K. Y., Tao, J., and Chen, S. (2015). Ebselen as a potent covalent inhibitor of New Delhi Metallo-β-lactamase (NDM-1). *Chemical Communications*, *51*(46), 9543−9546.

Choi, U. and Lee, C.-R. (2019). Distinct roles of outer membrane porins in antibiotic resistance and membrane integrity in *Escherichia coli*. *Frontiers in Microbiology*, *10*, 00953.

Chorell, K., Das, P. and Almqvist, F. (2007). Diverse functionalization of Thiazolo Ring-fused 2-pyridones. *The Journal of Organic Chemistry*, *72*(13), 4917-4924.

Christopeit, T. and Leiros, H.-K. S. (2016). Fragment-based discovery of inhibitor scaffolds targeting the Metallo-β-lactamases NDM-1 and VIM-2. *Bioorganic & Medicinal Chemistry Letters*, *26*(8), 1973 − 1977.

Christopeit, T., Albert, A. and Leiros, H.-K. S. (2016). Discovery of a novel covalent non-β-lactam inhibitor of the Metallo-β-lactamase NDM-1. *Bioorganic & Medicinal Chemistry*, *24*(13), 2947− 2953.

Concha, N. O., Rasmussen, B. A., Bush, K., and Herzberg, O. (1996). Crystal structure of the wide-spectrum binuclear zinc β-lactamase from *Bacteroides fragilis*. *Structure*, *4*(7), 823–836.

Crout, D. H. G. and Hedgecock, C. J. (1979). The base-catalysed rearrangement of α-acetolactate (2-hydroxy-2-methyl-3-oxobutanoate): A novel carboxylate ion migration in a tertiary ketol rearrangement. *Journal of the Chemical Society, Perkin Transactions, 1*, 1982-1989.

Dahl, J. (2008). File:Gram-negative cell wall.svg. Retrieved January 14, 2023, from https://commons.wikimedia.org/wiki/File:Gram_negative_cell_wall.svg.

Dal Peraro, M., Vila, A. J., Carloni, P., and Klein, M. L. (2007). Role of zinc content on the catalytic efficiency of B1 metallo β-lactamases. *Journal of the American Chemical Society*, *129*(10), 2808–2816.

Damblon, C., Raquet, X., Lian, L. Y., Lamotte-Brasseur, J., Fonze, E., Charlier, P., … Frère, J. M. (1996). The catalytic mechanism of beta-lactamases: NMR titration of an active-site lysine residue of the TEM-1 enzyme. *Proceedings of the National Academy of Sciences*, *93*(5), 1747–1752.

Danton, F., Othman, M., Lawson, A. M., Moncol, J., Ghinet, A., Rigo, B. and Daıch, A. (2019). Phenyliodine(III) Diacetate/I₂-mediated domino approach for pyrrolo[1,4]thiazines and 1,4-thiazines by a one-pot morin rearrangement of *N,S*-Acetals. *Chemistry - A European Journal, 25*(24), 6113–6118.

Das, S., Ihssen, J., Wick, L., Spitz, U. and Shabat, D. (2020). Chemiluminescent carbapenem-based molecular probe for detection of Carbapenemase activity in live bacteria. *Chemistry – A European Journal*, *26*(16), 3647–3652.

Das, M., Das, B., De, A., Banerjee, S. and Samanta, A. (2019). Antimicrobial investigation and binding mode analysis of some newly synthesized 4-amino-5-((aryl substituted)-4H-1, 2, 4-triazole-3-yl)-thio linked hydroxamic acid derivatives. *Asian Journal of Pharmaceutical and Clinical Research*, 469–479.

Dawson, D. A., Masayasu, H., Graham, D. I. and Macrae, I. M. (1995). The neuroprotective efficacy of ebselen (a glutathione peroxidase mimic) on brain damage induced by transient focal cerebral ischaemia in the rat. *Neuroscience Letters*, *185*(1), 65–69.

de Koning, C. B., van Otterlo, W. A. L. and Michael, J. P. (2003). Amide rotamers of N-acetyl-1,3-dimethyltetrahydroisoquinolines: Synthesis, variable temperature NMR spectroscopy and molecular modelling. *Tetrahedron*, *59*(42), 8337–8345.

Delcour, A. H. (2009). Outer membrane permeability and antibiotic resistance. *Biochimica Et Biophysica Acta (BBA) - Proteins and Proteomics*, *1794*(5), 808–816.

Department of Health and Social Care. (2019, January 24). UK 5-Year action plan for antimicrobial resistance 2019 to 2024. Retrieved January 13, 2023, from https://www.gov.uk/government/publications/uk-5-year-action-plan-for-antimicrobial-resistance-2019-to-2024.

Dortet, L., Poirel, L. and Nordmann, P. (2014). Worldwide dissemination of the NDM-type carbapenemases in Gram-negative bacteria. *BioMed Research International*, *2014*, 1–12.

Drawz, S. M. and Bonomo, R. A. (2010). Three decades of β-lactamase inhibitors. *Clinical Microbiology Reviews*, *23*(1), 160 – 201.

Dubée, V., Bernut, A., Cortes, M., Lesne, T., Dorchene, D., Lefebvre, A. L., Hugonnet, J. -E., Gutmann, L., Mainardi, J. L., Herrmann, J. L., Gaillard, J. L., Kremer, L., Arthur, M. (2015a). β-lactamase inhibition by avibactam in *Mycobacterium abscessus*. *Journal of Antimicrobial Chemotherapy*, *70*(4), 1051 – 1058.

Dubée, V., Soroka, D., Cortes, M., Lefebvre, A. -L., Gutmann, L., Hugonnet, J. -E., Arthur, M. and Mainardi, J. L., (2015b). Impact of β-lactamase inhibition on the activity of ceftaroline against *Mycobacterium tuberculosis* and *Mycobacterium abscessus*. *Antimicrobial Agents and Chemotherapy*, *59*(5), 2938–2941.

Duthaler, R. O. and Wyss, B. (2011). Conversion of L-cysteine into D-α-amino acids and related transformations. *European Journal of Organic Chemistry*, *2011*(24), 4667–4680.

Easton, C. J., Hay, M. P. and Love, S. G. (1988). Regioselective formation of amidocarboxy-substituted free radicals. *Journal of the Chemical Society, Perkin Transactions 1*, (2), 265.

Eshtiwi, A., (2020). Computational Investigation of New Delhi Metallo-β-lactamase 1 (NDM-1) Inhibitors, PhD thesis, Aston University.

Esther, C. R. Jr., Esserman, D. A., Gilligan, P., Kerr, A. and Noone, P. G. (2010). Chronic *Mycobacterium abscessus* infection and lung function decline in cystic fibrosis. *Journal of Cystic Fibrosis*, *9*(2), 117 – 123.

Evans, L. E., Krishna, A., Ma, Y., Webb, T. E., Marshall, D. C., Tooke, C. L., Spencer, J., Clarke, T. B., Armstrong, A. and Edwards, A. M. (2019). Exploitation of antibiotic resistance as a novel drug target: Development of a β-lactamase-activated antibacterial prodrug. *Journal of Medicinal Chemistry*, *62*(9), 4411–4425.

Feng, H., Ding, J., Zhu, D., Liu, X., Xu, X., Zhang, Y., Zang, S., Wang, D. C., and Liu, W. (2014). Structural and mechanistic insights into NDM-1 catalyzed hydrolysis of cephalosporins. *Journal of the American Chemical Society*, *136*(42), 14694−14697.

Feng, H., Liu, X., Wang, S., Fleming, J., Wang, D. C. and Liu, W. (2017). The mechanism of NDM-1-catalyzed carbapenem hydrolysis is distinct from that of penicillin or cephalosporin hydrolysis. *Nature Communications*, *8*(1), 2242.

Finch, R., Davey, P., Wilcox, M. and Irving, W. (2012). *Antimicrobial Chemotherapy*. 6th ed. New York: Oxford University Press.

Fisher, J. F. and Mobashery, S. (2016). β-lactam resistance mechanisms: Gram-positive bacteria and *Mycobacterium tuberculosis*. *Cold Spring Harbor perspectives in medicine*, *6*(5), a025221.

Floto, R. A., Olivier, K. N., Saiman, L., Daley, C. L., Herrmann, J. L., Nick, J. A., Noone, P. G., Bilton, D., Corris, P., Gibson, R. L., Hempstead, S. E., Koetz, K., Sabadosa, K. A., Sermet-Gaudelus, I., Smyth, A. R., Ingen, J. A., Wallace, R. J., Winthrop, K. L., Marshall, B. C., Haworth, C. S. (2016). US Cystic Fibrosis Foundation and European Cystic Fibrosis Society Consensus Recommendations for the management of non-tuberculous mycobacteria in individuals with cystic fibrosis. *Thorax, 71*(1), i1–22.

Fraga, H., Esteves da Silva, J. C. and Fontes, R. (2004). Identification of luciferyl adenylate and Luciferyl coenzyme A synthesized by firefly luciferase. *ChemBioChem, 5*(1), 110–115.

Gao, W., Xing, B., Tsien, R. Y. and Rao, J. (2003). Novel fluorogenic substrates for imaging β-lactamase gene expression. *Journal of the American Chemical Society, 125*(37), 11146–11147.

García-Sáez, I., Hopkins, J., Papamicael, C., Franceschini, N., Amicosante, G., Rossolini, G. M., Galleni, M., Frère, J. M., and Dideberg, O. (2003). The 1.5-Å structure of Chryseobacterium meningosepticum zinc β-lactamase in complex with the inhibitor, D-captopril. *Journal of Biological Chemistry. 278*(26), 23868 – 23873.

Ghosh, S. S., Dakoji, S., Tanaka, Y., Cho, Y. J. and Mobashery, S. (1996). Properties of analogues of an intermediate in the process of mechanism-based inactivation of carboxypeptidase A. *Bioorganic & Medicinal Chemistry, 4*(9), 1487–1492.

Gibson, R. M., Christensen, H. and Waley, S. G. (1990). Site-directed mutagenesis of β-lactamase I. single and double mutants of glu-166 and lys-73. *Biochemical Journal, 272*(3), 613–619.

González, M. M. and Vila, A. J. (2016). An elusive task: A clinically useful inhibitor of metallo-β-lactamases. In: Supuran C., Capasso C. eds. *Zinc enzyme inhibitors. Topics in Medicinal Chemistry*, Springer-Cham, 22, 1-34.

González, M. M., Kosmopoulou, M., Mojica, M. F., Castillo, V., Hinchliffe, P., Pettinati, I., Brem, J., Schofield, C. J., Mahler, G., Bonomo, R. A., Llarrull, L. I., Spencer, J. and Vila, A. J. (2015). Bisthiazolidines: A substrate-mimicking scaffold as an inhibitor of the NDM-1 carbapenemase. *ACS Infectious Diseases, 1*(11), 544 -554.

Gootz, T. D. (2006). The forgotten gram-negative bacilli: What genetic determinants are telling us about the spread of antibiotic resistance. *Biochemical Pharmacology, 71*(7), 1073–1084.

Gracia-Victoria, J., Osante, I., Cativiela, C., Merino, P. and Tejero, T. (2018). Self-regeneration of chirality with L-cysteine through 1,3-dipolar cycloadditions between diazoalkanes and enantiomerically pure thiazolines: Experimental and computational studies. *The Journal of Organic Chemistry, 83*(7), 3960–3972.

Green, M. and Thorp, D. M. (1967). The mechanism of reaction of phosphorus pentachloride and thionyl chloride with carboxylic esters. *Journal of the Chemical Society B: Physical Organic*, 1067 – 1068.

Groundwater, P. W., Xu, S., Lai, F., Varadi, L., Tan, J., Perry, J. D. and Hibbs, D. E. (2016). New Delhi metallo-β-lactamase-1: Structure, inhibitors and detection of producers. *Future Medicinal Chemistry, 8*(9), 993–1012.

Guilbault, G. G. (1990). *Practical fluorescence*. 2nd ed. New York: Marcel Dekker.

Guo, Y., Wang, J., Niu, G., Shui, W., Sun, Y., Zhou, H., Zhang, Y., Yang, C., Lou, Z., and Rao, Z. (2011). A structural view of the antibiotic degradation enzyme NDM-1 from a superbug. *Protein and Cell, 2*(5), 384 – 394.

Hananya, N. and Shabat, D. (2017). A glowing trajectory between bio- and chemiluminescence: From Luciferin-based probes to triggerable dioxetanes. *Angewandte Chemie International Edition, 56*(52), 16454–16463.

Hananya, N. and Shabat, D. (2019). Recent advances and challenges in Luminescent Imaging: Bright outlook for chemiluminescence of dioxetanes in water. *ACS Central Science, 5*(6), 949–959.

Hananya, N., Eldar Boock, A., Bauer, C. R., Satchi-Fainaro, R. and Shabat, D. (2016). Remarkable enhancement of chemiluminescent signal by Dioxetane–fluorophore conjugates: Turn-on chemiluminescence probes with color modulation for sensing and imaging. *Journal of the American Chemical Society*, *138*(40), 13438–13446.

Hancock, R. E., and Brinkman, F. S. (2002). Function of *pseudomonas* porins in uptake and efflux. *Annual Review of Microbiology*, *56*(1), 17–38.

Hansen, J. J. and Krogsgaard-Larsen, P. (1980). Isoxazole amino-acids as glutamic acid agonists. synthesis of some analogues and homologues of ibotenic acid. *Journal of the Chemical Society, Perkin Transactions 1*, 1826-1833.

Hecker, S. J., Reddy, K. R., Lomovskaya, O., Griffith, D. C., Rubio-Aparicio, D., Nelson, K., Tsivkovski, R., Dongxu Sun, Sabet, M., Tarazi, Z., Parkinson, J., Totrov, M., Boyer, S. H., Glinka, T. W., Pemberton, O. A., Yu Chen, and Dudley, M. N. (2020). Discovery of cyclic boronic acid QPX7728, an ultrabroad-spectrum inhibitor of serine and metallo-β-lactamases. *Journal of Medicinal Chemistry*, *63*(14), 7491–7507.

Hecker, S. J., Reddy, K. R., Totrov, M., Hirst, G. C., Lomovskaya, O., Griffith, D. C., King, P., Tsivkovski, R., Sun, D., Sabet, M., Tarazi, Z., Clifton, M. C., Atkins, K., Raymond, A., Potts, K. T., Abendroth, J., Boyer, S. H., Loutit, J. S., Morgan, E. E., Durso, S. and Dudley, M. N. (2015). Discovery of a cyclic boronic acid β-lactamase inhibitor (RPX7009) with utility vs class A serine carbapenemases. *Journal of Medicinal Chemistry*, *58*(9), 3682–3692.

Hu, Z., Periyannan, G., Bennett, B., and Crowder, M. W. (2008). Role of the Zn_1 and Zn_2 site in metallo-β-lactamase L1. *Journal of the American Chemical Society*. *130*(43), 14207 – 14216.

Huggins, M. T., Kesharwani, T., Buttrick, J. and Nicholson, C. (2020). Variable temperature NMR experiment studying restricted bond rotation. *Journal of Chemical Education*, *97*(5), 1425–1429.

Huntley, J. J. A., Scrofani, S. D. B., Osborne, M. J., Wright, P. E. and Dyson, H. J. (2000). Dynamics of the metallo-β-lactamase from *bacteroides fragilis* in the presence and absence of a tight-binding inhibitor. *Biochemistry*, *39*(44), 13356–13364.

Huy, P., Neudörfl, J.-M. and Schmalz, H.-G. (2011). A practical synthesis of *trans*-3-substituted proline derivatives through 1,4-Addition. *Organic Letters*, *13*(2), 216–219.

Hwu, J. R., Jain, M. L., Shwu-Chen, T. and Hakimelahi, G. H. (1996). Ceric ammonium nitrate in the deprotection of tert-butoxycarbonyl group. *Tetrahedron Letters*, *37*(12), 2035–2038.

Isozumi, H., Hoshimoto, S., Matsunaga, H. and Kunieda, T. (2003). Chiral functionalization of 2(3H)-thiazolone. New route to chiral synthons for 2-amino thiols. *Heterocycles*, *59*(1), 323-332.

Jackson, M. B., Mander, L. N. and Spotswood, T. M. (1983). Reduction of N-substituted azetidin-2-ones to Azetidines. *Australian Journal of Chemistry*, *36*(4), 779 - 788.

Jarand, J., Levin, A., Zhang, L., Huitt, G., Mitchell, J. D. and Daley, C. L. (2011). Clinical and microbiologic outcomes in patients receiving treatment for *Mycobacterium abscessus* pulmonary disease. *Clinical Infectious Diseases*, *52*(5), 565–571.

Jin, W. B., Xu, C., Cheng, Q., Qi, X. L., Gao, W., Zheng, Z., Chan, E. W. C., Leung, Y. C., Chan, T. H., Wong, K. Y., Chen, S. and Chan, K. (2018). Investigation of synergistic antimicrobial effects of the drug combinations of meropenem and 1,2-benzisoselenazol-3(2h)-one derivatives on carbapenem-resistant Enterobacteriaceae producing NDM-1. *European Journal of Medicinal Chemistry*, *155*, 285–302.

Johshita, H., Sasaki, T., Matsui, T., Hanamura, T., Masayasu, H., Asano, T. and Takakura, K. (1990). Effects of ebselen (PZ 51) on Ischaemic Brain Oedema after focal ischaemia in cats. *Brain Edema VIII*, *51*, 239–241.

Jones, R. N., Wilson, H. W. and Novick, W. J. (1982b). In vitro evaluation of pyridine-2-azo-p-dimethylaniline cephalosporin, a new diagnostic chromogenic reagent, and comparison with nitrocefin, cephacetrile, and other beta-lactam compounds. *Journal of Clinical Microbiology*, *15*(4), 677–683.

Jones, R. N., Wilson, H. W., Novick, W. J., Barry, A. L. and Thornsberry, C. (1982a). In vitro evaluation of CENTA, a new beta-lactamase-susceptible chromogenic cephalosporin reagent. *Journal of Clinical Microbiology*, *15*(5), 954–958.

Ju, L.-C., Cheng, Z., Fast, W., Bonomo, R. A. and Crowder, M. W. (2018). The continuing challenge of metallo-β-lactamase inhibition: Mechanism matters. *Trends in Pharmacological Sciences*, *39*(7), 635–647.

Jubeh, B., Breijyeh, Z. and Karaman, R. (2020). Antibacterial prodrugs to overcome bacterial resistance. *Molecules*, *25*(7), 1543.

Kallen, R. G. (1971). Mechanism of reactions involving Schiff base intermediates. Thiazolidine Formation from L-cysteine and formaldehyde. *Journal of the American Chemical Society*, *93*(23), 6236–6248.

Karsisiotis, A. I., Damblon, C. F., and Roberts, G. C. K. (2013). Solution structures of the *Bacillus cereus* metallo-β-lactamase BcII and its complex with the broad spectrum inhibitor *R*-thiomandelic acid. *Biochemical Journal*, *456*(3), 397–407.

Kaushik, A., Ammerman, N. C., Lee, J., Martins, O., Kreiswirth, B. N., Lamichhane, G., Parrish, N. M. and Nuermberger, E. L. (2019). *in vitro* activity of the new β-lactamase inhibitors Relebactam and Vaborbactam in combination with β-lactams against *Mycobacterium abscessus* complex clinical isolates. *Antimicrobial Agents and Chemotherapy*, *63*(3), e02623-18.

Kaushik, A., Gupta, C., Fisher, S., Story-Roller, E., Galanis, C., Parrish, N. and Lamichhane, G. (2017). Combinations of avibactam and carbapenems exhibit enhanced potencies against drug-resistant *Mycobacterium abscessus*. *Future Microbiology*, *12*(6), 473–480.

Ke, W., Bethel, C. R., Thomson, J. M., Bonomo, R. A. and van den Akker, F. (2007). Crystal structure of KPC-2: insights into Carbapenemase activity in class A β-lactamases. *Biochemistry*, *46*(19), 5732–5740.

Khan, A. U., Maryam, L. and Zarrilli, R. (2017). Structure, genetics and worldwide spread of New Delhi metallo-β-lactamase (NDM): A threat to public health. *BMC Microbiology*, *17*(1), 101.

Kil, J., Harruff, E. E. and Longenecker, R. J. (2022). Development of ebselen for the treatment of sensorineural hearing loss and tinnitus. *Hearing Research*, *413*, 108209.

Kil, J., Lobarinas, E., Spankovich, C., Griffiths, S. K., Antonelli, P. J., Lynch, E. D. and Le Prell, C. G. (2017). Safety and efficacy of ebselen for the prevention of noise-induced hearing loss: A randomised, double-blind, placebo-controlled, phase 2 trial. *The Lancet*, *390*(10098), 969–979.

Kim, Y., Tesar, C., Mire, J., Jedrzejczak, R., Binkowski, A., Babnigg, G., Sacchettini, J. and Joachimiak, A. (2011). Structure of apo- and monometalated forms of NDM-1 — a highly potent carbapenem-hydrolyzing metallo-β-lactamase. *PLoS ONE*, *6*(9), e24621.

King, A. M., Reid-Yu, S. A., Wang, W., King, D. T., De Pascale, G., Strynadka, N. C., Walsh, T. R., Coombes, B. K. and Wright, G. D. (2014). Aspergillomarasmine A overcomes metallo-β-lactamase antibiotic resistance. *Nature*, *510*(7506), 503–506.

King, D. and Strynadka, N. (2011). Crystal structure of New Delhi metallo-β-lactamase reveals molecular basis for antibiotic resistance. *Protein Science*, *20*(9), 1484–1491.

King, D. T. and Strynadka, N. C. J. (2013). Targeting metallo-β-lactamase enzymes in antibiotic resistance. *Future Medicinal Chemistry*, *5*(11), 1243–1263.

King, D. T., King, A. M., Lal, S. M., Wright, G. D. and Strynadka, N. C. (2015). Molecular mechanism of avibactam-mediated β-lactamase inhibition. *ACS Infectious Diseases*, *1*(4), 175–184.

King, D. T., Worrall, L. J., Gruninger, R. and Strynadka, N. C. J. (2012). New Delhi metallo-β-lactamase: Structural insights into β-lactam recognition and inhibition. *Journal of the American Chemical Society*, *134*(28), 11362–11365.

Klingler, F.-M., Wichelhaus, T. A., Frank, D., Cuesta-Bernal, J., El-Delik, J., Müller, H. F., Sjuts, H., Göttig, S., Koenigs, A., Pos, K. M., Pogoryelov, D. and Proschak, E. (2015). Approved drugs containing thiols as inhibitors of metallo-β-lactamases: Strategy to combat multidrug-resistant bacteria. *Journal of Medicinal Chemistry*, *58*(8), 3626–3630.

Krajnc, A., Brem, J., Hinchliffe, P., Calvopiña, K., Panduwawala, T. D., Lang, P. A., Kamps, J. J. A. G., Tyrrell, J. M., Widlake, E., Saward, B. G., Walsh, T. R., Spencer, J. and Schofield, C. J. (2019). Bicyclic boronate VNRX-5133 inhibits metallo- and serine-β-lactamases. *Journal of Medicinal Chemistry*, *62*(18), 8544–8556.

Krishnamurty, K. V. and Harris, G. M. (1961). The chemistry of the metal oxalato complexes. *Chemical Reviews*, *61*(3), 213−246.

Krishnan, N. P.,Nguyen, N. Q., Papp-Wallace K. M., Bonomo, R. A., van den Akker, F. (2015). Inhibition of klebsiella β-lactamases (SHV-1 and KPC-2) by Avibactam: A structural study. *PLOS ONE*, *10*(9), e0136813.

Kubyshkin, V. and Budisa, N. (2017). Amide rotation trajectories probed by symmetry. *Organic & Biomolecular Chemistry*, *15*(32), 6764–6772.

Kumar, P., Chauhan, V., Silva, J. R., Lameira, J., d'Andrea, F. B., Li, S. G., Ginell, S. L., Freundlich, J. S., Alves, C. N., Bailey, S., Cohen, K. A., Lamichhane, G. (2017a). *Mycobacterium abscessus* L, D-transpeptidases are susceptible to inactivation by carbapenems and cephalosporins but not penicillins. *Antimicrobial Agents and Chemotherapy*, *61*(10), e00866-17.

Kumar, P., Kaushik, A., Lloyd, E. P., Li, S.-G., Mattoo, R., Ammerman, N. C., Bell, D. T., Perryman, A. L., Zandi, T. A., Ekins, S., Ginell, S. L., Townsend, C. A., Freundlich, J. S., Lamichhane, G. (2017b). Non-classical transpeptidases yield insight into new antibacterials. *Nature Chemical Biology*, *13*(1), 54–61.

Lamotte-Brasseur, J., Dive, G., Dideberg, O., Charlier, P., Frère, J. M., & Ghuysen, J. M. (1991). Mechanism of acyl transfer by the class A serine *β*-lactamase of *streptomyces albus* g. *Biochemical Journal*, *279*(1), 213–221.

Langley, G. W., Cain, R., Tyrrell, J. M., Hinchliffe, P., Calvopiña, K., Tooke, C. L., Widlake, E., Dowson, C. G., Spencer, J., Walsh, T. R., Schofield, C. J., Brem, J. (2019). Profiling interactions of vaborbactam with metallo-β-lactamases. *Bioorganic & Medicinal Chemistry Letters*, *29*(15), 1981–1984.

Lanyon-Hogg, T., Ritzefeld, M., Masumoto, N., Magee, A. I., Rzepa, H. S. and Tate, E. W. (2015). Modulation of amide bond rotamers in 5-acyl-6,7-dihydrothieno[3,2-*c*]pyridines. *The Journal of Organic Chemistry*, *80*(9), 4370–4377.

Lassaux, P., Traoré, D. A., Loisel, E., Favier, A., Docquier, J. D., Sohier, J. S., Laurent, C., Bebrone, C., Frère, J. M., Ferrer, J. L., Galleni, M. (2011). Biochemical and structural characterization of the subclass B1 metallo-β-lactamase Vim-4. *Antimicrobial Agents and Chemotherapy*, *55*(3), 1248–1255.

Lavollay, M., Fourgeaud, M., Herrmann, J.-L., Dubost, L., Marie, A., Gutmann, L., Arthur, M. and Mainardi, J.-L. (2011). The peptidoglycan of *Mycobacterium abscessus* is predominantly cross-linked by L, D-transpeptidases. *Journal of Bacteriology*, *193*(3), 778–782.

Lefebvre, A.-L., Le Moigne, V., Bernut, A., Veckerlé, C., Compain, F., Herrmann, J. L., Kremer, L., Arthur, M. and Mainardi, J.-L. (2017). Inhibition of the β-lactamase Bla$_{mab}$ by avibactam improves the *in vitro* and *in vivo* efficacy of imipenem against *Mycobacterium abscessus*. *Antimicrobial Agents and Chemotherapy*, *61*(4), e02440-16.

Li, J., Chen, L., Du, L. and Li, M. (2013). Cage the firefly luciferin! – A strategy for developing bioluminescent probes. *Chemical Society Reviews*, *42*(2), 662–676.

Li, N., Xu, Y., Xia, Q., Bai, C., Wang, T., Wang, L., He, D., Xie, N., Li, L., Wang, J., Zhou, H. G., Xu, F., Yang, C., Zhang, Q., Yin, Z., Guo, Y., Chen, Y. (2014). Simplified captopril analogues as NDM-1 inhibitors. *Bioorganic & Medicinal Chemistry Letters*, *24*(1), 386–389.

Liao, D., Yang, S., Wang, J., Zhang, J., Hong, B., Wu, F., and Lei, X. (2016). Total synthesis and structural reassignment of aspergillomarasmine A. *Angewandte Chemie International Edition*, *55*(13), 4291–4295.

Linciano, P., Cendron, L., Gianquinto, E., Spyrakis, F. and Tondi, D. (2019). Ten years with New Delhi metallo-β-lactamase-1 (NDM-1): From structural insights to inhibitor design. *ACS Infectious Diseases*, *5*(1), 9–34.

Liu, B., Trout, R. E. L., Chu, G.-H, McGarry, D., Jackson, R. W., Hamrick, J. C., Daigle, D. M., Cusick, S. M., Pozzi, C., Luca, F. D., Benvenuti, M., Mangani, S., Docquier, J.-D., Weiss, W. J., Pevear, D. C., Xerri, L. and Burns, C. J. (2019). Discovery of Taniborbactam (VNRX-5133): A broad-spectrum serine- and metallo-β-lactamase inhibitor for carbapenem-resistant bacterial infections. *Journal of Medicinal Chemistry*, *63*(6), 2789–2801.

Liu, X.-L., Shi, Y., Kang, J. S., Oelschlaeger, P. and Yang, K.-W. (2015). Amino acid thioester derivatives: A highly promising scaffold for the development of metallo-β-lactamase L1 inhibitors. *ACS Medicinal Chemistry Letters*, *6*(6), 660–664.

Livermore, D. M. (2012). Current epidemiology and growing resistance of Gram-negative pathogens. *The Korean Journal of Internal Medicine*, *27*(2), 128–142.

Llarrull, L. I., Tioni, M. F. and Vila, A. J. (2008). Metal content and localization during turnover in *B. cereus* metallo-β-lactamase. *Journal of the American Chemical Society*, *130*(47), 15842–15851.

Lopeman, R. C., Harrison, J., Rathbone, D. L., Desai, M., Lambert, P. A. and Cox, J. A. (2020). Effect of amoxicillin in combination with imipenem-relebactam against mycobacterium abscessus. *Scientific Reports*, *10*(1).

Lund Myhre, C. E. and Nielsen, C. J. (2004). Optical properties in the UV and visible spectral region of organic acids relevant to tropospheric aerosols. *Atmospheric Chemistry and Physics*, *4*(7), 1759–1769.

Lynch, E. and Kil, J. (2009). Development of ebselen, a glutathione peroxidase mimic, for the prevention and treatment of noise-induced hearing loss. *Seminars in Hearing*, *30*(01), 047–055.

Martínez-Martínez, L. (2008). Extended-spectrum β-lactamases and the permeability barrier. *Clinical Microbiology and Infection*, *14*, 82–89.

Massova, I., and Mobashery, S. (1998). Kinship and diversification of bacterial penicillin-binding proteins and β-lactamases. *Antimicrobial Agents and Chemotherapy*, *42*(1), 1–17.

Mattoo, R., Lloyd, E. P., Kaushik, A., Kumar, P., Brunelle, J. L., Townsend, C. A., Lamichhane, G. (2017). LDTmav2, a nonclassical transpeptidase and susceptibility of *mycobacterium avium* to carbapenems. *Future Microbiology*, *12*(7), 595–607.

Medjahed, H., Gaillard, J.-L. and Reyrat, J.-M. (2010). Mycobacterium abscessus: A new player in the mycobacterial field. *Trends in Microbiology*, *18*(3), 117–123.

Meini, M. -R., Llarrull, L. I. and Vila, A. J. (2015). Overcoming differences: The catalytic mechanism of metallo-β-lactamases. *FEBS Letters*, *589*(22), 3419–3432.

Meir, M., Bifani, P. and Barkan, D. (2018). The addition of avibactam renders piperacillin an effective treatment for mycobacterium abscessus infection in an in vivo model. *Antimicrobial Resistance & Infection Control*, *7*(1), 151.

Mercuri, P. S., García-Sáez, I., De Vriendt, K., Thamm, I., Devreese, B., Van Beeumen, J., Dideberg, O., Rossolini, G. M., Frère, J. M., and Galleni, M. (2004). Probing the specificity of the subclass B3FEZ-1 metallo-β-lactamase by site-directed mutagenesis. *Journal of Biological Chemistry*, *279*(32), 33630–33638.

Mimoto, T., Kato, R., Takaku, H., Nojima, S., Terashima, K., Misawa, S., Fukazawa, T., Ueno, T., Sato, H., Shintani, M., Kiso, Y. and Hayashi, H. (1999). Structure−activity relationship of small-sized HIV

protease inhibitors containing Allophenylnorstatine. *Journal of Medicinal Chemistry*, *42*(10), 1789–1802.

Minasov, G., Wang, X. and Shoichet, B. K. (2002). An ultrahigh resolution structure of TEM-1 β-lactamase suggests a role for Glu166 as the general base in acylation. *Journal of the American Chemical Society*, *124*(19), 5333–5340.

Mobashery, S. and Johnston, M. (1986). Reactions of Escherichia coli TEM β-lactamase with Cephalothin and with C_{10}-dipeptidyl cephalosporin esters. *Journal of Biological Chemistry*, *261*(17), 7879–7887.

Moellering, R. C. (2010). NDM-1 — a cause for worldwide concern. *New England Journal of Medicine*, *363*(25), 2377–2379.

Mojica, M. F., Bonomo, R. and Fast, W. (2016). B1-metallo-β-lactamases: Where do we stand? *Current Drug Targets*, *17*(9), 1029–1050.

Mollard, C., Moali, C., Papamicael, C. Damblon, C., Vessilier, S., Amicosante, G., Schofield, C. J., Galleni, M., Frere, J. and Roberts, G. C. K. (2001). Thiomandelic acid, a broad spectrum inhibitor of zinc β-lactamases. *Journal of Biological Chemistry*, *276*(48), 45015–45023.

Moloughney, J. G., Thomas, J. D. and Toney, J. H. (2005). Novel IMP-1 Metallo-β-lactamase inhibitors can reverse meropenem resistance in *Escherichia coli* expressing IMP-1. *FEMS Microbiology Letters*, *243*(1), 65–71.

Money, R. W. and Davies, C. W. (1938). The solubility of barium oxalate in aqueous salt solutions. *The Journal of the Chemical Society,* 2098−2100.

Montalbetti, C. A. G. N. and Falque, V. (2005). Amide bond formation and peptide coupling. *Tetrahedron*, *61*(46), 10827–10852.

Morales-Rios, M. S., Suarez-Castillo, O. R. and Joseph-Nathan, P. (2002). First total syntheses of dihydroflustramine C and flustramine E, alkaloids from the marine bryozoan *Flustra foliacea*. *Tetrahedron*, *58*(8), 1479–1484.

Muneeswara M., Sundaravelu N. and Sekar G. (2019) NBS-mediated synthesis of β-keto sulfones from benzyl alcohols and sodium arenesulfinates. *Tetrahedron*, *75*(25), 3479-3484.

Murray, C. L. J. *et al*. (2022). Global burden of bacterial antimicrobial resistance in 2019: a systematic analysis. *Lancet*, 399: 629–55.

Mycobacterium abscessus in healthcare settings. (2010, November 24). Retrieved January 14, 2023, from https://www.cdc.gov/hai/organisms/
mycobacterium.html.

Nagasawa, H. T., Goon, D. J., Zera, R. T. and Yuzon, D. L. (1982). Prodrugs of L-cysteine as liver-protective agents. 2(R, S)-methylthiazolidine-4(R)-carboxylic acid (MTCA), a latent cysteine. *Journal of Medicinal Chemistry*, *25*(5), 489–491.

Nicolaou, K. C., Nevalainen, M., Safina, B. S., Zak, M. and Bulat, S. (2002). A biomimetically inspired synthesis of the dehydropiperidine domain of Thiostrepton. *Angewandte Chemie International Edition*. *41*(11), 1941 - 1945.

Nikaido, H. (2003). Molecular basis of bacterial outer membrane permeability revisited. *Microbiology and Molecular Biology Reviews*, *67*(4), 593–656.

Niu, X., Wang, X., Gao, Y., Yu, Y., Yana, Y., Wang, G., Sun, L. and Wang, H. (2019). Insight into the inhibition mechanism and structure–activity relationship of 2,6-dipicolinic acid and its analogue to New Delhi metallo-β-lactamase-1. *Molecular Simulation*, *45*(6), 525–531.

O'Callaghan, C. H., Morris, A., Kirby, S. M. and Shingler, A. H. (1972). Novel method for detection of β-lactamases by using a chromogenic cephalosporin substrate. *Antimicrobial Agents and Chemotherapy*, *1*(4), 283–288.

Ogawara, H. (2015). Penicillin-binding proteins in Actinobacteria. *The Journal of Antibiotics*, *68*(4), 223–245.

Oliver, G. L., Dann, J. R. and Gates, J. W. (1958). Preparation of thiazolidines and related compounds: Lactams and lactamidines. *Journal of the American Chemical Society*, *80*(3), 702–707.

Olsen, L., Jost, S., Adolph, H. -W., Pettersson, I., Hemmingsen, L. and Jørgensen, F. S. (2006). New leads of metallo-β-lactamase inhibitors from structure-based pharmacophore design. *Bioorganic & Medicinal Chemistry*, *14*(8), 2627–2635.

O'Neill, J., Antimicrobial resistance: Tackling a crisis for the health and Wealth of Nations: December 2014 (2014). London: Review on Antimicrobial Resistance.

Pagès, J.-M. and Amaral, L. (2009). Mechanisms of drug efflux and strategies to combat them: Challenging the efflux pump of Gram-negative bacteria. *Biochimica Et Biophysica Acta (BBA) - Proteins and Proteomics*, *1794*(5), 826–833.

Pages, J.-M., Amaral, L. and Fanning, S. (2011). An original deal for new molecule: Reversal of efflux pump activity, a rational strategy to combat gram-negative resistant bacteria. *Current Medicinal Chemistry*, *18*(19), 2969–2980.

Pagès, J.-M., James, C. E., and Winterhalter, M. (2008). The Porin and the permeating antibiotic: A selective diffusion barrier in Gram-negative bacteria. *Nature Reviews Microbiology*, *6*(12), 893–903.

Pala, L., Sirec, T. and Spitz, U. (2020). Modified enzyme substrates for the detection of bacteria: A Review. *Molecules*, *25*(16), 3690.

Parnham, M. J. and Sies, H. (2013). The early research and development of ebselen. *Biochemical Pharmacology*, *86*(9), 1248–1253.

Paul-Soto, R., Bauer, R., Frère, J.-M., Galleni, M., Meyer-Klaucke, W., Nolting, H., Rossolini, G. M., De Seny, D., Hernandez-valladares, M., Zeppezauer, M. and Adolph, H.-W. (1999). Mono- and binuclear Zn^{2+}-β-lactamase. *Journal of Biological Chemistry*, *274*(19), 13242−13249.

Pellegrini, N., Refouvelet, B., Crini, G., Blacque, O., Kubicki, M. M. and Robert, J.-F. (1999). New dipeptides containing thiazolidine-4-carboxylic acid derivatives: Synthesis and characterization using NMR techniques and X-ray data. *Chemical and Pharmaceutical Bulletin*, *47*(7), 950–955.

Perrin, C. L. (2003). Physical Organic Chemistry. In: Meyers, R. A. ed. *Encyclopedia of Physical Science and Technology*. 3rd ed. San Diego: Academic Press, pp. 211 – 243.

Perry, D. L. (2011). *Handbook of inorganic compounds*. Boca Raton, Florida: CRC Press.

Piddock, L. J. (2006). Multidrug-resistance efflux pumps? not just for resistance. *Nature Reviews Microbiology*, *4*(8), 629–636.

Pinho e Melo, T. M. V. D., Santos, C. I. A., Rocha Gonsalves, A. M. A., Paixão, J. A., Beja, A. M., and Ramos Silva, M. (2003). Synthesis of novel tricyclic isoindole derivatives. *Tetrahedron Letters*, *44*(45), 8285–8287.

Pinho e Melo, T. M. V. D., Santos, C. I. A., Rocha Gonsalves, A. M. A., Paixão, J. A. and Beja, A. M. (2004). Synthesis of tricyclic isoindoles and thiazolo[3,2-c][1,3]benzoxazines. *Tetrahedron*, *60*(18), 3949–3955.

Rajakanthan, A., De Jongh, P. A. J. M., Town, J. S., Wilson, P. and Kempe, K. (2019). A sequential native chemical ligation – thiol-Michael addition strategy for polymer-polymer ligation. *Polymer Chemistry*, *10*(38), 5242–5250.

Rajapaksha, P., Elbourne, A., Gangadoo, S., Brown, R., Cozzolino, D. and Chapman, J. (2019). A review of methods for the detection of pathogenic microorganisms. *The Analyst*, *144*(2), 396–411.

Ramirez, A., Ruggiero, M., Aranaga, C., Cataldi, A., Gutkind, G., de Waard, J. H., Araque, M. and Power, P. (2017). Biochemical characterization of β-lactamases from *Mycobacterium abscessus* complex and genetic environment of the β-lactamase-encoding gene. *Microbial Drug Resistance*, *23*(3), 294–300.

Ramli, F. F., Cowen, P. J. and Godlewska, B. R. (2022). The potential use of Ebselen in treatment-resistant depression. *Pharmaceuticals*, *15*(4), 485.

Ratner, S. and Clarke, H. T. (1937). The action of formaldehyde upon cysteine. *Journal of the American Chemical Society*, *59*(1), 200–206.

Refouvelet, B., Harraga, S., Nicod, L., Robert, J. F., Seilles, E., Couquelet, J., Tronche, P. (1994). Immunomodulatory agents: Dioxothiadiazabicyclo[3.3.0]octanes and their 2-spiro derivatives. *Chemical and Pharmaceutical Bulletin*, *42*(5), 1076–1083.

Riemenschneider, W. and Tanifuji, M. (2011). Oxalic acid. Ullmann's *Encyclopedia* of Industrial Chemistry; Wiley-VCH: Weinheim, 2011.

Rotondo, C. M. and Wright, G. D. (2017). Inhibitors of metallo-β-lactamases. *Current Opinion in Microbiology*, *39*, 96–105.

Royen, H. and Fortkamp, U. (2016). Rare Earth Elements - Purification, Separation and Recycling. Technical Report No. C211, Swedish Environmental Research Institute, September 2016.

Rukavishnikov, A., Gee, K. R., Johnson, I. and Corry, S. (2011). Fluorogenic cephalosporin substrates for β-lactamase TEM-1. *Analytical Biochemistry*, *419*(1), 9–16.

Rumble, J. R., Lide, D. R. and Bruno, T. J. (2018). *CRC handbook of chemistry and physics: a ready-reference book of chemical and physical data*. CRC Press: Boca Raton, Florida.

Sabath, L. D. and Abraham, E. P. (1966). Zinc as a cofactor for cephalosporinase from *Bacillus cereus* 569. *Biochemical Journal*, *98*(1), 11c – 13c.

Saito, I., Asano, T., Sano, K., Takakura, K., Abe, H., Yoshimoto, T., Kikuchi, H., Ohta, T. and Ishibashi, S. (1998). Neuroprotective effect of an antioxidant, Ebselen, in patients with delayed neurological deficits after aneurysmal subarachnoid hemorrhage. *Neurosurgery*, *42*(2), 269–277.

Sako, M., Totani, R., Hirota, K., and Maki, Y. (1992). First synthesis of 5,6,7,8-tetrahydro-8-thiafolic acid. *Chemical and Pharmaceutical Bulletin*, *40*(1), 49 – 52.

Santucci, M., Spyrakis, F., Cross, S., Quotadamo, A., Farina, D., Tondi, D., de Luca, F., Docquier, J. D., Prieto, A. I., Ibacache, C., Blázquez, J., Venturelli, A., Cruciani, G. and Costi, M. P. (2017). Computational and biological profile of boronic acids for the detection of bacterial serine- and metallo-β-lactamases. *Scientific Reports*, *7*(1), 17716.

Sassi, M. and Drancourt. M. (2014). Genome analysis reveals three genomospecies in *Mycobacterium abscessus. BMC Genomics*, *15*(1), 359.

Schindler, P. and Huber, G. (1980). Use of PADAC, a novel chromogenic β-lactamase substrate, for the detection of β-lactamase producing organisms and assay of β-lactamase inhibitors/inactivators. In: U. Brodbeck, U. ed. *Enzyme inhibitors*. Weinheim: Verlag Chemie, 169-176.

Schnaars, C., Kildahl-Andersen, G., Prandina, A., Popal, R., Radix, S. L., Le Borgne, M., Gjoen, T., Andresen, A. M. S., Heikal, A., Økstad, O. A., Fröhlich, C., Samuelsen, Ø., Lauksund, S., Jordheim, L. P., Rongved, P., Åstrand, O. A. H. (2018). Synthesis and preclinical evaluation of TPA-based zinc chelators as metallo-β-lactamase inhibitors. *ACS Infectious Diseases*, *4*(9), 1407–1422.

Seitz,T., Fu, P., Haut, F., Adam, L., Habicht, M., Lentz, D., MacMillan, J. B. and Christmann, M. (2016). One-pot synthesis of 5-hydroxy-4*h*-1,3-thiazin-4-ones: Structure revision, synthesis, and NMR shift dependence of Thiasporine A. *Organic Letters*, *18*(13), 3070–3073.

Shaikh, S., Fatima, J., Shakil, S., Rizvi, S. M. and Kamal, M. A. (2015). Antibiotic resistance and extended spectrum beta-lactamases: Types, epidemiology and treatment. *Saudi Journal of Biological Sciences*, *22*(1), 90–101.

Shannon, K. and Phillips, I. (1980). β-lactamase detection by three simple methods: Intralactam, Nitrocefin and acidimetric. *Journal of Antimicrobial Chemotherapy*, *6*(5), 617–621.

Shimamura, T., Ibuka, A., Fushinobu, S., Wakagi, T., Ishiguro, M., Ishii, Y. and Matsuzawa H. (2002). Acyl-intermediate structures of the extended-spectrum class A β-lactamase, Toho-1, in complex with cefotaxime, Cephalothin, and Benzylpenicillin. *Journal of Biological Chemistry*, *277*(48), 46601–46608.

Sies, H. (1993). Ebselen, a selenoorganic compound as glutathione peroxidase mimic. *Free Radical Biology and Medicine*, *14*(3), 313–323.

Sies, H. and Parnham, M.J. (2020). Potential therapeutic use of ebselen for COVID-19 and other respiratory viral infections. *Free Radical Biology and Medicine*. *156*, 107–112.

Singh, S. B. and Barrett, J. F. (2006). Empirical antibacterial drug discovery—foundation in natural products. *Biochemical Pharmacology*, *71*(7), 1006–1015.

Skagseth, S., Akhter, S., Paulsen, M. H., Muhammad, Z., Lauksund, S., Samuelsen, Ø., Leiros, H. S., Bayer, A. (2017). Metallo-β-lactamase inhibitors by bioisosteric replacement: Preparation, activity and binding. *European Journal of Medicinal Chemistry*, *135*, 159–173.

Somboro, A. M., Tiwari, D., Bester, L. A., Parboosing, R., Chonco, L., Kruger, H. G., Arvidsson, P. I., Govender, T., Naicker, T. and Essack, S. Y. (2015). NOTA: A potent metallo-β-lactamase inhibitor. *Journal of Antimicrobial Chemotherapy*, *70*(5), 1594–1596.

Song, G. -Q., Wang, W. -M., Li, Z. -S., Wang, Y. and Wang, J. -G. (2018). First identification of Isatin-β-thiosemicarbazones as novel inhibitors of New Delhi metallo-β-lactamase-1: Chemical synthesis, biological evaluation and molecular simulation. *Chinese Chemical Letters*, *29*(6), 899–902.

Soroka, D., Dubee, V., Soulier-Escrihuela, O., Cuinet, G., Hugonnet, J. E., Gutmann, L., Mainardi, J. L. and Arthur, M. (2014). Characterization of broad-spectrum mycobacterium abscessus class A β-lactamase. *Journal of Antimicrobial Chemotherapy*, *69*(3), 691–696.

Soroka, D., Li de la Sierra-Gallay, I., Dubée, V., Triboulet, S., van, Tilbeurgh, H., Compain, F., Ballell, L., Barros, D., Mainardi, J. -L., Hugonnet, J. -E., Arthur, M. (2015). Hydrolysis of clavulanate by *Mycobacterium tuberculosis* β-lactamase BlaC harboring a canonical SDN motif. *Antimicrobial Agents and Chemotherapy*, *59*(9), 5714–5720.

Soroka, D., Ourghanlian, C., Compain, F., Fichini, M., Dubee, V., Mainardi, J. -L., Hugonnet, J. -E. and Arthur, M. (2017). Inhibition of β-lactamases of mycobacteria by avibactam and clavulanate. *Journal of Antimicrobial Chemotherapy*, *72*(4), 1081 – 1088.

Stella, V., Borchardt, R., Hageman, M., Oliyai, R., Maag, H. and Tilley, J. (2007). *Prodrugs: challenges and Rewards*. New York: Springer New York.

Strynadka, N. C. J., Martin, R., Jensen, S. E., Gold, M. and Jones, J. B. (1996). Structure-based design of a potent transition state analogue for TEM-1 β-lactamase. *Nature Structural & Molecular Biology*, *3*(8), 688–695.

Suaifan, G.A.R.Y, Mahon, M. F., Arafat, T. and Threadgill, M. D. (2006). Effects of steric bulk and stereochemistry on the rates of diketopiperazine formation from N-aminoacyl-2,2-dimethylthiazolidine-4-carboxamides (DMT dipeptide amides)—a model for a new prodrug linker system. *Tetrahedron*, *62*(48), 11245-11266.

Thakare, R., Kaul, G., Shukla, M., Kesharwani, P., Srinivas, N., Dasgupta, A., Chopra, S. (2020). Repurposing nonantibiotic drugs as antibacterials. In: Kesharwani, P., Chopra, S. and Dasgupta, A. ed(s). *Drug discovery targeting drug-resistant bacteria*. London: Academic press, pp. 105-138.

Thomas, T. (1808). IV. on oxalic acid. *Philosophical Transactions of the Royal Society of London*, *98*, 63–95.

Thomas, P. W., Cammarata, M., Brodbelt, J. S. and Fast, W. (2014). Covalent Inhibition of New Delhi metallo-β-lactamase-1 (NDM-1) by Cefaclor. *ChemBioChem, 15*(17), 2541 − 2548.

Toney, J. H., Hammond, G. G., Fitzgerald, P. M., Sharma, N., Balkovec, J. M., Rouen, G. P., Olson, S. H., Hammond, M. L., Greenlee, M. L. and Gao, Y. -D. (2001). Succinic acids as potent inhibitors of plasmid-borne imp-1 metallo-β-lactamase. *Journal of Biological Chemistry*, *276*(34), 31913–31918.

Tripathi, R. and Nair, N. N. (2015). Mechanism of meropenem hydrolysis by New Delhi metallo-β-lactamase. *ACS Catalysis*, *5*(4), 2577–2586.

Trivedi, M. K., Sethi, K. K., Panda, P. and Jana, S. (2017). A comprehensive physicochemical, thermal, and spectroscopic characterization of zinc (II) chloride using X-ray diffraction, particle size distribution, differential scanning calorimetry, thermogravimetric analysis/differential thermogravimetric analysis, ultraviolet-visible, and Fourier transform-infrared spectroscopy. *International Journal of Pharma-ceutical Investigation*, *7*(1), 33 – 40.

Tuley, A. and Fast, W. (2018). The taxonomy of covalent inhibitors. *Biochemistry*, *57*(24), 3326–3337.

Unemo, M., and Nicholas, R. A. (2012). Emergence of multidrug-resistant, extensively drug-resistant and untreatable gonorrhoea. *Future Microbiology*, 7(12), 1401–1422.

van Berkel, S. S., Brem, J., Rydzik, A. M., Salimraj, R., Cain, R., Verma, A., Owens, R. J., Fishwick, C. W. G., Spencer, J. and Schofield, C. J. (2013). Assay platform for clinically relevant metallo-β-lactamases. *Journal of Medicinal Chemistry*, *56*(17), 6945–6953.

Verma, A., Kore, R., Corbin, D. R. and Shiflett, M. B. (2019). Metal recovery using oxalate chemistry: A technical review. *Industrial and Engineering Chemistry Research*, *58*(34), 15381–15393.

Viswanatha, T., Marrone, L., Goodfellow, V., & Dmitrienko, G. I. (2008). Assays for B-lactamase activity and inhibition. In: Champney, W.S. eds. *New Antibiotic Targets. Methods In Molecular Medicine™*. Humana Press. *142*, 239–260.

Wade, J. D., Bedford, J., Sheppard, R. C. and Tregear, G. W. (1991). *Journal* of *Peptide Research, 4, 194.*

Wang, F., Cassidy, C. and Sacchettini, J. C. (2006). Crystal structure and activity studies of the *Mycobacterium tuberculosis* β-lactamase reveal its critical role in resistance to β-lactam antibiotics. *Antimicrobial Agents and Chemotherapy*, *50*(8), 2762–2771.

Wang, Z., Fast, W. and Benkovic, S. J. (1998). Direct observation of an enzyme-bound intermediate in the catalytic cycle of the metallo-β-lactamase from *Bacteroides fragilis*. *Journal of the American Chemical Society*, *120*(41), 10788–10789.

Watson, D. G. (2012). *Pharmaceutical Analysis: A Textbook for Pharmacy Students and Pharmaceutical Chemist*. Edinburgh, UK: Elsevier Churchill Livingstone.

Webber, M. A. and Piddock, L. J. V. (2003). The importance of efflux pumps in bacterial antibiotic resistance. *Journal of Antimicrobial Chemotherapy*, *51*(1), 9–11.

William, N. S. (1972). *Vanadyl Oxalate Compounds and Process for Producing Same*. U.S. Patent US3689515A.

Woodman, E. K., Chaffey, J. G., Hopes, P. A., Hose, D. R. and Gilday, J. P. (2009). *N, N′*-carbonyldiimidazole-mediated amide coupling: Significant rate enhancement achieved by acid catalysis with imidazole·HCl. *Organic Process Research & Development*, *13*(1), 106–113.

World Health Organization. (2012). The evolving threat of antimicrobial resistance: options for action: executive summary. World Health Organization. https://apps.who.int/iris/handle/10665/75389.

Wu, K.-M. (2009). A new classification of Prodrugs: Regulatory perspectives. *Pharmaceuticals*, *2*(3), 77–81.

Wu, W., Feng, Y., Tang, G., Qiao, F., McNally, A. and Zong, Z. (2019). NDM metallo-β-lactamases and their bacterial producers in Health Care Settings. *Clinical Microbiology Reviews*, *32*(2), e00115 - 18.

Xiang, Y., Chang, Y. -N., Ge, Y., Kang, J. S., Zhang, Y. -L., Liu, X. L., Oelschlaeger, P., and Yang, K. -W. (2017). Azolylthioacetamides as a potent scaffold for the development of metallo-β-lactamase inhibitors. *Bioorganic & Medicinal Chemistry Letters*, *27*(23), 5225–5229.

Xie, H., Mire, J., Kong, Y., Chang, M., Hassounah, H. A., Thornton, C. N., Sacchettini, J. C., Cirillo, J. D., Rao, J. H. (2012). Rapid point-of-care detection of the tuberculosis pathogen using a BlaC-specific fluorogenic probe. *Nature Chemistry*, *4*(10), 802–809.

Yamaguchi, T., Sano, K., Takakura, K., Saito, I., Shinohara, Y., Asano, T. and Yasuhara, H. (1998). Ebselen in acute ischemic stroke. *Stroke*, *29*(1), 12–17.

Yamaguchi, Y., Kuroki, T., Yasuzawa, H., Higashi, T., Jin, W., Kawanami, A., Yamagata, Y., Goto, M., and Kurosaki, H. (2005). Probing the role of asp-120(81) of metallo-β-lactamase (IMP-1) by site-directed mutagenesis, kinetic studies, and X-ray crystallography. *Journal of Biological Chemistry*, *280*(21), 20824–20832.

Yang, H., Aitha, M., Hetrick, A. M., Richmond, T. K., Tierney, D. L. and Crowder, M. W. (2012). Mechanistic and spectroscopic studies of metallo-β-lactamase NDM-1. *Biochemistry*, *51*(18), 3839–3847.

Yang, S., Wang, T., Zhou, Y., Shi, L., Lu, A. and Wang, Z. (2021). Discovery of cysteine and Its derivatives as novel antiviral and antifungal agents. *Molecules*, *26*(2), 383.

Yao, H., So, M.-kyung and Rao, J. (2007). A bioluminogenic substrate for in vivo imaging of β-lactamase activity. *Angewandte Chemie International Edition*, *46*(37), 7031–7034.

Yong, D., Toleman, M. A., Giske, C. G., Cho, H. S., Sundman, K., Lee, K. and Walsh, T. R. (2009). Characterization of a new metallo- β-lactamase gene, bla$_{NDM-1}$, and a novel erythromycin esterase gene carried on a unique genetic structure in *Klebsiella pneumoniae* sequence type 14 from India. *Antimicrobial agents and chemotherapy*, *53*(12), 5046 – 5054.

Yoshizumi, A., Ishii, Y., Kimura, S., Saga, T., Harada, S., Yamaguchi, K., Tateda, K., Livermore, D. M., Woodford, N. and Livermore, D. M. (2013). Efficacies of calcium–EDTA in combination with imipenem in a murine model of sepsis caused by *Escherichia coli* with NDM-1 β-lactamase. *Journal of Infection and Chemotherapy*, *19*(5), 992–995.

Zervosen, A., Valladares, M. H., Devreese, B., Prosperi-Meys, C., Adolph, H. -W., Mercuri, P. S., Vanhove, M., Amicosante, G., van Beeumen, J., Frere, J. M. and Galleni, M. (2001). Inactivation of *Aeromonas hydrophila* metallo-β-lactamase by cephamycins and Moxalactam. *European Journal of Biochemistry*, *268*(13), 3840–3850.

Zhai, L., Zhang, Y. -L., Kang, J. S., Oelschlaeger, P., Xiao, L., Nie, S. -S., and Yang, K. -W. (2016). Triazolylthioacetamide: A valid scaffold for the development of New Delhi metallo-β-lactmase-1 (NDM-1) inhibitors. *ACS Medicinal Chemistry Letters*, *7*(4), 413–417.

Zhang, GM., and Hao, Q. (2011). Crystal structure of NDM-1 reveals a common β-lactam hydrolysis mechanism. *The FASEB Journal*, *25*(8), 2574–2582.

Zhang, J., Wang, S., Wei, Q., Guo, Q., Bai, Y., Yang, S., Song, F., Zhang, L. and Lei, X. (2017). Synthesis and biological evaluation of aspergillomarasmine A derivatives as novel NDM-1 inhibitor to overcome antibiotics resistance. *Bioorganic & Medicinal Chemistry*, *25*(19), 5133–5141.

Zhang, Y. -L., Yang, K. -W., Zhou, Y. -J., LaCuran, A. E., Oelschlaeger, P., and Crowder, M. W. (2014). Diaryl-substituted azolylthioacetamides: Inhibitor discovery of New Delhi metallo-β-lactamase-1 (NDM-1). *ChemMedChem*, *9*(11), 2445–2448.

Zhang, Y.-L., Xiao, J.-M., Feng, J.-L., Yang, K.-W., Feng, L., Zhou, L.-S. and Crowder, M. W. (2013). A novel fluorogenic substrate for dinuclear zn(ii)-containing metallo-β-lactamases. *Bioorganic & Medicinal Chemistry Letters*, *23*(6), 1676–1679.

Zhao, L., Huang, W., Liu, H., Wang, L., Zhong, W., Xiao, J., Hu, Y., Li, S. (2006). FK506-binding protein ligands: Structure-based design, synthesis, and neurotrophic/neuroprotective properties of substituted 5,5-dimethyl-2-(4-thiazolidine)carboxylates. *Journal of Medicinal Chemistry*, *49*(14), 4059-4071.

Zhao, L.-X., Wu, H., Zou, Y.-L., Wang, Q.-R., Fu, Y., Li, C.-Y., & Ye, F. (2018). Design, synthesis, and safener activity of novel methyl (R)-N-benzoyl/dichloroacetyl-thiazolidine-4-carboxylates. *Molecules*, *23*(1), 155.

Zhu, K., Lu, J., Liang, Z., Kong, X., Ye, F., Jin, L., … Luo, C. (2013). A quantum mechanics/molecular mechanics study on the hydrolysis mechanism of New Delhi metallo-β-lactamase-1. *Journal of Computer-Aided Molecular Design*, *27*(3), 247–256.

Zhu, L., Yuan, Z., Simmons, J. T. and Sreenath, K. (2014). Zn(II)-coordination modulated ligand photophysical processes – the development of fluorescent indicators for imaging biological Zn(II) ions. *Royal Society of Chemistry Advances*, *4*(39), 20398–20440.

Appendix

UV absorbance for spectrophotometric detection of Zn(II)-bis cyclo-oxamide complex

Wavelength (nm)	Comp. 94	0.01 mL	0.02 mL	0.03 mL	0.04 mL	0.05 mL	0.06 mL
198	0.083	0.084	0.123	0.153	0.176	0.213	0.237
199	0.084	0.083	0.132	0.162	0.2	0.232	0.248
200	0.096	0.097	0.151	0.191	0.24	0.28	0.293
201	0.105	0.107	0.167	0.216	0.269	0.316	0.333
202	0.129	0.137	0.211	0.283	0.345	0.412	0.441
203	0.145	0.153	0.235	0.319	0.39	0.467	0.507
204	0.172	0.179	0.283	0.392	0.48	0.577	0.64
205	0.194	0.198	0.32	0.451	0.56	0.674	0.754
206	0.203	0.205	0.336	0.475	0.593	0.715	0.804
207	0.217	0.216	0.358	0.511	0.644	0.786	0.889
208	0.222	0.22	0.367	0.525	0.664	0.814	0.924
209	0.231	0.225	0.379	0.546	0.697	0.86	0.988
210	0.234	0.227	0.383	0.555	0.71	0.878	1.014
211	0.239	0.23	0.39	0.568	0.732	0.909	1.055
212	0.242	0.231	0.394	0.576	0.747	0.932	1.087
213	0.244	0.232	0.396	0.58	0.753	0.942	1.1
214	0.245	0.233	0.397	0.584	0.761	0.955	1.119
215	0.246	0.232	0.397	0.585	0.763	0.959	1.127
216	0.245	0.232	0.396	0.585	0.764	0.962	1.136
217	0.245	0.231	0.395	0.584	0.764	0.962	1.139
218	0.244	0.229	0.391	0.58	0.76	0.959	1.138
219	0.241	0.228	0.388	0.574	0.754	0.952	1.132
220	0.24	0.227	0.386	0.57	0.749	0.947	1.127
221	0.236	0.225	0.381	0.563	0.738	0.935	1.114
222	0.234	0.224	0.378	0.558	0.732	0.927	1.106
223	0.23	0.221	0.371	0.546	0.716	0.908	1.086
224	0.224	0.216	0.362	0.532	0.697	0.886	1.059
225	0.221	0.214	0.357	0.524	0.687	0.873	1.044
226	0.213	0.208	0.346	0.507	0.661	0.842	1.008
227	0.209	0.205	0.339	0.496	0.647	0.823	0.987
228	0.199	0.199	0.326	0.474	0.617	0.787	0.943
229	0.195	0.195	0.319	0.464	0.603	0.77	0.923
230	0.187	0.189	0.308	0.445	0.579	0.74	0.887
231	0.181	0.184	0.298	0.428	0.559	0.713	0.855
232	0.179	0.181	0.293	0.42	0.548	0.7	0.839
233	0.175	0.176	0.284	0.405	0.528	0.672	0.805
234	0.172	0.173	0.279	0.397	0.517	0.658	0.788
235	0.168	0.168	0.269	0.38	0.493	0.627	0.749
236	0.165	0.165	0.263	0.371	0.481	0.61	0.728
237	0.159	0.158	0.251	0.35	0.453	0.575	0.683
238	0.151	0.151	0.237	0.328	0.424	0.537	0.635
239	0.147	0.147	0.229	0.317	0.408	0.517	0.61
240	0.137	0.138	0.212	0.293	0.375	0.475	0.559
241	0.131	0.133	0.203	0.281	0.358	0.454	0.532
242	0.121	0.124	0.187	0.258	0.327	0.415	0.485

243	0.113	0.117	0.175	0.239	0.302	0.385	0.448
244	0.11	0.114	0.17	0.231	0.292	0.372	0.431
245	0.105	0.109	0.16	0.216	0.271	0.345	0.399
246	0.102	0.106	0.154	0.208	0.26	0.331	0.382
247	0.097	0.101	0.145	0.194	0.241	0.307	0.352
248	0.093	0.097	0.138	0.181	0.225	0.287	0.328
249	0.09	0.094	0.132	0.17	0.211	0.269	0.305
250	0.089	0.092	0.129	0.165	0.204	0.259	0.294
251	0.086	0.089	0.122	0.154	0.189	0.24	0.271
252	0.082	0.085	0.116	0.144	0.176	0.223	0.25
253	0.081	0.083	0.113	0.139	0.17	0.216	0.241
254	0.079	0.08	0.108	0.13	0.159	0.201	0.223
255	0.078	0.079	0.105	0.126	0.153	0.193	0.213
256	0.074	0.075	0.099	0.117	0.14	0.176	0.192
257	0.072	0.073	0.094	0.112	0.132	0.167	0.18
258	0.067	0.068	0.086	0.103	0.118	0.15	0.159
259	0.064	0.065	0.082	0.098	0.111	0.142	0.15
260	0.06	0.061	0.076	0.09	0.101	0.13	0.135
261	0.057	0.059	0.072	0.083	0.094	0.122	0.125
262	0.056	0.058	0.07	0.081	0.092	0.118	0.121
263	0.055	0.056	0.068	0.076	0.087	0.112	0.114
264	0.055	0.056	0.067	0.075	0.085	0.109	0.11
265	0.054	0.054	0.066	0.072	0.081	0.104	0.103
266	0.054	0.054	0.065	0.07	0.079	0.101	0.1
267	0.053	0.052	0.062	0.067	0.074	0.095	0.092
268	0.05	0.05	0.058	0.063	0.069	0.089	0.085
269	0.049	0.049	0.056	0.061	0.067	0.086	0.081
270	0.047	0.046	0.052	0.058	0.062	0.08	0.075
271	0.045	0.045	0.051	0.056	0.06	0.078	0.072
272	0.043	0.042	0.048	0.053	0.056	0.074	0.067
273	0.043	0.042	0.047	0.052	0.055	0.072	0.065
274	0.042	0.04	0.045	0.049	0.053	0.069	0.062
275	0.041	0.04	0.044	0.048	0.052	0.068	0.06
276	0.04	0.039	0.043	0.047	0.05	0.065	0.058
277	0.04	0.038	0.042	0.045	0.049	0.063	0.055
278	0.04	0.038	0.042	0.045	0.048	0.063	0.054
279	0.039	0.037	0.04	0.043	0.046	0.061	0.052
280	0.039	0.036	0.039	0.043	0.045	0.059	0.05
281	0.037	0.034	0.037	0.041	0.043	0.057	0.047
282	0.036	0.033	0.035	0.041	0.042	0.056	0.046
283	0.035	0.032	0.034	0.039	0.04	0.054	0.044
284	0.034	0.031	0.033	0.038	0.039	0.053	0.043
285	0.034	0.031	0.033	0.037	0.039	0.052	0.042
286	0.034	0.031	0.033	0.037	0.039	0.051	0.042
287	0.034	0.032	0.034	0.036	0.039	0.051	0.041
288	0.034	0.032	0.034	0.036	0.039	0.051	0.041
289	0.034	0.032	0.035	0.036	0.039	0.051	0.041
290	0.034	0.032	0.034	0.036	0.038	0.05	0.04
291	0.033	0.031	0.033	0.036	0.037	0.048	0.039
292	0.033	0.031	0.032	0.035	0.036	0.048	0.038

Wavelength							
293	0.032	0.03	0.031	0.034	0.035	0.047	0.037
294	0.031	0.029	0.03	0.034	0.034	0.046	0.036
295	0.03	0.028	0.029	0.033	0.034	0.045	0.035
296	0.03	0.027	0.028	0.032	0.033	0.045	0.034
297	0.029	0.026	0.027	0.031	0.033	0.044	0.034
298	0.029	0.026	0.027	0.03	0.033	0.044	0.033
299	0.029	0.026	0.027	0.03	0.033	0.044	0.033
300	0.029	0.026	0.028	0.03	0.033	0.044	0.034

Wavelength (nm)	Comp. 94	0.01 mL	0.02 mL	0.03 mL	0.04 mL	0.05 mL	0.06 mL
198	0.083	0.072	0.113	0.152	0.168	0.199	0.217
199	0.084	0.082	0.121	0.164	0.185	0.218	0.242
200	0.096	0.1	0.139	0.2	0.223	0.264	0.291
201	0.105	0.109	0.159	0.226	0.253	0.3	0.334
202	0.129	0.136	0.204	0.293	0.34	0.404	0.435
203	0.145	0.15	0.229	0.331	0.388	0.463	0.494
204	0.172	0.178	0.279	0.398	0.481	0.577	0.619
205	0.194	0.198	0.318	0.456	0.56	0.674	0.737
206	0.203	0.206	0.333	0.48	0.593	0.714	0.789
207	0.217	0.217	0.356	0.517	0.644	0.782	0.885
208	0.222	0.222	0.364	0.531	0.664	0.81	0.92
209	0.231	0.229	0.378	0.552	0.698	0.858	0.977
210	0.234	0.231	0.384	0.56	0.712	0.877	1
211	0.239	0.235	0.393	0.572	0.734	0.908	1.04
212	0.242	0.238	0.4	0.58	0.75	0.93	1.074
213	0.244	0.239	0.402	0.583	0.756	0.94	1.088
214	0.245	0.241	0.405	0.587	0.766	0.954	1.109
215	0.246	0.241	0.405	0.587	0.769	0.959	1.116
216	0.245	0.242	0.405	0.587	0.772	0.964	1.124
217	0.245	0.241	0.405	0.585	0.772	0.963	1.126
218	0.244	0.24	0.402	0.582	0.768	0.96	1.127
219	0.241	0.238	0.398	0.577	0.761	0.952	1.121
220	0.24	0.237	0.396	0.574	0.756	0.947	1.117
221	0.236	0.233	0.391	0.566	0.744	0.935	1.102
222	0.234	0.231	0.388	0.561	0.737	0.927	1.094
223	0.23	0.226	0.379	0.55	0.72	0.908	1.072
224	0.224	0.22	0.368	0.536	0.7	0.884	1.045
225	0.221	0.216	0.361	0.528	0.688	0.871	1.03
226	0.213	0.207	0.346	0.509	0.661	0.839	0.993
227	0.209	0.202	0.337	0.498	0.644	0.82	0.971
228	0.199	0.193	0.322	0.477	0.613	0.784	0.927
229	0.195	0.189	0.316	0.468	0.599	0.767	0.907
230	0.187	0.183	0.308	0.45	0.575	0.737	0.872
231	0.181	0.179	0.301	0.435	0.555	0.711	0.84
232	0.179	0.177	0.298	0.427	0.546	0.697	0.824
233	0.175	0.172	0.289	0.412	0.525	0.67	0.79
234	0.172	0.169	0.284	0.403	0.514	0.655	0.773
235	0.168	0.164	0.274	0.386	0.491	0.624	0.735

236	0.165	0.161	0.269	0.377	0.479	0.608	0.715
237	0.159	0.155	0.257	0.356	0.452	0.572	0.671
238	0.151	0.148	0.242	0.334	0.422	0.534	0.624
239	0.147	0.143	0.234	0.322	0.406	0.514	0.599
240	0.137	0.133	0.213	0.296	0.371	0.472	0.547
241	0.131	0.127	0.202	0.283	0.354	0.451	0.521
242	0.121	0.116	0.183	0.26	0.322	0.412	0.474
243	0.113	0.11	0.172	0.241	0.297	0.382	0.437
244	0.11	0.107	0.167	0.233	0.287	0.368	0.42
245	0.105	0.101	0.157	0.218	0.265	0.341	0.388
246	0.102	0.098	0.151	0.21	0.254	0.327	0.371
247	0.097	0.092	0.141	0.195	0.234	0.302	0.341
248	0.093	0.088	0.136	0.184	0.219	0.282	0.317
249	0.09	0.086	0.132	0.174	0.205	0.264	0.295
250	0.089	0.085	0.13	0.168	0.198	0.255	0.284
251	0.086	0.081	0.122	0.157	0.183	0.235	0.261
252	0.082	0.077	0.116	0.147	0.17	0.218	0.24
253	0.081	0.076	0.114	0.142	0.164	0.211	0.231
254	0.079	0.074	0.11	0.134	0.153	0.196	0.213
255	0.078	0.073	0.107	0.129	0.147	0.188	0.203
256	0.074	0.068	0.098	0.119	0.132	0.17	0.182
257	0.072	0.065	0.091	0.112	0.124	0.161	0.17
258	0.067	0.057	0.078	0.101	0.108	0.143	0.148
259	0.064	0.054	0.073	0.096	0.102	0.136	0.139
260	0.06	0.05	0.067	0.088	0.092	0.124	0.125
261	0.057	0.049	0.065	0.082	0.086	0.116	0.115
262	0.056	0.048	0.065	0.08	0.083	0.112	0.111
263	0.055	0.048	0.064	0.076	0.079	0.106	0.104
264	0.055	0.047	0.064	0.075	0.077	0.103	0.101
265	0.054	0.046	0.061	0.072	0.073	0.097	0.094
266	0.054	0.045	0.06	0.07	0.071	0.094	0.091
267	0.053	0.044	0.058	0.066	0.066	0.089	0.083
268	0.05	0.042	0.053	0.061	0.061	0.083	0.076
269	0.049	0.041	0.051	0.059	0.059	0.08	0.072
270	0.047	0.037	0.044	0.054	0.053	0.074	0.066
271	0.045	0.036	0.041	0.052	0.051	0.072	0.063
272	0.043	0.034	0.038	0.049	0.048	0.068	0.058
273	0.043	0.034	0.038	0.048	0.047	0.067	0.057
274	0.042	0.033	0.037	0.045	0.045	0.064	0.054
275	0.041	0.033	0.037	0.044	0.045	0.063	0.052
276	0.04	0.033	0.036	0.043	0.043	0.06	0.05
277	0.04	0.032	0.036	0.041	0.042	0.058	0.048
278	0.04	0.032	0.036	0.041	0.042	0.058	0.047
279	0.039	0.032	0.034	0.039	0.04	0.056	0.045
280	0.039	0.031	0.032	0.038	0.039	0.055	0.043
281	0.037	0.029	0.028	0.035	0.036	0.052	0.04
282	0.036	0.028	0.026	0.034	0.035	0.051	0.039
283	0.035	0.027	0.024	0.032	0.034	0.05	0.037
284	0.034	0.027	0.025	0.031	0.034	0.049	0.036
285	0.034	0.027	0.025	0.031	0.034	0.048	0.036

Wavelength (nm)							
286	0.034	0.027	0.027	0.031	0.034	0.047	0.036
287	0.034	0.028	0.028	0.032	0.034	0.047	0.035
288	0.034	0.028	0.03	0.032	0.033	0.046	0.035
289	0.034	0.028	0.03	0.032	0.032	0.046	0.034
290	0.034	0.026	0.028	0.031	0.031	0.044	0.032
291	0.033	0.025	0.025	0.03	0.029	0.043	0.031
292	0.033	0.024	0.024	0.029	0.028	0.042	0.03
293	0.032	0.023	0.021	0.028	0.027	0.042	0.029
294	0.031	0.023	0.021	0.027	0.027	0.041	0.028
295	0.03	0.022	0.019	0.026	0.027	0.04	0.028
296	0.03	0.022	0.019	0.025	0.026	0.04	0.028
297	0.029	0.022	0.019	0.025	0.027	0.04	0.028
298	0.029	0.023	0.021	0.024	0.028	0.04	0.028
299	0.029	0.023	0.022	0.024	0.028	0.04	0.028
300	0.029	0.024	0.024	0.025	0.029	0.04	0.028

Wavelength (nm)	Comp.96	0.01 mL	0.02 mL	0.03 mL	0.04 mL	0.05 mL	0.06 mL
198	0.042	0.032	0.064	0.09	0.116	0.138	0.146
199	0.048	0.032	0.071	0.099	0.124	0.152	0.165
200	0.054	0.042	0.085	0.118	0.152	0.187	0.199
201	0.06	0.048	0.098	0.134	0.174	0.212	0.227
202	0.073	0.06	0.127	0.173	0.232	0.27	0.298
203	0.08	0.067	0.14	0.192	0.262	0.304	0.337
204	0.093	0.078	0.164	0.226	0.313	0.365	0.412
205	0.101	0.085	0.179	0.251	0.347	0.414	0.472
206	0.104	0.088	0.184	0.26	0.36	0.433	0.496
207	0.108	0.092	0.191	0.274	0.379	0.461	0.532
208	0.109	0.094	0.194	0.279	0.387	0.471	0.545
209	0.111	0.096	0.198	0.285	0.397	0.486	0.565
210	0.111	0.097	0.199	0.287	0.401	0.492	0.573
211	0.112	0.099	0.2	0.29	0.407	0.5	0.585
212	0.112	0.1	0.201	0.291	0.41	0.505	0.592
213	0.112	0.1	0.2	0.292	0.411	0.507	0.594
214	0.111	0.101	0.2	0.291	0.412	0.508	0.596
215	0.11	0.101	0.199	0.291	0.411	0.508	0.596
216	0.109	0.1	0.197	0.289	0.409	0.506	0.595
217	0.108	0.1	0.196	0.287	0.407	0.504	0.593
218	0.107	0.1	0.194	0.284	0.404	0.499	0.588
219	0.106	0.099	0.192	0.281	0.399	0.493	0.582
220	0.106	0.099	0.191	0.279	0.396	0.489	0.578
221	0.105	0.098	0.189	0.275	0.389	0.481	0.569
222	0.104	0.097	0.188	0.273	0.385	0.476	0.564
223	0.103	0.096	0.185	0.268	0.377	0.466	0.552
224	0.101	0.094	0.181	0.261	0.367	0.453	0.537
225	0.1	0.092	0.178	0.258	0.361	0.446	0.529
226	0.098	0.09	0.173	0.25	0.348	0.43	0.51
227	0.097	0.088	0.171	0.245	0.341	0.421	0.499
228	0.095	0.085	0.166	0.237	0.328	0.404	0.479

229	0.093	0.084	0.163	0.233	0.321	0.397	0.471
230	0.091	0.081	0.159	0.225	0.311	0.383	0.456
231	0.089	0.08	0.154	0.219	0.301	0.372	0.444
232	0.088	0.079	0.152	0.216	0.296	0.366	0.438
233	0.085	0.078	0.148	0.21	0.287	0.355	0.424
234	0.084	0.077	0.145	0.206	0.282	0.349	0.417
235	0.082	0.076	0.141	0.199	0.272	0.336	0.402
236	0.081	0.075	0.138	0.196	0.267	0.329	0.393
237	0.078	0.073	0.133	0.187	0.255	0.313	0.374
238	0.074	0.07	0.126	0.177	0.24	0.294	0.352
239	0.072	0.068	0.122	0.171	0.232	0.285	0.34
240	0.067	0.063	0.114	0.159	0.215	0.263	0.313
241	0.064	0.06	0.109	0.152	0.206	0.252	0.299
242	0.06	0.056	0.101	0.14	0.189	0.232	0.274
243	0.057	0.052	0.095	0.131	0.176	0.216	0.256
244	0.055	0.051	0.093	0.127	0.171	0.209	0.247
245	0.053	0.048	0.087	0.119	0.159	0.195	0.231
246	0.051	0.047	0.084	0.115	0.153	0.188	0.222
247	0.049	0.044	0.08	0.108	0.143	0.175	0.206
248	0.047	0.043	0.076	0.102	0.135	0.164	0.195
249	0.046	0.042	0.073	0.098	0.128	0.155	0.185
250	0.046	0.041	0.072	0.095	0.124	0.151	0.179
251	0.044	0.039	0.068	0.09	0.116	0.141	0.167
252	0.042	0.038	0.064	0.085	0.109	0.132	0.157
253	0.041	0.037	0.063	0.082	0.106	0.128	0.152
254	0.04	0.037	0.061	0.079	0.101	0.121	0.144
255	0.04	0.036	0.059	0.076	0.097	0.116	0.138
256	0.037	0.034	0.055	0.071	0.09	0.107	0.126
257	0.035	0.032	0.052	0.067	0.085	0.101	0.118
258	0.032	0.028	0.047	0.06	0.076	0.09	0.104
259	0.031	0.026	0.045	0.057	0.072	0.085	0.098
260	0.028	0.024	0.042	0.052	0.065	0.078	0.089
261	0.027	0.022	0.039	0.049	0.061	0.072	0.083
262	0.026	0.022	0.038	0.047	0.059	0.07	0.081
263	0.026	0.022	0.037	0.046	0.056	0.067	0.077
264	0.026	0.022	0.036	0.045	0.055	0.065	0.076
265	0.025	0.022	0.036	0.044	0.053	0.062	0.072
266	0.025	0.022	0.035	0.043	0.052	0.061	0.07
267	0.024	0.021	0.033	0.04	0.049	0.057	0.065
268	0.022	0.019	0.031	0.037	0.046	0.053	0.059
269	0.021	0.018	0.03	0.036	0.044	0.05	0.056
270	0.019	0.016	0.027	0.033	0.04	0.046	0.05
271	0.019	0.015	0.026	0.031	0.038	0.044	0.048
272	0.017	0.014	0.024	0.029	0.036	0.042	0.044
273	0.017	0.013	0.024	0.028	0.035	0.04	0.043
274	0.016	0.013	0.023	0.027	0.034	0.039	0.041
275	0.016	0.013	0.022	0.026	0.033	0.038	0.04
276	0.015	0.013	0.021	0.026	0.032	0.036	0.039
277	0.015	0.013	0.021	0.025	0.031	0.035	0.038
278	0.015	0.012	0.021	0.024	0.031	0.035	0.037

279	0.014	0.012	0.02	0.023	0.03	0.033	0.035
280	0.013	0.011	0.019	0.023	0.029	0.032	0.034
281	0.012	0.01	0.017	0.021	0.027	0.03	0.031
282	0.012	0.009	0.017	0.02	0.026	0.03	0.029
283	0.011	0.008	0.016	0.019	0.025	0.028	0.028
284	0.011	0.009	0.015	0.018	0.025	0.027	0.027
285	0.011	0.009	0.015	0.018	0.024	0.027	0.027
286	0.011	0.01	0.016	0.018	0.024	0.027	0.028
287	0.011	0.01	0.016	0.019	0.024	0.027	0.028
288	0.012	0.01	0.017	0.019	0.024	0.027	0.028
289	0.012	0.01	0.017	0.019	0.024	0.026	0.028
290	0.012	0.01	0.016	0.019	0.023	0.026	0.026
291	0.012	0.009	0.016	0.018	0.022	0.025	0.025
292	0.011	0.008	0.015	0.018	0.022	0.024	0.024
293	0.01	0.007	0.014	0.017	0.021	0.023	0.022
294	0.01	0.007	0.014	0.017	0.02	0.023	0.022
295	0.009	0.007	0.013	0.016	0.02	0.022	0.021
296	0.009	0.007	0.013	0.015	0.02	0.022	0.021
297	0.009	0.007	0.013	0.015	0.02	0.022	0.021
298	0.009	0.007	0.013	0.015	0.02	0.022	0.022
299	0.009	0.008	0.013	0.015	0.02	0.022	0.022
300	0.01	0.009	0.014	0.016	0.021	0.023	0.023

Wavelength (nm)	Comp. 96	0.01 mL	0.02 mL	0.03 mL	0.04 mL	0.05 mL	0.06 mL
198	0.042	0.035	0.061	0.094	0.114	0.134	0.138
199	0.048	0.038	0.07	0.104	0.128	0.146	0.161
200	0.054	0.047	0.087	0.123	0.155	0.177	0.207
201	0.06	0.052	0.101	0.139	0.18	0.204	0.238
202	0.073	0.065	0.131	0.18	0.233	0.268	0.307
203	0.08	0.073	0.144	0.202	0.261	0.303	0.346
204	0.093	0.084	0.169	0.237	0.311	0.366	0.418
205	0.101	0.091	0.185	0.263	0.351	0.412	0.477
206	0.104	0.093	0.19	0.272	0.365	0.429	0.5
207	0.108	0.096	0.197	0.284	0.387	0.457	0.537
208	0.109	0.097	0.199	0.288	0.394	0.467	0.55
209	0.111	0.099	0.203	0.294	0.404	0.481	0.57
210	0.111	0.099	0.203	0.296	0.408	0.487	0.577
211	0.112	0.099	0.204	0.298	0.412	0.494	0.587
212	0.112	0.099	0.204	0.299	0.415	0.497	0.593
213	0.112	0.099	0.204	0.299	0.415	0.498	0.596
214	0.111	0.098	0.204	0.298	0.415	0.499	0.597
215	0.11	0.098	0.203	0.297	0.414	0.498	0.597
216	0.109	0.098	0.202	0.295	0.412	0.496	0.595
217	0.108	0.097	0.201	0.294	0.41	0.494	0.593
218	0.107	0.096	0.198	0.291	0.406	0.489	0.587
219	0.106	0.096	0.196	0.287	0.401	0.482	0.581
220	0.106	0.095	0.194	0.285	0.398	0.479	0.577
221	0.105	0.094	0.191	0.28	0.391	0.47	0.568

222	0.104	0.093	0.189	0.277	0.386	0.465	0.563
223	0.103	0.092	0.185	0.271	0.377	0.455	0.55
224	0.101	0.089	0.18	0.263	0.366	0.442	0.536
225	0.1	0.088	0.178	0.26	0.361	0.435	0.528
226	0.098	0.085	0.172	0.251	0.347	0.419	0.509
227	0.097	0.084	0.168	0.246	0.339	0.41	0.499
228	0.095	0.081	0.162	0.236	0.325	0.394	0.479
229	0.093	0.08	0.159	0.232	0.319	0.386	0.47
230	0.091	0.078	0.154	0.224	0.308	0.373	0.455
231	0.089	0.077	0.15	0.217	0.299	0.362	0.442
232	0.088	0.076	0.148	0.214	0.295	0.356	0.435
233	0.085	0.074	0.143	0.207	0.285	0.345	0.422
234	0.084	0.074	0.141	0.204	0.281	0.339	0.415
235	0.082	0.072	0.136	0.197	0.27	0.326	0.399
236	0.081	0.071	0.134	0.193	0.265	0.319	0.391
237	0.078	0.069	0.128	0.184	0.253	0.303	0.371
238	0.074	0.066	0.121	0.174	0.238	0.284	0.349
239	0.072	0.064	0.117	0.168	0.23	0.275	0.337
240	0.067	0.059	0.108	0.155	0.212	0.254	0.311
241	0.064	0.057	0.104	0.149	0.202	0.243	0.297
242	0.06	0.052	0.096	0.137	0.186	0.223	0.273
243	0.057	0.049	0.089	0.127	0.173	0.207	0.253
244	0.055	0.048	0.087	0.123	0.167	0.2	0.245
245	0.053	0.045	0.081	0.115	0.155	0.186	0.228
246	0.051	0.043	0.078	0.111	0.149	0.179	0.22
247	0.049	0.041	0.073	0.103	0.139	0.166	0.204
248	0.047	0.04	0.069	0.097	0.131	0.156	0.192
249	0.046	0.038	0.066	0.092	0.124	0.147	0.181
250	0.046	0.038	0.064	0.089	0.12	0.142	0.176
251	0.044	0.036	0.061	0.084	0.112	0.132	0.164
252	0.042	0.034	0.057	0.078	0.105	0.123	0.153
253	0.041	0.034	0.056	0.076	0.102	0.119	0.148
254	0.04	0.033	0.053	0.072	0.097	0.112	0.139
255	0.04	0.032	0.052	0.07	0.094	0.108	0.134
256	0.037	0.03	0.047	0.064	0.085	0.098	0.122
257	0.035	0.028	0.044	0.061	0.08	0.092	0.115
258	0.032	0.024	0.039	0.054	0.07	0.082	0.101
259	0.031	0.022	0.037	0.051	0.066	0.077	0.095
260	0.028	0.02	0.033	0.046	0.06	0.07	0.086
261	0.027	0.019	0.031	0.042	0.055	0.065	0.079
262	0.026	0.019	0.03	0.041	0.054	0.063	0.077
263	0.026	0.019	0.029	0.039	0.051	0.059	0.073
264	0.026	0.018	0.029	0.038	0.05	0.058	0.071
265	0.025	0.018	0.028	0.037	0.048	0.054	0.067
266	0.025	0.018	0.027	0.036	0.047	0.052	0.065
267	0.024	0.017	0.025	0.034	0.044	0.048	0.06
268	0.022	0.015	0.023	0.031	0.04	0.044	0.055
269	0.021	0.014	0.022	0.029	0.038	0.042	0.052
270	0.019	0.012	0.019	0.027	0.034	0.038	0.047
271	0.019	0.011	0.018	0.025	0.032	0.037	0.044

272	0.017	0.01	0.017	0.024	0.03	0.034	0.041
273	0.017	0.01	0.016	0.023	0.029	0.033	0.039
274	0.016	0.01	0.015	0.022	0.028	0.031	0.037
275	0.016	0.01	0.015	0.021	0.027	0.03	0.036
276	0.015	0.009	0.014	0.02	0.026	0.029	0.035
277	0.015	0.009	0.014	0.019	0.025	0.028	0.033
278	0.015	0.009	0.013	0.019	0.025	0.027	0.032
279	0.014	0.008	0.013	0.018	0.024	0.026	0.03
280	0.013	0.008	0.012	0.018	0.023	0.025	0.029
281	0.012	0.006	0.01	0.016	0.021	0.023	0.026
282	0.012	0.005	0.01	0.016	0.02	0.022	0.025
283	0.011	0.005	0.009	0.015	0.019	0.021	0.024
284	0.011	0.005	0.009	0.014	0.019	0.02	0.023
285	0.011	0.006	0.009	0.014	0.018	0.02	0.023
286	0.011	0.006	0.009	0.014	0.019	0.02	0.023
287	0.011	0.007	0.01	0.014	0.019	0.019	0.023
288	0.012	0.007	0.01	0.014	0.018	0.019	0.023
289	0.012	0.007	0.01	0.014	0.018	0.019	0.023
290	0.012	0.006	0.009	0.013	0.017	0.018	0.021
291	0.012	0.005	0.008	0.013	0.016	0.017	0.02
292	0.011	0.004	0.007	0.012	0.015	0.016	0.019
293	0.01	0.004	0.007	0.011	0.014	0.015	0.018
294	0.01	0.003	0.007	0.011	0.014	0.015	0.017
295	0.009	0.003	0.006	0.011	0.013	0.015	0.017
296	0.009	0.003	0.006	0.011	0.013	0.014	0.016
297	0.009	0.003	0.006	0.011	0.014	0.014	0.016
298	0.009	0.004	0.007	0.011	0.014	0.015	0.017
299	0.009	0.005	0.007	0.011	0.015	0.015	0.017
300	0.01	0.006	0.008	0.011	0.015	0.015	0.018

Wavelength (nm)	Comp.98	0.01 mL	0.02 mL	0.03 mL	0.04 mL	0.05 mL	0.06 mL
198	0.04	0.045	0.081	0.103	0.131	0.157	0.18
199	0.045	0.047	0.094	0.114	0.145	0.174	0.201
200	0.06	0.05	0.115	0.141	0.178	0.217	0.244
201	0.068	0.055	0.131	0.162	0.208	0.249	0.279
202	0.087	0.068	0.165	0.216	0.279	0.331	0.367
203	0.096	0.075	0.182	0.244	0.317	0.375	0.416
204	0.11	0.09	0.212	0.292	0.384	0.454	0.517
205	0.121	0.101	0.232	0.328	0.434	0.52	0.602
206	0.124	0.105	0.24	0.342	0.452	0.546	0.637
207	0.128	0.11	0.252	0.362	0.48	0.588	0.69
208	0.129	0.113	0.256	0.37	0.489	0.603	0.712
209	0.129	0.117	0.261	0.381	0.505	0.627	0.745
210	0.129	0.119	0.263	0.385	0.511	0.636	0.758
211	0.129	0.121	0.266	0.391	0.519	0.649	0.778
212	0.127	0.123	0.267	0.395	0.524	0.657	0.792

213	0.127	0.124	0.268	0.396	0.525	0.66	0.797
214	0.125	0.125	0.268	0.397	0.525	0.663	0.803
215	0.124	0.125	0.267	0.397	0.525	0.663	0.804
216	0.122	0.125	0.266	0.396	0.522	0.661	0.803
217	0.121	0.125	0.265	0.395	0.521	0.659	0.801
218	0.119	0.125	0.262	0.391	0.515	0.653	0.796
219	0.118	0.124	0.26	0.386	0.508	0.645	0.787
220	0.118	0.123	0.258	0.383	0.505	0.64	0.782
221	0.117	0.122	0.254	0.376	0.496	0.629	0.769
222	0.117	0.121	0.252	0.372	0.491	0.623	0.761
223	0.116	0.119	0.246	0.362	0.48	0.608	0.744
224	0.114	0.116	0.24	0.352	0.467	0.59	0.723
225	0.113	0.115	0.236	0.346	0.459	0.581	0.712
226	0.111	0.111	0.228	0.333	0.443	0.559	0.686
227	0.11	0.109	0.223	0.325	0.433	0.546	0.671
228	0.108	0.105	0.214	0.311	0.415	0.523	0.643
229	0.107	0.104	0.21	0.305	0.406	0.512	0.63
230	0.104	0.101	0.203	0.294	0.391	0.493	0.607
231	0.102	0.099	0.197	0.284	0.377	0.477	0.586
232	0.1	0.097	0.195	0.279	0.371	0.469	0.576
233	0.098	0.095	0.189	0.269	0.359	0.452	0.554
234	0.096	0.094	0.186	0.264	0.352	0.443	0.543
235	0.093	0.091	0.179	0.254	0.337	0.424	0.518
236	0.091	0.089	0.176	0.248	0.329	0.413	0.505
237	0.087	0.086	0.168	0.235	0.311	0.39	0.475
238	0.082	0.081	0.158	0.221	0.29	0.364	0.443
239	0.08	0.079	0.153	0.213	0.279	0.35	0.426
240	0.074	0.073	0.141	0.195	0.257	0.32	0.39
241	0.071	0.07	0.134	0.186	0.245	0.304	0.371
242	0.066	0.064	0.122	0.169	0.223	0.276	0.338
243	0.062	0.06	0.113	0.156	0.205	0.254	0.311
244	0.061	0.058	0.109	0.15	0.197	0.244	0.299
245	0.057	0.054	0.102	0.138	0.182	0.225	0.275
246	0.056	0.052	0.098	0.133	0.175	0.215	0.264
247	0.053	0.049	0.09	0.122	0.161	0.198	0.242
248	0.05	0.046	0.085	0.114	0.15	0.184	0.225
249	0.048	0.044	0.081	0.107	0.14	0.172	0.21
250	0.047	0.043	0.079	0.104	0.135	0.165	0.202
251	0.045	0.04	0.074	0.096	0.125	0.152	0.186
252	0.042	0.038	0.069	0.089	0.116	0.141	0.172
253	0.041	0.037	0.067	0.087	0.112	0.136	0.165
254	0.04	0.035	0.064	0.081	0.104	0.126	0.154
255	0.039	0.034	0.062	0.079	0.1	0.121	0.147
256	0.036	0.031	0.057	0.071	0.091	0.109	0.133
257	0.035	0.03	0.054	0.067	0.086	0.103	0.125
258	0.032	0.026	0.048	0.059	0.077	0.09	0.11
259	0.03	0.025	0.045	0.055	0.072	0.085	0.104
260	0.028	0.022	0.04	0.05	0.065	0.076	0.094
261	0.027	0.021	0.038	0.046	0.06	0.07	0.087
262	0.026	0.02	0.037	0.045	0.057	0.068	0.084

263	0.025	0.019	0.035	0.042	0.055	0.064	0.079
264	0.025	0.019	0.035	0.042	0.053	0.062	0.077
265	0.024	0.018	0.034	0.04	0.051	0.059	0.072
266	0.024	0.018	0.033	0.039	0.049	0.057	0.069
267	0.022	0.017	0.032	0.036	0.045	0.052	0.064
268	0.021	0.016	0.029	0.033	0.041	0.048	0.059
269	0.02	0.015	0.028	0.032	0.04	0.045	0.056
270	0.018	0.013	0.025	0.029	0.037	0.041	0.05
271	0.018	0.013	0.024	0.027	0.035	0.039	0.048
272	0.016	0.012	0.022	0.025	0.032	0.036	0.044
273	0.016	0.012	0.022	0.024	0.031	0.034	0.043
274	0.015	0.011	0.021	0.023	0.029	0.032	0.04
275	0.015	0.011	0.02	0.023	0.028	0.031	0.039
276	0.014	0.01	0.02	0.022	0.027	0.03	0.037
277	0.013	0.01	0.019	0.021	0.025	0.028	0.035
278	0.013	0.01	0.019	0.021	0.024	0.028	0.034
279	0.012	0.009	0.018	0.02	0.023	0.026	0.032
280	0.012	0.009	0.018	0.019	0.022	0.025	0.031
281	0.01	0.008	0.016	0.018	0.021	0.023	0.028
282	0.01	0.008	0.016	0.017	0.02	0.021	0.027
283	0.009	0.007	0.015	0.016	0.018	0.02	0.025
284	0.009	0.007	0.014	0.015	0.017	0.019	0.024
285	0.009	0.007	0.014	0.015	0.017	0.018	0.023
286	0.009	0.007	0.014	0.015	0.016	0.018	0.023
287	0.009	0.007	0.015	0.015	0.016	0.018	0.023
288	0.01	0.007	0.015	0.015	0.016	0.018	0.023
289	0.01	0.007	0.015	0.015	0.016	0.018	0.022
290	0.01	0.007	0.015	0.014	0.016	0.017	0.021
291	0.01	0.006	0.014	0.013	0.016	0.016	0.02
292	0.01	0.006	0.013	0.012	0.015	0.016	0.019
293	0.009	0.005	0.013	0.012	0.014	0.014	0.018
294	0.009	0.005	0.012	0.011	0.014	0.014	0.018
295	0.008	0.005	0.012	0.011	0.013	0.013	0.017
296	0.007	0.005	0.011	0.011	0.012	0.013	0.016
297	0.006	0.005	0.011	0.011	0.011	0.012	0.015
298	0.006	0.005	0.011	0.011	0.011	0.012	0.015
299	0.006	0.005	0.011	0.011	0.011	0.012	0.015
300	0.007	0.005	0.012	0.011	0.011	0.012	0.015

Wavelength (nm)	Comp.98	0.01 mL	0.02 mL	0.03 mL	0.04 mL	0.05 mL	0.06 mL
198	0.04	0.047	0.072	0.101	0.13	0.14	0.176
199	0.045	0.051	0.081	0.115	0.15	0.155	0.188
200	0.06	0.057	0.103	0.142	0.182	0.196	0.227
201	0.068	0.062	0.118	0.167	0.211	0.225	0.265
202	0.087	0.078	0.155	0.22	0.283	0.314	0.363
203	0.096	0.086	0.173	0.248	0.319	0.36	0.419

204	0.11	0.1	0.204	0.3	0.387	0.448	0.518
205	0.121	0.109	0.227	0.338	0.44	0.517	0.603
206	0.124	0.113	0.235	0.353	0.458	0.544	0.636
207	0.128	0.117	0.247	0.375	0.486	0.586	0.691
208	0.129	0.119	0.251	0.382	0.496	0.602	0.711
209	0.129	0.121	0.257	0.392	0.511	0.626	0.747
210	0.129	0.122	0.258	0.396	0.517	0.635	0.758
211	0.129	0.123	0.261	0.402	0.525	0.649	0.779
212	0.127	0.123	0.262	0.405	0.53	0.658	0.793
213	0.127	0.123	0.263	0.406	0.532	0.661	0.799
214	0.125	0.124	0.263	0.407	0.533	0.665	0.805
215	0.124	0.124	0.263	0.407	0.532	0.665	0.807
216	0.122	0.124	0.261	0.406	0.53	0.663	0.806
217	0.121	0.124	0.26	0.404	0.528	0.662	0.804
218	0.119	0.123	0.258	0.4	0.523	0.656	0.799
219	0.118	0.122	0.255	0.395	0.516	0.647	0.789
220	0.118	0.121	0.253	0.392	0.512	0.642	0.784
221	0.117	0.119	0.249	0.385	0.502	0.63	0.77
222	0.117	0.119	0.247	0.381	0.497	0.623	0.762
223	0.116	0.117	0.241	0.371	0.485	0.607	0.743
224	0.114	0.114	0.234	0.36	0.471	0.589	0.722
225	0.113	0.113	0.231	0.354	0.463	0.579	0.71
226	0.111	0.109	0.222	0.34	0.446	0.556	0.682
227	0.11	0.107	0.217	0.332	0.436	0.543	0.667
228	0.108	0.104	0.208	0.318	0.416	0.518	0.637
229	0.107	0.102	0.204	0.311	0.407	0.507	0.623
230	0.104	0.1	0.198	0.301	0.392	0.489	0.6
231	0.102	0.098	0.193	0.291	0.378	0.472	0.58
232	0.1	0.096	0.19	0.286	0.372	0.464	0.57
233	0.098	0.094	0.185	0.277	0.359	0.447	0.55
234	0.096	0.092	0.182	0.272	0.352	0.438	0.539
235	0.093	0.09	0.175	0.261	0.337	0.419	0.515
236	0.091	0.088	0.172	0.255	0.328	0.408	0.502
237	0.087	0.085	0.163	0.242	0.31	0.384	0.473
238	0.082	0.081	0.154	0.227	0.289	0.358	0.441
239	0.08	0.079	0.148	0.219	0.278	0.344	0.424
240	0.074	0.073	0.135	0.2	0.255	0.313	0.387
241	0.071	0.07	0.129	0.19	0.243	0.298	0.368
242	0.066	0.064	0.117	0.173	0.221	0.269	0.333
243	0.062	0.06	0.108	0.159	0.202	0.247	0.306
244	0.061	0.058	0.104	0.153	0.195	0.237	0.294
245	0.057	0.054	0.097	0.142	0.179	0.217	0.27
246	0.056	0.052	0.093	0.136	0.172	0.208	0.258
247	0.053	0.049	0.085	0.125	0.158	0.19	0.237
248	0.05	0.046	0.08	0.117	0.146	0.176	0.22
249	0.048	0.044	0.076	0.11	0.136	0.163	0.205
250	0.047	0.043	0.074	0.106	0.131	0.157	0.197
251	0.045	0.041	0.069	0.099	0.121	0.144	0.181
252	0.042	0.038	0.065	0.092	0.111	0.132	0.167
253	0.041	0.037	0.063	0.089	0.107	0.127	0.16

254	0.04	0.036	0.06	0.083	0.099	0.117	0.149
255	0.039	0.035	0.058	0.081	0.095	0.112	0.142
256	0.036	0.032	0.052	0.073	0.086	0.099	0.127
257	0.035	0.03	0.049	0.068	0.081	0.093	0.12
258	0.032	0.026	0.042	0.059	0.072	0.08	0.104
259	0.03	0.024	0.039	0.056	0.067	0.075	0.098
260	0.028	0.022	0.035	0.05	0.06	0.066	0.088
261	0.027	0.021	0.033	0.046	0.054	0.061	0.081
262	0.026	0.02	0.032	0.045	0.052	0.058	0.078
263	0.025	0.019	0.031	0.043	0.049	0.054	0.073
264	0.025	0.019	0.031	0.042	0.048	0.053	0.071
265	0.024	0.019	0.03	0.04	0.045	0.049	0.066
266	0.024	0.018	0.029	0.039	0.043	0.047	0.064
267	0.022	0.017	0.027	0.036	0.04	0.042	0.059
268	0.021	0.016	0.025	0.033	0.036	0.038	0.053
269	0.02	0.015	0.023	0.032	0.035	0.035	0.051
270	0.018	0.013	0.02	0.028	0.032	0.031	0.045
271	0.018	0.013	0.019	0.027	0.03	0.029	0.043
272	0.016	0.012	0.018	0.024	0.027	0.027	0.04
273	0.016	0.012	0.017	0.024	0.026	0.025	0.038
274	0.015	0.011	0.016	0.022	0.024	0.023	0.036
275	0.015	0.011	0.016	0.022	0.024	0.022	0.035
276	0.014	0.011	0.015	0.021	0.022	0.021	0.033
277	0.013	0.01	0.015	0.02	0.021	0.019	0.031
278	0.013	0.01	0.015	0.02	0.02	0.019	0.03
279	0.012	0.01	0.014	0.019	0.019	0.017	0.029
280	0.012	0.009	0.013	0.018	0.018	0.016	0.027
281	0.01	0.008	0.012	0.016	0.017	0.014	0.025
282	0.01	0.008	0.011	0.015	0.016	0.013	0.024
283	0.009	0.008	0.01	0.014	0.015	0.012	0.022
284	0.009	0.007	0.01	0.014	0.014	0.011	0.021
285	0.009	0.007	0.01	0.014	0.014	0.011	0.021
286	0.009	0.007	0.01	0.014	0.013	0.01	0.02
287	0.009	0.007	0.01	0.014	0.013	0.01	0.02
288	0.01	0.008	0.01	0.014	0.012	0.009	0.019
289	0.01	0.007	0.01	0.014	0.012	0.009	0.019
290	0.01	0.007	0.01	0.013	0.012	0.008	0.017
291	0.01	0.007	0.009	0.012	0.011	0.007	0.016
292	0.01	0.006	0.009	0.011	0.011	0.006	0.015
293	0.009	0.006	0.008	0.01	0.01	0.005	0.014
294	0.009	0.006	0.008	0.01	0.009	0.005	0.014
295	0.008	0.005	0.007	0.009	0.009	0.004	0.013
296	0.007	0.005	0.007	0.009	0.009	0.004	0.013
297	0.006	0.005	0.007	0.009	0.008	0.004	0.013
298	0.006	0.005	0.007	0.01	0.008	0.004	0.013
299	0.006	0.006	0.007	0.01	0.008	0.004	0.013
300	0.007	0.006	0.008	0.01	0.007	0.004	0.013

Wavelength (nm)	Comp. 103	0.01 mL	0.02 mL	0.03 mL	0.04 mL	0.05 mL	0.06 mL
198	0.135	0.12	0.128	0.169	0.194	0.213	0.243
199	0.149	0.133	0.145	0.189	0.217	0.236	0.267
200	0.185	0.166	0.186	0.234	0.273	0.297	0.323
201	0.212	0.189	0.219	0.272	0.322	0.346	0.369
202	0.274	0.244	0.296	0.375	0.438	0.476	0.496
203	0.306	0.272	0.336	0.43	0.506	0.549	0.572
204	0.362	0.322	0.408	0.539	0.642	0.693	0.724
205	0.403	0.358	0.463	0.628	0.76	0.826	0.873
206	0.417	0.371	0.487	0.66	0.812	0.888	0.94
207	0.437	0.389	0.52	0.716	0.896	0.994	1.058
208	0.443	0.395	0.532	0.739	0.924	1.042	1.112
209	0.451	0.402	0.551	0.771	0.976	1.122	1.205
210	0.453	0.404	0.557	0.782	0.997	1.152	1.244
211	0.453	0.405	0.563	0.796	1.025	1.196	1.313
212	0.449	0.403	0.564	0.798	1.041	1.224	1.362
213	0.446	0.401	0.561	0.797	1.043	1.231	1.379
214	0.438	0.394	0.553	0.786	1.035	1.237	1.402
215	0.433	0.39	0.547	0.779	1.028	1.235	1.408
216	0.422	0.38	0.534	0.76	1.007	1.221	1.406
217	0.415	0.375	0.526	0.748	0.993	1.209	1.401
218	0.401	0.363	0.507	0.721	0.96	1.175	1.377
219	0.386	0.349	0.485	0.688	0.919	1.128	1.334
220	0.378	0.342	0.472	0.67	0.895	1.1	1.306
221	0.361	0.326	0.444	0.63	0.843	1.038	1.237
222	0.352	0.317	0.43	0.609	0.814	1.005	1.2
223	0.333	0.3	0.4	0.566	0.758	0.937	1.123
224	0.314	0.282	0.371	0.525	0.703	0.872	1.046
225	0.305	0.274	0.357	0.505	0.678	0.842	1.011
226	0.288	0.258	0.331	0.468	0.63	0.784	0.941
227	0.279	0.25	0.318	0.451	0.607	0.757	0.909
228	0.265	0.237	0.298	0.423	0.57	0.711	0.854
229	0.259	0.232	0.29	0.412	0.556	0.692	0.832
230	0.25	0.224	0.278	0.396	0.532	0.662	0.798
231	0.244	0.219	0.27	0.383	0.515	0.639	0.772
232	0.242	0.216	0.266	0.377	0.507	0.629	0.76
233	0.236	0.212	0.259	0.367	0.492	0.61	0.737
234	0.234	0.209	0.256	0.361	0.485	0.6	0.725
235	0.228	0.205	0.249	0.35	0.469	0.58	0.7
236	0.225	0.203	0.245	0.344	0.46	0.569	0.686
237	0.219	0.197	0.237	0.331	0.442	0.544	0.657
238	0.211	0.19	0.226	0.316	0.421	0.517	0.624
239	0.206	0.186	0.221	0.308	0.41	0.503	0.607
240	0.196	0.177	0.208	0.29	0.387	0.475	0.57
241	0.19	0.173	0.201	0.281	0.374	0.46	0.55
242	0.181	0.165	0.189	0.264	0.352	0.432	0.515
243	0.174	0.158	0.179	0.25	0.333	0.407	0.485
244	0.171	0.156	0.175	0.244	0.324	0.397	0.473
245	0.165	0.15	0.167	0.232	0.308	0.376	0.447

246	0.162	0.148	0.163	0.226	0.3	0.366	0.433
247	0.157	0.143	0.155	0.215	0.285	0.346	0.409
248	0.154	0.14	0.149	0.206	0.272	0.329	0.389
249	0.151	0.137	0.144	0.198	0.26	0.313	0.37
250	0.149	0.135	0.142	0.194	0.254	0.305	0.361
251	0.146	0.132	0.136	0.185	0.242	0.289	0.342
252	0.143	0.128	0.131	0.177	0.23	0.275	0.324
253	0.141	0.127	0.129	0.174	0.225	0.268	0.316
254	0.139	0.125	0.124	0.167	0.215	0.254	0.3
255	0.138	0.123	0.122	0.163	0.21	0.247	0.291
256	0.134	0.119	0.115	0.153	0.198	0.233	0.271
257	0.131	0.116	0.111	0.148	0.191	0.225	0.261
258	0.125	0.111	0.104	0.138	0.178	0.21	0.24
259	0.122	0.108	0.1	0.133	0.172	0.203	0.23
260	0.118	0.104	0.095	0.125	0.161	0.189	0.214
261	0.115	0.101	0.091	0.119	0.152	0.178	0.201
262	0.114	0.1	0.089	0.117	0.149	0.173	0.196
263	0.113	0.099	0.087	0.112	0.143	0.165	0.187
264	0.113	0.098	0.086	0.11	0.14	0.161	0.182
265	0.111	0.096	0.083	0.106	0.133	0.153	0.172
266	0.11	0.095	0.081	0.103	0.13	0.148	0.166
267	0.108	0.093	0.077	0.097	0.122	0.138	0.154
268	0.105	0.089	0.073	0.091	0.114	0.128	0.142
269	0.103	0.087	0.071	0.088	0.11	0.124	0.135
270	0.099	0.084	0.066	0.081	0.102	0.115	0.123
271	0.097	0.082	0.064	0.078	0.098	0.111	0.117
272	0.094	0.079	0.06	0.073	0.091	0.102	0.107
273	0.093	0.078	0.059	0.07	0.087	0.098	0.102
274	0.091	0.076	0.056	0.066	0.082	0.091	0.095
275	0.09	0.075	0.055	0.065	0.08	0.089	0.091
276	0.089	0.074	0.053	0.062	0.076	0.084	0.085
277	0.088	0.073	0.052	0.059	0.072	0.079	0.081
278	0.087	0.072	0.051	0.058	0.071	0.077	0.078
279	0.085	0.07	0.05	0.056	0.068	0.074	0.074
280	0.084	0.069	0.049	0.054	0.066	0.072	0.072
281	0.082	0.067	0.047	0.052	0.063	0.07	0.067
282	0.081	0.066	0.046	0.05	0.062	0.068	0.066
283	0.079	0.065	0.044	0.048	0.059	0.065	0.062
284	0.078	0.064	0.043	0.047	0.057	0.063	0.06
285	0.078	0.064	0.043	0.046	0.057	0.061	0.059
286	0.077	0.063	0.042	0.046	0.055	0.059	0.057
287	0.077	0.063	0.042	0.046	0.055	0.058	0.056
288	0.076	0.063	0.042	0.046	0.054	0.057	0.055
289	0.076	0.062	0.041	0.045	0.054	0.056	0.054
290	0.074	0.061	0.04	0.044	0.053	0.055	0.052
291	0.072	0.06	0.039	0.043	0.051	0.053	0.05
292	0.071	0.059	0.038	0.043	0.051	0.053	0.049
293	0.069	0.057	0.037	0.041	0.049	0.051	0.047
294	0.068	0.057	0.036	0.04	0.048	0.05	0.046
295	0.067	0.055	0.035	0.039	0.046	0.049	0.044

296	0.066	0.055	0.035	0.038	0.046	0.048	0.044
297	0.065	0.053	0.034	0.037	0.044	0.046	0.043
298	0.064	0.053	0.034	0.036	0.043	0.044	0.042
299	0.064	0.053	0.034	0.036	0.042	0.044	0.042
300	0.064	0.053	0.034	0.036	0.042	0.042	0.041

Wavelength (nm)	Comp. 103	0.01 mL	0.02 mL	0.03 mL	0.04 mL	0.05 mL	0.06 mL
198	0.135	0.117	0.133	0.169	0.181	0.219	0.235
199	0.149	0.136	0.152	0.192	0.203	0.244	0.258
200	0.185	0.171	0.197	0.235	0.259	0.3	0.314
201	0.212	0.197	0.229	0.273	0.306	0.346	0.361
202	0.274	0.256	0.311	0.373	0.425	0.472	0.485
203	0.306	0.287	0.353	0.426	0.493	0.547	0.562
204	0.362	0.336	0.434	0.538	0.629	0.697	0.723
205	0.403	0.371	0.493	0.63	0.748	0.838	0.871
206	0.417	0.383	0.516	0.666	0.799	0.901	0.94
207	0.437	0.401	0.548	0.722	0.885	1.01	1.055
208	0.443	0.406	0.56	0.741	0.922	1.053	1.105
209	0.451	0.413	0.578	0.772	0.982	1.128	1.195
210	0.453	0.413	0.584	0.784	1.004	1.159	1.231
211	0.453	0.413	0.589	0.798	1.033	1.208	1.298
212	0.449	0.41	0.588	0.801	1.047	1.243	1.346
213	0.446	0.407	0.585	0.798	1.048	1.256	1.361
214	0.438	0.4	0.575	0.787	1.043	1.264	1.379
215	0.433	0.396	0.569	0.779	1.037	1.262	1.383
216	0.422	0.386	0.554	0.76	1.016	1.246	1.38
217	0.415	0.38	0.545	0.749	1.004	1.234	1.374
218	0.401	0.367	0.525	0.722	0.971	1.2	1.348
219	0.386	0.353	0.502	0.688	0.929	1.155	1.303
220	0.378	0.345	0.489	0.67	0.904	1.127	1.274
221	0.361	0.327	0.46	0.629	0.85	1.063	1.206
222	0.352	0.318	0.445	0.607	0.822	1.028	1.169
223	0.333	0.3	0.414	0.564	0.764	0.959	1.093
224	0.314	0.281	0.384	0.521	0.709	0.893	1.019
225	0.305	0.272	0.369	0.501	0.683	0.862	0.983
226	0.288	0.255	0.342	0.464	0.634	0.803	0.915
227	0.279	0.247	0.329	0.447	0.612	0.775	0.883
228	0.265	0.233	0.309	0.418	0.573	0.726	0.829
229	0.259	0.228	0.301	0.407	0.558	0.706	0.808
230	0.25	0.22	0.288	0.389	0.533	0.675	0.775
231	0.244	0.214	0.279	0.376	0.514	0.65	0.749
232	0.242	0.212	0.275	0.37	0.506	0.64	0.738
233	0.236	0.207	0.268	0.359	0.49	0.62	0.715
234	0.234	0.205	0.264	0.354	0.482	0.61	0.704
235	0.228	0.201	0.257	0.342	0.466	0.589	0.68
236	0.225	0.199	0.253	0.336	0.458	0.578	0.667
237	0.219	0.194	0.244	0.323	0.438	0.552	0.638
238	0.211	0.187	0.233	0.308	0.417	0.525	0.607

239	0.206	0.183	0.227	0.3	0.406	0.511	0.59
240	0.196	0.174	0.214	0.282	0.383	0.483	0.554
241	0.19	0.169	0.207	0.273	0.371	0.468	0.535
242	0.181	0.161	0.195	0.257	0.349	0.439	0.5
243	0.174	0.154	0.186	0.243	0.329	0.414	0.472
244	0.171	0.152	0.181	0.237	0.32	0.403	0.46
245	0.165	0.146	0.173	0.225	0.304	0.382	0.435
246	0.162	0.144	0.169	0.219	0.296	0.371	0.422
247	0.157	0.139	0.161	0.208	0.28	0.351	0.398
248	0.154	0.135	0.155	0.198	0.266	0.332	0.379
249	0.151	0.133	0.149	0.19	0.254	0.315	0.361
250	0.149	0.131	0.146	0.185	0.247	0.307	0.352
251	0.146	0.127	0.141	0.177	0.235	0.291	0.333
252	0.143	0.124	0.135	0.169	0.223	0.276	0.316
253	0.141	0.123	0.133	0.165	0.218	0.269	0.308
254	0.139	0.121	0.128	0.158	0.207	0.255	0.293
255	0.138	0.119	0.125	0.154	0.202	0.248	0.284
256	0.134	0.115	0.119	0.145	0.19	0.233	0.265
257	0.131	0.112	0.115	0.14	0.184	0.226	0.255
258	0.125	0.106	0.108	0.13	0.171	0.211	0.235
259	0.122	0.103	0.104	0.126	0.165	0.204	0.225
260	0.118	0.099	0.098	0.118	0.154	0.19	0.209
261	0.115	0.096	0.094	0.112	0.145	0.178	0.197
262	0.114	0.095	0.092	0.109	0.141	0.173	0.192
263	0.113	0.093	0.09	0.105	0.135	0.164	0.183
264	0.113	0.093	0.088	0.103	0.132	0.161	0.179
265	0.111	0.092	0.086	0.098	0.125	0.152	0.168
266	0.11	0.09	0.084	0.095	0.121	0.147	0.163
267	0.108	0.088	0.08	0.089	0.113	0.137	0.151
268	0.105	0.084	0.075	0.083	0.105	0.127	0.139
269	0.103	0.082	0.073	0.08	0.101	0.123	0.133
270	0.099	0.078	0.068	0.074	0.094	0.114	0.121
271	0.097	0.077	0.066	0.072	0.09	0.11	0.115
272	0.094	0.074	0.062	0.066	0.083	0.101	0.104
273	0.093	0.073	0.061	0.064	0.08	0.097	0.1
274	0.091	0.071	0.058	0.06	0.074	0.09	0.093
275	0.09	0.071	0.057	0.058	0.072	0.087	0.09
276	0.089	0.069	0.055	0.055	0.068	0.082	0.084
277	0.088	0.068	0.053	0.053	0.064	0.078	0.079
278	0.087	0.068	0.053	0.052	0.062	0.076	0.077
279	0.085	0.066	0.051	0.05	0.059	0.072	0.073
280	0.084	0.065	0.05	0.048	0.058	0.071	0.07
281	0.082	0.063	0.048	0.046	0.055	0.069	0.066
282	0.081	0.062	0.047	0.045	0.054	0.067	0.064
283	0.079	0.06	0.045	0.043	0.051	0.064	0.061
284	0.078	0.06	0.044	0.042	0.049	0.062	0.058
285	0.078	0.059	0.044	0.041	0.049	0.06	0.057
286	0.077	0.059	0.043	0.04	0.047	0.058	0.056
287	0.077	0.059	0.043	0.04	0.046	0.057	0.055
288	0.076	0.059	0.042	0.039	0.045	0.055	0.054

289	0.076	0.058	0.042	0.039	0.045	0.054	0.053
290	0.074	0.057	0.041	0.038	0.044	0.052	0.051
291	0.072	0.055	0.04	0.036	0.042	0.051	0.048
292	0.071	0.054	0.039	0.036	0.041	0.05	0.047
293	0.069	0.052	0.038	0.035	0.04	0.049	0.045
294	0.068	0.051	0.037	0.034	0.039	0.048	0.044
295	0.067	0.05	0.036	0.033	0.038	0.047	0.043
296	0.066	0.05	0.036	0.032	0.037	0.046	0.042
297	0.065	0.049	0.035	0.031	0.035	0.045	0.041
298	0.064	0.049	0.034	0.03	0.034	0.043	0.041
299	0.064	0.049	0.034	0.03	0.034	0.042	0.04
300	0.064	0.049	0.034	0.03	0.033	0.041	0.04

Wavelength (nm)	Comp 106	0.01 mL	0.02 mL	0.03 mL	0.04 mL	0.05 mL	0.06 mL
198	0.065	0.044	0.094	0.098	0.136	0.184	0.188
199	0.069	0.047	0.101	0.104	0.144	0.195	0.204
200	0.077	0.046	0.119	0.125	0.175	0.222	0.241
201	0.085	0.05	0.133	0.141	0.2	0.247	0.268
202	0.108	0.059	0.169	0.185	0.262	0.318	0.356
203	0.12	0.065	0.186	0.207	0.294	0.358	0.404
204	0.14	0.079	0.221	0.244	0.355	0.44	0.498
205	0.154	0.089	0.247	0.274	0.405	0.508	0.577
206	0.159	0.094	0.257	0.287	0.424	0.536	0.611
207	0.166	0.101	0.272	0.306	0.454	0.581	0.663
208	0.168	0.105	0.276	0.314	0.465	0.598	0.685
209	0.171	0.11	0.283	0.325	0.481	0.623	0.719
210	0.172	0.112	0.285	0.329	0.487	0.633	0.732
211	0.173	0.115	0.288	0.334	0.495	0.648	0.753
212	0.173	0.117	0.29	0.339	0.501	0.658	0.766
213	0.172	0.117	0.29	0.34	0.503	0.662	0.771
214	0.172	0.119	0.29	0.343	0.506	0.667	0.778
215	0.171	0.12	0.29	0.344	0.507	0.669	0.781
216	0.17	0.121	0.289	0.344	0.508	0.669	0.783
217	0.17	0.122	0.288	0.344	0.507	0.669	0.783
218	0.168	0.122	0.286	0.342	0.506	0.668	0.782
219	0.165	0.121	0.283	0.34	0.502	0.664	0.778
220	0.164	0.121	0.281	0.339	0.5	0.662	0.775
221	0.16	0.12	0.277	0.335	0.495	0.657	0.769
222	0.159	0.119	0.275	0.333	0.491	0.653	0.764
223	0.155	0.117	0.27	0.327	0.483	0.644	0.754
224	0.151	0.115	0.264	0.32	0.474	0.633	0.742
225	0.148	0.113	0.26	0.316	0.469	0.626	0.734
226	0.144	0.11	0.253	0.307	0.457	0.611	0.717
227	0.141	0.109	0.248	0.303	0.45	0.602	0.707
228	0.137	0.106	0.241	0.294	0.437	0.586	0.687
229	0.135	0.105	0.238	0.29	0.431	0.578	0.677

230	0.133	0.103	0.233	0.283	0.42	0.565	0.661
231	0.13	0.101	0.229	0.276	0.41	0.553	0.647
232	0.129	0.1	0.226	0.273	0.405	0.547	0.64
233	0.126	0.097	0.221	0.266	0.395	0.534	0.624
234	0.124	0.095	0.218	0.262	0.389	0.527	0.616
235	0.121	0.092	0.212	0.254	0.377	0.511	0.597
236	0.119	0.091	0.209	0.25	0.37	0.502	0.586
237	0.115	0.088	0.202	0.241	0.356	0.481	0.563
238	0.111	0.085	0.195	0.23	0.339	0.459	0.536
239	0.109	0.083	0.19	0.225	0.33	0.447	0.522
240	0.103	0.079	0.179	0.211	0.31	0.419	0.489
241	0.1	0.076	0.173	0.203	0.299	0.404	0.472
242	0.094	0.071	0.162	0.189	0.279	0.376	0.439
243	0.089	0.067	0.153	0.177	0.261	0.353	0.412
244	0.087	0.065	0.149	0.172	0.254	0.343	0.4
245	0.082	0.061	0.141	0.161	0.238	0.322	0.376
246	0.08	0.059	0.137	0.156	0.23	0.312	0.363
247	0.075	0.054	0.129	0.145	0.214	0.291	0.339
248	0.072	0.051	0.123	0.137	0.202	0.274	0.319
249	0.069	0.049	0.117	0.129	0.19	0.259	0.302
250	0.067	0.047	0.115	0.125	0.184	0.252	0.293
251	0.064	0.044	0.108	0.117	0.172	0.235	0.274
252	0.06	0.041	0.102	0.109	0.16	0.22	0.255
253	0.059	0.039	0.1	0.106	0.155	0.213	0.247
254	0.056	0.037	0.095	0.099	0.145	0.199	0.231
255	0.054	0.036	0.092	0.096	0.139	0.192	0.223
256	0.05	0.032	0.086	0.087	0.127	0.175	0.204
257	0.048	0.03	0.081	0.083	0.12	0.166	0.193
258	0.043	0.026	0.073	0.073	0.107	0.147	0.172
259	0.041	0.024	0.069	0.068	0.101	0.139	0.162
260	0.038	0.022	0.064	0.062	0.092	0.126	0.147
261	0.036	0.02	0.06	0.057	0.085	0.117	0.136
262	0.035	0.019	0.059	0.055	0.082	0.114	0.132
263	0.033	0.017	0.056	0.051	0.076	0.107	0.124
264	0.032	0.016	0.055	0.05	0.074	0.104	0.121
265	0.031	0.015	0.052	0.047	0.069	0.097	0.113
266	0.03	0.014	0.051	0.045	0.066	0.093	0.109
267	0.028	0.013	0.048	0.042	0.061	0.086	0.1
268	0.027	0.012	0.045	0.038	0.056	0.079	0.092
269	0.026	0.011	0.043	0.036	0.054	0.075	0.087
270	0.023	0.009	0.04	0.032	0.049	0.068	0.079
271	0.023	0.009	0.038	0.03	0.046	0.064	0.076
272	0.021	0.008	0.036	0.028	0.043	0.059	0.07
273	0.021	0.008	0.035	0.027	0.042	0.057	0.067
274	0.02	0.007	0.034	0.025	0.039	0.054	0.063
275	0.02	0.007	0.034	0.025	0.038	0.052	0.061
276	0.019	0.006	0.032	0.023	0.036	0.049	0.057
277	0.019	0.006	0.032	0.022	0.034	0.046	0.054
278	0.018	0.006	0.031	0.022	0.033	0.045	0.053
279	0.018	0.005	0.03	0.02	0.031	0.042	0.05

280	0.017	0.005	0.029	0.019	0.03	0.04	0.048
281	0.016	0.004	0.027	0.018	0.028	0.037	0.044
282	0.015	0.004	0.026	0.017	0.027	0.035	0.042
283	0.014	0.003	0.025	0.016	0.025	0.033	0.04
284	0.014	0.003	0.024	0.015	0.024	0.032	0.038
285	0.014	0.003	0.024	0.015	0.024	0.031	0.037
286	0.014	0.003	0.024	0.014	0.023	0.03	0.036
287	0.014	0.003	0.024	0.014	0.022	0.03	0.035
288	0.014	0.003	0.024	0.014	0.022	0.03	0.035
289	0.014	0.003	0.024	0.014	0.021	0.029	0.034
290	0.013	0.003	0.023	0.013	0.02	0.028	0.033
291	0.013	0.003	0.022	0.012	0.019	0.027	0.031
292	0.012	0.003	0.021	0.012	0.019	0.026	0.03
293	0.012	0.002	0.02	0.011	0.018	0.024	0.029
294	0.012	0.002	0.02	0.011	0.018	0.024	0.028
295	0.011	0.002	0.02	0.011	0.017	0.023	0.027
296	0.011	0.002	0.02	0.011	0.017	0.022	0.026
297	0.012	0.002	0.02	0.011	0.017	0.022	0.026
298	0.012	0.003	0.02	0.011	0.017	0.022	0.025
299	0.012	0.003	0.021	0.011	0.017	0.022	0.025
300	0.013	0.003	0.021	0.011	0.017	0.022	0.026

Wavelength (nm)	Comp. 106	0.01 mL	0.02 mL	0.03 mL	0.04 mL	0.05 mL	0.06 mL
198	0.065	0.043	0.097	0.104	0.146	0.169	0.193
199	0.069	0.049	0.1	0.117	0.157	0.183	0.208
200	0.077	0.054	0.121	0.144	0.19	0.223	0.253
201	0.085	0.058	0.137	0.158	0.216	0.25	0.281
202	0.108	0.07	0.178	0.204	0.277	0.321	0.362
203	0.12	0.077	0.199	0.228	0.308	0.363	0.409
204	0.14	0.092	0.237	0.273	0.372	0.448	0.504
205	0.154	0.102	0.262	0.309	0.426	0.522	0.587
206	0.159	0.106	0.271	0.323	0.446	0.552	0.622
207	0.166	0.111	0.285	0.341	0.476	0.597	0.673
208	0.168	0.113	0.29	0.347	0.487	0.613	0.693
209	0.171	0.117	0.297	0.357	0.504	0.637	0.725
210	0.172	0.118	0.3	0.361	0.509	0.647	0.738
211	0.173	0.119	0.302	0.367	0.518	0.661	0.758
212	0.173	0.12	0.303	0.371	0.524	0.672	0.771
213	0.172	0.121	0.303	0.372	0.526	0.676	0.776
214	0.172	0.121	0.302	0.374	0.528	0.682	0.782
215	0.171	0.122	0.302	0.375	0.529	0.683	0.784
216	0.17	0.122	0.3	0.375	0.529	0.685	0.786
217	0.17	0.123	0.299	0.374	0.528	0.685	0.786
218	0.168	0.122	0.297	0.372	0.526	0.684	0.785
219	0.165	0.122	0.293	0.369	0.522	0.679	0.78
220	0.164	0.121	0.291	0.368	0.52	0.677	0.777
221	0.16	0.12	0.287	0.363	0.514	0.67	0.77

222	0.159	0.119	0.284	0.36	0.511	0.665	0.765
223	0.155	0.117	0.278	0.354	0.503	0.655	0.755
224	0.151	0.115	0.272	0.346	0.493	0.643	0.742
225	0.148	0.114	0.268	0.342	0.487	0.636	0.734
226	0.144	0.111	0.26	0.332	0.474	0.62	0.716
227	0.141	0.11	0.255	0.327	0.467	0.611	0.706
228	0.137	0.107	0.248	0.317	0.453	0.593	0.686
229	0.135	0.106	0.245	0.312	0.447	0.585	0.677
230	0.133	0.103	0.24	0.305	0.436	0.57	0.661
231	0.13	0.101	0.235	0.299	0.426	0.557	0.646
232	0.129	0.1	0.233	0.295	0.42	0.551	0.639
233	0.126	0.097	0.227	0.288	0.409	0.537	0.623
234	0.124	0.095	0.224	0.284	0.403	0.529	0.614
235	0.121	0.092	0.218	0.275	0.391	0.512	0.595
236	0.119	0.09	0.215	0.27	0.384	0.503	0.584
237	0.115	0.088	0.208	0.26	0.368	0.482	0.561
238	0.111	0.085	0.2	0.249	0.351	0.459	0.535
239	0.109	0.083	0.195	0.242	0.342	0.446	0.52
240	0.103	0.078	0.184	0.227	0.321	0.419	0.488
241	0.1	0.076	0.177	0.218	0.31	0.404	0.47
242	0.094	0.071	0.165	0.203	0.288	0.375	0.437
243	0.089	0.067	0.156	0.19	0.27	0.352	0.41
244	0.087	0.065	0.152	0.185	0.262	0.341	0.398
245	0.082	0.061	0.144	0.173	0.246	0.32	0.374
246	0.08	0.059	0.14	0.167	0.237	0.309	0.361
247	0.075	0.054	0.131	0.156	0.221	0.288	0.337
248	0.072	0.051	0.125	0.146	0.208	0.27	0.317
249	0.069	0.048	0.119	0.139	0.196	0.254	0.3
250	0.067	0.046	0.117	0.135	0.189	0.245	0.29
251	0.064	0.043	0.11	0.126	0.176	0.228	0.271
252	0.06	0.04	0.104	0.117	0.164	0.212	0.253
253	0.059	0.038	0.101	0.113	0.159	0.205	0.245
254	0.056	0.036	0.096	0.106	0.148	0.191	0.229
255	0.054	0.034	0.094	0.103	0.143	0.183	0.221
256	0.05	0.031	0.086	0.093	0.13	0.166	0.201
257	0.048	0.029	0.082	0.088	0.123	0.157	0.19
258	0.043	0.025	0.073	0.077	0.109	0.139	0.169
259	0.041	0.024	0.069	0.072	0.103	0.132	0.159
260	0.038	0.021	0.063	0.065	0.093	0.119	0.145
261	0.036	0.019	0.06	0.06	0.086	0.11	0.134
262	0.035	0.018	0.058	0.058	0.083	0.106	0.13
263	0.033	0.016	0.056	0.054	0.078	0.099	0.122
264	0.032	0.015	0.054	0.053	0.075	0.095	0.118
265	0.031	0.014	0.052	0.049	0.07	0.088	0.11
266	0.03	0.013	0.05	0.047	0.067	0.084	0.106
267	0.028	0.012	0.047	0.044	0.062	0.076	0.098
268	0.027	0.011	0.044	0.04	0.056	0.069	0.089
269	0.026	0.01	0.042	0.038	0.054	0.066	0.085
270	0.023	0.008	0.038	0.033	0.048	0.059	0.077
271	0.023	0.008	0.037	0.031	0.046	0.057	0.073

272	0.021	0.007	0.034	0.029	0.043	0.052	0.067
273	0.021	0.007	0.034	0.028	0.041	0.05	0.065
274	0.02	0.006	0.033	0.026	0.039	0.046	0.061
275	0.02	0.006	0.032	0.025	0.037	0.045	0.059
276	0.019	0.005	0.031	0.024	0.035	0.041	0.056
277	0.019	0.005	0.03	0.022	0.033	0.038	0.052
278	0.018	0.004	0.029	0.022	0.032	0.037	0.051
279	0.018	0.004	0.028	0.02	0.03	0.034	0.048
280	0.017	0.004	0.027	0.019	0.029	0.033	0.046
281	0.016	0.003	0.025	0.017	0.027	0.03	0.042
282	0.015	0.002	0.024	0.016	0.026	0.029	0.04
283	0.014	0.002	0.023	0.015	0.024	0.027	0.038
284	0.014	0.002	0.022	0.015	0.023	0.025	0.036
285	0.014	0.002	0.022	0.014	0.023	0.024	0.035
286	0.014	0.002	0.022	0.014	0.022	0.023	0.034
287	0.014	0.002	0.022	0.014	0.021	0.022	0.034
288	0.014	0.002	0.022	0.014	0.021	0.021	0.033
289	0.014	0.002	0.022	0.013	0.02	0.02	0.032
290	0.013	0.001	0.02	0.012	0.019	0.019	0.031
291	0.013	0.001	0.019	0.011	0.018	0.018	0.029
292	0.012	0.001	0.019	0.011	0.017	0.017	0.028
293	0.012	0.001	0.018	0.01	0.017	0.017	0.026
294	0.012	0.001	0.017	0.01	0.016	0.016	0.026
295	0.011	0.001	0.017	0.009	0.016	0.015	0.025
296	0.011	0.001	0.017	0.009	0.016	0.015	0.024
297	0.012	0.001	0.017	0.01	0.016	0.015	0.024
298	0.012	0.001	0.018	0.01	0.016	0.014	0.024
299	0.012	0.002	0.018	0.01	0.016	0.014	0.024
300	0.013	0.002	0.019	0.011	0.016	0.014	0.024